VLHC HEPAP Subpanel Report

- **EXECUTIVE SUMMARY**

Section 1. PHYSICS and DETECTOR ISSUES

- Summary of the Very Large Hadron Collider Physics and Detector Workshop — G. Anderson et al.
- I. Introduction
- II. New Strong Dynamics Working Group — E. Simmons, J. Womersley,
- III. Supersymmetry Working Group — G. W. Anderson
- IV. Exotics Working Group — U. Baur, S. Eno
- V. Full Rapidity Physics Working Group — A. Brandt, C. Taylor
- VI. Precision Measurements of Heavy Objects Working Group — F. Olness, R. Scalise
- VII. Multiple Interactions Working Group — S. Snow, F. Paige
- VIII. Tracking Working Group — F. Borcherding, T.Han
- IX. Calorimetry Working Group — D. Khazins, J. Lykken
- X. Muon Working Group — T. LeCompte, M.Berger
- XI. Summary

Section 2. ACCELERATOR PHYSICS

- Introduction and Design Goals — S. Mishra
- Lattice Design of the 3 TeV Injector — S. Mishra
- 50 TeV High Field Lattice: Observations from a Golden Cell — L. Michelotti
- Beam Transfer Lines for a VLHC — F. Bieniosek et al.
- Slow Extraction from the 3 TeV Injector for the VLHC — J. Marriner
- Alignment Issues for the 3 TeV Ring — C. T. Murphy
- RF Requirements for a 3 TeV Collider Ring — I. Kourbanis
- Beam Abort and Collimation for a 3x3 TeV Hadron Collider — A. I. Drozhdin, N. V. Mokhov
- Beam Abort for a 50x50 TeV Hadron Collider — A. I. Drozhdin et al.
- Transverse Resistive Wall Instability in a Very Large Hadron Collider — J-F. Ostiguy
- Electron-Cloud Instability in the VLHC — F. Zimmerman
- Beam Stability Issues in the 3 TeV Low-Field Collider — K-Y. Ng
- A Damper to Suppress Low Frequency Transverse Instabilities in the VLHC — J. Marriner
- Pipetron: Beam Dynamics with Noise — V. Shiltsev
- External Noise Issues in VLHC — V. Shiltsev
- Transverse Mode Coupling Instability in the VLHC — V. V. Danilov and V. D. Shiltsev
- Synchrotron Radiation in the VLHC — T. Kroc

Section 3. ACCELERATOR SYSTEMS

- Status Report on the Transmission Line Magnet — G. W. Foster
- Local Alignment of the Transmission Line Magnet — G. W. Foster
- Permanent Magnet for the Transfer Lines from the Main Injector To the 3 TeV VLHC Injector — G. W. Foster
- Design and operation of an experimental "Double-C" Transmission Line Magnet — G. W. Foster et al.
- Cryogenic System for the 3 TeV Injector Study — M. McAshan
- Examination of the Proposed VLHC Vacuum System — T. Anderson
- Instrumentation: Beam Intensity and Longitudinal Measurements — A. Hahn
- Position Monitors for the 3 TeV High Energy Booster — J. Crisp
- High Field Magnet R&D for VLHC — H. Glass et al.
- Thoughts on Controls/Instrumentation for 3 TeV Booster and VLHC — R. Goodwin et al.

Section 4. CONVENTIONAL CONSTRUCTION AND SITE CONSIDERATIONS

- Geology and Tunneling — J. Lach et al
- Dehumidification Options — S. Krstulovich et al
- 3 TeV RF Cooling System Design Proposal and Cost Estimate — J. A. Satti

Section 5. Five Year Plan for VLHC R&D

- Proposed Research and Development Plan — E. Malamud

APPENDIX

- An e^+e^- Top Factory in a 50 + 50 TeV Hadron Collider Tunnel — J. Norem et al
- Electron/Proton and Electron/Positron Collider Options — J. Norem
- The e/P option in the 3 TeV Booster — D. Krakauer & J. Norem

Executive Summary

This report is an update on work done by the VLHC Study Group since Snowmass '96 on a superconducting 100 TeV cm pp collider, $\geq 10^{34}$ cm^{-2} sec^{-1} luminosity. A VLHC in this energy range is a "discovery machine," whether or not Higgs or SUSY is discovered at the Tevatron or LHC. It is the only presently considered route to the 10 TeV mass scale. The goal of the VLHC study group and R&D efforts is to reduce the cost/TeV by about a factor of ten from the present cost.

Two approaches are being discussed for creating the VLHC:

- very high field magnets, perhaps using new HTS materials.
- low-field superferric magnet using existing technology.

This report has been prepared for the HEPAP Subpanel: "Planning for the future of the U.S. High Energy Physics." It supplements presentations made at Fermilab on August 13 by M. Albrow, S. Mishra, G.W. Foster, and E. Malamud. It is a compilation of work done since the distribution of two earlier documents:

- the "Pink Book," Selected Reports submitted to the Proceedings of the DPF/DPB Summer Study (Snowmass '96), and
- the "Yellow Book," collected transparencies from the VLHC Physics and Detector Workshop held at Fermilab March 13-15, 1997.

In our presentations to the Subpanel we discussed a staged approach to extending the energy frontier in the post-LHC era. Our current thinking is to use the 150 GeV Main Injector, inject into a 3 TeV "booster" and from there into the VLHC. We choose a conservative factor of 20 in dynamic range of the magnets.

We have focused considerable attention on the 3 TeV low-field "injector," a machine slightly larger than LEP/LHC in circumference. The cost of the machine (excluding a possible physics program) is comparable to the Main Injector. The 3 TeV low-field "booster" can also be regarded as a Tevatron replacement; in the Fermilab tradition many Tevatron components can be "recycled." The 3 TeV machine will be a demonstration of all the necessary technologies and their associated costs for constructing a machine 20x larger, and will be the benchmark for manufacturing the components, installing and servicing them. A modest physics program could be carried out during construction of the 100 TeV cm collider. Over the next year various physics options (fixed target, pbar-p, pp, ep) will be explored for the 3 TeV machine.

The proposed R&D plan for the 3 TeV low-field injector is such that construction could begin as the NuMI funding "bump" tapers down, and ramp up further, when US funding for LHC is essentially complete. Civil construction and construction of the technical components for the 3 TeV injector would proceed in parallel and could be completed in 4 years.

This report is divided into 5 sections plus one Appendix in which e^+e^- and ep options are discussed.

Section 1: Physics and Detector Issues

This section has a summary of the March VLHC Physics and Detector Workshop, "Physics at the energy frontier beyond the LHC." The VLHC will be designed to investigate physics beyond the Standard Model and outside the reach of any lepton collider. The workshop explored the physics that could be opened up in the 5-10 TeV mass scale with the new collider and explored in some detail the tradeoff between center of mass energy and luminosity. There are many challenges for the VLHC detectors, but for a luminosity comparable to the LHC luminosity, the detectors appears to be feasible. Their cost should not be ignored in the overall cost optimization of the VLHC.

Supersymmetric particles may be discovered prior to VLHC turn on, but some may be too heavy to study well at LHC. The SUSY-breaking mechanism occurs at a still higher mass scale, and may involve "messenger" particles within the VLHC range. Above 1 TeV interactions among W's and Z's may show rich structure. The Standard Model has dramatic phenomena (instantons, tunneling between vacua) in the 10's of TeV region which might be detectable. The VLHC, and past experience with hadron colliders supports this claim, should be a "discovery machine" as well as being superior in thoroughly studying any new physics found at LHC.

Section 2: Accelerator Physics

In this section, there are a number of papers dealing with the 4 different machines (high field, low field, 3 and 50 TeV) under study. The parameter tables also include luminosity values for use of the 3 TeV machine as a pbar-p or pp collider. Parameters for the 3 TeV machine depend on its uses: a demonstration project; a modest 3 TeV physics program; or simply an injector to the 50 TeV collider.

The low field lattice design is alternating gradient so that no quadrupoles are needed. This allows the accelerator structures to be made in long lengths. The system is modular allowing maximal use of automation in manufacture, installation and maintenance. The 150 GeV lines from the Main Injector are simple FODO beam lines using permanent magnet quadrupoles and therefore not requiring a water cooling system.

Since the Snowmass 96 workshop we have paid considerable attention to the beam stability in the 2 cm warm bore of the low-field VLHC. We belive that the issues have been addressed and that the design is workable. A solution to the resistive wall coupled bunch instability requires a modest feedback system. We are performing computational and experimental work on the vacuum pipe impedance, relevant for the understanding of both the single bunch and coupled bunch instabilities.

Section 3: Accelerator Systems

Work has been done at Fermilab on a 2 T combined function magnet that can be used in the 3 TeV booster and the 50 TeV collider. An innovative design by G. W. Foster called the double-C or transmission line magnet uses a single 75 kA of superconducting cable to energize two magnet gaps. This is a warm bore, warm iron magnet. The small cold mass allows rapid cool

down. The most economical approach is to use NbTi conductor, cooled with liquid helium. A simple cryogenic system has been designed. Because of the "magic" of iron which concentrates the stored energy in the gaps where the beams circulate, the amount of superconductor required is small. The conductor is at a force null so a low heat leak structure is possible. Furthermore, the field at the conductor is only 1 T, so one can take advantage of the factor of 10 increase in J_c in NbTi at low fields since the Tevatron was built. The base technology to build this magnet is in hand and a 50m prototype is under development.

High-field magnets ($B \geq 9$ T) using either Nb_3Sn or high-temperature superconductor (HTS) are some years away. Using magnets of field strength of about 10 T, or higher, will result in synchrotron radiation damping of the beam emittance, which gives a boost to machine performance, and is an advantage over a low-field design.

Section 4: Conventional Construction and Site Considerations

Both the 3 TeV and 50 TeV machines would be built deep underground in what has been called by contractors that make tunnels in hard rock "ideal" for tunnel boring machines. This is a uniform layer of dolomite ~400 feet below the surface of the Fermilab region.

A reference siting for the 3 TeV "booster" has been made and we are working with one of the major contractors from the Chicago deep tunnel project to obtain cost estimates for the civil construction using conventional tunnel boring machine techniques. The 3 TeV "booster" is 34 km in circumference.

Section 5: Five Year Plan for VLHC R&D

The overall R&D goal is to demonstrate feasibility and cost. The proposed R&D plan is divided into 7 areas, each with a set of goals. A five-year effort totaling approximately $25M is outlined. Whatever approach is followed the main motivation driving the R&D is to lower the cost/TeV by a factor of 10 relative to current capabilities. Both capital and operating costs are important.

A major goal is to complete by the end of 1998 a design study of the 3 TeV low-field injector and to be nearing completion of a design study for the 50 TeV machine.

Public Outreach

Gaining public support is part of our challenge. We need to begin work on this early. We have many different constituencies to talk to. The project name, logo, and mission statement are important. We must understand the role of the Media and use the many different types of formal and informal education to communicate our message. We can learn from successes and failures from other large scientific projects. Community involvement in the initial stages is essential.

The development of a 75 kA transmission line in a deep underground tunnel, installed and serviced robotically, is of interest to the electric utility industry. Partnerships based on common goals are another important way to gain public support.

Conclusions

The VLHC project can build on Fermilab's core competencies in

- accelerators and colliders
- large project management
- international collaboration

In the coming year we will continue to work on the physics case and preliminary detector parameters, accelerator parameters, lattice, and dynamics, R&D on magnets including the use of HTS and together with industry work on tunneling and robotics. Our goals are aggressive and depend on sufficient resources becoming available. Clearly if Fermilab did not have an incredibly rich physics program on its menu for the next decade we could go even faster; but obviously exploitation of the new Main Injector and the luminosity upgrades in the Tevatron must be the lab's highest priority. However we as a field also need to invest in the future, to make sure that the long term physics program based on machines with true discovery potential, will be as rich as it will be for the next decade.

Section 1: PHYSICS and DETECTOR ISSUES

G. Anderson, et al., "Summary of the Very Large Hadron Collider Physics and Detector Workshop"

I. Introduction

II. E. Simmons, J. Womersley, "New Strong Dynamics Working Group"

III. G. W. Anderson, "Supersymmetry Working Group"

IV. U.Baur, S.Eno, "Exotics Working Group"

V. A. Brandt, C.Taylor, "Full Rapidity Physics Working Group"

VI. F. Olness, R. Scalise, "Precision Measurements of Heavy Objects Working Group"

VII. S. Snow, F. Paige, "Multiple Interactions Working Group"

VIII. F. Borcherding, T. Han, "Tracking Working Group"

IX. D. Khazins, J. Lykken, "Calorimetry Working Group"

X. T. LeCompte, M. Berger, "Muon Working Group"

XI. Conclusions

FERMILAB-CONF-97/ 318-T

Summary of the Very Large Hadron Collider Physics and Detector Workshop

Physics at the high energy frontier beyond the LHC

March 13-15, 1997

Fermi National Accelerator Laboratory, Batavia, Illinois

G. Anderson (Fermilab), U. Baur (SUNY at Buffalo), M. Berger (Indiana University), F. Borcherding (Fermilab), A. Brandt (Fermilab), D. Denisov (Fermilab, Co-Chair and Co-editor), S. Eno (University of Maryland), T. Han (University of California–Davis), S. Keller (Fermilab, Co-Chair and Co-editor), D. Khazins (Duke University), T. LeCompte (Argonne National Laboratory), J. Lykken (Fermilab), F. Olness (Southern Methodist University), F. Paige (Brookhaven National Laboratory), R. Scalise (Southern Methodist University), E. H. Simmons (Boston University), G. Snow (University of Nebraska–Lincoln), C. Taylor (Case Western Reserve University), J. Womersley (Fermilab).

Abstract

One of the options for an accelerator beyond the LHC is a hadron collider with higher energy. Work is going on to explore accelerator technologies that would make such a machine feasible. This workshop concentrated on the physics and detector issues associated with a hadron collider with an energy in the center of mass of the order of 100 to 200 TeV.

I. INTRODUCTION

The Very Large Hadron Collider Physics and Detector workshop took place at Fermilab in March 1997. In this paper we summarize the activities of the working groups during the workshop.

This workshop was motivated by the accelerator work [1] [1] that has been started on new technologies for a post-LHC Very Large Hadron Collider (VLHC). Obviously, physics and detector issues, along with accelerator technology and budget constraint, must guide us to select appropriate and realistic energy and luminosity for such a machine.

As is well known, the last largely unexplored sector of the Standard Model (SM), the Higgs sector, will be investigated over the next decade or so by the Tevatron, HERA, LEP, and LHC. Any post-LHC machine will be built to explore physics beyond the SM. At this point in time, we do not have any experimental evidence for the physics beyond the SM, and it is therefore difficult to make the case for any specific accelerator beyond the LHC. Therefore, our goal is to make the case for accelerator and detector developments that would allow us to build a hadron collider for a lower cost than with current technologies.

Some preliminary work was done during the Snowmass 96 [2] workshop, where the EHLQ [3] paper was used as a guide. Contrary to what is sometimes assumed, it is not necessary to increase the luminosity proportionally to the square of the energy. In fact for the production of heavy objects, each time the accelerator energy is increased by a factor of 2, the cross section increases by more than a factor of 10. For this to be true, the heavy object has to be detectable at the lower energy accelerator. The increase in cross section is due to the simple fact that the average Bjorken-x probed is decreased when the accelerator energy is increased and that the parton distribution function are larger at smaller x.

For this workshop it was therefore decided to concentrate on a center of mass energy (E_{cm}) between 100 TeV and 200 TeV and a luminosity ($\mathcal{L}$) between $10^{34} cm^{-2} s^{-1}$ and $10^{35} cm^{-2} s^{-1}$. These ranges are testing the limits of the detector and accelerator capabilities and allow one to investigate the tradeoff between E_{cm} and $\mathcal{L}$. The increase in E_{cm} and $\mathcal{L}$ from the LHC to the VLHC are about the same as the increase between the Tevatron and the LHC. We will see that with these parameters the scales of physics beyond the SM that can be probed are about an order of magnitude larger than the scales probed at the LHC.

One of the conclusions reached during the Snowmass 96 workshop was that it would be interesting to concentrate on scenarios of physics beyond the SM that have a chance to reveal themselves before the VLHC and study their implications for a VLHC. This was done in several studies during this workshop.

Due to the discovery nature of the VLHC, it is clear that we need to consider multipurpose detectors. No major problems with detector design were uncovered during the Snowmass 96 study.

About 150 participants attended the workshop which consisted of one day of plenary talks, one day of working group meetings and one half day of working group summaries by the conveners. Before going to the summary of the different working groups we provide here a brief synopsis of the plenary talks.

P. Sphicas (MIT) started with a broad sweep from the first hadron collider, the ISR, to the VLHC. He summarized the impresssive achievements of hadron colliders over the last 25 years and the current outstanding questions. G. Dugan (Cornell University) summarized the activity of the accelerator group during the Snowmass 96 workshop. Both the low and high field options were considered, with a center of mass energy of 100 TeV, a peak luminosity of $10^{34} cm^{-2} s^{-1}$ and 16ns bunch spacing. It is currently believed that there is an overall luminosity upgrade potential for the low and high field options of a factor of 5 and 10, respectively. P. Bloch (CERN) reviewed the main components of the LHC detectors. C. Hill (Fermilab) summarized the basic principles of the SM and possible scenarios of physics beyond the SM (e.g., SUSY, Technicolor, Topcolor.). F. Wilczek (IAS, Princeton) gave his view of the future of particle physics, describing the success and deficiencies of the SM and the wonders of unification and SUSY. P. Grannis (SUNY Stony Brook) closed the workshop with a talk entitled:" The Future Beckons". He analysed lessons of the past and drew morals for future decisions. He presented both depressing and optimistics scenarios, and warned us against the danger of hasting our decision to support a specific machine before Nature gives us some clues of what the appropriate machine is. [2]

We now turn to the working group summaries.

[1] The references for the introduction and conclusions are at the end of the paper, the references for the working group summaries are at the end of the respective sections.

[2] The collection of transparencies of the plenary talks and working group summary talks is available, please send your request for a copy to vlhc@fnth32.fnal.gov.

II. NEW STRONG DYNAMICS WORKING GROUP

Elizabeth Simmons
Boston University
John Womersley
Fermi National Accelerator Laboratory

The New Strong Dynamics working group considered what a VLHC could reveal about new strong interactions, such as might be involved in electroweak symmetry breaking (EWSB). We tried to identify new physics that would be uniquely visible at a VLHC (as opposed to the LHC, NLC, or a muon collider). We also considered the appropriate center of mass energy and luminosity for a hadron collider intended to explore this physics and whether the traditional 'rules of thumb' about energy-luminosity trade-offs hold.

The working group met for a total of four hours during the VLHC workshop. Group discussions were initiated (and ultimately summarized) by the following presentations:

- Introduction and Overview (J. Womersley)
- Non-Standard Higgs (V. Koulovassilopoulos)
- Multiple W Production (W. Kilgore)
- Strong WW Scattering (K. Cheung)
- Deca-TeV Unified Compositeness (Y. Pirogov)
- Summary (E. Simmons)

Many other physicists including S. Chivukula, P. Grannis, C. Hill, T. LeCompte and F. Paige also made valuable contributions.

One thread of our discussion centered around the feasibility of using the VLHC to study a 'non-standard Higgs': a scalar boson with a mass of 400 to 800 GeV with non-standard couplings to weak gauge bosons and fermions[1]. Looking in the decay channel $H \to ZZ \to \ell^+\ell^-\ell^+\ell^-$, it appears that this scalar can be discovered as easily as a standard Higgs. A careful measurement might then make it possible to distinguish whether the width of the discovered object differed from that of the standard model prediction by more than a few percent. Both the discovery and identification capabilities of a VLHC would be superior to those of the LHC; a muon collider of the right energy might also do a reasonable job. The relatively low mass of this scalar makes it easier to study at a lower-energy (60-100 TeV) VLHC than at a higher-energy (200 TeV) machine.

In particular, Koulovassilopoulos *et al.* studied the possibility that the WWH coupling is rescaled relative to the standard model value by a factor ξ. The decay width of the heavy Higgs is proportional to ξ^2, and a collider's ability to detect the non-standard nature of the Higgs can be described in terms of its sensitivity to deviations of ξ from 1.0. Their results for the LHC and several possible VLHC accelerators are listed in Table I.

$\sqrt{s}$, $\mathcal{L}(\mathrm{cm}^{-2}s^{-1})$	Sensitivity to ξ		
	m_H (GeV)		
	400	600	800
14 TeV, 10^{33}	60%*	—	—
14 TeV, 10^{34}	20%*	40%*	—
50 TeV, 10^{34}	7%	12%	20%
50 TeV, 10^{35}	3%	4%	7%
100 TeV, 10^{34}	6%	8%	12%
100 TeV, 10^{35}	$2-3\%$	3%	5%
200 TeV, 10^{34}	—	25%	30%
200 TeV, 10^{35}	—	8%	12%

Table I: Sensitivity to the parameter ξ at the LHC and VLHC for various value of the luminosity and CM energy. The starred entries indicate that the value given applies only for $\xi > 1$, whereas for $\xi < 1$ the sensitivity is substantially worse.

Another topic was production and detection of multiple (longitudinal) weak gauge bosons at high energies. The idea is that just as pion scattering above the ρ resonance is dominated by multiple pion production, so might $W_L W_L$ scattering (in a strongly-interacting regime) result at high energies in multi-W_L final states. Kilgore[2] estimates the total cross section σ_{WW} to be $\sim$ 100 fb at the "ρ" peak and $\sim$ 20 fb asymptotically at higher $\sqrt{\hat{s}}$. If the acceptance is of order 50%, then the observable cross section of $\sim$ 10 fb would imply that it is not reasonable to require more than $\sim$ 1 of the W's to decay leptonically. If one of the W's is required to decay leptonically and each of the others becomes a single 'fat' hadronic jet, the dominant background will arise from standard production of one W plus multiple gluon jets. Unlike multiple W production the cross section for this process would fall rapidly with increasing jet multiplicity and the multiple-W signal might become apparent above $n_{\mathrm{jets}} \sim 5-8$. The current rough estimate is that with an integrated luminosity of 100 fb^{-1}, about 100 signal events (and almost no background) might remain after all cuts and branching ratios are included. Other suggestions for reducing background and improving signal included allowing more than one W to decay leptonically or identifying tau leptons resulting from $W \to \tau\nu_\tau$ decays.

A third focus was on how well the VLHC compares with the LHC in studying strong $V_L V_L$ scattering in the gold-plated modes where the vector bosons decay leptonically and the silver-plated modes where two Z bosons are produced and one decays to neutrinos[3]. Since (at tree level) the only hadronic activity in the detector in the signal events would result from the spectator quarks that radiated the $W_L^l s$, a forward jet tag and central jet veto can reduce background. It appears that the VLHC would do much better than the LHC at detecting the simple excess of $V_L V_L$ final states that would indicate the presence of a strongly-coupled electroweak symmetry-breaking sector. Furthermore, the VLHC would more clearly determine which specific final states ($W^\pm W^\pm, ZZ, W^+W^-, WZ$) showed the largest excesses – information that would help distinguish among competing models of the strong electroweak interactions. It is interesting to note that, based on these studies, cutting on measured missing E_T may not be required for W identification. This is potentially important for detector design.

Mode	σ_B	$\sigma_S(S/\sqrt{B})$	
		1 TeV Higgs	Rescaled $\pi\pi$
$\sqrt{s} = 14$ TeV, 100 fb^{-1}			
$W^\pm W^\pm$	0.037	0.065(3.4)	0.2(11)
ZZ	0.006	0.042(5.1)	0.0085(1.0)
W^+W^-	0.13	0.18(5.0)	0.05(1.3)
$W^\pm Z$	0.05	0.016(0.7)	0.04(1.8)
$\sqrt{s} = 60$ TeV, 100 fb^{-1}			
$W^\pm W^\pm$	0.83	1.4(15)	4.9(54)
ZZ	0.2	1.3(29)	0.3(6.9)
W^+W^-	5.2	7.3(32)	3.5(15)
$W^\pm Z$	1.1	0.38(3.6)	1.5(14)
$\sqrt{s} = 100$ TeV, 100 fb^{-1}			
$W^\pm W^\pm$	1.9	2.9(21)	10(72)
ZZ	0.5	2.8(40)	0.68(9.6)
W^+W^-	12	16(45)	9.4(27)
$W^\pm Z$	3.2	0.7(3.9)	4.0(22)
$\sqrt{s} = 200$ TeV, 100 fb^{-1}			
$W^\pm W^\pm$	4.9	6.8(31)	2.4(110)
ZZ	1.3	6.2(52)	1.8(15)
W^+W^-	40	40(62)	28(43)
$W^\pm Z$	10	3.1(6.6)	15(47)

Table II: Signal and background cross sections σ_S and σ_B (in femtobarns), and signal significance $S/\sqrt{B}$, for two models of vector-boson pair production in various final states, for the LHC and for various VLHC options.

For instance, Cheung *et al.* examined the signal of a strong EWSB sector at the LHC and VLHC in several longitudinal diboson final states. They employed the general type of cuts described above and evaluated the significance $S/\sqrt{B}$ (where S and B are the number of signal and background events) assuming an integrated luminosity of 100fb^{-1}. Table II shows their results for two models of strong EWSB: a 1 TeV Higgs and a rescaled $\pi\pi$ scattering model (including chirally coupled ρ, σ and f_0 states) scaled from QCD.

Finally, it was acknowledged that the existence of compositeness at scales of order 10 TeV, as discussed in [4], might give rise to new interesting resonances at energies accessible to the VLHC.

Drawing any firm conclusions about the physics of the VLHC is currently impossible, because we do not know what underlies electroweak symmetry breaking. For the purposes of this working group we assume that it involves some new strong dynamics. It then seems reasonable to conclude that:

- The VLHC should be designed to probe the TeV scale in detail, since the physics associated with electroweak symmetry breaking will be there. This is the only scale at which we can currently say much about the possibilities for new physics. If the LHC has discovered this physics, the VLHC will be able to explore it in depth. If this physics lies just beyond the reach of the LHC, we will nonetheless know it must exist, and the VLHC will catch it.
- At the same time, the VLHC should have an ultimate reach of 10 TeV or more at the partonic scale, so that it can be sensitive to any relatively low-lying phenomena associated with flavor physics.
- The VLHC detector(s) will need to be capable of identifying final states involving multiple vector bosons. This will require good capability for measuring the charge and momentum of leptons, and the energy and direction of hadronic jets (including forward jets associated with spectator quarks). It is not clear if missing E_T measurement will have a high priority. Tagging the jets associated with high-energy top quarks or taus would also be very useful, because the physics of flavor-symmetry breaking might be expected to give top- and tau-enriched signals. Tagging heavy flavor in the environment of the VLHC will be an interesting challenge!
- While a compelling case for studying the TeV scale exists, far less is known about what might lie at higher scales. A challenge to theorists is to identify the possibilities for 10 TeV-scale physics. For instance, it would be interesting to know the extent to which specific classes of experimental results at lower energies (e.g. observing a particular spectrum of technipions at the LHC) would help narrow the options at higher scales.

However nature has chosen to construct the world, we can be sure that if it involves new strong dynamics the VLHC will have a rich spectrum of new physics to explore.

REFERENCES

[1] D. Kominis and V. Koulovassilopoulos, Phys. Rev. D **52** (1995) 2737; Phys. Rev. D **51** (1995) 282.

[2] W. Kilgore (with M. Peskin), presentation to the Very Large Hadron Collider Physics and Detector Subgroup, 1996 DPF/DPB Summer Study on New Directions in High Energy Physics (Snowmass 1996).

[3] J. Bagger *et al.*, Phys. Rev. D **52** (1995) 3878.

[4] V. V. Kabachenko and Yu. F. Pirogov, "Unified Compositeness of Leptons, Quarks and Higgs Bosons," hep-ph/9612275.

III. SUPERSYMMETRY WORKING GROUP

Greg W. Anderson
Fermi National Accelerator Laboratory

Assessing the role of a VLHC as a tool for studying supersymmetry at this point in time is a problematic enterprise. This question depends largely and significantly on what is and is not seen in future collider experiments. As a candidate for physics just beyond the standard model, supersymmetry presents us with a large variety of models and frameworks. Still, in this context, it is reasonable to ask "under what circumstances would a very high energy collider like the VLHC further, or possibly complete, our understanding of weak-scale supersymmetry?" The principal scenarios which could require a very high energy accelerator fall into two classes: Models with a multi-scale superpartner spectrum, and models with gauge mediated supersymmetry breaking. [3]

If the physics just beyond the standard model is supersymmetric, naturalness requires an abundance of superpartners with masses below a few hundred GeV[1]. These new spectra should be well within the range of the LHC and a 1.5 TeV NLC, and it is likely the lighter of these particles will be accessible at the Tevatron and perhaps LEP-II. If no evidence of supersymmetry is seen by the time the LHC is in operation, supersymmetry will have little motivation as the physics just beyond the weak-scale. In this case, it is supersymmetry and not the VLHC which is lacking motivation and one would expect new dynamics of the type discussed by other groups in the VLHC study. If SUSY does appear at the weak-scale, it will be discovered by the next generations of accelerators (Tevatron, LEP-II, LHC). Moreover, the LHC and a 1-1.5 TeV NLC could provide us with considerable information about the spectroscopy and interactions of superparticles. What might we learn about SUSY at these colliders that would argue for a higher energy machine such as the VLHC?

It is possible that pre-VLHC experiments would only uncover part of the supersymmetric spectrum. Although the simplest formulations of weak-scale supersymmetry would place *all* of the superpartners below a few–several hundred GeV, it is tenable for some superpartners to appear at a higher scale[2]. Because the first two generations of squarks and sleptons couple less strongly to the Higgs sector, it is possible for them to have masses of several TeV without violating naturalness unacceptably. Supersymmetry requires at least two Higgs doublets, and if the multi-TeV scale involves new dynamics, it is also conceivable for part of the Higgs sector to have masses as heavy as a few TeV[2]. Evidence for a multi-scale superpartner spectrum would be inferred from the absence of some modes of superpartner production. Moreover, the radiative effects of multi-TeV superpartners would induce a non-decoupling violation of the equality between the gauge couplings of bosons and gauginos. This violation can occur at the $1-10\%$ level for multi-TeV scale superpartners [3].

The most compelling case for a VLHC would arise if future collider experiments could probe the dynamics of supersymmetry breaking. Any supersymmetric theory of physics beyond the standard model must contain a mechanism for breaking supersymmetry and a method (messenger) for communicating this breaking to the superpartners of the standard model particles. Hence, any SUSY discovery immediately implies the existence of two, possibly distinct, scales beyond the weak-scale: the fundamental scale of SUSY breaking and the messenger scale. A typical superpartner mass $\tilde{m}$ is related to the messenger scale M and the dimension-two supersymmetry breaking vev F by:

$$\tilde{m} \propto \eta \frac{F}{M} \tag{1}$$

here we include a parameter η as a placeholder for additional suppressions which can be supplied by dimensionless couplings. If supersymmetry breaking is mediated by gravitational interactions, $M = M_{Pl}$, requiring $\sqrt{F} \sim 10^{10} GeV$ a scale so high as to be irrelevant for conceivable collider experiments. If supersymmetry breaking is communicated by gauge interactions, M is replaced by the mass of heavy vector-like messenger fields and the parameter η contains a factor $\alpha/4\pi$. For $\sqrt{F} \sim M$, it is possible that the messengers of supersymmetry breaking and the fundamental scale of SUSY breaking itself are as low as $10-10^2$ TeV. However even with gauge mediation these relatively low scales are not inevitable. Anything resembling a "no-lose" theorem for the VLHC would rely both our ability to determine that supersymmetry breaking has been communicated by gauge interactions, and on our ability to place an upper bound on the messenger scale.

We have at least two ways of distinguishing gauge-mediated SUSY breaking from gravitationally mediated SUSY breaking. In their simplest forms, these two mechanisms for mediating SUSY breaking lead to rather different patterns of superpartner masses (see for example Figs. 10–11 of Ref. [4]). A more dramatic diagnostic comes from the decays of superpartners. In gravitationally mediated models, the lightest superpartner–LSP, typically the lightest neutralino – $\tilde{\chi}_1^0$ is stable. [4] In gauge mediated models, the gravitino, with a mass typically on the scale of eV's takes on the role of the LSP. In this case, distinctive decays of the next to lightest superpartners–NLSP, into the gravitino *e.g.*, $\tilde{\chi}_1^0 \to \gamma + \tilde{G}$ may occur inside the detector, leading to signatures with two-photons, missing energy and various combinations of jets and leptons[5, 6, 7, 8]. (For other possibilities see for example [9]).

The more challenging task is determining if the messenger sector and/or the fundamental scale of supersymmetry breaking is within reach of the VLHC. We can hope to learn something about a potential multi-TeV messenger scale from the mass spectra of superpartners and from their decays to gravitinos.

The field(s) responsible for SUSY breaking, whether fundamental or composite may have both supersymmetry preserving and dimension-two supersymmetry breaking vevs which we denote by S and F_S respectively. In the simplest models, if the

[3] Of course, other possible motivations for a VLHC, including extended gauge groups, extended heavy Higgs sectors, or additional heavy exotic-particles are compatible with weak-scale SUSY, but these augmentations are not specific to SUSY models, and these subjects are treated in detail by the New Strong Dynamics, and Exotics groups.

[4] Assuming R-parity conservation.

field responsible for supersymmetry breaking couples to a pair of messengers with a Yukawa coupling λ, each supermultiplet of messengers will split into a pair of heavy and light scalars along with an intermediate mass fermion. In this case messenger masses can be written in terms of two parameters[7]:

$$\begin{aligned} M_f &= \frac{\Lambda}{x} \\ M_{\ell,h} &= \frac{\Lambda}{x}\sqrt{1 \mp x} \end{aligned} \tag{2}$$

The scale $\Lambda = F_S/S$, is roughly a factor of 10^2 larger than a typical superpartner mass, and will be determined once the magnitudes of superpartner masses are measured *e.g.*, $m_{\tilde{g}}, m_{\tilde{q}} \sim \frac{\alpha_s}{4\pi}\Lambda$. The residual uncertainty in the values of messenger masses is parameterized by $x = F_S/\lambda S^2 = \lambda^{-1}\Lambda^2/F_S$. For simplicity we neglect variations in λ across different messenger representations. In order to avoid unwanted breaking of color, x is bounded from above by one. For fixed superpartner masses, as $x \to 0$, messenger particles become inaccessibly heavy, even for a VLHC.

The appearance of heavy messenger representations, induce soft supersymmetry breaking masses for the SM superpartners through loop corrections. At a renormalization group scale $\mu \sim M_f$ the induced gaugino masses, M_a and scalar superpartner masses $\tilde{m}$ take the form: [7, 10, 11]:

$$\begin{aligned} M_a &= \frac{\alpha_a}{4\pi}\Lambda \sum_i n_a(i) g(x_i) \\ \tilde{m}^2 &= 2\Lambda^2 \sum_a \left(\frac{\alpha_a}{4\pi}\right)^2 C_a \sum_i n_a(i) f(x_i), \end{aligned} \tag{3}$$

where C_a is the quadratic Casimir invariant of the MSSM superpartner field, and $n_a(i)$ is the Dynkin index of the i-th messenger pair. For the minimal $\mathbf{5} + \bar{\mathbf{5}}$ model, the sum over messenger representations: $\sum_i n_1(i) = \sum_i n_2(i) = \sum_i n_3(i) = 1$.

The superpartner mass spectrum depends on x in two ways, so a precise measurement of the superpartner spectrum can in principle be used to place an upper-bound on the messenger sector. The masses in Eq. 3 must be renormalized down to low energy. This induces a logarithmic dependence of the superpartner masses on x. However, the softness of this logarithmic dependence makes the prospect of obtaining an upper bound on messenger masses low enough to provide a guarantee for the discovery at a VLHC appear quite challenging.

In the fortunate circumstances that x is close to one, and upper-bound on the messenger scale could be achieved by examining the ratio of gaugino and scalar superpartner masses. For small x, the functions $g(x)$ and $f(x)$ are very close to one, and the only dependence of superpartner masses on the messenger scale is the logarithmic dependence discussed above. As x approaches 1 the functions $f(x)$ and $g(x)$ depart from values close to one. In this case examination of scalar superpartner–gaugino mass ratios may provide a quantitative measure of the messenger scale. The relevant quantity is $\sqrt{f}/g$, which is always less than unity and approaches 1 for $x \to 0$. $\sqrt{f}/g \lesssim .8$ (.9) ((.95)), requires $x \gtrsim .9$ (.72) ((.54)) respectively. This approach also appears quite challenging, unless x is quite close to one. Moreover, the simple dependence of the superpartner mass ratios on $\sqrt{f}/g$ occurs at messenger energy scales, and this contribution must be disentangled from renormalization effects, the dependence on the messenger content, and other effects. However, these fortuitously large values of x also coincide with the light messenger masses we have the best chance of probing. Our ability to use superpartner mass measurements to place an upper bound on the messenger scale which lie within the reach of a VLHC requires that future colliders make reasonably precise measurements of superpartner masses.

Recent studies of the potential for superpartner mass measurements at the LHC appear quite promising. For example, Hinchliffe *et.al*, [12] were able to extract superpartner mass measurements at the level of $\sim 10\%$ and $\sim 20\%$ for Snowmass LHC study. However, the precision of these measurements depends on were one is in SUSY parameter space, and these analyses are not model independent. How precisely, and model-independently we will be able to measure superpartner masses at the LHC is not yet known. More detailed analyses have been made concerning precision measurements achievable at an NLC [13]. If at all possible, bounding the messenger scale significantly may require a future lepton collider, but whether this is a necessity will not be clear for some time.

An upper bound on the messenger scale could also be inferred from upper bounds on the displaced vertex in NLSP decay. The gravitino coupling to superpartners diminishes significantly as the scale supersymmetry breaking increases. Accordingly, a shorter lifetime for the NLSP requires a lower scale of supersymmetry breaking and lighter messenger masses. Rewriting Eq. 2 for the messenger fermion mass, a bound on F can be translated into a bound on the messenger scale M:

$$M_f = \lambda \frac{F_S}{\Lambda} < \lambda \frac{F_{tot}}{\Lambda} \lesssim \frac{F_{tot}}{\Lambda} \tag{4}$$

here we make a distinction between F_S and F_{tot} because there may be other sources of supersymmetry breaking in addition to the SUSY breaking field coupled to messenger fields. Because Λ can be in principle determined by measurements of superpartner masses, an upper-bound on the messenger scale can be found if we can place and upper bound on F_{tot} or equivalently an upper bound on the distance to the displaced vertex. The decay width for the lightest neutralino into a gravitino in gauge mediated models is

$$\Gamma(\tilde{\chi}_1^0 \to \tilde{G}\gamma) = 20\kappa \left(\frac{m_{\tilde{\chi}_1^0}}{100\ \mathrm{GeV}}\right)^5 \left(\frac{\sqrt{F}}{10\ \mathrm{TeV}}\right)^{-4} \mathrm{eV} \tag{5}$$

where κ is the photino content of $\tilde{\chi}_1^0$. The probability that the neutralino travels a distance x before decaying in the detector is $P(x) = 1 - e^{-x/L}$, where

$$L = \frac{9.9 \times 10^{-3}\mu m}{\kappa} \left(\frac{m_{\tilde{\chi}_1^0}}{100 GeV}\right)^{-5} \left(\frac{\sqrt{F_{tot}}}{10\ \mathrm{TeV}}\right)^4 \left(E^2_{\tilde{\chi}_1^0}/m^2_{\tilde{\chi}_1^0} - 1\right)^{\frac{1}{2}}. \tag{6}$$

Leading to the bound:

$$M_f \lesssim 10 \text{ TeV} \left(\frac{100 \text{ TeV}}{\Lambda}\right) \left(\frac{\kappa L}{0.99\ \mu\text{m}}\right)^{1/2} \left(\frac{100 \text{ GeV}}{m_{\tilde{\chi}_1^0}}\right)^{5/2} \left(E^2_{\tilde{\chi}_1^0}/m^2_{\tilde{\chi}_1^0} - 1\right)^{-\frac{1}{4}} \quad (7)$$

So this method will challenge our ability to resolve relatively small displaced vertices as well.

In both cases, establishing that messengers lie within reach of a VLHC requires relatively large values of x, relatively light values of F, and reliable measurements of superpartner masses. On one hand combining these fortunate circumstances may appear to be wishful, but the fortunate circumstances under which we would be able to identify and place reliable upper-bounds messenger scale overlap with those where multi-TeV messenger states are light enough to be accessible at a VLHC. Good luck is when preparation and opportunity meet, and we should be prepared to exploit this opportunity if it arises.

We conclude with a few remarks about the collider signatures of the messenger sector. If light enough, messenger particles would be pair produced at the VLHC. Heavy messenger scalars will decay to messenger fermions by radiating gauginos and messenger fermions will decay to the lighter messenger scalars by radiating gauginos as well. Renormalizable Yukawa interactions between messenger fields and standard model fields potentially introduce flavor changing neutral currents, spoiling the principle motivation for low energy 10–100 TeV SUSY breaking. In the absence of such couplings the lightest messenger fields contain conserved quantum numbers and are stable. The presence of nonrenormalizable operators may induce messenger decay, but not on time scales relevant to collider searches. Planck mass suppressed dim-5 operators, would for example lead messengers to decay with lifetimes of $\sim 10^{-1}$–10^{-2} s[10].

The apparent unification of gauge couplings at high energies $\sim 10^{16}$ GeV is most naturally accommodated by messenger representations in complete $SU(5)$ representation. In the minimal messenger model, the messengers are contained in the $\mathbf{5} + \bar{\mathbf{5}}$ representation of $SU(5)$. Under the standard model gauge group $SU(3) \times SU(2) \times U(1)$. The $\bar{\mathbf{5}}$ representation decomposes as:

$$\bar{\mathbf{5}} = (\bar{\mathbf{3}}, \mathbf{1}, \frac{\mathbf{1}}{\mathbf{3}}) + (\mathbf{1}, \mathbf{2}, -\frac{\mathbf{1}}{\mathbf{2}}). \quad (8)$$

Together with the 5, the lightest scalar messenger states will these states will have the quantum numbers of and has the same quantum numbers as $SU(2)$-singlet down squarks– D^c, and left handed slepton doublet – L respectively. The colored scalar messenger states hadronize to form multi-TeV objects with the same quantum numbers as a neutron or proton, and would look like a canon ball in the detector.

In the absence of a discovery of supersymmetry at or before the LHC SUSY provides little motivation for a VLHC. However, it should be understood in this case that it is supersymmetry and not the VLHC which is lacking motivation.

If the world is supersymmetric above the weak scale and supersymmetry breaking is transmitted to the standard model superpartners by gauge interactions, the VLHC may be a logical step in the worlds future high energy physics program. However, this is not inevitable. Supersymmetry could be found at the several hundred GeV scale without giving us any compelling reason to expect another layer of structure at the multi-TeV scale. The case for such a machine will rest on what nature provides for us, and on our ability to exploit the Tevatron, LEP-II and the LHC.

REFERENCES

[1] G. W. Anderson and D. J. Castaño, Phys. Lett. **B347**, (1995) 300; Phys. Rev. **D52** (1995) 1693; Phys. Rev. **D53** (1996) 2403. G. W. Anderson, D. J. Castaño and A. Riotto, Phys. Rev. **D55** (1997) 2950.

[2] S. Dimopoulos, G. F. Giudice, Phys. Lett. **B357** (1995) 573-578; A. G. Cohen, D. B. Kaplan, and A. E. Nelson, Phys. Lett. **B388** (1996) 588-598.

[3] Hsin-Chia Cheng, J. L. Feng, and N. Polonsky, FERMILAB-PUB-97-205-T, hep-ph/9706476; FERMILAB-PUB-97-177-T, hep-ph/9706438; E. Katz, L. Randall, and S. Su, MIT-CTP-2646, hep-ph/9706478; D. Pierce, M. Nojiri and Y. Yamada, SLAC-PUB-7558, hep-ph/9707244.

[4] J. A. Bagger, K. T. Matchev, D. M. Pierce and R.-J.Zhang, Phys. Rev. **D55** (1997) 3188-3200.

[5] P. Fayet, Phys. Lett. **B70** (1977) 461; Phys. Lett. **B86** (1979) 272; Phys. Lett. **B175** (1986) 471.

[6] N. Cabibbo, G. R. Farrar, and L. Maiani, Phys. Lett. **B105** (1981) 155; M. K. Gaillard, L. Hall, I. Hinchliffe, Phys. Lett. **B116**(1982) 279; J. Ellis, J. S. Hagelin, Phys.. Lett. **B122** (1983) 303; D. A. Dicus, S. Nandi, and J. Woodside, Phys. Lett. **B258**(1991) 231.

[7] M. Dine, A. E. Nelson, Phys. Rev. **D48** (1993) 1277; M. Dine, A. E. Nelson, Y. Shirman, Phys. Rev. **D51** (1995) 1362; M. Dine, A. E. Nelson, Y. Nir, Y. Shirman, Phys. Rev. **D53** (1996) 2658.

[8] S. Dimopoulos, M. Dine, S. Raby, S. Thomas, Phys. Rev. Lett. **76** (1996) 3494 .

[9] S. Ambrosanio, G. D. Kribs, and S. P. Martin, hep-ph/9703211

[10] S. Dimopoulos, G. G. Giudice, A. Pomarol, Phys. Lett **B389** (1996) 37-42.

[11] S. P. Martin, hep-ph/9608224.

[12] I. Hinchliffe, F. E. Paige, M. D. Shapiro, J. Soderqvist and W. Yao, Phys. Rev. **D55** (1997) 5520-5540.

[13] T. Tsukamoto, K. Fujii, H. Murayama, M. Yamaguchi, and Y. Okada, Phys. Rev. **D51** (1995) 3153; J. L. Feng, H. Murayama, M. E. Peskin, and X. Tata, Phys. Rev. **D52** (1995) 1418.

IV. EXOTICS WORKING GROUP

U. Baur
SUNY at Buffalo
S. Eno
University of Maryland

A. Introduction

We summarize the reach of the VLHC for contact interactions and new heavy particles in non-supersymmetric extensions of the Standard Model.

The Standard Model (SM) of strong and electroweak interactions, based on the gauge group $SU(3)_C \times SU(2)_L \times U(1)_Y$, has been extremely successful phenomenologically. It has provided the theoretical framework for the description of a very rich phenomenology spanning a wide range of energies, from the atomic scale up to the Z boson mass. However, the SM has a number of shortcomings. In particular, it does not explain the origin of mass, the observed hierarchical pattern of fermion masses, and why there are three generations of quarks and leptons. It is widely believed that at high energies deviations from the SM will appear, signaling the presence of new physics.

Many theoretical models which attempt to overcome the shortcomings of the SM either involve new gauge symmetries, or predict that quarks and leptons are composite objects. A common feature of these models are new interactions and new heavy particles. The mass of these objects is in general given by the energy scale of the new interaction. At low energies, their existence is signalled by four fermion contact interactions. A hadron collider with a center of mass energy of 100 TeV or more (VLHC) would offer an excellent chance to search for contact interactions and also, directly, for the new heavy particles associated with new interactions.

In this brief report, we discuss the potential of the VLHC to search for contact interactions associated with quark and lepton compositeness, and illustrate the discovery mass reach for new heavy states by describing the search for excited quarks [1] in some detail. In addition, we list benchmark results for additional gauge bosons [2] and leptoquarks [3], which are predicted by many grand unified models. We also briefly comment on the discovery mass reach for colorons [4] and axigluons [5] which appear in models with extended strong interaction gauge symmetries. Supersymmetric and technicolor particle searches at the VLHC are described in Refs. [6] and [7] and are therefore not discussed here.

B. Contact Interactions

The repetition of the three generations of quarks and leptons suggests that they are bound states of more fundamental fermions, and perhaps bosons, bound together by a new interaction which is characterized by an energy scale Λ^+. At energies much smaller than Λ^+, the substructure of quarks and leptons is signalled by the appearance of four fermion contact interactions which arise from the exchange of bound states of the subconstituents [8]. The lowest order contact terms are dimension 6 four-fermion interactions which can affect jet and Drell-Yan production at a hadron collider. Compared with the SM terms, they are suppressed by a factor $1/\Lambda^{+2}$. The signature for four-quark contact interactions, for example, would be an excess of events at large transverse energy, E_T, similar to that observed by CDF in inclusive jet production at the Tevatron in Run 1a [9].

However, from the CDF measurement of the jet inclusive cross section it is apparent that it is difficult to discover a signal for contact interactions by looking for an excess of events at high transverse energies, due to uncertainties in the parton distribution functions, ambiguities in QCD calculations, and systematic uncertainties in jet energy measurements [10]. Another signal for quark – quark contact interactions, which is not very sensitive to theoretical or jet energy uncertainties, is the dijet angular distribution which is more isotropic than that predicted by QCD if contact terms are present. Both CDF [11] and DØ [12] have found good agreement with the shape predicted by QCD. The DØ dijet angular distribution is shown in Fig. 1. The quantity χ shown here is related to the scattering angle in the center of mass frame, θ^*, by $\chi = (1+|\cos\theta^*|)/(1-|\cos\theta^*|)$. Using a model with left-handed contact interactions, DØ sets a preliminary 95% confidence level (CL) limit on the interaction scale, Λ^+, of $\Lambda^+ > 2.0$ TeV [12]. CDF obtains a 95% CL limit of $\Lambda^+ > 1.8$ TeV [11]. From the inclusive jet analysis, the dijet angular distribution and other searches for contact interactions at the Tevatron [13], as well as searches at the CERN $p\bar{p}$ collider [14] and simulations carried out for the LHC [15], we conclude that the compositeness scale reach of a hadron collider is roughly equal to its center of mass energy, $\sqrt{s}$. Detailed simulations for the VLHC, however, have not been carried out so far.

C. Excited Quarks

Conclusive evidence for a new layer of substructure would be provided by the direct observation of excited states of the known quarks and leptons. In the following we shall concentrate on excited quarks with spin 1/2 and weak isospin 1/2. The coupling between excited spin 1/2 quarks, ordinary quarks and gauge bosons is uniquely fixed to be of magnetic moment type by gauge invariance. Excited quarks decay into quarks and a gluon, photon or a W/Z boson, or, via contact interactions into $\bar{q}qq'$ final states [16]. Subsequently, only decays via gauge interactions are considered. Excited quarks are then expected to decay predominantly via strong interactions; radiative decays and decays into a quark and a W/Z boson will typically appear at $\mathcal{O}(\alpha/\alpha_s)$, *i.e.* at the few per cent level [17].

In hadronic collisions, excited quarks can be produced singly via quark gluon fusion. The subsequent $q^* \to qg$ decay leads to a peak in the two jet invariant mass distribution located at $m(jj) = M^*$, where M^* is the excited quark mass. UA2 [18], CDF [19, 20] and DØ [21] have searched for q^* production in the dijet invariant mass distribution. Figure 2 shows the region of the excited quark coupling $f = f' = f_s$ versus M^* plane excluded by those experiments. Here, f, f' and f_s are the strength of the $SU(2)_L, U(1)_Y$ and $SU(3)_C$ couplings of the q^* to quarks and the SM gauge fields when the scale of the magnetic moment coupling is set equal to M^*. For $f = f' = f_s = 1$,

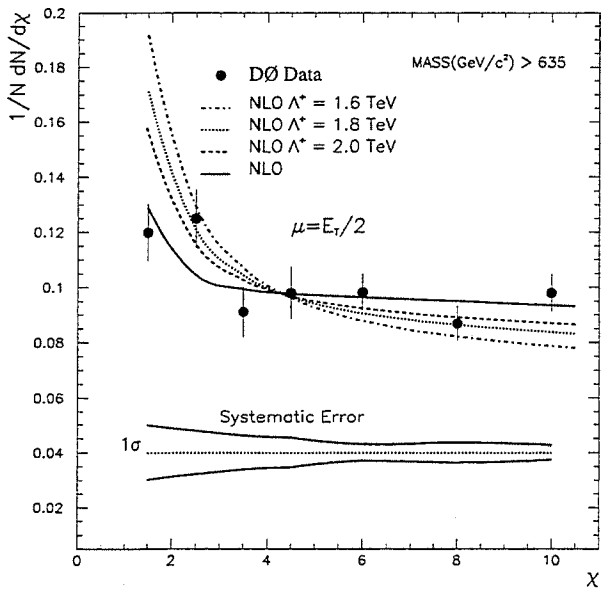

Figure 1: The DØ dijet angular distribution (points) for dijet masses larger than 635 GeV compared to predictions of NLO QCD (solid line), and NLO QCD with a quark contact interaction for various values of Λ^+.

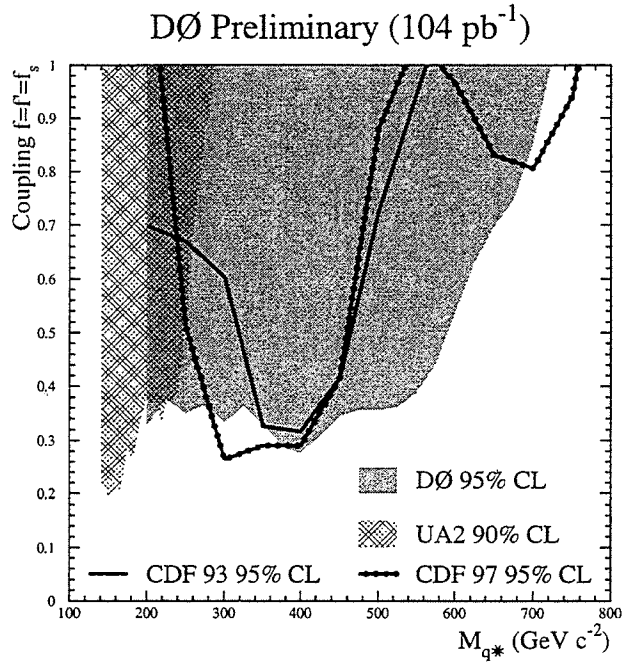

Figure 2: The region of the excited quark coupling versus mass plane excluded by UA2, CDF and DØ measurements.

CDF sets a lower 95% CL limit of $M^* > 760$ GeV (with the exception of the region 570 GeV $< M^* <$ 580 GeV), whereas DØ finds a (preliminary) bound of $M^* > 725$ GeV (95% CL). Only first generation excited quarks, u^* and d^*, are considered. The u^* and d^* are assumed to be degenerate in mass.

The discovery reach of the VLHC in this model has been studied in Ref. [1], assuming a Gaussian dijet invariant mass resolution of $\sigma = 0.1\, m(jj)$, which is similar to that of the CDF detector. Since $\Gamma(q^*) \approx 0.04\, M^*$ in the model considered, approximately 90% of the two jet events from an excited quark will be in the mass window $0.84\, M^* < m(jj) < 1.16\, M^*$. To estimate the mass reach, the differential cross section is integrated within this window for both the q^* signal and the QCD background. The QCD background rate is then used to find the $5\,\sigma$ discovery cross section. This is defined as the cross section which is above the background by $5\,\sigma$, where σ is the statistical error on the measured cross section.

The discovery mass reach for excited quarks at the VLHC is shown in Fig. 3 for three different machine energies as a function of the integrated luminosity. For an integrated luminosity of 10^4 fb^{-1}, the mass reach at a pp collider with center of mass energy of 50 TeV (200 TeV) is $M^* = 25$ TeV (78 TeV). However, an excited quark with a mass of 25 TeV would be discovered at a pp collider with $\sqrt{s} = 100$ TeV with only 13 fb^{-1}. In this case, doubling the collider energy is equivalent to an increase in integrated luminosity of almost a factor 1000. A similar result is obtained from other heavy particle searches.

D. Additional Vector Bosons and Leptoquarks

The discovery of new gauge bosons, W', Z', would signal an extension of the SM gauge group by an additional factor such as $U(1)$ or $SU(2)$. Z' bosons appear in most Grand Unified Theories. W' bosons are typical for models which restore the left-right symmetry at high energies. The mass reach of a hadron collider for new gauge bosons is model dependent due to the variations in their couplings to quarks and leptons. At hadron colliders, new gauge bosons can be produced directly via quark – antiquark annihilation, $q\bar{q}' \to W'$ and $q\bar{q} \to Z'$. CDF [22] and DØ [23] have searched for W' (including righthanded W bosons) and Z' bosons in a variety of models. The limits obtained vary between 565 GeV and 720 GeV. The discovery reach of the VLHC for new gauge bosons has been investigated in Ref. [2]. Only the leptonic decays of the W' and Z' bosons, which are virtually background free, were used in this analysis. At a 200 TeV pp collider, with an integrated luminosity of 1000 fb^{-1}, Z' bosons with mass up to $M_{Z'} = 40 - 50$ TeV can be detected [2], whereas the mass reach for W' bosons is 50 – 60 TeV, depending on the details of the model considered.

Many Grand Unified Theories predict the existence of leptoquarks, LQ, which are spin 0 (scalar) or spin 1 (vector) color triplet objects coupling to a quark – lepton pair. Searches for leptoquarks have been performed at LEP [24], HERA [25] and the Tevatron [26]. The most stringent bounds presently come from Tevatron data which exclude, at 95% CL, scalar (vector) first generation leptoquarks with $B(LQ \to eq) = \beta = 0.5$ if their mass is $M_{LQ} < 192$ GeV (270 GeV) [27]. Leptoquarks can be produced either singly or in pairs at a hadron collider. The cross

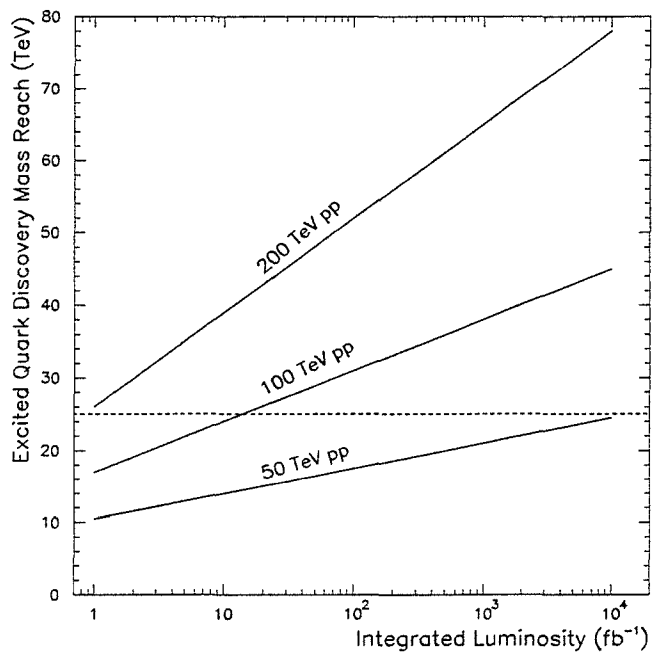

Figure 3: The $5\,\sigma$ discovery mass reach for $pp \to q^* \to jj$ is shown as a function of the integrated luminosity for a VLHC with center of mass energy of 50 TeV, 100 TeV and 200 TeV (solid lines). The horizontal dashed line illustrates what integrated luminosity is necessary to discover an excited quark with mass $M^* = 25$ TeV.

section for single production depends on unknown Yukawa couplings of the leptoquark. Pair production, on the other hand, proceeds via QCD interactions, and therefore depends only on the leptoquark spin. Unless the Yukawa couplings are large, pair production dominates. The discovery reach of the VLHC for leptoquarks has been studied in Ref. [3]. At a proton – proton collider with $\sqrt{s} = 200$ TeV and an integrated luminosity of 1000 fb^{-1}, one should be able to detect scalar (vector) leptoquarks with a mass up to $M_{LQ} \approx 14$ TeV ($M_{LQ} \approx 23$ TeV), if $\beta = 0.5$. For $\beta = 1$, the mass reach is higher by about 1 TeV.

If leptoquarks are sufficiently light, the VLHC will make it possible to probe the Yukawa couplings of leptoquarks. At a 100 TeV proton – proton collider, Yukawa couplings as small as $\lambda/e = 10^{-3}$ ($\lambda/e = 10^{-5}$) [e is the electric charge unit] can be probed for $M_{LQ} = 2$ TeV ($M_{LQ} = 1$ TeV) [28].

At a $p\bar{p}$ collider, the search limits for new gauge bosons and leptoquarks are both about 20 – 30% higher than those found for pp collisions with the same center of mass energy [2, 3].

E. Colorons and Axigluons

In the coloron [4] model, the symmetry group of the strong interactions, $SU(3)_C$, is replaced by a $SU(3)_1 \times SU(3)_2$ group, which is spontaneously broken to $SU(3)_C$ at an unknown scale v. The corresponding color octet of massive gauge bosons (colorons) couples vector-like to quarks. In the axigluon [5] model, the gauge group is $SU(3)_L \times SU(3)_R$, and the coupling of the massive color octet vector bosons (axigluons) to quarks is axial vector-like. Colorons and axigluons can be produced via $q\bar{q}$ annihilation, and lead to a peak in the two jet invariant mass distribution, very much like an excited quark. CDF has searched for these particles in the dijet channel, and places a lower limit of 980 GeV (95% CL) on their mass [19]. The discovery reach of the VLHC for these particles has not been estimated yet. It is expected that colorons and axigluons in the multi-ten TeV range can be discovered at a 200 TeV pp collider.

F. Conclusions

In this brief report, we have discussed the search for contact interactions and new heavy particles, which appear in popular non-supersymmetric extensions of the SM, at the VLHC. The search potential of the VLHC for these new states is truly enormous; for a collider with a center of mass energy of 100 TeV or more, the limits are in general in the multi-ten TeV region. To maximize the heavy particle search potential, the VLHC should strive to the highest energy possible. It should be emphasized, however, that there are no models which firmly predict the existence of new particles in the region of interest for the VLHC. On the other hand, in a situation where first signs of new physics are observed at the LHC in the form of contact interactions, but the scale of new physics is too high to allow production of the associated new states directly, the VLHC will be a perfect tool for an in-depth investigation of the beyond the Standard Model frontier.

G. Acknowledgments

We would like to thank H. Frisch for stimulating discussions. This research has been supported in part by the National Science Foundation, grant PHY-9600770, and the Department of Energy, grant DEFG0296ER41015.

REFERENCES

[1] R. Harris, FERMILAB-Conf-96-285-E, Proceedings of the Workshop *"New Directions in High Energy Physics"*, Snowmass, CO, June 25 – July 12, 1996, p. 1010.

[2] T. Rizzo, SLAC-PUB-7279, Proceedings of the Workshop *"New Directions in High Energy Physics"*, Snowmass, CO, June 25 – July 12, 1996, p. 900.

[3] T. Rizzo, SLAC-PUB-7284, Proceedings of the Workshop *"New Directions in High Energy Physics"*, Snowmass, CO, June 25 – July 12, 1996, p. 953.

[4] E. Simmons, Phys. Rev. **D55**, 1678 (1997).

[5] P. Frampton and S. Glashow, Phys. Lett. **B190**, 157 (1987); J. Bagger, C. Schmidt, and S. King, Phys. Rev. **D37**, 1188 (1988).

[6] G. Anderson, these proceedings.

[7] E. Simmons and J. Womersley, these proceedings.

[8] E. Eichten, K. Lane, and M. Peskin, Phys. Rev. Lett. **50**, 811 (1980).

[9] F. Abe *et al.* (CDF Collaboration), Phys. Rev. Lett. **77**, 438 (1996).

[10] J. Huston *et al.*, Phys. Rev. Lett. **77**, 444 (1996).

[11] F. Abe *et al.* (CDF Collaboration), Phys. Rev. Lett. **77**, 5336 (1996).

[12] M. Bhattacharjee (DØ Collaboration), talk given at the *"Hadron Collider Physics XII"* Conference, Stony Brook, NY, June 5 – 11, 1997.

[13] F. Abe *et al.* (CDF Collaboration), FERMILAB-Pub-97-171-E, submitted to Phys. Rev. Letters.

[14] J. Alitti *et al.* (UA2 Collaboration), Phys. Lett. **B257**, 232 (1991).

[15] I. Hinchliffe and J. Womersley, FERMILAB-Conf-96-432, Proceedings of the Workshop *"New Directions in High Energy Physics"*, Snowmass, CO, June 25 – July 12, 1996, p. 101.

[16] U. Baur, M. Spira and P. Zerwas, Phys. Rev. **D42**, 815 (1990).

[17] U. Baur, I. Hinchliffe and D. Zeppenfeld, Int. J. of Mod. Phys. **A2**, 1285 (1987).

[18] J. Alitti *et al.* (UA2 Collaboration), Nucl. Phys. **B400**, 3 (1993).

[19] F. Abe *et al.* (CDF Collaboration), Phys. Rev. **D55**, R5623 (1997).

[20] F. Abe *et al.* (CDF Collaboration), Phys. Rev. Lett. **74**, 3538 (1995).

[21] L. Sawyer (DØ Collaboration), talk given at the *"Hadron Collider Physics XII"* Conference, Stony Brook, NY, June 5 – 11, 1997.

[22] F. Abe *et al.* (CDF Collaboration), Phys. Rev. Lett. **74**, 2900 (1995) and FERMILAB-Pub-97-122-E, submitted to Phys. Rev. Letters.

[23] S. Abachi *et al.*, (DØ Collaboration), Phys. Lett. **B358**, 405 (1995); Phys. Rev. Lett. **76**, 3271 (1996), and Phys. Lett. **B385**, 471 (1996); C. Gerber (DØ Collaboration), Proceedings of the *"DPF96"*, Minneapolis, MN, August 1996.

[24] P. Mättig, CERN-PPE/96-187 (December 1996), to appear in the Proceedings of the *"28th International Conference on High Energy Physics"*, Warsaw, July 1996.

[25] S. Aid *et al.* (H1 Collaboration), Phys. Lett. **B369**, 173 (1996).

[26] F. Abe *et al.* (CDF Collaboration), Phys. Rev. Lett. **75**, 1012 (1995); S. Abachi *et al.* (DØ Collaboration), Phys. Rev. Lett. **75**, 3618 (1995).

[27] D. Norman (DØ Collaboration), FERMILAB-Conf-97-224-E, to appear in the Proceedings of the *"Hadron Collider Physics XII"* Conference, Stony Brook, NY, June 5 – 11, 1997; H. Kambara (CDF Collaboration), talk given the *"Hadron Collider Physics XII"* Conference, Stony Brook, NY, June 5 – 11, 1997.

[28] T. Rizzo, talk given at the *"VLHC Workshop"*, Fermilab, March 1997.

V. FULL RAPIDITY PHYSICS WORKING GROUP

Andrew Brandt
Fermi National Accelerator Laboratory
Cyrus Taylor
Case Western Reserve University

Members of the working group include: M. Albrow, W. Baker, J. Bantley, P. Bloch, A. Brandt, K. Goulianos, P. Hanlet, T. Heuring, C. Lundstedt, H. de Motta, F. Paige, D. Rainwater, V. Simak, A. Santoro, G. Snow, C. Taylor, and L. Voyvodic.

Particle production at a VLHC operating at $\sqrt{s} = 100$ TeV will span some 24 units of rapidity. Such an accelerator should include a detector and interaction region optimized for full acceptance[1]. Design goals for such a detector should include:

- all charged particles, photons and neutrons of generic p_t should be observed and their energies/momenta well measured over all of phase space
- diffractive and elastically scattered protons should be well measured
- muon identification should be extended into the far forward regions
- the physics of rapidity gaps should not be compromised

While no full acceptance detector has ever operated at collider energies, such a detector, FELIX, is being proposed for the LHC[2]. The lessons learned in the design and operation of FELIX will provide the basis for a full acceptance detector at the VLHC.

The need for a full acceptance detector at the VLHC follows from basic kinematics. Physics on the energy frontier is necessarily central and will largely be the domain of optimized central detectors, conversely, any physics not on the energy frontier is forward physics, and will benefit from a full acceptance detector.

A second point is that a full acceptance detector should operate in an environment of $\sim$ 1 interaction per beam crossing. This ensures that global event structure can be determined, event by event. In contrast, central detectors operating on the energy frontier will also be operating on the luminosity frontier, with many collisions per beam crossing. This observation also has a corollary: any precision physics or standard physics will likely be done well by a full acceptance detector.

Finally, one should state the obvious: a central detector, optimized for high-p_t physics at the energy frontier in messy environments will only be sensitive to a small fraction of the kinematically allowed phase space. The discovery potential of a full acceptance detector operating in unexplored regions of phase space should thus be noted.

A few examples illustrate the scope of a full acceptance detector at the VLHC.

A. The small-x frontier

Hard processes at the VLHC span a kinematically allowed region in (x, Q^2) given by

$$x_1 x_2 \geq \frac{4E_t^2}{s}, Q^2 \geq E_{tmin}^2 \tag{9}$$

where x_1, x_2 are the momentum fractions of the two partons involved in the hard scattering, and E_{tmin} is the minimum transverse energy needed to identify the process. Thus, at $\sqrt{s} = 100$ TeV, for scattering to two jets with $E_{tmin} \sim 10$ GeV, one can probe the proton structure down to $x \sim 4 * 10^{-8}$. This is some 4 orders of magnitude smaller than the HERA limit, and will be an extremely interesting domain of QCD[3].

B. Forward particle tags

Particle production in the fragmentation region has never been studied at collider energies. A full acceptance detector, with complete coverage for neutral particles down to zero degrees, and with complete charged particle tracking, will not only measure such production exquisitely, it will also be able to tag leading particles. For example, detecting leading deltas or neutrons tags the rest of the event as a collision between a beam nucleon with the exchanged non-strange meson. The VLHC thus becomes an effective meson-proton collider. One can similarly tag on both sides, defining meson-meson interactions, tag on strange meson exchange, and so on. Aside from the rich physics program that this capability will allow, it is also necessary for total cross section measurements which are crucial for determining the cross sections for all physics processes.

C. Rapidity gap phenomena

While perturbative QCD has been extremely successful at describing and predicting many aspects of the strong interactions, many fundamental processes cannot yet be calculated in this language. Processes such as elastic and diffractive scattering are instead still understood in terms of Regge theory, with elusive objects like the "Pomeron" playing a central role in current phenomenology. The study of such processes, in particular hard diffractive processes, has expanded dramatically in recent years[4], with pioneering work at UA8, followed by important ongoing studies at HERA and the Tevatron. It should be noted that all of these current or past experiments would have benefited tremendously from increased coverage. A full acceptance detector at the VLHC will be able to do all of this physics superbly, allowing a continuous transition from the clearly perturbative regime into the non-perturbative regime in a controlled manner.

D. Cosmic ray phenomena

All experimental information about particle interactions at the highest energies comes from cosmic ray experiments. LHC energies correspond to primary cosmic rays of about 100 PeV (10^{17} eV); particles with energies of 10^{20} eV have been observed. While fraught with problems of limited statistics and complicated systematics, cosmic ray experimentalists can point

with pride to a number of important discoveries, including a prediscovery of charm. It is thus important to take note of the fact that there are a number of anomalies reported in studies of cosmic ray interactions hinting at unusual physics, not anticipated in the standard model. These anomalies are observed at energies beyond the reach of current accelerators. Further, since cosmic ray experiments track energy flow, their sensitivity is typically in the fragmentation region, beyond the reach of current (central) collider detectors. A full acceptance detector should be designed keeping these anomalies in mind. The list of anomalies includes reports of anomalous mean free paths, anomalous forward heavy flavor production, anomalous attenuation of secondary hadrons, anomalies in the energy fraction of air showers, scaling anomalies, anomalies in the charged to neutral ratio (Centauros and anti-Centauros), and anomalously parallel multi-muon bundles. Only detectors with good acceptance in the very forward direction can test these claims in an accelerator environment.

E. Summary

The task of designing a full acceptance detector for the VLHC is non-trivial, and requires careful coordination with the design of the machine itself. The starting point is necessarily the magnetic architecture, which must be integrated into the machine lattice. The design of FELIX, a possible full acceptance detector for the LHC, should serve as a prototype for discussing the design of a full rapidity detector at the VLHC.

Important features of the FELIX design which may translate to the VLHC include:

1. The relatively low luminosity should permit an insertion in which focusing quadrupoles are located a large distance from the collision point. In FELIX, this distance is more than 100 m.

2. The requirement of complete calorimetric coverage for neutrals demands a precision zero degree calorimeter. This requires that the beams be separated by a significant transverse distance (in FELIX, 42 cm) at the location of the zero degree calorimeter. The beam separation is defined in FELIX by the requirement that the experiment co-habit with the RF cavities, located 140 m from the beam.

3. The dipole fields needed to move the beams through the experimental area within the above constraints will play a dual role as spectrometer analysis magnets and consequently should have the largest possible aperture.

4. While the central region is not the focus of the proposed experiment, it should nevertheless have a good central detector. Such a detector might be built around elements of the preceeding generation of collider detectors. It need not be of the quality of the high p_t central VLHC detector, but should also not be neglected.

Although it is premature to begin detailed work on possible optics for an insertion at the VLHC, the need for a long straight section is clear and should be built into any VLHC design at the earliest stage. Simple scaling with the beam energy (which seems reasonable given constants such as transverse shower sizes in calorimeters) would suggest that the zero degree calorimeter should be located at least 700 m from the collision point. The required beam separation at this point would imply that a straight section with a total length of 2.8–4 km seems appropriate.

A full acceptance detector will provide a powerful tool for the study of physics at the VLHC. While low in cost compared to detectors concentrating on physics at the energy frontier in the central region, a full acceptance detector will combine a strong program of physics complementary to other detectors with a substantial discovery potential, particularly for the "unexpected".

REFERENCES

[1] L. Jones, M. Albrow, H. R. Gustafson and C. Taylor, "Forward Physics with the Pipetron", Proceedings of the DPF/DPB Summer Study on New Directions for High-Energy Physics, Snowmass, CO, 1996, p. 291.

[2] K. Eggert and C. Taylor, "FELIX, a full acceptance detector for the CERN LHC", to be published in the Proceedings of the VIIth International Symposium of Very High Energy Cosmic Ray Interactions, Karlsruhe, 1996. Also see the FELIX web pages, http://www.cern.ch/FELIX

[3] "FELIX Potential for small-x Parton Measurements in proton-proton (-nucleus) Collisions", L. Alvaro, M. Strikman and J. Whitmore, FELIX Working paper, http://www.cern.ch/FELIX/Physics/paperi.html

[4] M. Albrow, et al., "QCD Subgroup on Diffractive and Forward Physics", Proceedings of the DPF/DPB Summer Study on New Directions for High-Energy Physics, Snowmass, CO, 1996, p. 1109.

VI. PRECISION MEASUREMENTS OF HEAVY OBJECTS WORKING GROUP

Frederick Olness
Southern Methodist University
Randall Scalise
Southern Methodist University

A. Introduction

We report on the activities of the Precision Measurements of Heavy Objects working group. The following people contributed to the writing of this summary: Marcel Demarteau, Vassilis Koulovassilopoulos, Joseph Lykken, Stephen Parke(convener during the workshop), Erich Varnes, G. P. Yeh (convener during the workshop).

The topics discussed by the Precision Measurements of Heavy Objects working group spanned a very wide range; consequently, it is impossible to cover each topic in depth. Therefore, in this report we will primarily focus on the issues most relevant to a VLHC machine. In the following, we mention only the highlights, and refer the reader to the literature for more specific questions.

B. Parton Distributions for VLHC

Global QCD analysis of lepton-hadron and hadron-hadron processes has made steady progress in testing the consistency of perturbative QCD (pQCD) within many different sets of data, and in yielding increasingly detailed information on the universal parton distributions.[5]

We present the kinematic ranges covered by selected facilities relevant for the determination of the universal parton distributions. While we would of course like to probe the full $\{x, Q\}$ space, the small x region is of special interest. For example, the rapid rise of the F_2 structure function observed at HERA suggests that we may reach the parton density saturation region more quickly than anticipated. Additionally, the small x region can serve as a useful testing ground for BFKL, diffractive phenomena, and similar processes. Conversely, the production of new and exotic phenomena generally happens in the region of relatively high x and Q.

This compilation provides a useful guide to the planning of future experiments and to the design of strategies for global analyses. Another presentation regarding future and near-future machines is given in the 1996 Snowmass Structure Functions Working Group report [1].

Here we will simply mention a few features which are particularly relevant for such a very high energy facility as a VLHC.

As we see in Fig. 4, the VLHC will probe an $\{x, Q\}$ region far beyond the range of present data. To accurately calculate processes at a VLHC, we must have precise PDF's in this complete kinematic range. Determining the PDF's in the small x regime is a serious problem since there will be no other measurement in the extreme kinematic domain required by VLHC. For the large

[5]PDF sets are available via WWW on the CTEQ page at http://www.phys.psu.edu/~cteq/ and on the The Durham/RAL HEP Database at http://durpdg.dur.ac.uk/HEPDATA/HEPDATA.html.

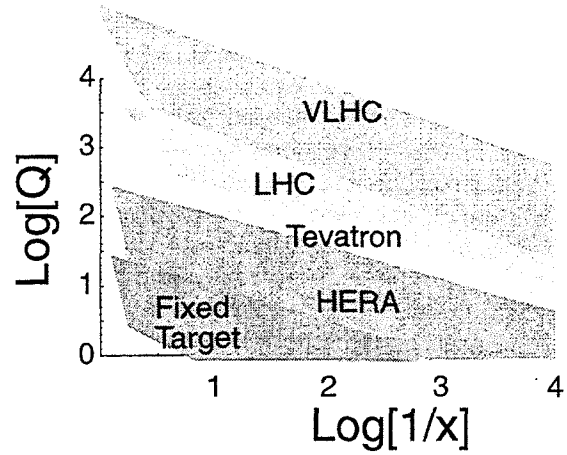

Figure 4: Kinematic range of various machines. Note the small x range is clipped in this plot. The Q scale is in GeV and the logs are base 10.

x and Q region, the PDF's at large Q can, in principle, be determined via the standard QCD DGLAP evolution, but in practice uncertainties from the small x region can contaminate this region.

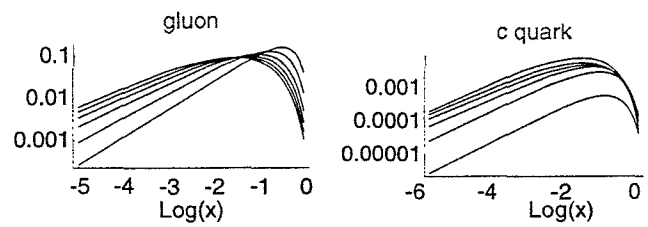

Figure 5: Evolution of the a) gluon and b) charm PDF's in Q *vs.* x. We display $x^2 f_{i/P}(x, Q)$ for $Q = \{2, 10^1, 10^2, 10^3, 10^4, 10^5\}$ GeV.

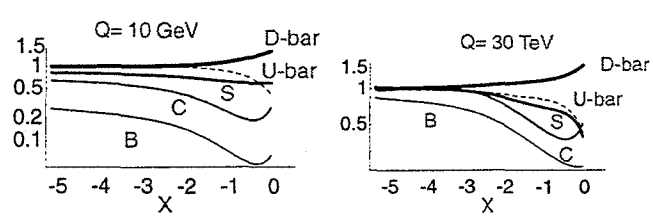

Figure 6: Flavor democracy at a) 10 GeV and b) 30 TeV. We compare the individual parton distributions $f_{i/P}(x, Q)$ to that of the average sea, $(\bar{u} + \bar{d})/2$.

In Fig. 5, we display the evolution of the PDF's for a selection of partons. For the gluon and the valence quarks, we see a decrease at high x and an increase at low x with $x \sim 0.1$ as the crossing point. In contrast, for the heavy quark PDF's, we see

generally an increase with increasing Q. The momentum fraction of the partons *vs.* energy scale is shown in Table III. An interesting feature to note here is the approximate "flavor democracy" at large energy scales; that is, as we probe the proton at very high energies, the influence of the quark masses becomes smaller, and all the partonic degrees of freedom carry comparable momentum fractions. To be more precise, we see that at the very highest energy scales relevant for the VLHC, the strange and charm quark are on par with the up and down sea, (while the bottom quark lags behind a bit). This feature is also displayed in Fig. 6 where we show these contributions for two separate scales. In light of this observation, we must dispense with preconceived notions of what are "traditionally" heavy and light quarks, and be prepared to deal with all quark on an equal footing at a VLHC facility. This approach is discussed in the following section.

Table III: Momentum fraction (in percent) carried by separate partons as a function of the energy scale Q.

Q	g	$\bar{u}$	$\bar{d}$	s	c	b
3 GeV	46	5	7	3	1	0
10 GeV	48	6	8	4	2	0
30 GeV	48	6	8	5	3	1
100 GeV	48	7	8	5	3	2
300 GeV	49	7	8	6	4	2
1 TeV	49	7	8	6	4	3
3 TeV	49	7	8	6	4	3
10 TeV	50	7	9	6	5	4
30 TeV	50	7	9	7	6	4
100 TeV	51	7	10	7	7	4

C. Heavy Quark Hadroproduction

Improved experimental measurements of heavy quark hadroproduction has increased the demand on the theoretical community for more precise predictions [2, 3, 4, 5, 6]. The first Next-to-Leading-Order (NLO) calculations of charm and bottom hadroproduction cross sections were performed some years ago [3]. As the accuracy of the data increased, the theoretical predictions displayed some shortcomings: 1) the theoretical cross-sections fell well short of the measured values, and 2) they displayed a strong dependence on the unphysical renormalization scale μ. Both these difficulties indicated that these predictions were missing important physics.

These deficiencies can, in part, be traced to large contributions generated by logarithms associated with the heavy quark mass scale, such as[6] $\ln(s/m_Q^2)$ and $\ln(p_T^2/m_Q^2)$. Pushing the calculation to one more order, formidable as it is, would not necessarily improve the situation since these large logarithms persist to every order of perturbation theory. Therefore, a new approach was required to include these logs.

[6]Here, m_Q is the heavy quark mass, s is the energy squared, and p_T is the transverse momentum.

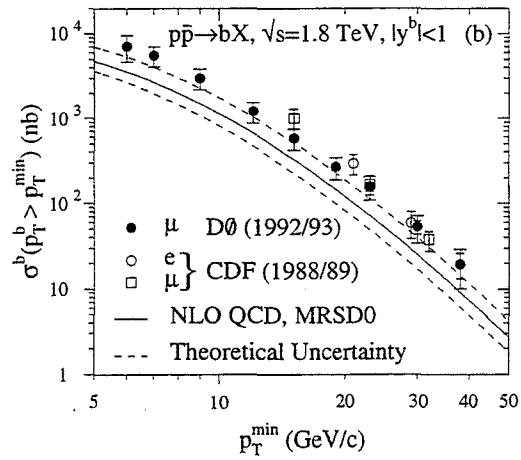

Figure 7: Heavy quark hadroproduction data. *Cf.*, Ref. [2].

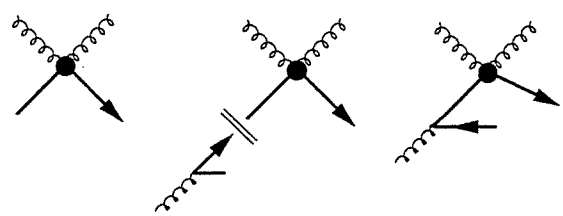

Figure 8: a) Generic leading-order diagram for heavy-flavor excitation (LO-HE), $gQ \to gQ$. b) Subtraction diagram for heavy-flavor excitation (SUB-HE), ${}^1f_{g\to Q} \otimes \sigma(gQ \to gQ)$. c) Next-to-leading-order diagram for heavy-flavor creation (NLO-FC).

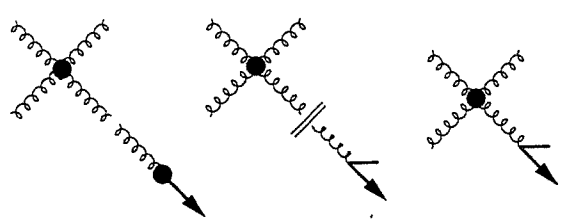

Figure 9: a) Generic leading-order diagram for heavy-flavor fragmentation (LO-HF), $\sigma(gg \to gg) \otimes D_{g\to Q}$. b) Subtraction diagram for heavy-flavor fragmentation (SUB-HF), $\sigma(gg \to gg) \otimes {}^1d_{g\to Q}$. c) Next-to-leading-order diagram for heavy-flavor creation (NLO-FC).

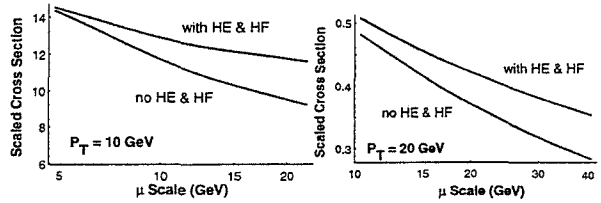

Figure 10: The scaled differential cross section $p_T^5\, d^2\sigma/dp_T^2/dy$ at $p_T = 10, 20\,\mathrm{GeV}$ and $y = 0$ in $(pb - \mathrm{GeV}^3)$ *vs.* μ. The lower curves are the heavy quark production cross sections *ignoring* heavy-flavor excitation (HE) and heavy-flavor fragmentation (HF). The upper curves are the heavy quark production cross sections *including* HE and HF. *Cf.*, Ref. [6].

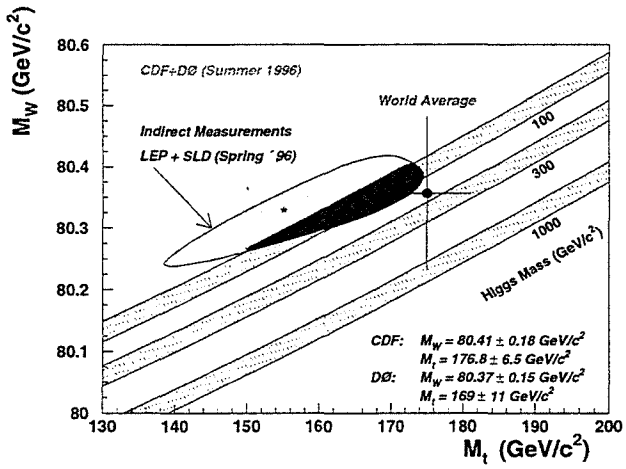

Figure 11: Plot of M_W *vs.* M_t with DØ and CDF preliminary measurements of the W boson and top quark masses. Bands indicate the Standard Model constraints for different Higgs mass values. Indirect measurements from LEP I are also shown. (June, 1997) Taken from Ref. [9].

In 1994, Cacciari and Greco[5] observed that since the heavy quark mass played a limited dynamical role in the high p_t region, one could instead use the massless NLO jet calculation convoluted with a fragmentation into a massive heavy quark pair to compute more accurately the production cross section in the region $p_t \gg m_Q$. In particular, they find that the dependence on the renormalization scale is significantly reduced.

A recent study[6] investigated using initial-state heavy quark PDF's and final-state fragmentation functions to resum the large logarithms of the quark mass. The principle ingredient was to include the leading-order heavy-flavor excitation (LO-HE) graph (Fig. 8) and the leading-order heavy-flavor fragmentation (LO-HF) graph (Fig. 9) in the traditional NLO heavy quark calculation [3]. These contributions can not be added naively to the $\mathcal{O}(\alpha_s^3)$ calculation as they would double-count contributions already included in the NLO terms; therefore, a subtraction term must be included to eliminate the region of phase space where these two contributions overlap. This subtraction term plays the dual role of eliminating the large unphysical collinear logs in the high energy region, and minimizing the renormalization scale dependence in the threshold region. The complete calculation including the contribution of the heavy quark PDF's and fragmentation functions 1) increases the theoretical prediction, thus moving it closer to the experimental data, and 2) reduces the μ-dependence of the full calculation, thus improving the predictive power of the theory. (Cf., Fig 10.)

In summary, the wealth of data on heavy quark hadroproduction will allow for precise tests of many different aspects of the theory, namely radiative corrections, resummation of logs, and multi-scale problems. Resummation of the large logs associated with the mass is an essential step necessary to bring theory in agreement with current experiments and to make predictions for the VLHC.

D. W Mass Studies

The W boson mass is one of the fundamental parameters of the standard model; its precision measurement can be used in conjunction with the top mass to extract information on the Higgs boson mass. The W boson mass has already been measured precisely, and the current world average is: $M_W = 80.356 \pm 0.125\,\mathrm{GeV}/c^2$.

Here, we focus on issues which are unique to a VLHC facility, and refer the reader to the literature for details regarding other topics [7, 8, 9, 10]. The question addressed in the working group session was to consider the expected precision for M_W at the VLHC in comparison to what will be available from competing facilities at VLHC turn-on. For our estimates, we use $\sqrt{s} = 100$ TeV, $\Delta t = 16.7$ ns (the bunch spacing), $\sigma_{tot} \simeq 120$ mb, and 20 interactions per crossing.

For W events produced in a hadron collider environment there are essentially only two observables that can be measured: *i)* the lepton momentum, and *ii)* the transverse momentum of the recoil system. The transverse momentum of the neutrino must be inferred from these two observables. The W boson mass can be extracted from either the lepton transverse momentum distribution, or the transverse mass: $M_T = \sqrt{2p_T^e p_T^\nu(1 - \cos\phi^{e\nu})}$, where $\phi^{e\nu}$ is the angle between the electron and neutrino in the transverse plane.

It is important to note that the following estimates necessitate a large extrapolation from $\sqrt{s} = 1.8$ TeV to $\sqrt{s} = 100$ TeV. For the W decays, the observed number distribution in pseudorapidity (η) can be estimated by scaling results from the CERN $Sp\bar{p}S$ and the Fermilab Tevatron. The shoulder of the pseudorapidity plateau is ~ 3 for $\sqrt{s} = 630\,\mathrm{GeV}$, and ~ 4 for $\sqrt{s} = 1.8$ TeV. This yields an estimate in the range of ~ 5 to 9 for a $\sqrt{s} = 100$ TeV VLHC. Assuming coverage out to $|\eta| \leq 4$, we obtain $\sim$ 1400 charged tracks in the detector calorimeter with which we must contend for the missing E_T calculation, ($\not{E}$). Scaling the $\langle p_T \rangle$ up to $\sqrt{s} = 100$ TeV we estimate $\langle p_T \rangle \simeq 865\,MeV$ for minimum bias tracks. Assuming $N_{ch}/N_\gamma = 1$ yields an average E_T flow of 2 TeV in the detector. Using current $\not{E}_T$ resolutions of $\sim 4 - 5$ GeV, we estimate $\sigma(\not{E}_T) \simeq 25 - 30$ GeV for VLHC.

Two fundamental problems we encounter at a VLHC are mul-

tiple interactions and pile-up. Multiple interactions are produced in the same crossing as the event triggered on. The effects are "instantaneous;" *i.e.*, the electronic signals are added to the trigger signals and subjected to the same electronics. Pile-up effects are out-of-time signals from interactions in past and future buckets caused by "memory" of the electronics. Both cause a bias and affect the resolution, but in different ways. The effect of pile-up is strongly dependent on the electronics used in relation to the bunch spacing.

The bottom line is the estimation of the total uncertainty on the W mass, δM_W. For a luminosity of 2 fb^{-1}, δM_W is about 20 MeV for both the transverse mass and lepton transverse momentum fits. For an increased luminosity of $10 fb^{-1}$, the transverse mass fit might improve to $\delta M_W \sim 15\, MeV$, with minimal improvement for the determination from the lepton transverse momentum distribution. It should be noted that these estimates have quite a few caveats—additional study would be required before taking these numbers as guaranteed predictions. In Table IV, we compare these estimations with the anticipated uncertainty from upcoming experiments. Clearly the VLHC will not greatly improve the determination of M_W. The situation becomes more difficult when one insists that the VLHC detectors be capable of *precisely* measuring the relatively low energy leptons from the M_W decay.

Table IV: Anticipated limits on δM_W from present and future facilities. (This compilation is taken from Ref. [9].)

FACILITY	δM_W (MeV/c^2)	$\mathcal{L}$
NuTeV	~ 100	—
HERA	~ 60	$1000\, pb^{-1}$
LEP2	$\sim$ 35-45	$500\, pb^{-1}$
Tevatron	~ 55	$1\, fb^{-1}$
Tevatron	~ 18	$10\, fb^{-1}$
LHC	$\lesssim 15$	$10\, fb^{-1}$
VLHC	~ 20	$1\, fb^{-1}$
VLHC	~ 15	$10\, fb^{-1}$

E. The Top Quark

The mass of the recently discovered top quark is determined by the CDF and DØ collaborations from $t\bar{t}$ production at the Tevatron. For the details of this discovery and measurement, we refer the reader to Refs. [11, 12, 13, 14].

In Table V, we display the anticipated accuracy on the top quark mass at the Tevatron as estimated in the TeV2000 report [15]. Since this report, statistical techniques have been improved such that one would expect a precision of $\delta m_t \sim 1.5$ GeV with 10 fb^{-1}, assuming other sources of systematics are negligible.

Moving on to the LHC, the top production cross section is $\sim$ 100 times greater than at TeV2000, so with a luminosity of $\sim 100 fb^{-1}/year$, we expect $\sim$ 1000 more top events after one LHC year. Assuming naively that the errors scale as $1/\sqrt{N}$ (where N is the number of events), we would obtain $\delta m_t \sim 50$ MeV.

The challenges of the VLHC are quite similar to the LHC regarding this measurement. A precision measurement of the top quark mass at this level (or better) places stringent demands on the jet calibration. Even with large control samples of Z + jets and γ + jets, uncertainties due to the ambiguous nature of jet definitions will persist. The large number of multiple interactions at LHC and VLHC complicates this analysis (in a manner similar to that discussed for the W boson mass measurement). Therefore, in order to improve upon existing measurements, the VLHC detectors will need to be extremely well designed and understood.

Table V: Anticipated accuracy on the top quark mass, as estimated by the TeV2000 report.

Source	$70\, pb^{-1}$	$1\, fb^{-1}$	$10\, fb^{-1}$
Statistics	25	6.2	2
Jet Scale	11	2.7	0.9
Backgrounds	4	1	0.3
Total	27.6	6.9	2.2

F. Probing a nonstandard Higgs boson at a VLHC

We have studied the potential of a VLHC to observe a nonstandard Higgs boson (i.e. a spin-0 isospin-0 particle with nonstandard couplings to weak gauge bosons and possibly fermions) and distinguish it from the Standard Model Higgs boson. Results are presented for different options for the energy ($\sqrt{s}$ = 50, 100, 200 TeV) and luminosity ($\mathcal{L} = 10^{33} - 10^{35} cm^{-2} s^{-1}$) and compared to those obtained for the LHC in [16].

Our analysis is based on the gold-plated channel $H \to ZZ \to l^+l^-l^+l^-$ and assumes cuts on the final-state leptons, which are given by $|\eta^l| < 3$, $p_T^l > 0.5 \times 10^{-3}\sqrt{s}$. We studied Higgs masses in the range from 400 to 800 GeV (600-800 GeV for $\sqrt{s} = 200$ TeV), where the lower limit is due to the cuts and the upper limit is theoretically motivated.

The two relevant parameters that encode the deviations from the Standard Model (SM) are ξ and y_t, the $HW^+W^-(HZZ)$ and $Ht\bar{t}$ couplings relative to the SM respectively. We found that a nonstandard Higgs should be detected for practically all values of ξ, y_t and $\mathcal{L}$ in the entire mass range studied, a situation which is not so clear for the LHC, particularly for the larger masses.

A nonstandard Higgs boson can be distinguished from the SM one by a comparison of its width Γ_H and the total cross-section. Due to theoretical uncertainties in the latter, we chose to use as a criterion only the measurement of the width. Following the procedure of [16] we quantified the statistical significance of a deviation from the SM prediction by constructing the probability density function according to which the possible measurements of the SM width are distributed. Postulating that a nonstandard Higgs boson is "distinguishable" if its width differs from the SM value by at least 3σ, we were able to determine the precision

with which the parameter ξ can be measured at the LHC and a VLHC. This is summarized in Table I for the case of $y_t = 1$. We deduce that, for the purpose of precision measurements of the Higgs couplings, a lower energy VLHC with higher luminosity is preferred to that of a higher energy with lower luminosity — a conclusion that is due to the low-mass character of the physics of interest.

Consequently, we find that for Higgs masses in the range from 400 to 800 GeV, the Higgs-Z-Z coupling can be measured to within a few percent at the VLHC, depending on the precise mass and collider parameters.

G. Supersymmetry

Supersymmetry (SUSY) is a dominant framework for formulating physics beyond the standard model in part due to the appealing phenomenological and theoretical features. SUSY is the only possible extension of the spacetime symmetries of particle physics, SUSY easily admits a massless spin-2 (graviton) field into the theory, and SUSY appears to be a fundamental ingredient of superstring theory. Given the large number of excellent recent reviews and reports on SUSY [17, 18, 19], we will focus here on the issues directly related to the VLHC.

One specific question which was addressed in the working group meeting was: Is the VLHC a precision machine for standard weak-scale SUSY with sparticle masses in the range 80 GeV to 1 TeV? Probably not, for the following reasons.

- An order of magnitude increase in sparticle production rates will yield minimal gains, *except* for sparticles in the range $\gtrsim$ 1 TeV.
- Multiple interactions, degraded tracking, calibration, and b-tagging issues complicate reconstruction of the SUSY decay chains.

On the contrary, VLHC looks best if SUSY has some heavy surprises such as $\gtrsim$ 1 TeV squarks, or $\sim$ 10 TeV SUSY messengers.

One example of a plausible SUSY scenario would be heavy first and second generation squarks and sleptons (to suppress FCNC's) with a characteristic mass in the range of $\sim$ 3 TeV [19]. While the gauginos and the third generation squarks and sleptons would be within reach of the LHC, investigation of $\{\widetilde{u}, \widetilde{d}, \widetilde{e}, \widetilde{\nu_e},\}$ and $\{\widetilde{c}, \widetilde{s}, \widetilde{\mu}, \widetilde{\nu_\mu}\}$ in the multi-TeV energy range would require a higher energy facility such as the VLHC.

An estimate of the heavy squark signal over the weak-scale SUSY background and conventional channels (such as $t\bar{t}$) indicates that a VLHC can observe heavy quarks in the $\sim$ 3 TeV mass range; such a heavy squark is difficult to reach at the LHC. One might expect on order of $10^3 - 10^4$ signal events/year. Of course, background rejection is a serious outstanding question, and the efficiently of b-tagging and high p_t lepton detection, for example, are crucial to suppressing the backgrounds.

H. Conclusions

While these individual topics are diverse, there are some common themes we can identify with respect to a VLHC machine. First, a very high energy hadron collider does not appear to be the machine of choice for precision measurements in the energy range $\lesssim$ 500 GeV. The competition from Tevatron, HERA, LEP, and LHC are formidable in this region. To obtain comparable precision, the VLHC is handicapped by numerous factors including multiple interactions, large multiplicity, and large $\not{E}$.

In contrast, the strong suit of the VLHC is clearly its kinematic reach. Should there be unexpected sparticles in the $\gtrsim$ TeV range, the VLHC would prove useful in exploring this range. Of course our intuition as to what might exist in the $\sim$10 TeV regime is not as refined as the $\lesssim$ 1 TeV regime which will be explored in the near-future; however what we discover in this energy range can provide important clues as to where we should search with a VLHC.

REFERENCES

[1] 1996 Snowmass Structure Functions Working Group report, hep-ph/9706470. And references therein.

[2] CDF Collaboration: V. Papadimitriou. FERMILAB-CONF-95-128-E. DØ Collaboration: L. Markosky. FERMILAB-CONF-95-137-E; Kamel A. Bazizi. FERMILAB-CONF-95-238-E.

[3] P. Nason, ETH-PT/88-11. P. Nason, S. Dawson, R. K. Ellis, Nucl. Phys. **B327** (1989) 49 , Err. -ibid. B335 (1990) 260. ibid. **B303** (1988) 607. M. L. Mangano, P. Nason, G. Ridolfi. ibid. **B405** (1993) 507. W. Beenakker, H. Kuijf, W. L. van Neerven, J. Smith, Phys.Rev. **D40** (1989) 54.

[4] J. Collins, W. Tung., Nucl. Phys. **B278** (1986) 934. F. Olness, W.-K. Tung, Nucl. Phys. **B308** (1988) 813. M. Aivazis, F. Olness, W. Tung, Phys. Rev. Lett. 65 (1990) 2339. Phys.Rev. **D50**, 3085 (1994). M. Aivazis, J. Collins, F. Olness, W. Tung, Phys. Rev. **D50**(1994) 3102.

[5] M. Cacciari, M. Greco, Nucl. Phys. **B421**(1994) 530. Z.Phys.**C69** (1996) 459. B. Mele, P. Nason, Phys.Lett.**B245** (1990) 635. Nucl.Phys.**B361**(1991) 626.

[6] F. I. Olness, R. J. Scalise, and W.-K. Tung, SMU-HEP-96/08; J. C. Collins, F. I. Olness, R. J. Scalise, and W.-K. Tung, CTEQ-616 (in preparation).

[7] "Precision Electroweak Measurements," M. Demarteau, DPF, 1996, FERMILAB-Conf-96/354.

[8] "Electroweak Results from the Tevatron," M. Demarteau, Snowmass, 1996, Fermilab-Conf-96/353.

[9] "Precision Electroweak Physics at Future Collider Experiments," U. Baur and M. Demarteau, talk given at 1996 DPF/DPB Summer Study on New Directions for High-energy Physics (Snowmass 96), Snowmass, CO, 25 Jun - 12 Jul 1996, p. 499.

[10] "Future Electroweak Physics at the Fermilab Tevatron," Report of the TEV-2000 Study Group, (D. Amidei *et al.*), FERMILAB-PUB-96-082, Apr 1996.

[11] CDF Collaboration, (F. Abe *et al.*), "Observation of Top Quark Production in $\bar{p}p$ Collisions," Phys. Rev. Lett. **74** (1995) 2626-2631.

[12] DØ Collaboration, (S. Abachi *et al.*), "Observation of the Top Quark," Phys. Rev. Lett. **74** 2632 (1995).

[13] DØ Collaboration, (S. Abachi *et al.*), "Direct Measurement of the Top Quark Mass," hep-ex/9703008.

[14] DØ Collaboration, (B. Abbott *et al.*), "Measurement of the Top Quark Mass Using Dilepton Events," hep-ex/9706014.

[15] D. Amidei and R. Brock, *eds.* Future ElectroWeak Physics at the Fermilab Tevatron: Report of the TeV2000 Study Group. FERMILAB-Pub-96/082.

[16] "The Profile Of A Nonstandard Higgs Boson At The LHC," Dimitris Kominis, Vassilis Koulovassilopoulos, Phys. Rev. **D52** (1995) 2737.

[17] "Introduction to Supersymmetry," J. D. Lykken, Talk given at Theoretical Advanced Study Institute in Elementary Particle Physics (TASI 96): Fields, Strings, and Duality, Boulder, CO, 2-28 Jun 1996, FERMILAB-PUB-96-445-T, hep-th/9612114.

[18] "Report of the Supersymmetry Theory Subgroup," J. Amundson *et al.*, report of the Snowmass Supersymmetry Theory Working Group, Sep 1996, p. 655.

[19] A. Bartl *et al.*, "Supersymmetry at LHC," Presented at 1996 DPF/DPB Summer Study on New Directions for High-Energy Physics (Snowmass 96), Snowmass, CO, 25 Jun - 12 Jul 1996, p. 693.

VII. MULTIPLE INTERACTIONS WORKING GROUP

G. Snow
University of Nebraska-Lincoln
F. Paige
Brookhaven National Laboratory

The Multiple Interactions working group was charged with investigating issues related to the large number of interactions per crossing envisioned for the VLHC at design luminosity. Presentations and discussions focused on the following topics: corrections to the calorimetric measurements of single-particle and jet energies in the presence of many interactions, multiple interaction corrections to luminosity measurements at the Tevatron, and the measurement of the luminosity in the VLHC environment. As the Tevatron luminosity increased into the range 10^{31} cm^{-2} s^{-1} during Run I, the CDF and DØ experiments learned to cope with increasing, yet small number $(1-5)$ of interactions per crossing. The LHC at CERN will provide a more difficult training ground since there will be in average 17 interactions per crossing at the design luminosity of 10^{34} cm^{-2} s^{-1}.

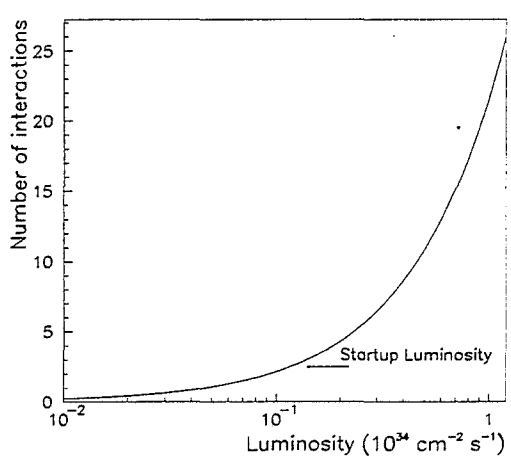

Figure 12: Average number of interactions per crossing as a function of luminosity at the VLHC. The horizontal axis is a log scale labeled in units of 10^{34} cm^{-2} s^{-1}.

The problem with multiple interactions at the VLHC will be worse, yet comparable to the situation at the LHC. The design luminosities are identical (10^{34} cm^{-2} s^{-1}) and the luminous region for a given bunch crossing will be a few cm longitudinally for both machines. While the time between bunch crossings is 25 nsec at the LHC and the bunches are separated by 7.5 m, these numbers are 17 nsec and 5 m, respectively, for the VLHC. Fig. 12 shows the number of interactions per bunch crossing expected at the VLHC as a function of luminosity, assuming an inelastic proton-proton cross section of 130 mbarn. At design luminosity, each beam crossing will yield about 22 interactions.

Both the LHC and the VLHC will likely come online with instantaneous luminosities at least a factor of 10 lower than the design luminosity. Fig. 12 shows that at start-up luminosity, there will only be a few interactions per crossing, so the multiple interaction problem will be similar to that faced at the Tevatron. As discussed below VLHC will benefit from low-luminosity running at start-up, both for physics and detector calibration reasons.

The much higher center-of-mass energy of the VLHC, however, will make the underlying event problem more difficult than at the LHC, since the particle multiplicity and average minimum-bias E_T will be higher. Still an average E_T density of 10's of GeV per unit $\eta - \phi$ at the VLHC design luminosity is manageable if one is searching for high mass particles and jets at $\sqrt{s} =$ 100 TeV.

A precise knowledge of the proton-proton luminosity at a VLHC interaction region is an essential ingredient in the measurement of absolute cross sections in a VLHC experiment. Monitoring the instantaneous luminosity is also important for making corrections to the data for detector effects related to the number of interactions per beam crossing.

The "counting zeros" technique is used by the DØ and CDF experiments at the Fermilab Tevatron collider and leads to an uncertainty of order 5%. A modified version of this technique is expected to yield similar precision at the VLHC even in the presence of large numbers of interactions per bunch crossing.

The counting zeros technique works as follows [1]. Two sets of luminosity monitors, symmetrically located on each side of the interaction region, count the fraction of times a given bunch crossing results in no detected particles on either side. The luminosity is inferred from the rate of such zeros.

The probability of having an empty crossing where a forward/backward coincidence is not recorded is given by:

$$P(0) = e^{-\overline{n}_1}\,(2\,e^{-\overline{n}_2/2} - e^{-\overline{n}_2})$$

where $\overline{n}_1$ is the average number of forward/backward coincidences and $\overline{n}_2$ is average number of one-side hits (but not both). $\overline{n}_1$ and $\overline{n}_2$ are related to the instantaneous luminosity L via:

$$\overline{n}_1 = (\epsilon_1^{sd}\sigma^{sd} + \epsilon_1^{dd}\sigma^{dd} + \epsilon_1^{hc}\sigma^{hc})\,\tau\,L$$

and

$$\overline{n}_2 = (\epsilon_2^{sd}\sigma^{sd} + \epsilon_2^{dd}\sigma^{dd} + \epsilon_2^{hc}\sigma^{hc})\,\tau\,L$$

Here, $\sigma^{sd}, \sigma^{dd}, \sigma^{hc}$ are the cross sections for single-diffractive, double-diffractive, and hard-core scattering, $\epsilon_1^{sd}, \epsilon_1^{dd}, \epsilon_1^{hc}$ are the acceptances for forward/backward coincidences for these processes, $\epsilon_2^{sd}, \epsilon_2^{dd}, \epsilon_2^{hc}$ are the corresponding acceptances for one-side hits, and τ is the bunch crossing time.

In order to track the luminosity as it decreases through the lifetime of an accelerator store (typically from a few hours to a day), for example, one would like to monitor the luminosity with a

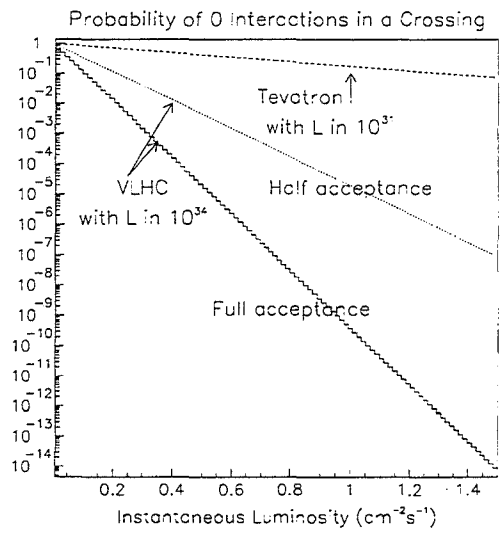

Figure 13: The probability of detecting zero interactions in a crossing vs. instantaneous luminosity for the Tevatron (full acceptance Level-0 array) and the VLHC (full and half acceptance arrays).

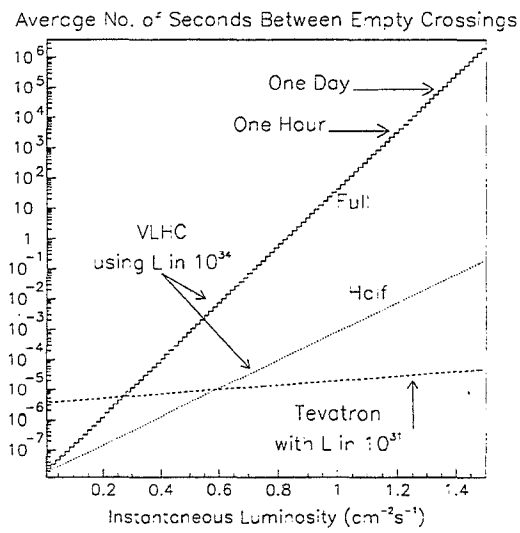

Figure 14: The average number of seconds between detected empty crossings vs. instantaneous luminosity for the Tevatron (full acceptance Level-0 array) and the VLHC (full and half acceptance arrays).

statistical uncertainty of about 1% every few seconds or minutes. This calls for counting of order 10^4 zeros in this period. These rates are achieved in the DØ experiment with the fine-grained Level-0 array of scintillation counters [2] which subtend the high-η region on both sides of the interaction region. The Level-0 counters are nearly 100% efficient for detecting a forward/backward coincidence from a hard-core scattering event, the dominant process among those listed above, since the two beam jets almost always send particles into the two arrays.

Fig. 13 shows the probability of detecting zero interactions per crossing as a function of luminosity for the DØ configuration and for a similar high-acceptance, high-efficiency "Level-0" array located in a VLHC experiment. Fig. 14 shows the same information in an alternate way – the average number of seconds between empty crossings vs. luminosity. One sees that a full-acceptance array at the VLHC results in having to wait several minutes between empty crossings at the design luminosity. The rates of detected zeros can be effectively increased, however, by decreasing the ϵ_1 and ϵ_2 terms in the above relations. This can be achieved by using an array of luminosity counters which have a smaller geometric acceptance or are less efficient for detecting minimum-ionizing particles, accomplished by raising discriminator thresholds.

Fig. 12 and 13 also show that the VLHC situation for a half-acceptance array starts to approach that of the Tevatron. Extrapolating further, the figures indicate that acceptance terms of order 10% those used at the Tevatron will result in zero-counting rates which give negligible statistical uncertainty in the luminosity measurement at the VLHC design luminosity. Fast timing for such counters will be necessary to distinguish between the bunch crossings separated by 17 nsec. Tevatron Level-0 counters, with 200 psec time resolution, have already demonstrated the ability to distinguish particles in neighboring buckets which are separated by about 15 nsec.

The calibration of the luminosity counters at the VLHC will require running the VLHC at low luminosity, where there is an average of one interaction per crossing. This will likely be the default scenario during the start-up of the machine. Many physics measurements require low-luminosity running as well: studies of elastic scattering and diffraction dissociation, studies of rapidity gaps between jets, etc. Another important step in calibrating the luminosity counters will be to run the VLHC at a lower center-of-mass energy where the total proton-proton cross section and its components (hard-core, elastic, single-diffractive, and double-diffractive) have been accurately measured. The LHC center-of-mass energy of 14 TeV would be the obvious low-energy target. Hence, the VLHC machine designers should incorporate into their planning the possibility of running the machine stably at this energy. Running the VLHC at the LHC center-of-mass energy will be useful for cross check-

ing other ingredients in cross-section calculations besides luminosity, as well as studying the $\sqrt{s}$-dependence of many physics processes.

REFERENCES

[1] "A Proposal for the DØ Upgrade Luminosity Monitor", J. Bantly, et al., DØ Note 2860, February 23, 1996.

[2] "The DØ Detector", S. Abachi et al., Nucl. Instr. & Meth. **A338**, 185 (1994).

VIII. TRACKING WORKING GROUP

F. Borcherding
Fermi National Accelerator Laboratory
Tao Han
University of California–Davis

A. Introduction

Good tracking has been and will continue to be a key ingredient for high energy physics experiments. Good tracking will require an inner tracker which can achieve precise measurements of the vertex positions for both the initial and displaced vertices. This good tracking will also require an outer tracker which can supply a precision position at large lever arm for momentum measurements and which can be used as a seed for track finding into the inner tracker. The tracker must be resistant to radiation damage particularly in its inner layers which are closest to the beam.

The machine parameters specify 100 TeV center of mass energy and a peak luminosity of $10^{34} cm^{-2} sec^{-1}$. With a bunch spacing of 17ns there will be about 20 interactions per crossing. Extrapolations of the minimum bias cross section are uncertain but indicate that each collision will generate about 10^2 particles for central ($\eta < 1.5$) and of the same order for each of forward and backward ($1.5 < \eta < 3$) regions. This produces some 4×10^3 charged tracks on average per crossing. For tracking to work well the occupancy needs to be kept to about 1% which leads to a requirement of 4×10^5 channels per tracking layer.

It is important to have a precision determination of the momenta of very high energy charged leptons (as discussed by T. Han [1]). For one meter of tracking in a four Tesla field, using fifteen planes, each with 50 μm resolution, the $\frac{\sigma_p}{p}$ resolution for a 10 TeV particle is 25%. For two meters of tracking this drops to 10%. Getting to 2.5% in one meter requires 5 μm resolution. Remember that 50 μm resolution is the 'goal' for the LHC detectors. Also needed is effective second vertex detection. For a two plane system the impact parameter resolution is a function of the ratio of the inner to outer radius. Therefore the inner radii must be small, close to the beam, or the outer radii becomes very large.

B. Inner Tracking with Pixels

For the high radiation levels and instantaneous rates of the VLHC the best choice for inner tracking appears to be pixels (as discussed by S. Kwan [2]). Even at $\sqrt{s}$ = 100 TeV but with a luminosity of about that at the LHC the requirements placed on the pixels by rate considerations are about the same. There pixel detectors of the order of 10^8 channels are planned with r-ϕ hit resolutions of about 15 μm. But at the VLHC the momentum of the high momentum tracks will be almost a factor of ten higher. One way to preserve momentum resolution is to improve tracker resolution by a factor of ten. Some work has been done which suggest that this factor of ten is possible, but reading out the many more smaller pixels could remain a problem [3].

C. Outer Tracking with Gas Chambers

A promising approach to solving these difficult problems appears to be the combination of the tried and true proportional mode gas avalanche counter and new techniques of surface treatments and photo lithography (as discussed by P. Rubinov [4]). This is already a very active field which has produced ideas such as the Micro Strip Gas Chambers (MSGCs), Micro Gap Chambers (MGCs), Gas Electron Multiplier (GEM) and more. Already one of the LHC detectors (CMS) has committed to developing the MSGCs for tracking as the most promising path of achieving the required performance. For the VLHC, only incremental improvements beyond the LHC application would be required. Gas detectors created with micro technology offer the following parameters:

- Spatial resolution - 40 μm is achievable without difficulty.
- Timing resolution - The very short charge collection times allow a timing resolution of approximately 10ns with current technologies.
- Low mass - Intrinsically, a 3mm gas gap at 1 atm is sufficient for the detection of minimum ionizing particles with full efficiency, but in practice all the material is in the support.
- High rate capability - Up to 10^6 particles/mm^2/sec is currently achievable (r > 190mm at VLHC).
- Segmentation - Strips of as long as 30cm can be used, or they can be as small as 200 μm for MSGCs or even less for MGCs.
- Radiation hardness - Able to withstand several megarads of ionizing radiation. With current technologies, MSGCs can be made to work for up to 10 years in an LHC environment.

Gas detectors is a very active field that is in the process of rapid evolution. Some promising ideas, such as the GEM are only now beginning to be explored. Currently the following parameters can be achieved simultaneously using MSGCs:

- 40 μm spatial resolution
- 10^6 particles/mm^2/sec rate capability
- up to 100mC/cm of collected charge without aging with good control of the gas purity.
- 11ns RMS time resolution.

Further developments such as combining the MSGC with the Gas Electron Multiplier are expected to extend the performance by allowing much higher gains and significantly improved reliability as well as extending the rate capability by another order of magnitude.

D. Scintillating Fibers

Scintillating fibers are a viable technology at high luminosity (as discussed by F.Borcherding [5]). A fiber tracker could start at an inner radius of 1.6m if that layer is segmented into 10 sections in z and the fiber diameter is as small as 0.5mm. A fiber tracker for the VLHC then could have eight layers each with $2x10^5$ channels located at radii of 1.5 to 3.0m.

The Upgrade DØ detector at FNAL will use VLPCs to convert photons seen in its fiber tracker and has a total channel count of just under 10^5 in eight layers [6]. It is not unreasonable to expect to build a detector eight to ten times as large for about the same cost in over a decade from now. A modest extrapolation of the VLPC technology indicates that the channel count could be increased 4-fold with no increase in the number of VLPC chips. There is some evidence that 0.5mm diameter fibers will produce enough photons to work with the present VLPCs [7]. A major factor would be in the cost and room needed for the 16 fold increase in clear wave guide fibers. This would be greatly reduced if the VLPCs which must operate at about 6.5 degrees K could be moved closer to the fiber tracker. The electronics could be greatly streamlined over the DØ design by requiring only one bit of information for each channel. The present front end pick off chip for DØ does this for 16 channels. This chip could be evolved up to 64 or 128 channels and a pipelined output stage added.

E. 3D Pixels

Today's silicon strips and tomorrow's pixels are 2-D technology with the electrodes etched on the surface of a silicon wafer (as discussed by S. Parker [8]). In 3-D technology the electrodes would extend through the wafer thickness. Here the n- and p-strips instead of laying on the surface are columns extending through the 300 μm wafer thickness. The depletion voltage for 3-D pixels is very much smaller than that for 2-D pixels. The signal amplitude is also very much greater and arrives within 1ns. The chip industry in the past has been focused on surface features. In the future, however, it will probably move into 3-D structures in its quest for denser and denser circuits. In such an industry 3-D pixel manufacture could become economically viable.

REFERENCES

[1] T. Han this workshop.

[2] S. Kwan this workshop.

[3] G. J. Kenny, S.I.Parker and V.Z.Peterson. " A Prototype Monolithic Pixel Detector", NIM A342 (1994) p. 59.

[4] P. Rubinov this workshop and private communication.

[5] F. Borcherding this workshop.

[6] S. Abachi et al., " The DØ Upgrade ", FERMILAB-CONF-95-177-E, Jul 1995, 54 pp. Submitted to International Europhysics Conference on High Energy Physics (HEP 95), Brussels, Belgium, 27 Jul - 2 Aug 1995. Adams et al., " A Detailed Study of Plastic Scintillating Strips with Axial Wavelength Shifting Fiber and VCLPC Readout", Nucl. Instrum. and Meth. A366 (1995) 263, FERMILAB PUB-95/027-E.

[7] A. Bross private communication.

[8] S. Parker this workshop.

IX. CALORIMETRY WORKING GROUP

D. Khazins
Duke University
J. Lykken
Fermi National Accelerator Laboratory

A. Introduction

The calorimetry looks as the most feasible part of the detector, even with the VLHC luminosity of $10^{34} cm^{-2} s^{-1}$. The radiation doses in the calorimeters and their occupancies increase very modestly with the collider energy. Based on the phenomenology developed by D.E. Groom [1], the calorimetry radiation doses at the collider energy of 100 TeV are only 2 times higher of those at the LHC with the same luminosity. Similar conclusions are followed from N. Mohov's calculations [2]. There are many calorimetry techniques which potentially fit the VLHC conditions, as it was demonstrated at this Workshop.

B. Scintillator calorimeters

This well established technique can be used for the barrel part of the detector in spite of its limited radiation resistance (about 4 Mrad, according to estimations of A. Pla-Dalmau [3]). However, chances to use scintillator for the forward/backward parts of the detector (pseudorapidity $\eta > 2$) do not look realistic even at the luminosity of $10^{34} cm^{-2} s^{-1}$.

Performance of the CMS scintillator hadronic calorimeter in combination with the $PbWO_4$ crystal electromagnetic (EM) calorimeter was discussed by J. Freeman [4]. The problem with this combination is a non-uniform response to the hadronic and EM parts of the shower (e/h $\neq$ 1) which causes non-linear amplitude versus energy dependence for hadrons and a degradation of the hadronic energy resolution (increase of the constant term). However, this degradation is relatively small, and author concludes that it is less important than non-gaussian tails in the calorimeter response function due to cracks and dead areas in real calorimeters.

C. $PbWO_4$ crystal calorimeters

The CMS crystal EM calorimeter was reported by R. Rusack [5]. The lead tungstate crystals ($PbWO_4$) allow to construct a compact EM calorimeter (the radiation length is 0.89 cm, Moliere radius is 2 cm) with excellent energy resolution:

$$\frac{\sigma_E}{E} = \frac{2\%}{\sqrt{E}} \oplus 0.5\% \oplus \frac{0.15}{E} \text{ (E in GeV).}$$

The long term radiation resistance of the crystal is also good, 10 Mrad has been demonstrated. Nevertheless, the ability of the $PbWO_4$ calorimeter to work in high radiation fields still is not clear. First, there is so called 'short term' radiation damage which may vary the crystal light output in some unpredictable way, thus deteriorating the calorimeter resolution. Another point of concern is the radiation resistance of the silicone avalanche photodiode (APD), which was accepted by CMS as a photodetector for the crystals.

Both, the $PbWO_4$ crystals and especially the APD, are very sensitive to the temperature variations. However, with the proper temperature monitoring, corrections could be made and the calorimeter energy resolution should not suffer.

Apparently, we will have more data on this promising technique in the near future due to intensive studies for CMS.

D. Quartz fiber calorimeters

This new type of calorimetry was presented by O. Ganel [6]. The calorimeter is a kind of 'spaghetti' calorimeter with fibers made of quartz (amorphous silica) instead of scintillator plastic. Pure quartz is very radiation hard, 30 Grad is achievable. Quartz fibers detect Cherenkov light which yields low-intensive but extremely fast signal, an output signal of several nanosecond width has been observed.

The calorimeter EM energy resolution is determined by the photo-electron statistics (yield is 0.8 ph.e./GeV):

$$\frac{\sigma_E}{E} = \frac{(100-140)\%}{\sqrt{E}}.$$

Since the quartz fibers pick up only Cherenkov light from fast electrons the calorimeter is practically non-sensitive to the hadronic energy. Nevertheless, it can be used for the hadron energy measurements at very high energies, due to high EM component in the hadronic shower which logarithmically increases with energy. Clearly, the hadronic energy resolution is not very good, basically, it is 2 - 3 times worse than that for the conventional (scintillator, liquid argon) calorimeters.

Another feature of the quartz fiber calorimeter is narrow hadronic shower (64 mm diameter), because it detects the EM core of the hadronic shower only. This feature may be used for better jet-jet resolution at very high rapidity regions where radius of jet cone is less than the width of the hadronic shower.

E. Diamond calorimeters

Diamond detectors (presented by R. Stone-Rutgers [7]) allow to construct very compact, radiation hard ($\rangle$ 100 Mrad), robust, and very fast ($\sim$ 1ns readout) sampling calorimeters. One such calorimeter has been constructed and tested with a reasonable EM energy resolution:

$$\frac{\sigma_E}{E} \sim \frac{20\%}{\sqrt{E}} \oplus 1.5\% \oplus \frac{8\%}{E}.$$

The main problem with this technique is the diamond price. Presently, the cost of the diamond calorimeter is one or two order of magnitude higher than other types of calorimeters. However, the technology development may change the situation.

F. High pressure tube gas calorimeters

Although the first calorimeter with gas ionization readout has been tested back in 1979 [8] this technique has never been used in physics experiments by one reason: small signal. At low energies electronic noise dominates calorimeter energy resolution. However, with the energy increase and with the electronics improvement this technique presents very attractive option for the future colliders [9].

Gas ionization calorimeters are very radiation hard () 1 Grad) and fast (20 ns total width output signal has been demonstrated [10]). Due to high ion mobility in gases these calorimeters can work in high intensity radiation fields (100 rad/s) without signal degradation. Due to the lack of the gain the calorimeters are linear and stable. Finally, the gas ionization calorimeters are inexpensive, since their basic design is carbon steel tubes filled with argon based gas mixtures.

The tube design of the high-pressure (100 atm) gas-ionization calorimeters was presented by D. Khazins [11]. A tested hadronic calorimeter made of 0.5 inch diameter tubes had the energy resolution:

$$\frac{\sigma_E}{E} = \frac{70\%}{\sqrt{E}} \oplus 7.4\%.$$

Using a weighting procedure for the e/h compensation, authors managed to reduce the constant term to $\langle 3\%$. (It is not clear, however, how this or similar procedure could be beneficial in the case of jets.) The electronic noise of the tested calorimeter was equivalent to 4 GeV (r.m.s) per hadronic shower. Authors believe it could be reduced to 1 GeV or less.

An EM calorimeter made of 'wiggling' tubes had the energy resolution:

$$\frac{\sigma_E}{E} \sim \frac{32\%}{\sqrt{E}} \oplus 3\%.$$

It is somewhat worse than the expected value of $\frac{20\%}{\sqrt{E}} \oplus 1\%$, which implies that the wiggling calorimeter needs more R&D work. The EM calorimeter electronic noise was 0.3 GeV.

G. Moderate pressure gas calorimeters with planar electrode geometry

Another approach to the gas ionization calorimeters is being developed by a Serpukhov group (S. Denisov et al. [12]). They employ the standard sandwich geometry. A hadronic calorimeter filled with 90%Ar + 10%CF_4 gas mixture at 40 atm pressure has been tested. They are now looking for heavy carbon-fluorine gases to reduce the pressure to several atmospheres.

In the process of the calorimeter investigation the group discovered that they can control the calorimeter e/h ratio by adjusting the width and delay of the ADC gate signal. As the result they obtained a very low constant term in the hadronic energy resolution: 2.5% with the absorber made of steel and 0.1% with the lead absorber. This discovery opens possibilities for a really good hadronic and jet energy resolution at VLHC, because at those energies the constant term will dominate energy resolution.

H. Liquid argon calorimeters

The liquid argon calorimeters have not been presented at the Workshop. However, this well established and solid technique, undoubtedly, would be one of the main options for the VLHC detector. It is intrinsically radiation hard, linear, and stable. Energy resolution is very good for both hadrons and EM particles. The H1 group [13] obtained the hadronic resolution:

$$\frac{\sigma_E}{E} = \frac{51\%}{\sqrt{E}} \oplus 1.6\%,$$

using a weighting procedure for the e/h compensation. (Again, the low constant term may be not applicable for jets because of difference in energy distribution in jets and hadronic showers.)

The ATLAS group [14] has tested an accordion EM calorimeter with the resolution:

$$\frac{\sigma_E}{E} = \frac{7.7\%}{\sqrt{E}}$$

with a negligible constant term.

The drawback of the liquid argon technique is the low mobility of both electrons and ions. The big electron collection time, which is presently about 0.5 μsec, creates serious pileup problems for calorimetry. The positive ions build up a volume charge in the liquid argon gap which considerably distorts electric field in the gap at the dose rate about 1 rad/s. However, both these limitations strongly depend on the calorimeter design parameters (the gap size and voltage) and could be improved.

I. Calorimeter in situ calibration

At the last talk of the calorimetry group R. Vidal [15] considered several processes for the calorimeter in situ calibration. Decays $J/\psi \rightarrow \mu^+\mu^-$ and $Z \rightarrow e^+e^-$ can be used for the EM calorimeter calibration. The hadronic calorimeters may be calibrated with (Z + jets) events and with b-tagged W-bosons (decaying into two jets) from tt-bar events. The challenge is the in situ calibration at energies exceeding the weak boson masses.

REFERENCES

[1] D. E. Groom, "Ionizing Radiation Environment in SSC Detectors", Workshop on Radiation Hardness of Plastic Scintillator, Florida, 1990.

[2] N. Mokhov, "VLHC Radiation Levels", this Workshop.

[3] A. Pla-Dalmau, "Radiation damage in Plastic Scintillators", this Workshop.

[4] J. Freeman, "Non-compensating Calorimetry in CMS", this Workshop.

[5] R. Rusack, "The CMS Electromagnetic Calorimeter", this Workshop.

[6] O. Ganel, "Calorimetry Under Extreme Conditions", this Workshop.

[7] R. Stone-Rutgers, "Diamond Calorimetry", this Workshop

[8] V.I. Baskakov et al., Nucl. Instr. and Meth. 159 (1979) 83.

[9] N.D. Giokaris et al., Nucl. Instr. and Meth. A291 (1990) 552.

[10] V.E Konstantinov et al., ATLAS Internal Note CAL-NO-027 (1993)

[11] D.M. Khazins, "High-Pressure Gas-Ionization Tube Calorimeters", this Workshop.

[12] S. Denisov et al. "Recent Developments in the Gas Ionization Calorimetry with Planar Electrode Geometry", in Proceedings of the Fifth International Conference on Calorimetry in High Energy Physics, 1994, p. 380.

[13] A. Babaev, "Performance of the H1 Liquid Argon Calorimeter", ibid, p. 51.

[14] O. Benary et al., Nucl. Instr. and Meth A350 (1994) 131.

[15] R. Vidal, "In Situ Calibration", this Workshop.

X. MUON WORKING GROUP

T. LeCompte
Argonne National Laboratory
M. Berger
Indiana University

A. Introduction

Lepton identification is at the core of hadron collider physics. Leptons indicate the presence of an electroweak boson, either real or virtual. Electrons and muons (and to a lesser extent taus) can be identified at the trigger level, allowing these interesting events to be selected against the enormous background of QCD events.

Muons are simple to identify. Their long lifetime and high penetrating power virtually independent of energy makes them very distinctive: any charged particle that penetrates several meters of material is a muon. Unlike electrons, which can have their momenta measured by calorimetry, muons have to have their momentum measured in tracking, which becomes increasingly difficult at high p_T. The critical issue is not whether or not we can identify muons at the VLHC - we can. It's whether or not we can accurately measure their momentum.

B. Theoretical Issues: Which Muons Are We Looking For?

There are several processes of interest that can generate muons as signatures:

• Compositeness or a new contact interaction: here one signature is an increase in the Drell-Yan cross section at high $m(\mu^+\mu^-)$, and $p_T(\mu)$ can be several TeV.

• New gauge bosons, such as $Z' \to \mu^+\mu^-$. Again, $p_T(\mu)$ can be several TeV. Additionally, measuring the forward-backward asymmetry A_{FB} of this new Z' provides information on its couplings. This technique requires large η coverage for muons, and good resolution is needed since the asymmetry varies with $m(\mu^+\mu^-)$.

• Heavy squarks and gluinos. Weak scale supersymmetry (SUSY) will presumably be discovered at the LHC if not before. However some of the heavier states might be too heavy to be seen at the LHC or be produced in insufficient numbers to allow a detailed study of the complicated cascade decay. These particles can be pair produced at the VLHC, and many of these have muons as daughters, and these muons are expected to have $p_T(\mu)$ in the 100's of GeV range.

• Strongly Interacting Electroweak Symmetry Breaking: A hadron machine with the energy envisioned here is a "gauge boson collider," since the production mechanisms involving electroweak gauge bosons from the initial state partons becomes increasingly important. Any evidence uncovered at the LHC for a strongly interacting sector that breaks the electroweak symmetry would motivate a higher energy machine for study of the new interactions. Good charge determination for very energetic muons would allow the identification of various isospin channels in strong vector boson scattering. This is especially the case in the mode $W^+W^+ \to W^+W^+$ where the like-sign lepton signal must be separated from the unlike-sign Standard Model background.

• Multi-W production: While these W's tend to be at high p_T (and therefore generate high p_T muons), we would also like to measure the cross section for single W, WW, etc. production, and this means detection in some cases (when one of the W's is not highly boosted with respect to the lab frame) down to a few 10's of GeV.

• Other new particles: Other scenarios include the possibility of pair-producing leptoquarks which decay into a lepton and a quark jet or pair-producing vector-like quarks which have leptonic decays. New heavy particles exist in the messenger sector of gauge-mediated SUSY breaking models. If light enough some of these particles could be produced at the VLHC. One possible signal involving muons in the final state would be the production of a pair of (charged) messenger scalars which decay into a W and its (absolutely stable or relatively long-lived) neutral electroweak doublet partner, i.e. $\phi^+ \to \phi^0 W^+$. More generally the presence of new particles could enhance the number of muons observed at the VLHC.

This brings up the question of the purpose of a VLHC experiment: does it emphasize doing 10 TeV scale physics, or does it emphasize doing high statistics 1 TeV scale physics? The answer to this question depends on what the LHC does and does not discover, but it does have implications for detector design. For very massive objects, the acceptance is proportional to solid angle coverage, but for less massive objects, it is proportional to rapidity. A detector optimized for 10 TeV scale physics will invest more resources into the best momentum resolution in the central region, whereas a detector optimized for 1 TeV physics will opt to cover a larger region, with less emphasis on resolution. This increases the yield, but also makes A_{FB} measurements possible.

The best momentum measurement possible is desirable. The better the momentum resolution, the narrower peaks become, and the smaller the signal that can be identified over the background. Additionally, should (e.g.) a new Z' boson be discovered, measuring the width $\Gamma(Z')$ would be of intense interest. For intrinsic widths smaller than the detector resolution, this becomes extremely difficult.

C. Experimental Issues: How Do We Find Them?

The dynamic range of the VLHC muon system is unprecedented, ranging from a few 10's of GeV to a few 10's TeV. Even if one were to stipulate that muons from low p_T W bosons were uninteresting, it is impractical to build a detector with a thick enough muon absorber to be blind to these muons: approximately a meter of iron is required for a muon to lose 1 GeV via dE/dx.

Three strategies are commonly employed in measuring the momentum of muons: measure the momentum in a central tracker, measure the momentum in instrumented magnetized shielding, and measure the momentum in a special muon spectrometer outside the shielding.

It is unlikely that an independent muon tracker could measure the momentum better than a central tracker. An independent muon outer tracker covers a substantially larger volume,

which increases the channel count for a given number of measurements of a given resolution, and also reduces the practical magnetic field allowed because of stored energy considerations. The tracking group believes that an inner tracker using a large bore high field magnet and existing tracking technologies can reach momentum resolution of 10% or better for a 10 TeV track, which corresponds to a 3σ charge measurement for a 30 TeV muon. Although improved momentum resolution is always better, this is believed to be adequate to probe a broad range of physics.

It is expected that the dominant source of apparent high p_T muons will be low p_T muons that somehow get mismeasured to appear to be much straighter than they really are. While this is unlikely to happen to any particular muon, there are so many more low p_T muons than high p_T muons that non-Gaussian tails on the resolution could pose substantial problems. This is especially true at the trigger level, where only a subset of the detector information is available.

Clearly a second (and possibly even a third) momentum measurement to confirm the central tracker is desirable. It is certainly possible to build a tracking system inside the absorber (as DØ has done) or beyond the absorber (as ATLAS has done), at some cost. Additionally, properties of very energetic muons can be exploited.

A 2 TeV muon has the same velocity as a 10 GeV electron. Muons, therefore, begin to show features normally associated with electrons in their passage through matter. For example, a 1 GeV muon deposits (an average of) 3.5 GeV in 3m of iron. A 1 TeV muon deposits 9 GeV. If a VLHC detector built a 1 foot deep "muon calorimeter" at the extreme outer radius of the muon detector, this calorimeter would only need $30\%/\sqrt{E}$ resolution to provide 3σ separation. The main difficulty with this technique is shower fluctuations. Thicker calorimeters are less sensitive to fluctuations, although they are more expensive: to reduce the fluctuations by a factor of two requires a calorimeter four times thicker.

A second property that can be exploited is that muons of this velocity exhibit transition radiation, with an intensity proportional to γ. Historically, TRD's do not have the best track record, although most problems that have been experienced arise from trying to make TRD's that are lightweight and/or thin, so as not to degrade the track unnecessarily before its next measurement. Since the muon detectors are the last element to measure a particle, there is no incentive to make a TRD too thin. Relatively thick detectors with correspondingly large signals can be built. TRD's cannot be made arbitrarily thick, however, because a showering muon produces electrons, which have large γ. The TRD's would then respond to these electrons and (correctly) identify them as high velocity particles.

For a VLHC operating at luminosities of $10^{34} cm^{-2} s^{-1}$, muon identification and momentum measurement to better than 10% for a 10 TeV muon seems possible by simple extrapolation from known technologies. Non-Gaussian tails causing lower p_T muons to appear as higher p_T muons is a concern, which can be addressed by an additional momentum measurement and/or a velocity measurement using transition radiation or dE/dx.

A critical issue that has not yet been addressed is that of triggering. Experience has shown that triggering on muons is a more difficult problem than offline reconstruction; how much more difficult depends on the bandwidth limitations. Detector design may be driven by ease of triggering.

XI. CONCLUSIONS

Different scenarios of physics beyond the SM were investigated by the physics working groups and each time the potential of the VLHC was clearly demonstrated. Let us review the conclusions of the different working groups.

New Strong Dynamics Working Group. If strong dynamics is involved in electroweak symmetry breaking, the physics associated with it will first appear at the 1 TeV scale, and the VLHC will have the opportunity to explore it in more depth than the LHC. For example, if a Higgs is discovered in the 400-800 GeV range, the VLHC would be able to differentiate between a SM Higgs and a non-SM Higgs much better than the LHC. New strong dynamics as well as any phenomena associated with flavor physics would also give a rich structure in the 1-10 TeV range. A challenge to theorists is to identify the possibilities for 10 TeV-scale physics.

Supersymmetry Working Group. If SUSY is discovered at low energy, as many suspect it will be, and is gauge-mediated, one could then expect new gauge bosons in the 10-100 TeV range. A VLHC would be the right place to study these new particles as well as the heavy part of the SUSY spectrum.

Exotics Working Group. It is likely that not all outstanding questions will be answered by the LHC. Why are there three generations? What is the origin of the quark mixing matrix? Are there any connections between quarks and leptons? We can therefore expect some new phenomena that might manifest themselves by contact interactions and/or by new massive particles. The search potential of the VLHC for these new phenomena is truly enormous and the limits are in general in the multi-ten TeV region. We might never get any clues for these before the VLHC.

Full Rapidity Physics Working Group. A full acceptance detector will provide a powerfull tool and investigate physics complementary to the central, high Pt detector. The long straight section that is needed to insert such a detector should be included right from the start in the VLHC design.

Precision Measurements of Heavy Objects Working Group. The VLHC will not be competitive for precision measurements in the few 100 GeV mass scale, the competition from lower energy machines is too big in that region. The strong suit of the VLHC is clearly its kinematic reach.

Multiple Interaction Working Group. The average number of interactions per crossing at a luminosity of $10^{34} cm^{-2} s^{-1}$ should be about 22 for 17ns bunch spacing. The situation will be worse than, yet comparable to the situation at the LHC. The higher energy of the VLHC, however, will make the underlying event problem more difficult. This problem should be manageable if one is searching for relatively high energy particles and jets. The VLHC will benefit from low-luminosity running at start-up, both for physics and detector calibration reasons. Luminosity callibration would also require to operate the VLHC at the LHC energy.

Tracking Working Group. The total number of detector elements needed per tracking layer is estimated to be 4×10^5 in order to keep the occupancy down to 1%. To keep the momentum resolution of 10 TeV charged leptons in the few percent range will require a tracking resolution which is below the LHC goal, a challenging task. Different types of tracking detectors and their potential applications to the VLHC were discussed: two and three dimensional pixels for inner tracking, micro strip and micro gap gas chambers for outer tracking, and scintillating fibers.

Calorimetry Working Group. The calorimetry appears to be the most feasible part of the detector. The calorimetry radiation doses at E_{cm}=100 TeV are only 2 times higher than those at the LHC, with the same luminosity, and of course the energy resolution improves with energy. There are many calorimetry techniques which might fit the VLHC requirements of good time resolution, high radiation hardness and fine segmentation. The in situ calibration at high energies will be a challenge.

Muon Working Group. Muons are the signatures of many processes generated by physics beyond the SM and are simple to identify. Momentum measurement of 10 TeV muons to better than 10% seems possible with reasonable extrapolation from current technology. Non-Gaussian tails causing lower p_T muons to appear as higher p_T muons is a concern. This could be addressed by a second momentum measurement using transition radiation or the (relatively large at these energies) energy loss in a calorimeter. Triggering will be a serious challenge and will be limited by bandwidth consideration. Detector design may be driven by ease of triggering.

We note that the conclusions reached during the Snowmass 96 [2] workshop were confirmed by the specific studies done during the workshop.

The VLHC will be designed to investigate the unknown physics beyond the SM. It should be capable of investigating a broad spectrum of models which go beyond the SM. Much work remains to be done even though progress has been made during this workshop. We can however draw the following general conclusions. With the center-of-mass energy and luminosity considered at this workshop, the VLHC will be able to probe in detail the physics that will hopefully be discovered by the LHC at the 1 TeV mass scale. It will furthermore allow us to investigate scales that are about an order of magnitude larger (in some cases even larger) than the scales probed at the LHC. It will, however, be difficult for the VLHC to achieve competitive measurements at the 100 GeV mass scale.

For a luminosity comparable to the LHC luminosity, VLHC detectors seem feasible. There are however many challenges and new and/or old technologies should be pushed with the idea of decreasing the cost. Considering the cost of LHC-like detectors, it is clear that detectors should not be ignored in the overall cost optimization of the project. An increase of the accelerator energy increases its cost, but allow a decrease in luminosity (for fixed physics goal(s)) which more than likely will decrease the cost of the detector. The VLHC detector R&D effort should logically start once the LHC effort slows down.

We believe that the physics potential of a Very Large Hadron Collider warrants a strong R&D effort on accelerator technologies that would enable us to reach the necessary energy and luminosity within a reasonable cost.

Since the workshop we have started a VLHC Study Group; for more information see [4]. This workshop was sponsored by

Fermi National Accelerator Laboratory and the US Department of Energy

REFERENCES

[1] Mini-symposium "New low-cost approaches to high energy hadron colliders at Fermilab" at the May 3, 1996 APS Annual Meeting. G. Dugan, P. Limon, and M. Syphers, "Really Large Hadron Collider Working Group Summary", and E. Malamud, " New Technologies for a Future Superconducting Proton Collider at Fermilab", *Proceedings of the 1996 DPF/DPB Summer Study on New Directions for High Energy Physics*, Snowmass, CO, June 25 – July 12, 1996, p. 306.

[2] D. Denisov and S. Keller, "Summary of the Very Large Hadron Collider Physics and Detector Subgroup", *Proceedings of the 1996 DPF/DPB Summer Study on New Directions for High Energy Physics*, Snowmass, CO, June 25 – July 12, 1996, p. 277.

[3] E. Eichten, I. Hinchliffe, K. Lane, and C. Quigg, Rev. Mod. Phys. 56 (1984) 579-707; Addendum-ibid. 58 (1986) 1065-1073.

[4] See our web page: http://www-theory.fnal.gov/vlhc/vlhc.html

Section 2: ACCELERATOR PHYSICS

S. Mishra, "Introduction and Design Goals"

S. Mishra, "Lattice Design of the 3 TeV Injector"

L. Michelotti, "50 TeV high field lattice: Observations from a Golden Cell"

F. Bieniosek et al, "Beam Transfer Lines for a VLHC"

J. Marriner, "Slow Extraction from the 3 TeV Injector for the VLHC"

C. T. Murphy, "Alignment Issues for the 3 TeV Ring"

I. Kourbanis, "RF Requirements for a 3 TeV Collider Ring"

A. I. Drozhdin, N.V.Mokhov, "Beam Abort and Collimation for a 3x3 TeV Hadron Collider"

A. I. Drozhdin et al, "Beam Abort for a 50x50 TeV Hadron Collider"

J-F. Ostiguy, "Transverse Resistive Wall Instability in a Very Large Hadron Collider"

F. Zimmerman, "Electron-Cloud Instability in the VLHC"

K-Y. Ng, "Beam Stability Issues of 3 TeV Low-Field Collider"

J. Marriner, "A Damper to Suppress Low Frequency Transverse Instabilities in the VLHC"

V. Shiltsev, "Pipetron: Beam Dynamics with Noise"

V. Shiltsev, "External Noise Issues in VLHC"

V. V. Danilov and V.D. Shiltsev, "Transverse Mode Coupling Instability in the VLHC"

T. Kroc, "Synchrotron Radiation in the VLHC"

Introduction and Design Goals

C. S. Mishra
Fermilab

The goal of the Very Large Hadron Collider (VLHC) at Fermilab is to extend the energy frontier beyond the LHC and utilize Fermilab's injector chain of Linac, Booster and Main Injector. The design center of mass energy for the VLHC pp collider is 100 TeV, with an initial luminosity of 1e34 $cm^{-2}sec^{-1}$. The present design will provide an integrated luminosity of about 100 fb^{-1} per year. The design luminosity is limited by the detector's ability to trigger on high interactions per crossing. Present detector technologies limit the interactions per crossing to about 20. Considerable R&D are needed to determine the ultimate accelerator luminosity threshold from the point of view of beam stability. The accelerator luminosity is likely to increase with R&D and operating experiences.

This section of the report presents the current state our design and is by no means final. As discussed in the Accelerator Systems subsection we are investigating two different, magnet technologies, high field (10-12 Tesla) and low field (2 Tesla). At present accelerator design and calculations are being carried out for both magnet technologies. A specific magnet design exists for the low field option. The proposed site specific geometrical layout of accelerators using low field magnets, parameters of the injector and collider, basic layout of injection, extraction and abort lines, initial thoughts on the subject of beam stability and a conceptual damper design are discussed in this subsection.

The magnetic field quality at injection, eddy currents and hysteric effects limits the increase of energy from injection to maximum for a synchrotron. We have conservatively assumed this factor to be 20. We propose to use the Fermilab injector chain of Linac (400 MeV), Booster (8.9 GeV) and the Fermilab Main Injector (FMI) (150 GeV). These three are rapid cycling accelerators. The FMI can cycle to 150 GeV in about 1.5 sec. The FMI will be used as an injector to the VLHC. The VLHC will have two new accelerators, a 3 TeV High Energy Booster (HEB) and a 50 TeV, pp collider VLHC. Fig. 1 shows the schematic drawing of the Fermilab accelerators and injection lines to the HEB. Counter rotating protons will be injected into the HEB by extracting protons from the FMI at MI40 and MI62. These extractions are possible without any major modification to the FMI lattice. Antiprotons could also be extracted from FMI and injected into the 3 TeV HEB if a pbar-p collider physics program is of interest.

The 3 TeV low field injector will provide a relatively rapid cycling injector for the larger 50 TeV collider. It will be a new benchmark for HEP's ability to deliver machines with much lower cost/TeV. Since we are proposing a staged approach to VLHC, the 3 TeV low field injector will reduce the technical risk and overall cost of the VLHC at Fermilab. This new injector will test several accelerator physics and technology ideas and will provide needed technical R&D before we commit to build VLHC. A new 3 TeV injector does not disrupt the Tevatron physics program, which will be the flagship of HEP for at least next 10 years.

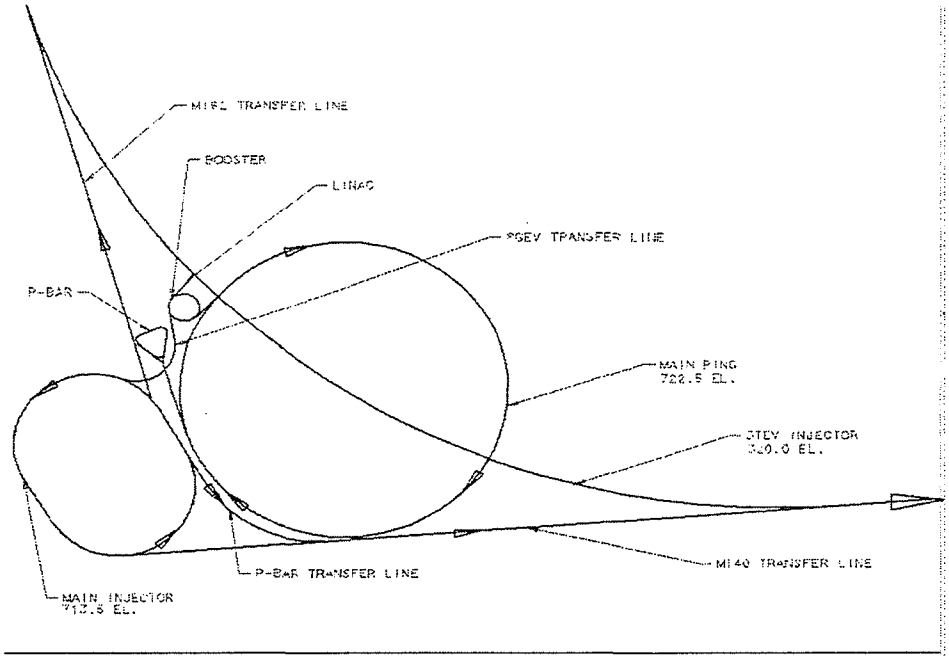

Fig 1 The schematic drawing of the Fermilab accelerators and injection lines to the HEB

The luminosity goals of VLHC at 100 TeV for both the low field and high field options are given in Table 1. The number of protons per bunch for both the machines are rather modest. The Fermilab Booster at present is capable of delivering 5×10^{10} protons/bunch. The bunch intensity has been adjusted to achieve a manageable number of interactions per crossing for the detectors. The current accelerator design does not include any beam cooling to reduce bunch emittance. It is possible to use the Recycler Ring with electron cooling to pre cool the protons before injection into the FMI. Table 1 conservatively assumes that the emittance through the Fermilab's injector chain will remain at its current level. We need to study the benefits and possibilities of using the Recycler Ring. One obvious benefit it will provide is that smaller bunch intensity will be required to achieve the same luminosity, due to smaller emittance of both the proton beams.

The high field option has advantages due to synchrotron radiation damping. The damping time is smaller than the storage time. As shown in Fig. 2 [1] the emittance of the bunch decreases as a function of store time due to synchrotron radiation. The luminosity of the collider is enhanced for relatively modest bunch intensities. The integrated luminosity of a 10 hours store vs. initial rms emittance for different VLHC options is shown in Fig 3 [1]. The integrated luminosity of the two high field cases is almost independent of the initial emittance because of synchrotron radiation damping. The low field integrated luminosity is a falling function of initial emittance, but at the emittance sigma of about 4-6 π mm-mr, where we plan to operate, it is relatively flat. As given in Table 1 the

integrated luminosity dictated by the interactions/crossing is the same for the two options ~100 fb^{-1} / year. The luminosity goal for the 3 TeV HEB if used as a collider is given in Table 2. It is possible to use the HEB as one of the two rings required for a 6 TeV center

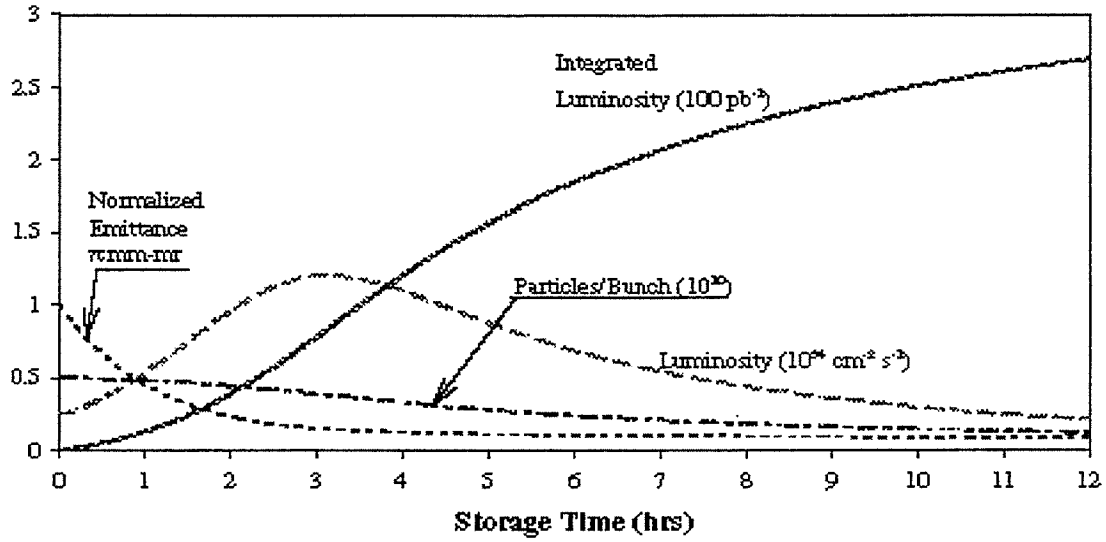

Fig 2. Beam parameters during a store for high-field VLHC

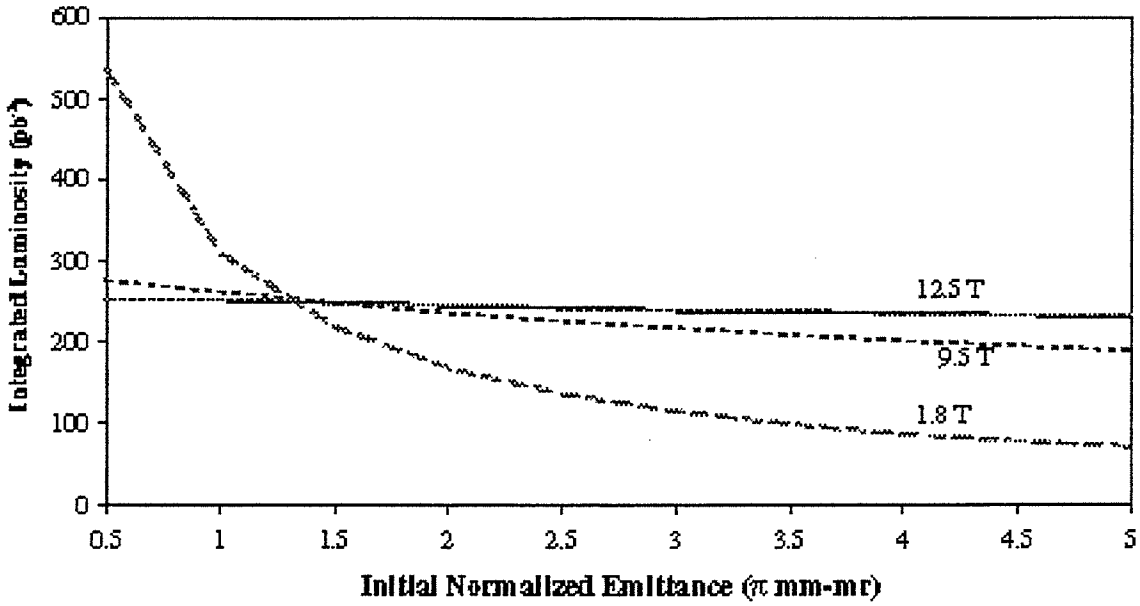

Fig 3. Integrated luminosity of 10 hours store vs. initial rms. emittance for VLHC

of mass pbar-p collider physics program. We will be required to install a second ring in the HEB tunnel and a low beta system. We regard the HEB as a demonstration machine for the final VLHC. The magnets built for the second ring can be used as magnets in the 50 TeV collider. The proton bunch intensities in the table are the present capabilities of the Fermilab accelerator. The luminosity is limited by the number of antiprotons available at the beginning of a store. We have assumed that the total number of antiprotons at the beginning of the store is 1E13, a planned goal for TeV33. We have reasons to believe that we can do better. The Recycler Ring will help achieve higher stacking rates; keeping only one interaction region will consume less antiprotons.

	50 TeV Collider p p option (Low Field)	50 TeV Collider p p option (High Field)
Proton Per Bunch	1.7E+10	1.2E+10
Number of Bunches	100000	16000
Revolution Frequency (kHz)	0.5	3.2
Beta Star at IP(m)	0.1	0.1
Proton Emittance(95%)	15	8
Form Factor	0.48	0.48
Typical Luminosity ($cm^{-2}sec^{-1}$)	1.1E+34	1.1E+34
Integrated Luminosity (fb^{-1}/year)	112	112
Interactions Per Crossing (Detector Acceptance Not Included)	28	28
Bunch Spacing (ns)	19	19
Inelastic Cross Section (mb)	127	127

Table 1. The Luminosity goals of VLHC at 100 TeV center of mass.

Table 2 also shows that we can achieve an integrated luminosity of 5 to 20 fb-1/year for pbar-p physics depending on magnet technology. Another advantageous feature of this collider is that we can collide pbar-p and pp at the same interaction region.

In this subsection, we have provided details of the present status of the 3 TeV low field lattice design. We are making progress on understanding the combined function vs. separated function lattice. We are in the process of developing lattices for all the four machines. These lattices will be used to study the details of magnet requirements, correction schemes and the beam stability.

The beam stability in VLHC has been center of our attention since the Snowmass 96 workshop. A few papers in this section detail our efforts on understanding the instabilities. Two instabilities appear potentially serious: the transverse coupled bunch instability and the mode-coupling single bunch instability. In both cases, the instabilities are driven by the resistive component of the vacuum pipe wall impedance, whose value scale linearly with the circumference of the machine. A serious concern is that at low frequencies it may be too costly to make the beam pipe thick enough to contain all the electromagnetic fields induced by the beam. This may have a significant impact on the value of the resistive wall impedance, in particular in the presence of iron pole pieces. Reliable estimates of the low frequency wall impedance must be obtained, especially in view of the fact that the standard formulae apply only to the situation where all electromagnetic fields are contained in the vacuum tube.

	3 TeV Collider pbar p option (Low Field)	3 TeV Collider p p option (High Field)	50 TeV Collider p p option (High Field)
Proton Per Bunch	2.7E+11	1.1E+11	2.7E+11
Proton/AntiProton Per Bunch	1.3E+10	1.1E+11	4.0E+10
Number of Bunches	790	790	250
Revolution Frequency (kHz)	8.8	8.8	30
Beta Star at IP(m)	0.25	0.25	0.25
Proton Emittance(95%)	15	15	15
Form Factor	0.56	0.56	0.56
Typical Luminosity ($cm^{-2}sec^{-1}$)	5.4E+32	1.9E+33	1.8E+33
Integrated Luminosity (fb^{-1}/year)	5.4	19.1	18.4
Interactions Per Crossing (Detector Acceptance Not Included)	6.2	22	19.6
Bunch Spacing (ns)	132	132	132
Inelastic Cross Section (mb)	80	80	80

Table 2. The Luminosity goals for the 3 TeV HEB if used as a collider.

In a paper we briefly outline transverse resistive wall instability theory. We then present preliminary numerical computations of the wall impedance at low frequency and

compare the results to those predicted by the standard theory. All computations were performed with a low frequency code since standard accelerator impedance codes cannot deal with situations where the fields are not all contained within the beam pipe.

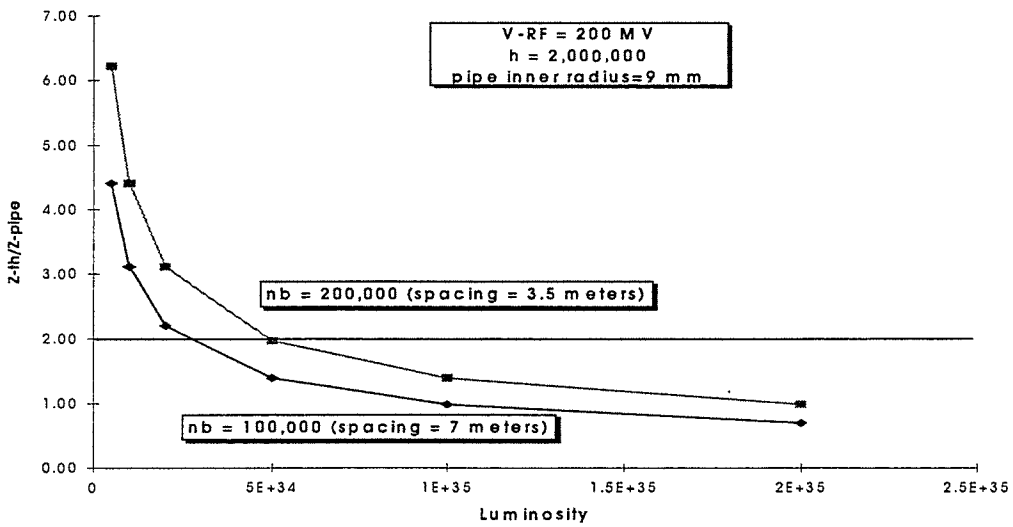

Fig 4. Change in TMCI threshold as a function of luminosity for different numbers of bunches.

In another paper on the subject of stability we present a conceptual design of a damper system to suppress low frequency transverse instabilities in the VLHC. The growth rate was estimated to be 1/3 of the revolution period. This instability is routinely suppressed with electronic feedback at operating machines such as the Main Ring and Tevatron, but was thought to be "beyond state of the art" for the VLHC presumably because the calculated growth time was shorter than the revolution period. The paper describes a design to damp low frequency instabilities in VLHC.

Transverse mode-coupling instability (TMCI) needs considerable attention in the VLHC design. As discussed by J. Rogers at Snowmass 96[2], it was thought to pose a significant problem to beam stability. We have been working on understanding this problem and its possible solution. Since this effect depends on several parameters which are not final yet and can be optimized, we feel that the effect of TMCI on the stability of the can be improved considerably. E. Malamud [3] has pointed out that by raising the RF voltage and frequency, or by reducing the change per bunch at injection and coalescing bunches part way up the ramp can reduce the effect. There are other possibilities, like changing the average beta function of the VLHC lattice. Fig. 4 shows the change in TMCI threshold as a function of luminosity for 100k and 200k bunches. Since the vacuum pipe impedance decreases as $1/(\text{gap})^3$, a less attractive solution is to increase the magnet gap. We are in process of optimizing these numbers and will provide detailed information in the Design Study.

In both high field and low field approaches we have to understand and solve the problems of emittance growth due to vibration and ground motion, although for low field approach the magnitude of this problem could be larger due to the larger circumference of the machine.

R&D plans for Accelerator Physics

As outlined in this section we are just beginning to work on a detailed design of HEB and VLHC accelerators. We need to develop a detailed design of these two accelerators with consideration of the magnetic field quality, aperture and stability of beam. The lattice and design parameters will be optimized for reliable operation of the machine. Several areas of high payoff R&D can be identified. Very high bandwidth stochastic cooling would be of great benefit. Methods of limiting noise induced emittance growth, including low vibration magnet mounts and use of an e-beam to extend the decoherence time introduced by the beam-beam tune shift.

Reference:

1. G. Dugan, P. Limon and M. Syphers, " Really Large Hadron Collider Working Group Summary," Snowmass 96.
2. J. T. Rogers "Collective Effects and Impedances in the RLHC(s)," Snowmass 96.
3. E. Malamud, Private Communications.

Lattice Design of the 3 TeV Injector for VLHC

(Low Field Approach)

C. S. Mishra

We present here preliminary design parameters for a 3 TeV proton injector, using the low field magnet technology. The Fermilab Main Injector will be used as an injector for this 3 TeV Machine. The design presented in this paper uses the low field combined function magnets with 2.15 Tesla dipole field.

This lattice design is very preliminary. We have not made beam dynamics studies with this lattice. This lattice and lattice parameters will be modified to improve the performance of the injector. The present working lattice parameters are given in Table 1.

Table 1

Design Parameters of 3 TeV Low Field Injector

Energy of Ring:	3 TeV
Injection Energy:	0.150 TeV
Ring Circumference:	34 Km (Including straight sections)
Number of Straight Sections:	2
Number of Utility Regions:	4
Length of Straight Section:	1.8 km
Length of Utility section:	0.1 km
Number of cells:	240
Length of cell:	125 m
Phase Advance per cell:	60 degrees
Number of Dipoles Per Half cell:	10

Length of a Dipole:	12.25 m
Dipole Field:	2.15 Tesla
Quadrupole Field in Dipole:	6.2e-4 (1/m^2)
Sextupole Field in Dipole:	6.0e-4 (1/m^3)

The lattice is made of combined function magnets. In the transmission line magnet, each 125 meters cell contains ten iron half-cores, each of which can in principle have an independent dipole, quadrupole and sextupole component. There are two types of combined function magnets (CFM) in the lattice, CFM with a quadrupole field and CFM with a sextupole field. The sextupole component has not been included in the CFM with quadrupole component to reduce the 2nd order effects introduced by the sextupole. Also by placing the sextupole at β_{max} locations in the cell we have reduced the overall sextupole strength in the lattice.

Choice of Lattice Parameters:

The 3 TeV injector lattice will have a minimal set of tune, chromaticity and higher order harmonics correctors. The fractional part of the tune will be set with a phase trombone like the Fermilab's Recycler. We would like to reduce the number and strength of these correctors in the lattice. The achievable quadrupole strengths in the CFM have been a major consideration in this lattice design.

In selecting these lattice parameters, we have made an attempt to minimize the required quadrupole strength in the combined function magnet, the dispersion in the ring and the beam size at injection. It is anticipated that the injected beam size from the Fermilab Main Injector at 150 GeV will be 15π mm-mr (95% Normalized emmittance).

The following two tables show the dependence of these parameters on phase advance and cell length. These parameters have been calculated by using a Mathcad program [1].

Dependence on Phase Advance

In this table we have varied the phase advance per cell keeping the rest of the lattice unchanged.

Phase Advance (deg)	**Quad Strength (T)**	**Beta Max (m)**	**Dispersion (m)**	**Beam Size (95%) at injection (mm)**
60	**166**	**207**	**3.7**	**4.5**
75	**203**	**200**	**2.65**	**4.4**
90	**236**	**205**	**2.04**	**4.43**

As expected the needed quadrupole strength is smallest for the cell with 60-degree phase

advance.

Dependence on Cell Length

In the following calculations we have fixed the phase advance per cell to 60 degrees and varied the cell length.

Cell Length (m)	Quad Strength (T)	Beta Max (m)	Dispersion (m)	Beam Size (95%) at injection (mm)
100	**200**	**173**	**2.61**	**4.1**
120	**166**	**207**	**3.7**	**4.5**
125	**160**	**216**	**4.1**	**4.62**
150	**133**	**259**	**5.9**	**5.1**
200	**100**	**346**	**10.47**	**6.1**
240	**83**	**415**	**15.1**	**6.8**

The required focusing strength decreases with increasing cell length. The maximum beta function, dispersion and beam size at injection increases with cell length. We have selected a cell length of 125 meters for further studies.

Cell Layout:

Each cell has ten CFM dipoles with focusing and defocusing sextupoles placed in between two focusing or defocusing quadrupoles. The dipole length of 12.25 meters has been selected for the ease of construction. The lattice has three types of cells, ARC Cell, Dispersion suppressor cell and straight section cell.

Arc Cell

DRIFT, CFM with F Quad, CFM with F Quad, CFM with F Sext, CFM with F Quad, CFM with F Quad, CFM with D Quad, CFM with D Quad, CFM with D Sext, CFM with D Quad, CFM with D Quad, DRIFT.

Dispersion Suppressor cell

The dispersion suppressor cell has the same layout as the arc cell. The CFM in the dispersion suppressor cells has half the bending strength as the arc cells. The quadrupole strength is the same as arc cell CFM. The middle dipole has no sextupole component.

Lattice Functions:

Beta (X, Y) max:	200 m
Beta (X, Y) min:	77 m

Dispersion max:	3.5 m
Chromaticity:	0.0

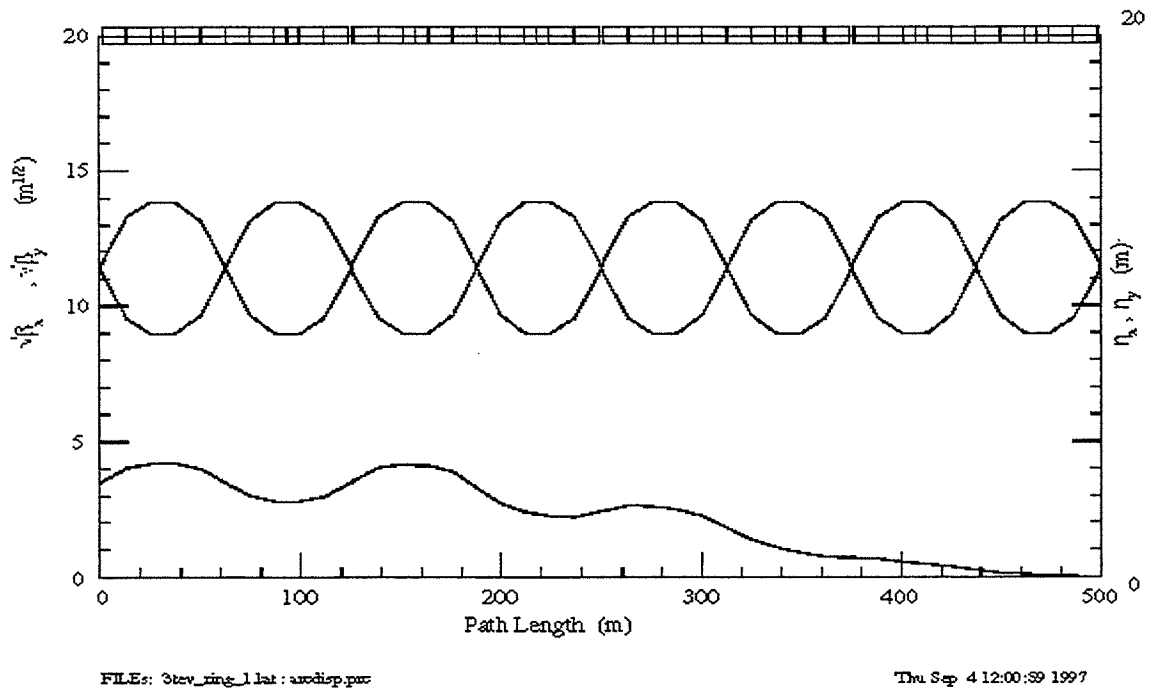

Fig. 1

Cell Lattice Functions

Based on the calculations performed using the Mathcad program[1] and calculations using MAD we have decided that the 3 TeV injector lattice should have 60 degrees phase advance per cell and a cell length of about 125 meters. Fig 1 shows the lattice function of an arc and dispersion suppressor cells.

The 60 degrees phase advance gives the smallest quadrupole strength and is ideal for the placement of correction elements in the lattice. We have chosen 125 meters of cell length; this increases the beta function, dispersion and beam size to an acceptable level while keeping the required quadrupole strength small. The dipole with the sextupole component is placed at the maximum beta in both planes to reduce the required sextupole strength.

Further Studies

As stated earlier this is the 0th order design of the 3 TeV low field injector lattice. Considerable work is needed to optimize the lattice parameters with magnetic field quality, aperture and stability of the beam under consideration.

Reference:

1. M. Syphers, Math Cad Program for Accelerator Modeling, Private communication.

50 TeV high field lattice: observations from a golden cell.

Leo Michelotti

This short note was written during a two-week "Futures" workshop held at Fermilab in July, 1997. It stresses the obvious point that the first important parameters that must be chosen in designing a high-field VLHC lattice are the phase advance and length of the standard cell. These decisions are not completely trivial and should be made only after some serious work has been done. Separated function and combined function machines are both under consideration.

God, grant me the serenity to accept the things I cannot change,
courage to change the things I can, and the wisdom to know the difference.
— Serenity Prayer
Reinhold Neibuhr

The principal thing that cannot be changed is the Lorentz force law, from which comes the ubiquitous expression relating momentum to magnetic rigidity, $p = eB\rho$. For singly charged particles, this is written in convenient units as follows,

$$B\rho \text{ [T-m]} = 3.33564\ldots \times p \text{ [GeV/c]} \quad .$$

While it is somewhat less immutable, we will consider the specification of building a circular p-p collider at $\sqrt{s} = 100$ TeV using 12.5 Tesla dipoles to be firmly established. From these is obtained the circumference that must be taken up by the arcs.

$$2\pi\rho = C_{\text{arcs}}[\text{km}] = 20.958\ldots \times p[\text{TeV/c}]/B[\text{T}] = 83.834\ldots$$

One reads of a high-field VLHC collider having a circumference of ≈ 100 km, which means that $\approx 20\%$ would not be in the arcs.

Two scenarios are under consideration: the first envisions that the ring will be built up from FODO cells, and the other proposes that it be built using combined function magnets. At this time, neither possibility has been excluded.

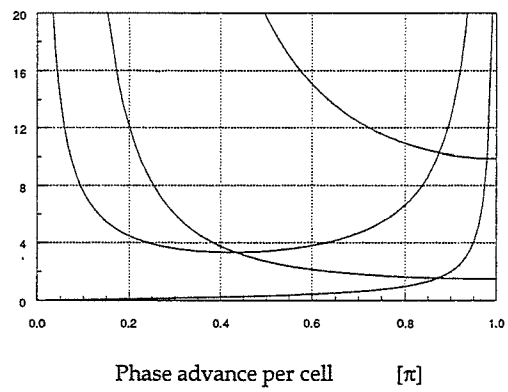

Figure 1: Normalized curves for the FODO model: $\beta_+/L, D_+\rho/L^2, N^2\alpha$, and $-\pi\xi/N$. .

1 Thin lens, FODO model

The key things that *can* be changed are the length, $2L$, and "phase advance," ψ, of the machine's "standard cell."[1] The thin lens FODO model has the advantage that one can derive a number of simple, analytic expressions relating first order optics parameters to the phase advance through a cell. To begin with, the maximum and minimum horizontal β – which occur at the "center" of the F and D quads, respectively – are given by one of the two equivalent expressions,

$$\beta_\pm/2L = \frac{1 \pm \sin(\psi/2)}{\sin\psi} \tag{1}$$

$$\beta_\pm/2f = \frac{1 \pm \sin(\psi/2)}{\cos(\psi/2)} \tag{2}$$

β_+ from Eq. 1 is plotted as one of the curves in Figure 1. Other scaled parameters of interest, for the same model, include the maximum and minimum dispersion,

$$\rho D_\pm/L^2 = D_\pm/L\theta = \frac{1}{\sin^2(\psi/2)} \pm \frac{1}{2\sin(\psi/2)} \ , \tag{3}$$

the natural chromaticity,

$$\xi/N = -\frac{1}{\pi}\tan(\psi/2) \ ,$$

[1]This number is actually the imaginary part of the log of the eigenvalue of the one-turn map through the cell; that is, $2\pi\nu$ of a standard cell. It literally applies to a machine constructed only from standard cells (and, if you will, perfectly matched straight sections).

and an approximate expression for the momentum compaction,

$$N^2\alpha \approx \left(\frac{\pi}{\sin(\psi/2)}\right)^2 ,$$

where $N = C_{\rm arcs}/2L$ is the number of standard cells. Some of these are also shown in Figure 1. (Derivations can be found in Edwards and Syphers[2] or Bryant and Johnsen[1].)

The minimum value of β_+ occurs at the value of $\sin(\psi/2)$ that satisfies the polynomial,

$$(s+1)(s^2+s-1) = 0$$

The first factor is not physical; the second is solved by the golden ratio,

$$\sin(\psi/2) = r_G = (\sqrt{5}-1)/2 = 0.618034\ldots \tag{4}$$

That it *is* the golden ratio is of no practical importance, but since it is the only original observation in this paper, we will make as much of it as possible. Accordingly, we call the FODO model designed so as to satisfy Eq.(4) a "golden cell," with "golden phase advance" per cell $\psi = 76.345\ldots^\circ$. Of much greater importance is the fact that the curve is rather flat over a large domain, so that minimizing β_+ is not a particularly restrictive constraint.

For the golden cell,

$$\min\beta_+ = (1/r_G^{3/2} + 1/r_G^{1/2}) \times L \approx 3.33019\ldots \times L \ .$$

We rewrite this in terms of the number of cells in the ring,

$$\begin{aligned} \min\beta_+[\mathrm{m}] &= (3\ 1/3)^2 \frac{\pi}{N}\frac{p[\mathrm{GeV/c}]}{B[\mathrm{T}]} \\ &\approx 140{,}000/N, \end{aligned}$$

where, for aesthetic purposes, we have substituted $(3\ 1/3)^2$ for $3.33564\ldots \times 3.33019\ldots$. A rather extreme upper bound on N can be found by examining its implications for the integrated quadrupole strength. Within the model,

$$B'l = \frac{2}{\pi}BN\sin(\psi/2) = \frac{2r_G}{\pi}BN = 0.39345\ldots \times BN \ ,$$

where $B'l$ is the integrated quad gradient, B is the dipole field, and N is the number of standard cells in the lattice; that last scaling coefficient applies to the golden cell only. Still assuming that $B = 12.5$ T, and $N \approx 500 - 1000$, we would need something like ≈ 15 m quadrupoles with operating gradients of $\approx 160 - 330$ T/m. By comparison, quadrupoles in Tevatron's standard cell have ≈ 78 T/m gradient and 1.7 m length. If we accept this as the upper limit on N, then $\beta_+ \geq 140 - 280$ m. Let's say, realistically, that we expect $\beta_+ \geq 300$ m from these simple considerations.

Similar expressions provide the values of other parameters in terms of r_G for the golden cell and the scaling parameters, L or, equivalently, N. For example,

$$\begin{aligned} \beta_- &= (1/r_G^{3/2} - 1/r_G^{1/2}) \times L = 0.78615\ldots \times L \ , \\ \alpha &\simeq (\pi/r_G)^2/N^2 = 25.83896\ldots/N^2 \ , \\ \xi &= -(r_G^{1/2}/\pi) \times N = -0.25024\ldots \times N \ . \end{aligned}$$

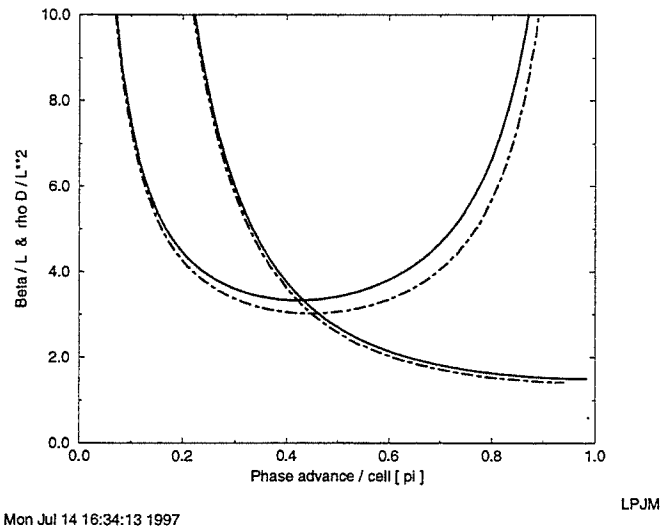

Figure 2: Comparison of β_+/L and $D_+\rho/L^2$ for the separated function FODO and combined function FD models.

The scaling coefficients are tabulated below for the golden cell and for cells with 60° and 90° phase advance.

	60°	Golden Cell	90°
β_+/L	$6/\sqrt{3} = 3.46...$	$1/r_G^{3/2} + 1/r_G^{1/2} = 3.33...$	$2+\sqrt{2} = 3.41...$
β_-/L	$2/\sqrt{3} = 1.15...$	$1/r_G^{3/2} + 1/r_G^{1/2} = 0.78...$	$2-\sqrt{2} = 0.58...$
$N^2\alpha$	$4\pi^2 = 39.47...$	$(\pi/r_G)^2 = 25.83...$	$2\pi^2 = 19.73...$
ξ/N	$-1/\pi\sqrt{3} = -0.18...$	$-r_G^{1/2}/\pi = -0.25...$	$-1/\pi = -0.31...$
$B'l/BN$	$1/\pi = 0.31...$	$2r_G/\pi = 0.39...$	$\sqrt{2}/\pi = 0.45...$

As a perhaps not totally worthless exercise, consider using the curve for $\beta_+/2f$, given by Eq.(2), rather than $\beta_+/2L$. Does one arrive at the same conclusions?

2 Combined function models

Curves analagous to those produced by Eq.(1) and Eq.(3) but for a combined function FD model are shown as the dashed lines in Figure 2; the solid lines are repetitions of the FODO calculations, put here for the sake of comparison. While the scaling properties are no longer exact, there are remarkably small differences when these results are plotted in this way.

However, the pure FD model has no spaces for sextupoles or drifts. If we take, instead, Mishra's lattice for the 3 TeV low field injector and alter the parameters so as to represent a 50 TeV high field cell, the the resultant β_+ is plotted in Figure 2, for 1000 cells, and Figure 2, for 500 cells. In the same figures are also plotted the quadrupole gradient required in the bends, in Tesla per meter and as a fraction of the magnetic

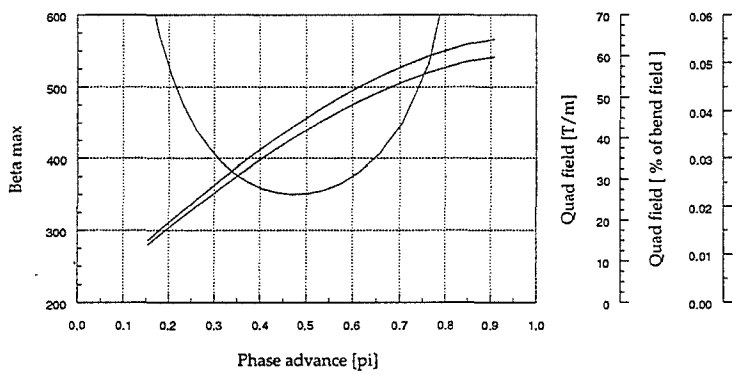

Figure 3: The β_+ curve and required quadupole fields for a combined function lattice with space for sextupole magnets. Here, $N = 1000$.

field at 1 cm from the center. We make only a few observations here. (a) $\min \beta_+$ occurs much closer to $\psi = 90°$ than $\psi = 76°$. (b) The curve is not as flat as before, so that the acceptable domain in ψ is smaller. (c) Most importantly, gradient fields have acceptable values; the gradient field at 1 cm will be $\leq 4\%$ of the bend field.

3 Key question

The key question is: what should be the cell length, or, equivalently, how many standard cells should there be in the ring? The scaling laws of the FODO model – and their approximate counterparts for the combined function models – only underscore the importance of this decision. Larger cells are more economical but will lead to a decreased aperture when nonlinear and error effects are taken into account. As a starting point, and only as a starting point, Glenn Goderre suggested in this workshop using the criterion: (a) $L[\mathrm{m}] \cdot \theta = 0.8$, a rule he obtained from an SSC memo by Courant, *et al.* Don Edwards has privately suggested a similar initial guess: (b) $N = \sqrt{C[\mathrm{ft}]}$. These are, in fact related; (a) implies that $N = 0.77\sqrt{C[\mathrm{ft}]}$, which is remarkably close to (b). If we apply (b) blindly to the 50 TeV machine, we get $N = 522$ and $L = 80$ [m], which are in the right ball park.

At the SSC, 100 m was chosen for the half cell length after considerable study, involving calculating dynamic and linear apertures using many independent tracking programs and checking the results for consistency. As a result of these studies, an empirical power law relating linear aperture to $L^{-3/4}$ was noted and used to fix the 100 m value. ($A[\mathrm{mm}] = 180 L[\mathrm{m}]^{-0.76}$, for coil diameter of 4 cm.) No corresponding studies were carried out for the combined function model or for either model with the levels of synchrotron radiation expected for the 50 TeV high field machine. (Synchrotron radiation damping and anti-damping

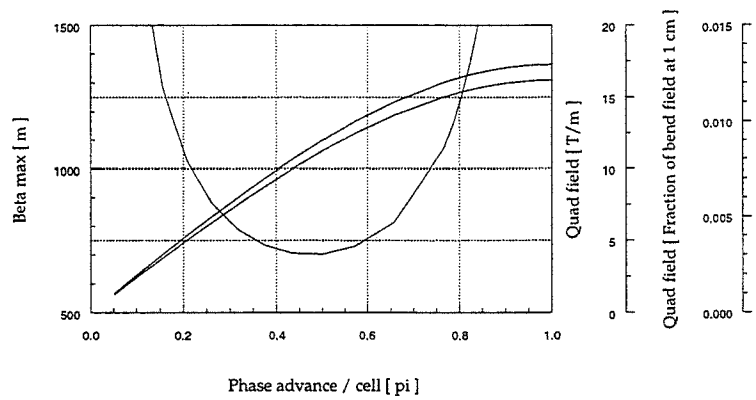

Figure 4: The β_+ curve and required quadupole fields for a combined function lattice with space for sextupole magnets. Here, $N = 500$.

must also be considered in making the choice between a FODO cell and a combined function cell.)

While it is likely that the final answer is still in the neighborhood of 100 m, *I would urge that we take this issue at least as seriously as was done at the SSC.* In particular, this means not making a recommendation after a quickly organized two-week workshop but only after taking the time to understand completely the SSC calculations and to do comparable studies of our own for both models under consideration.

With regard to the "Serenity Prayer," one word is used badly. Rather than "change the things I *can*," a better phrase would have been "change the things I *should*." It is worthwhile keeping that distinction in mind as we proceed to study the VLHC options.

References

[1] Philip J. Bryant and Kjell Johnsen. *The Principles of Circular Accelerators and Storage Rings*. Cambridge University Press, 1993.

[2] D. A. Edwards and M. J. Syphers. *An Introduction to the Physics of High Energy Accelerators*. John Wiley & Sons, New York, 1993.

VLHC-000 (1.0)
File: report1.tex (1.4)

Beam transfer lines for a VLHC

F. Bieniosek, N. Gelfand, D. E. Johnson, A. D. Russell, M.-J. Yang
Fermi National Accelerator Laboratory

September 10, 1997

1 Introduction

As part of the August 1997 Summer Study we have looked at the beamlines which will be required to transport 150 GeV protons and antiprotons from the Main Injector to the 3 TeV high energy VLHC booster and 3 TeV protons from the 3 TeV Booster to the 50 TeV ring.

2 Working assumptions

These considerations were developed under some standard assumptions.

- Beam will be extracted from the Main Injector at 150 GeV/c. Beam from the 3 TeV Booster to the VLHC will be transferred at 3 TeV/c.
- All geometry considerations assume the rings are located in a flat cordinate system. At this stage, no attempt is made to account for the curvature of the earth.
- The 3 TeV ring is at elevation 325′ (99.0 m). The Main Injector is at 714′ (217.6 m). The change in elevation is 389′ (118.6 m).
- Where ever possible beamlines will be composed of permanent magnets. The permanent magnets are described elsewhere[1]

3 Proton Transfer Lines From Main Injector to 3 TeV ring

Two extraction points have been identified for proton extraction from the Main Injector.

1. Beam can be extracted into the Main Injector abort line at MI40. A switching magnet subsequently deflects the beam through a 4″ hole passing through the dump assembly. The beam continues in the transfer line downstream of the dump and provides the counterclockwise beam in the 3 TeV Booster.

2. Protons are extracted at MI60 into the NuMI beamline. A switch magnet deflects the beam out of the NuMI channel and into the beamline to the 3 TeV Booster providing the clockwise beam.

3.1 Proton extraction at MI-40

The Main Injector beam is extracted to the dump at MI-40. The extraction elements comprise 2 fast kickers downstream of Q400 to deflect the beam across the septa of lambertsons at Q402 and into the extraction channel. A c-magnet and two B2 dipoles direct the beam to the dump. The beam size is controlled by three quadrupoles. Extraction to the 3 TeV ring is provided by 3 (2 may suffice) kickers or pulsed magnets and a lambertson to deflected the beam through a hole in the dump assembly which has been provided for this purpose. The lattice functions from M336 in the Main Injector ring to the end of the dump are shown in Figure 1. Note that $\beta_x \approx \beta_y \approx 260$ m, $\eta_x \approx 2.5$ m and $\eta_y \approx 0.8$ m at the downstream face of the dump, Table 3.3. Figure 2 shows a possible matching section and regular FODO structure which can be extended as needed to reach the injection point to the 3 TeV ring. The beamline is about 3000 m long.

3.2 Proton extraction via NuMI line

It is necessary to provide for counter-rotating protons (protons and antiprotons) in the 3 TeV ring and, later, in the 50 TeV ring. Extracting the beam at MI-60 into the NuMI channel and then separating from it near the NuMI pretarget hall provides a convenient and efficient means to deliver a clockwise moving beam to the 3 TeV ring. The length of this line is approximately 3000 m and, like the line from MI-40 should require minimal

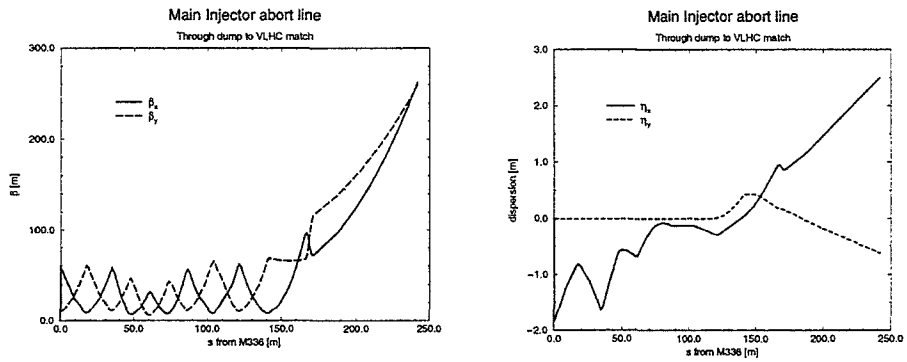

Figure 1: Lattice functions from M336 to downstream face of Main Injector abort dump.

horizontal bends. It will essentially duplicate the line from MI-40, excluding the kickers and lambertson required upstream of the dump.

3.3 150 GeV/c proton transfer line

The two proton transfer lines from the Main Injector are very similar except for the matching sections at the Main Injector end. A solution for the line from MI40 is discussed.

There are obviously many ways to transport 150 GeV beam from the Main Injector to the 3 TeV Booster. The range of options to be considered may be restricted by making a few reasonable assumptions. The first constraint is imposed by the need to limit the grade of the transport line to about 4%. This is desirable, for example, to facilitate the handling of magnets and other heavy equipment during installation and servicing and to simplify the task of supplying cooling water should it be necessary. This results in a beam line of $\approx$ 3 km length.

The length of the proposed beamline makes it reasonable to use permanent magnets for most of the bending, both horizontal and vertical. The benefits provided include simplicity, reduced cost, and operational stability. If correction is needed, small air-cooled dipoles may suffice.

The depth of the 3 TeV accelerator and the difficulty of working so far below the surface suggest that the transfer line lattice be the same as the lattice of 3 TeV accelerator. In that way all the matching of lattice functions and the dispersion can be done on the surface where power and water will be easily available.

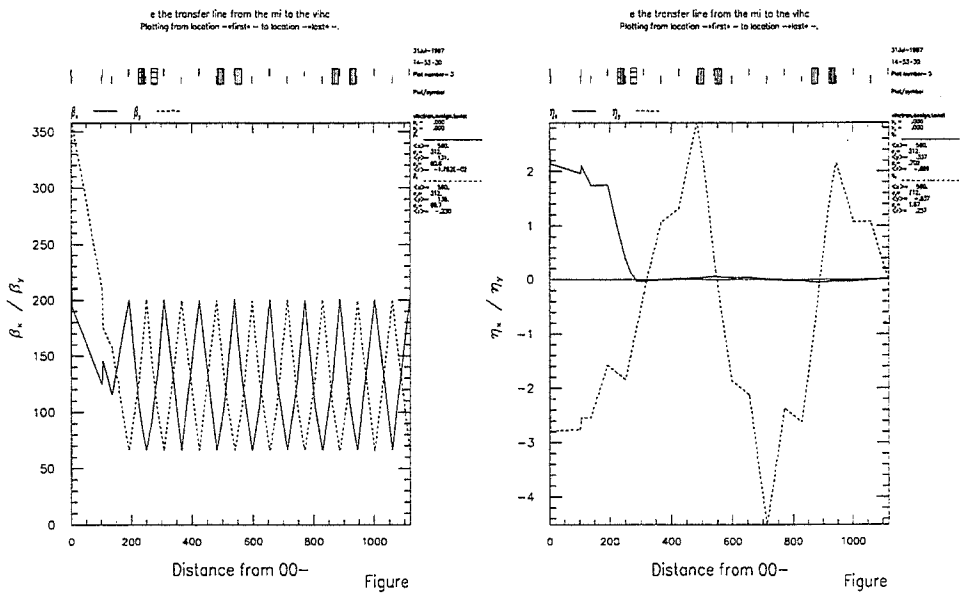

Figure 2: Amplitude functions β_x and β_y and dispersion functions η_x and η_y along the beam line.

The straight sections of the 3 TeV accelerator will presumably be FODO cells with 60° phase advance and $\beta_{max} \approx 200$ m. The straight sections are also expected to be dispersion free. Our transport line will be composed of the same FODO cells. On the surface we will match from the MI into the FODO string and kill the dispersion. The beam will then be bent down with a sequence of vertical bends (a total bend of 40 mr is needed) that results in no vertical dispersion. The requisite horizontal bends will also be done on the surface.

The maximum value of β in the matching section is less than 400 m, which seems quite reasonable given the initial conditions. Given the required bend strengths and gradients of the elements in the matching sections it is likely that some if not all of these could be permanent magnets.[1] The parameters of the quadrupoles, Table 2, in the standard cell can easily be achieved with permanent magnets.

The proposed beam line will, most likely, pass through different kinds of

[1]The lengths of the quadrupoles could be increased to reduce the required gradients. I see little purpose in trying to optimize the solution at this time. There should be plenty of time to do so when the VLHC moves onto the physical sheet.

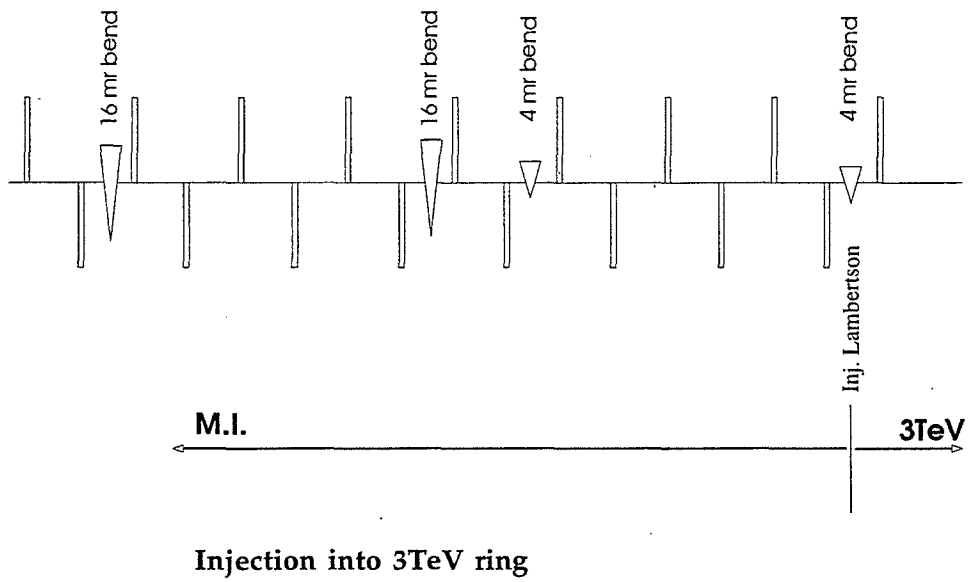

Figure 3: Layout of proposed matching section into the 3 TeV ring.

Function	Value
β_x	262.2358 m
β_y	259.3020 m
α_x	-2.0545
α_y	-1.4213
η_x	2.496 m
η_y	-0.633 m
η'_x	$24.602 \cdot 10^{-3}$
η'_y	$-10.816 \cdot 10^{-3}$

Table 1: Lattice functions for the extracted beam at the downstream end of the MI dump.

type	number	length	strength	field
dipole	1	20.000	14.1671 mr	.3544 T
dipole	1	20.000	-18.3478 mr	-.4590 T
dipole	1	20.000	-21.6522 mr	-.5417 T
quadrupole	29	2.000	.0981 m^{-1}	4.8115 T/m
quadrupole	1	2.000	.1614 m^{-1}	13.0291 T/m
quadrupole	1	2.000	-.1631 m^{-1}	-13.3146 T/m
quadrupole	1	2.000	.0264 m^{-1}	.3493 T/m
quadrupole	1	2.000	.0173 m^{-1}	.1493 T/m
quadrupole	1	2.000	.0084 m^{-1}	.0356 T/m
quadrupole	1	2.000	.0283 m^{-1}	.3996 T/m
quadrupole	29	2.000	-.0979 m^{-1}	-4.7922 T/m

Table 2: Major magnetic elements needed for 3 km long beamline, including matching section at Main Injector end.

rock and soil as it drops 400′ over its 3 km length. It seems likely that it will be subject to small unpredictable deformations as the temperature and the water level varies over the years. Thus, the beam line probably will require instrumentation to measure the beam position along the line and air cooled electromagnets to provide steering to compensate for the ground motion. Even though the lattice issues may admit to straight forward solutions the construction and operation of this transfer line may be challenging.

4 Antiprotons from MI-62

Antiprotons are extracted at MI-62 and transported through part of the A150 beamline until they can be deflected down and started through an $\approx 90°$ arc which joins the beamline from MI-40 approximately a third of the way along its length. The arc closely follows the outside of the Tevatron tunnel for much of its length while dropping to meet the other line at an elevation of about 600′.

Design considerations for 150 GeV pbar transfer from Main Injector to 3 TeV ring:

1. Extract from Main Injector using A150 beamline. This beamline transfers 150 GeV pbars from Main Injector to Tevatron. The beamline bends up and to the right, as the tunnel floor rises 5 ft. There is a 15 m clear gap in the beamline just after exiting the Main Injector. A

magnet switch could be installed here to bend the beam down to follow the floor of the enclosure. The beamline if extended in a straight line will pass through the wall of the NuMI tunnel.

2. A downward deflection of 40 mrad at this point using 3 or 4 vertical bend electromagnets will pass the beamline 10 ft underneath the floor of the Tevatron tunnel. Radius of curvature of the path to connect to the proton extraction line is about 1.5 km. It is reasonable to bend using permanent magnets as much as possible. Given $B\rho = 500$ T·m, the average bend field requirement is 3.3 kG. This field is probably near the practical limit of permanent magnet dipoles, after allowing space for focusing, trims, and diagnostics. We may want to add a few horizontal bend electromagnets in the beamline in addition to the vertical bend. But they could be clustered near the surface, for ease of access.

3. The beamline will pass underneath the Tevatron a second time, this time at a depth of about 130 ft. At junction with the proton transfer line, at least one more powered magnet switch will be required.

4. Total path length is roughly 1.5 km. A good fraction of this distance is taken up by permanent-magnet dipoles. Assuming a quad spacing of 40 m, 38 quad magnets will be required.

4.1 Injection at 150 GeV into 3 TeV ring

We assume that injection will be into a straight section. The most appealing assumption is to inject at the upstream end of the straight section. We assume that the center of the injected beam will be 18 cm above the circulating beam to allow the beam pipe to clear the first magnetic element. Then using $x = \theta\sqrt{\beta(s)\beta(0)}\sin(\Delta\phi)$ we can calculate the kick angle to flatten the injected beam. Table 3 shows typical requirements.

The calculation of injection into the 3 TeV ring was done with the assumption that:

1. The transfer line has a slope of -40 mr just before injection.

2. Beta function is already matched to that of the 3TeV ring and the transfer line is composed of FODO cells.

3. A kick of 4 mr is sufficient to clear the element up-stream of injection point.

	ϕ [deg]			
β_{max} $[m]$	60	70	80	90
100	1.04	0.96	0.91	0.90
200	0.52	0.48	0.46	0.45
300	0.35	0.32	0.30	0.30

Table 3: Integrated lambertson field(tesla·meter) to inject extract 150 GeV/c beam into 3 TeV/c ring for different cell parameters. The nominal beam displacement is 18 cm.

Therefore, the only matching requirement is that of the vertical dispersion function. A 4 mr bend unit is chosen because of the physical constrain of the permenant magnet. Before injection a pair of 16 mr bend are inserted into two half cells to give 32 mr kick with no dispersion function. Another 4 mr bend before injection and a 4 mr bend from lambertion complete the last 8 mr kick needed and results in zero final dispersion function. The bend arrangement is illustrated in Figure 3.

It is also possible to shorten the dispersion matching section by overlapping the 3-cell structure of 16 mr and 4 mr bends, if so needed.

5 Injection and extraction at 3 TeV

It is difficult at this stage to do more than estimate the requirements for the injection and extraction kickers and lambertson magnets. The nominal constraints include the following.

- Maximum β is 200 m.
- The cross section of combined function magnets is approximately 22 cm vertical by 30 cm horizontally.
- The working guess is that cross section of quadrupoles is about 30 cm by 30 cm.
- The injected beam is brought in vertically from above. Beam is extracted up.

The range of strengths required for the lambertson magnets is indicated in Table 4. These strengths are reasonable.

	ϕ [deg]			
β_{max} $[m]$	60	70	80	90
100	20.80	19.17	18.29	18.01
200	10.40	9.58	9.15	9.01
300	6.93	7.67	7.32	7.20

Table 4: Integrated lambertson field (tesla·meter) to inject (or extract) 3 TeV/c beam for different cell parameters. The nominal beam displacement is 18 cm.

Injection and extraction will most likely also require the use of a fast kicker magnet. Comparison with Table 4 suggests that kicker strengths would be reasonable provided that adequate space is allocated in the lattice for them.

REFERENCES

References

[1] Foster, G. W., Specialty Magnets for Pipetron Beam Transfers, unpublished working note.

Slow Extraction from the 3 TeV Injector for the VLHC

John Marriner
August 15, 1997

It has been proposed to build a 3 TeV injector for the VLHC on or near the Fermilab site. Such a machine could provide fixed target beams for physics both before and during the VLHC era. This note suggests possible parameters of the extraction system.

I have chosen to use 1/2 integer extraction with 0th harmonic octupoles. This scheme is used in the Tevatron. I chose it simply because I have the formulas handy. It may not be the best scheme. I chose the septum gap to be 6 mm and to assume that both the septum and the lambertson are placed at high beta locations (β=1200 m). The septum wires are placed at x_1=12 mm from the center of the aperture and the outside edge is therefore at x_2=12+6=18 mm. Assuming an aperture of 10 mm at β_{max} of a normal cell (β_{max} =300 m), the septum uses about 1/3 of the available aperture. This choice appears to allow sufficient space to develop the necessary step size as the septum is approached.

The VLHC injector parameters are pretty much up in the air. I have assumed the following:

Table I

Beam emittance (100%)		10 π	mm-mrad
Extraction Energy		3000	GeV
Beta at septum (β_s)		1200	m
Beta at lambertson (β_L)		1200	m
Aperture at β=300m		10	mm
Septum gap		6	mm
x_1	12		mm
x_2	18		mm

It can be shown that the extracted beam follows trajectories that circles in phase space. A possible trajectory for the extracted beam is shown in Figure 1. The radius of the circle describing the trajectory is

$$r_0^2 = -\frac{16\pi\Delta\nu}{3E}$$

where $\Delta\nu$ is the difference between the unperturbed tune and the nearest 1/2 integer (sometimes called the "tune defect") and where E is the strength of the 0th harmonic octupoles

$$E = \frac{\beta_s}{|B\rho|}\int_C \left[\frac{\beta(z)}{\beta_s}\right]^2 \frac{1}{6}\frac{d^3B}{dx^3}\cos[2\mu(z)]dz$$

The quantity k is defined as

$$k = \frac{q}{4\pi\Delta\nu}$$

where q is defined as the quadrupole fields that drive the 1/2 integer resonance.

$$q = \frac{1}{|B\rho|}\int_C \beta(z)\frac{dB}{dx}\cos[2\mu(z)]dz$$

It can be shown that the stable area is given by

$$\varepsilon_s = \frac{2\pi r_0^2}{\beta_s}\Gamma(k)$$

where

$$\Gamma(k) = \frac{2}{\pi}\left(\frac{1}{k}\sin^{-1}\sqrt{1-k} - \sqrt{k-k^2}\right)$$

and of course the stable area must be equal to the beam area to initiate the slow spill. The step size, the change in x per turn is given by:

$$\left.\frac{dx}{dn}\right|_{x=x_1} = 2\pi\Delta\nu p_1\left(-\frac{p_1^2 + x_1^2}{r_0^2} - k + 1\right)$$

where

$$p_1 = \sqrt{r_0^2 - \left(x_1^2 - x_c^2\right)}$$

and

$$x_c^2 = \frac{4q}{3|E|}.$$

It is desirable to have *dx/dn* large in order to obtain high efficiency, but it must be less than 1/2 the septum gap so that particles are not lost on the outside of the septum.

The following are the calculated results

Table II

k	0.840	
$\Delta\nu$	0.022	
$r0$	11.48	mm
x_c	10.52	mm
$2dx/dn$ at x_1=12 mm	6	mm
q	3.85	T
E	3.71×10^5	T/m^{-2}

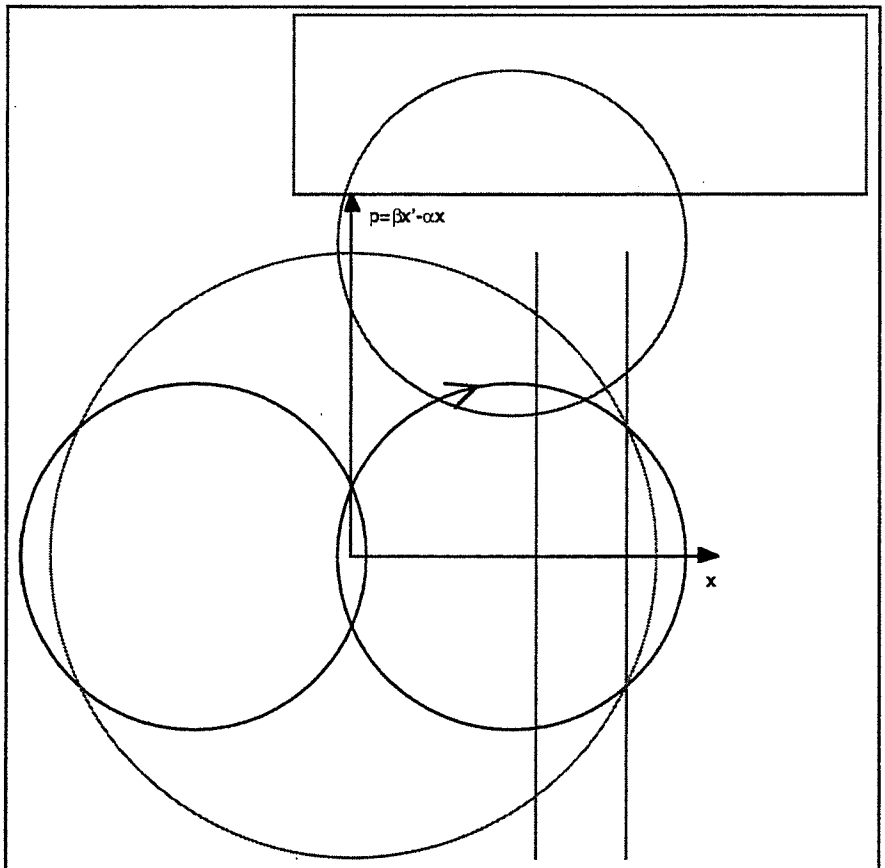

Figure 1. Schematic of the extraction scheme.

The strength of the quadrupoles required to drive the 1/2 integer resonance is very small. However, the octupole strength is substantial: equivalent to about 75 Tevatron spools. The requirements on the octupole strength could be reduced by chosing a different trajectory (with less curvature), but it doesn't seem like it is much of a problem to provide the octupole strength specified in Table II.

The step size as a function of x is shown in Figure 2. The density is equal to inverse of the step size and is shown in Figure 3. The density is approximately uniform over the septum gap and the extraction inefficiency is approximately the effective wire width divided by the septum gap. Assuming the wire width (25 μm) plus allignment tolerances lead to an effective width of 60 μm, the extraction efficiency would be 99%.

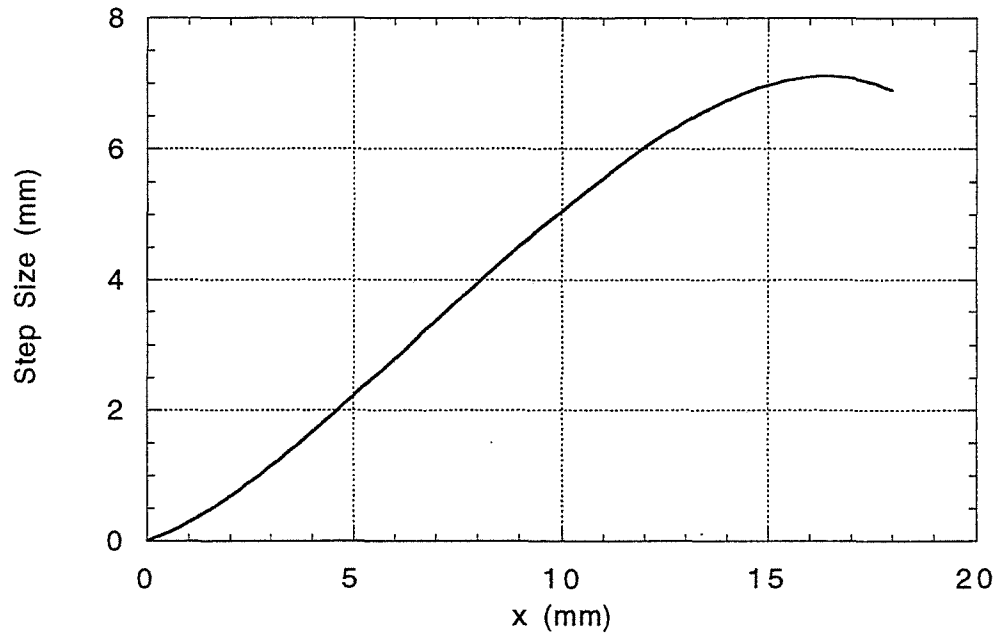

Figure 2. Step size versus horizontal position. The step size is the change in position after 2 turns.

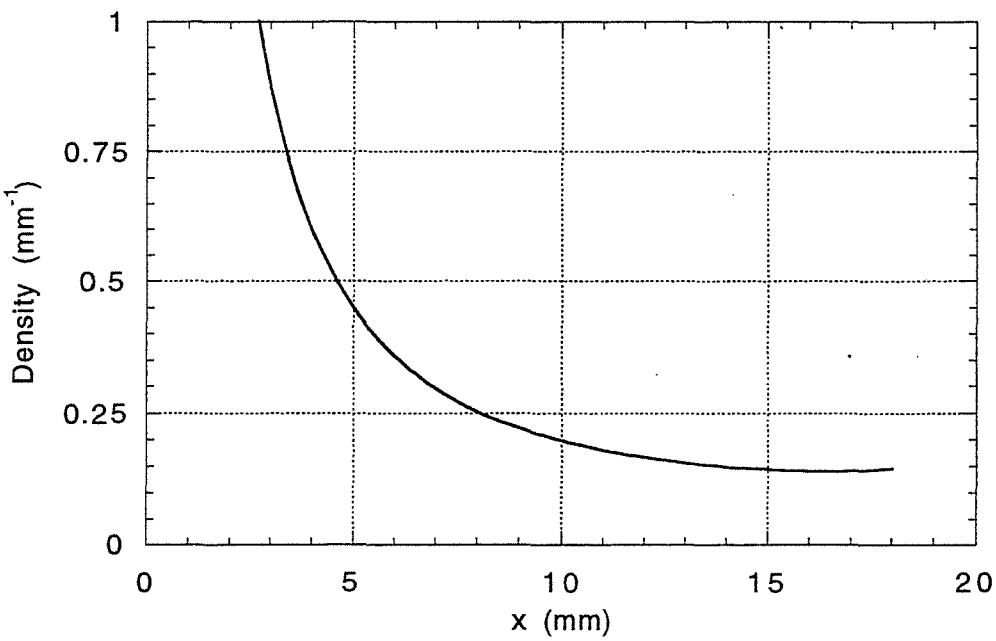

Figure 3. The relative density versus horizontal position at the septum. The density in the septum (12 to 18 mm) is approximately uniform.

Alignment Issues for the 3 TeV Ring
C. T. Murphy

Traditionally, separate function accelerators have always included a system of individually tunable correction dipoles, one at each quadrupole, to correct for the errors in quadrupole alignment, roll angle of the dipoles, and variations in the integral field of the dipoles. This note examines the possibility of doing without the correction dipoles, in the interest of economy, and instead realigning the quadrupoles rather frequently, based on an analysis of the beam orbit. This technique was in fact used for the Fermilab Main Ring, in which the correction dipoles were too weak to center the beam at 200 GeV. This realignment could be done in the customary manner or more inventively with a robot (an idea provided by Bill Foster), which would allow adjustments while beam was circulating, or at least without an access to the ring. Data is also presented on the rate at which the quadrupoles of several existing accelerators became misaligned.

Following the analysis and notation of Ref. [1], the maximum (98% probability) closed orbit distortion has been evaluated for assumed rms values of the misalignments. The analysis of Ref. [1] is based on the derivations of N. M. King [2] for a separate function machine; it is assumed that it would apply to a combined function machine to within a factor of two.

Let ΔQ_{rms} = the rms misalignment of the "quadrupoles" (the magnets in this case)

$\Delta B/B_{rms}$ = the rms variation of dipole field from magnet to magnet

$\Delta \Phi_{rms}$ = the rms roll angle of the dipoles

$\langle X\rangle_Q$, $\langle Y\rangle_Q$, $\langle X\rangle_B$, $\langle Y\rangle_\Phi$ = the maximum closed orbit distortions resulting from each of these misalignments.

For the values of the parameters, it has been assumed that:

ΔQ_{rms} = 0.1 mm (this has been achieved at LEP)

$\Delta B/B_{rms} = 2 \times 10^{-4}$ (from Bill Foster, achievable with magnet sorting)

$\Delta \Phi_{rms}$ = 0.17 mrad.

Of these parameters, the last one is the most questionable. It is derived assuming that the elevation of the left side of the magnet can be set to within 25 microns of the right side of the magnet - and that the mean magnetic plane of the magnet can be known that well relative to external fiducials. This parameter will need some R&D.

The equations of Ref. [1] also need some parameters of the ring, which are taken to be:

cell length = 172 m

number of dipoles per cell = 12

tune of machine = 33.18

phase advance per cell = 60°.

The resulting values of the maximum closed orbit distortions are:

$\langle X\rangle_Q = \langle Y\rangle_Q$ = 15 mm

$\langle X\rangle_B$ = 16 mm

$\langle Y\rangle_\Phi$ = 14 mm

which can be compared with the half widths of the vacuum tube, 15 x 9 mm. The conclusion is that at startup of the machine, one would probably not achieve a full turn of the beam before hitting the vacuum pipe. Either a few corrector magnets in each plane would be needed, or the

robot would have to make selected magnet realignments slightly upstream of the last place that the beam was lost. It appears very inefficient to send a crew into the ring to adjust magnets every time that the beam is lost at a new location.

It is also instructive to apply this same formalism to the Tevatron, where the misalignment parameters were well known at startup time and the initial tune-up is remembered The values of the parameters were:

$\Delta Q_{rmsH} = 0.56$ mm

$\Delta Q_{rmsV} = 0.30$ mm

$\Delta B/B_{rms} = 1 \times 10^{-3}$

$\Delta \Phi_{rms} = 0.28$ mrad.

The resulting values of the maximum closed orbit distortions are:

$\langle X \rangle_Q = 44$ mm

$\langle Y \rangle_Q = 23$ mm

$\langle X \rangle_B = 32$ mm

$\langle Y \rangle_\Phi = 9$ mm

which can be compared with the beam pipe radius of 32 mm. The following experiences are remembered from the first attempt to nurse the beam around the ring. After adjusting the first few correction dipoles in E-sector to compensate for injection errors, the beam went all the way from E15 to a beam dump at A0 (roughly one-third of the ring) without any correction dipoles. Later, when the rest of the ring had been installed and cooled, it took only a few correction dipoles to achieve the first complete turn.

In planning for how often it might be necessary to realign magnets, it is instructive to examine the rates at which the alignment of the SPS, the Tevatron, and LHC degenerated. In the SPS, which is the same size as the Main Ring but which is placed on bedrock ("molasse"), ΔQ_{rmsH} grew at the rate of 0.02 mm/yr over the course of 9 years, while ΔQ_{rmsV} grew at the rate of 0.05 mm/yr over a 4 year period. In the Tevatron, ΔQ_{rmsV} grew at the rate of 0.1 mm/yr in the first two years after the initial alignment, and then at a rate of 0.22 mm/yr in the next two years. The large difference between the SPS and Tevatron experience may be due to the fact that the Tevatron is placed on the glacial til (clay).

In LEP, which is also set in bedrock, but which crosses a fault line in Ferney-Voltaire and goes somewhat into the Jura mountains, ΔQ_{rmsV} grew at the rate of 0.14 mm/yr during the four years after initial alignment. This rms value is calculated after removing from the data two local "spikes" of 3 mm and 10 mm.

If the experience in the 3 TeV ring is comparable to that of LEP, and one wants to keep ΔQ_{rms} less than 0.025 mm relative to the initial beam-on alignment, then one would need to realign several times per year.

References:

1. C. Moore, C. T. Murphy, J. Norem, and M. Zisman, in "Accelerator Physics Issues for a Superconducting Super Collider", M. Tigner, ed. (Ann Arbor, 1983) 78.
2. N. M. King, in "Proceedings of the Second ICFA Workshop on Possibilities and Limitations of Accelerators and Detectors", U. Amaldi, ed. (Les Diablerets, 1979).

RF REQUIREMENTS FOR A 3 TEV COLLIDER RING

Ioanis Kourbanis

The purpose of this note is to investigate the possibility of using the existing Tevatron rf system in a large collider ring with injection momentum of 150 GeV/c and final momentum of 3 TeV/c. We are making the assumption that we will need to accelerate 860 proton bunches with 3×10^{11} ppb and 860 pbar bunches with 0.8E11 ppb. The bunch spacing is considered to be 132 nsec or 7 53 MHz bunches for a harmonic number of 6020. The collider ring is assumed to have a gamma-t of 35 and a radius R=5408.8 m resulting to a revolution frequency at injection of 8821.27 Hz.

TEV RF PARAMETERS

The Tev rf consists of a total of 8 cavities (4 for protons and 4 for pbars). A cavity consists of two quarter-wave resonators placed back to back with a coaxial drift tube separating the two accelerating gaps by π radians. Each cavity has a Q of ~7100, a shunt impedance of 1.2 $M\Omega$ and is capable of running cw with a peak accelerating voltage of 360 KV (1.44 MV total from 4 cavities). The rf power is supplied to each cavity by a 200 KW amplifier via a 9-3/16 inch copper transmission line. Cathode drive to the final Eimac Y567B tetrode is provided by a 14 tetrode cascode section. The amplifier and associated equipment reside in an equipment gallery above the beam enclosure. The cavities tune from 53,104,045 Hz at 150 GeV/c to 53,105,048 using a temperature control water system.

VLHC RF REQUIREMENTS

The rf system must in addition to creating bucket area, provide accelerating voltage and deliver energy to the beam. Here we assume that the collider proton and pbar bunches are formed through some form of coalescing in the collider injector and because of that a bucket area of at least 2 eV-sec is required. The accelerating voltage and power depend on the details of the rate of acceleration. In the example considered we assume a modified parabolic ramp with a total acceleration time of 500 sec. The momentum vs. time for that ramp is shown in Figure 1.

The accelerating rf voltage ($V\times\sin\phi_s$) required for the modified parabolic ramp considered is shown in Figure 2. The maximum accelerating voltage or energy gain per turn of 970kV per turn per proton is 1.36×10^{-9}Joules per second per proton or 353 W for 2.58×10^{14} protons (860 bunches$\times3\times10^{11}$ppb). This is the peak power which must be delivered to the proton beam by the (TeV) rf system. This power is to be delivered by all four cavities, i.e. each cavity must deliver 88.25kW. Assuming that each cavity is running at its maximum voltage of 360kV another 50kW of power is dissipated in each cavity. The total power required per cavity is 138.25kW which is less than the 200kW available from the power amplifier.

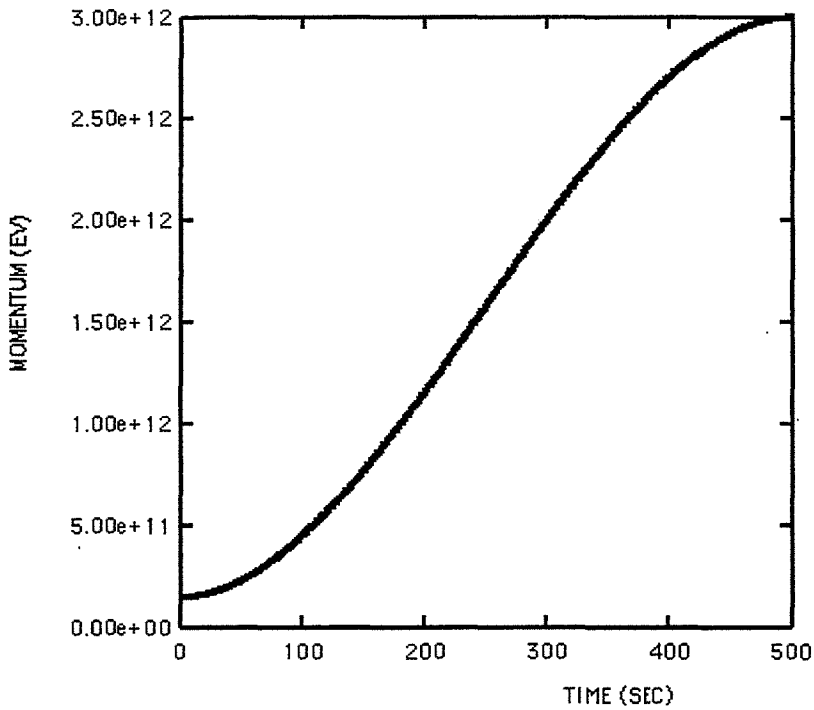

Figure 1: Momentum vs. time for the modified parabolic ramp.

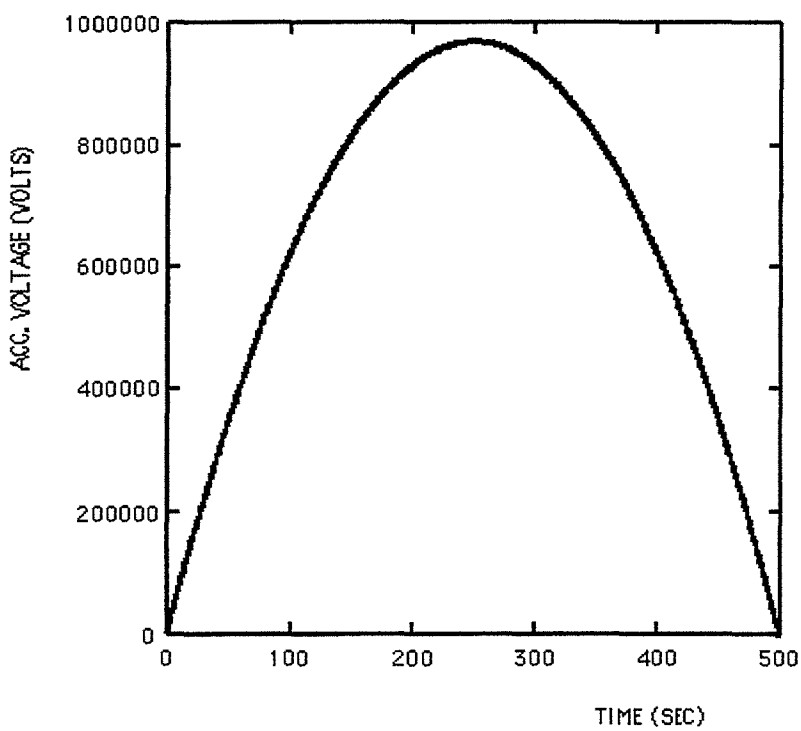

Figure 2: Accelerating voltage vs. time for the parabolic ramp.

Assuming a constant voltage of 1.44MV the bucket area available through the ramp is calculated. The results are plotted in Figure 3. As it can be seen from the figure the bucket area is always larger than the 2 eV-sec required. The synchronous phase angle ϕ_s is also calculated and is plotted in Figure 4.

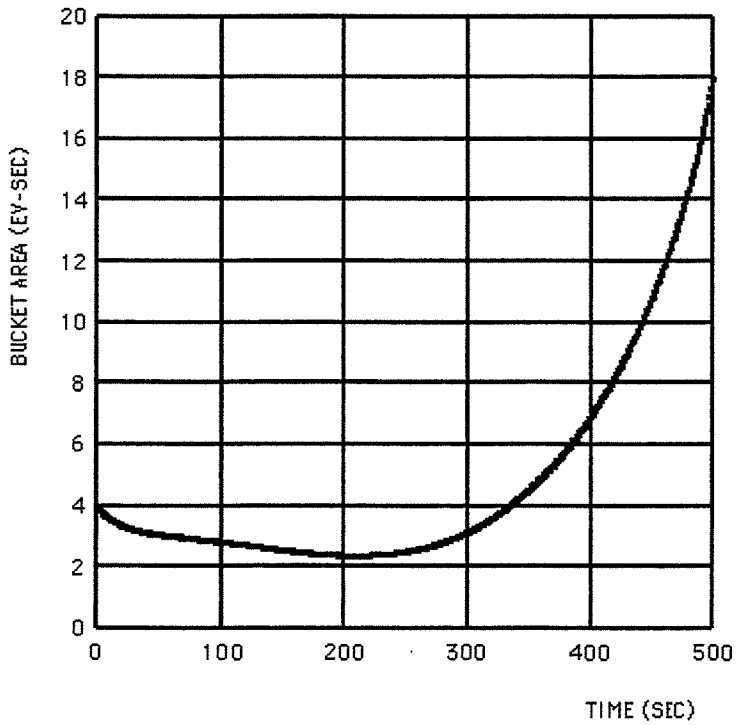

Figure 3: Bucket area vs. time for 1.44 MV rf voltage.

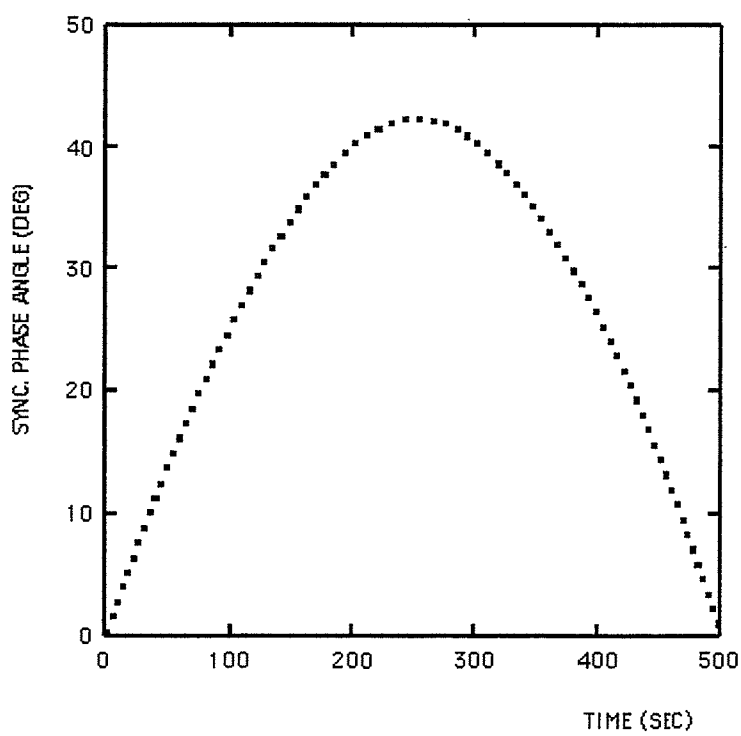

Figure 4: Synchronous phase angle ϕ_s vs. time for 1.44 MV rf voltage.

CONCLUSION

The TeV rf system can be used to accelerate up to 4.4×10^{14} protons (or pbars) in a 3 TeV collider with a 500 sec parabolic ramp, providing a bucket area larger than 2 eV-sec per bunch. Considering the fact that such a collider will be located very deep underground one might consider locating the cavities in a protective room in the tunnel itself. The replacement of the cascode drive section with a solid state amplifier will increase the reliability and will make that placement possible.

Beam Abort and Collimation for a 3×3 TeV Hadron Collider

A.I. Drozhdin and N.V. Mokhov

August 31, 1997

1 Beam Abort System

Design of a 3 TeV beam abort system follows the 3 TeV UNK abort system [1, 2] designed in IHEP (Protvino, Russia) a few years ago. The SSC and LHC experiences [3] are taken into account.

In a baseline case, a 3 TeV beam abort system is located in a special 800 m long straight section (Fig. 1). It consists of a kicker-magnet, two septum-magnets, and a set of bump-magnets. First septum-magnet has 1 mm thick septa and low field that allows to decrease a kicker strength. A thickness of the second septum-magnet increases from 5 to 20 mm with the magnetic field.

During the accelerator cycle the circulating beam is kept close to the extraction magnet septa by a set of bump-magnets. A kicker magnet is needed to put the beam into the septum aperture. To minimize the beam loss at the septa, the kicker rise time must be shorter than the distance between bunches. Fast ramping septum-magnets are used to decrease electric power. With a rise time of 350 μs one can extract the beam from the accelerator in 5 turns after the abort signal. One of the septum-magnet modules is on at injection. It gives a possibility to extract the beam over one turn and eliminate the accelerator component damage in a case of very fast instabilities at injection. The aperture of the septum-magnet should be large enough to extract the beam without losses over the machine cycle. The abort system magnet parameters are presented in Table 1.

A long distance between central quads is required to bypass the machine quadrupoles at extraction. It was found both in the SSC and LHC designs that to shorten the system, one can send the extracted beam through the beam pipe buried through the quadrupole yokes without deterioration of their performance. In the considered case it will decrease the straight section length from 800 m to about 400 m. Certainly, more studies are needed to investigate this possibility.

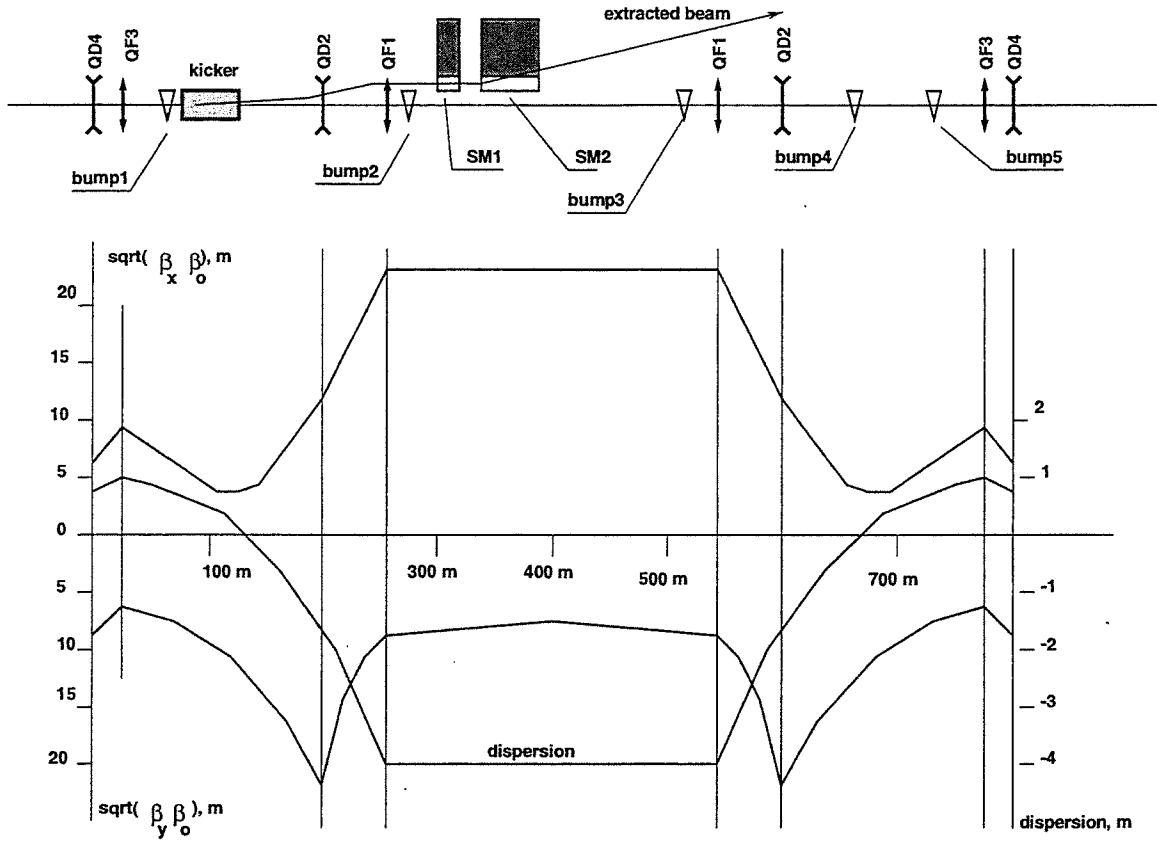

Figure 1: 3 TeV beam abort system layout.

2 Beam Collimation System

As in any other accelerator, some level of systematic beam loss is unavoidable in a 3 TeV machine certainly due to beam-gas scattering and slow diffusion processes (resonances, RF noise, ground motion, ...). This can cause quench of superconducting magnets, increased radiation levels and degradation of functional properties of the machine components. Significant fraction of beam loss can be localized in a few predetermined locations in the lattice with a dedicated beam cleaning system.

A two-stage beam collimation system can localize most of losses in the long straight section used for the abort system. System consists of a set of primary and secondary collimators (Fig. 2). A primary collimator, where a proton impact parameter is of the order of 1μm [7, 8], serves as a scattering target. As a result, the impact parameter on the thick downstream secondary collimators is drastically increased which results in significant increase of a scraping efficiency. Circulating beam is shaped in the horizontal and vertical plane by two separate primary collimators. A horizontal primary collimator is located upstream of the first thin septum-magnet of the abort system. A vertical

Table 1: Parameters of the abort system magnets.

Element	Length (m)	Magnetic field (T)
kicker	27	0.1
septum-magnet	9	0.1
septum-magnet	36	1.1
horizontal bump-magnet 1	2	1.2
horizontal bump-magnet 2	6	1.2
horizontal bump-magnet 3	6	1.2
horizontal bump-magnet 4	2	1.2
horizontal bump-magnet 5	2	1.2
vertical bump-magnet 1	3	1.2
vertical bump-magnet 2	12	1.2
vertical bump-magnet 3	15	1.2
vertical bump-magnet 4	15	1.2
vertical bump-magnet 5	6	1.2

primary collimator is placed downstream of the QD2 quadrupole at the beginning of the long drift. The primary collimators define the accelerator aperture at 6σ of the circulating beam in both directions.

Our studies show that at 3 TeV, a 5-mm thick tungsten target positioned at 6σ from the beam axis in both vertical and horizontal planes is a good choice. An optimal length of stainless steel secondary collimator is about 2 m. Each of them consists of a movable L-shaped jaw positioned at about 7σ from the beam axis in horizontal or vertical plane. The collimators are aligned parallel to the envelope of the circulating beam. A set of vertical and horizontal bump-magnets is used to keep the beam at the distance of 7σ from the secondary collimator jaws and to move the neutral and photon flux out of the superconducting coils.

3 Accidental Loss

A prefire of a single module of the abort kicker will result in a high amplitude coherent betatron oscillations of the beam. The disturbed beam can then hit a collimator jaw or other limiting aperture resulting in a significant component overheating or even damage. In a worst case, when a module prefire takes place just after the longitudinal abort gap, one needs to wait for the whole turn to extract the beam. For the SSC, two ways have been proposed [6] to mitigate the problem:

- start abort after a module prefire as soon as possible without synchronization with abort gap (asynchronous firing of beam abort kicker);

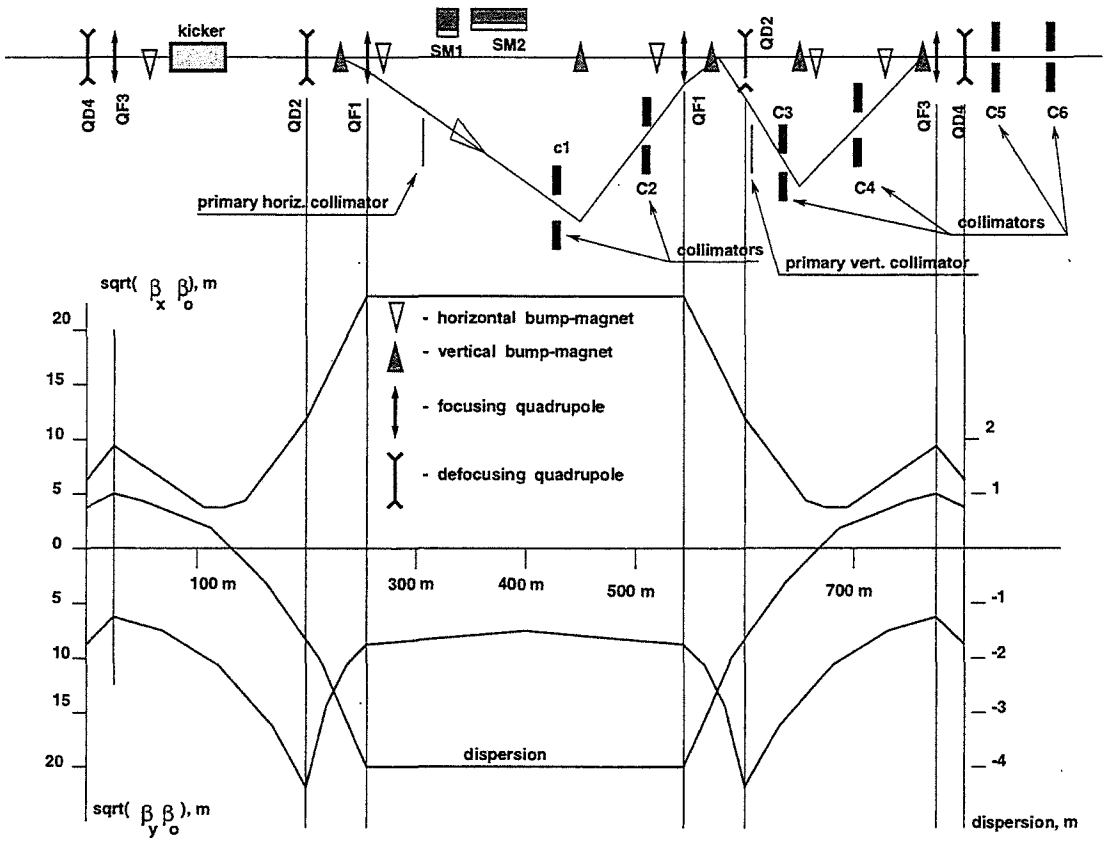

Figure 2: Beam collimation system layout.

- compensate a prefired module by a special module with the opposite magnetic field (antikicker). In this case the beam abort can be safely delayed until the gap comes, thus eliminating beam loss during the kicker rise time. The amount of beam loss depends on the delay between the moment of prefire and antikicker start.

The machine injection kicker misfire and prefire results in a coherent betatron oscillation of injected portion of the beam with pretty large amplitude causing the same problems [6] at injection. An asynchronous firing of the beam abort and beam injection kickers will spray the beam across the accelerator aperture (Fig. 3). Number of particles sprayed by the abort kicker is equal to $(\Delta t \times I)/t$. Here Δt - kicker rise time, T - revolution time, I - beam intensity. About half of this intensity will be sprayed across the abort beam line, and another half will come to the primary collimator (Fig. 3). Shadows (spoilers) can be used to protect collimators against overheating and damage. Pyrolytic graphite can be used as a material for shadows. This material can tolerate a temperature rise of 2500^oC before fracture. It can be coated with a

conductive material to reduce the resistive wall wakes.

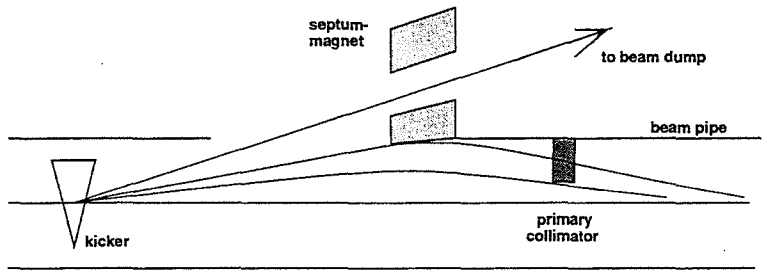

Figure 3: Asynchronous firing of beam abort kicker.

References

[1] I.S. Baishev, V.N. Chepegin, A.I. Drozhdin, Yu.S. Fedotov et al., Protection of Superconducting Magnets Against Irradiation. Proceedings of XIV International Particle Accelerator Conference, Tsukuba, Japan, 1989, part III, p.667.

[2] A.I.Drozhdin, Yu.S.Fedotov, M.A.Maslov, N.V.Mokhov, I.A.Yazynin. Calculation of losses and Protection Against Irradiation During Beam Abort and Loss Localization in the UNK. Proceedings of XIII Particle Accelerator Conference, Chicago, Illinois, 1989, v.1,p.255.

[3] The Large Hadron Collider, Conceptual Design, CERN/AC/95-05(LHC) October 20, 1995.

[4] I.Baishev, A.Drozhdin, N.Mokhov. STRUCT Program User's Reference Manuel. SSC-MAN-0034, February 1994.

[5] N.V.Mokhov, The MARS Code System User's Guide, Version 13(95), Fermilab-FN-628(1995).

[6] A.Drozhdin, N.Mokhov, B.Parker, Accidental Beam Loss in Superconducting Accelerators: Simulations, Consequences of Accidents and Protective Measures, SSCL-Preprint-556, February 1994.

[7] T.Risselada, The Effect of the Betatron Tune on the Impact Parameter at LHC Primary Collimators, CERN SL/Note 92-16(AP) (1992).

[8] M.Sidel, Determination of Diffusion Rates in the Proton Beam Halo of HERA, DESY-HERA 93-04 (1993).

BEAM ABORT FOR A 50×50 TEV HADRON COLLIDER

A.I. Drozhdin, N.V. Mokhov, C.T. Murphy and S. Pruss

July 25, 1997

0.1 Introduction

As currently designed, the low-field version of the VLHC has 1.12×10^{15} protons circulating at 50 TeV in each beam, i.e., 9 GJ per beam. This beam energy is equivalent to about 2000 kg of TNT. That is enough energy to cause severe damage to the machine and environment. The beams have sizes (sigma) of typically 0.07 mm in the arcs and 0.14 mm at the center of a utility straight (assuming a normalized emittance of 1π mm-mrad). Obviously, if such a beam goes astray, it will melt a hole through a magnet and do further damage outside the machine. The requirements for the reliability of a one-turn extraction mechanism are orders-of-magnitude greater than for the Tevatron, where a misfired extraction kicker magnet only causes a quench of the machine.

It turns out to be quite straight forward to kick the beams out of the machine towards absorbers. A scaled-up version of the LHC extraction beam lines calls for a mere 5 to 10 m of kicker magnets. The major difficulty lies in making the beams big enough that they will not crack a graphite absorber or reduce an air absorber to a vacuum in the center of the beam.

0.2 Beam Abort System

Like the Tevatron and the SSC, the LHC design uses fast kicker magnets to switch the circulating beam into the other aperture of Lambertson magnets. Unlike the Tevatron and the SSC, the circulating beam goes through the field-free hole in the Lambertson magnets, and the extracted beam is bent upward in the Lambertson magnets so as to clear the first quadrupole in the downstream half of the straight section. The total length of the straight section is 526 m. We have taken the length of the VLHC straight to be 2000 m. To scale the LHC straight section to the vLHC, we simply multiplied all the magnet spacings by the factor 2000/526. This leads to a layout for the RLHC straight section shown in Fig. 1. The values of β_{min} and the positions of the β_{min} in the horizontal and vertical planes were scaled up by the same factor, so that β_{min}=910 m in both planes for the VLHC. These are needed to calculate the effect of blow-up quadrupoles in the extraction line.

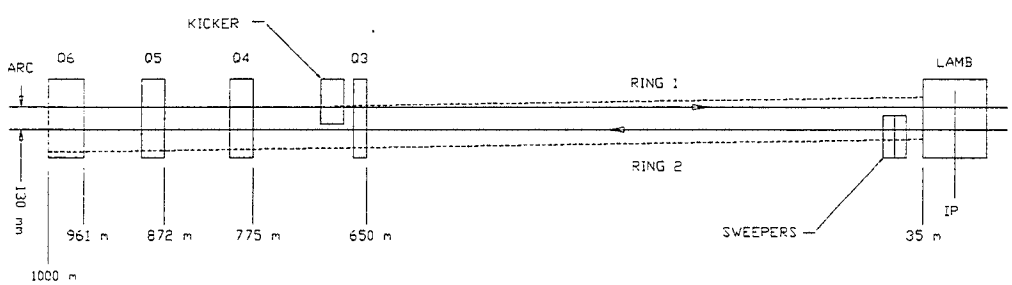

FIGURE 1 VLHC utility straight. The dashed lines are the extracted beams.

Fast kicker magnets located between Q3 and Q4 are used to kick the beams in one turn towards the magnetic aperture of the dual-bore Lambertson magnets. In the LHC, the separation of the circulating and extracted beams is 70 mm at the entrance to the Lambertson magnets; we have reduced that value to 25 mm, the value used at both the Tevatron and the SSC. The value needed is dependent on the beam size at injection at the Lambertson magnets. If the kicker magnets are placed close to Q3, 9.6 m of magnetic length are needed operating at the usual 0.6 T (the value assumed by both LHC and SSC). If the kickers are placed close to Q4, then Q3 gives an additional bend in the correct direction, and only 3.9 m of kickers are needed. Note that the LHC requires 14 m of kicker magnets.

The Lambertson magnets must bend the beam up sufficiently to clear Q3 in the downstream half of the straight section. In the absense of a real design for the VLHC quadrupoles, we have taken Q3 to have the same outside radius as the LHC Q3, reduced by half the difference in the beam separations in the two machines, so the radius is 200 mm. We then assume that the extracted beam must clear Q3 by 30 mm. The magnetic length of the Lambertson magnets, operating at 1 T, necessary for this clearance is 57.5 m. Note that the LHC requires 60 m.

0.3 Graphite Absorber

The first absorber considered was the standard Tevatron type graphite-core absorber, followed by aluminum with water cooling, followed by adequate steel to satisfy groundwater activation considerations. In order to determine the graphite dimensions and beam size necessary to contain the showers without cracking the graphite, shower development and energy deposition were simulated with the MARS13 code (Fig. 2).

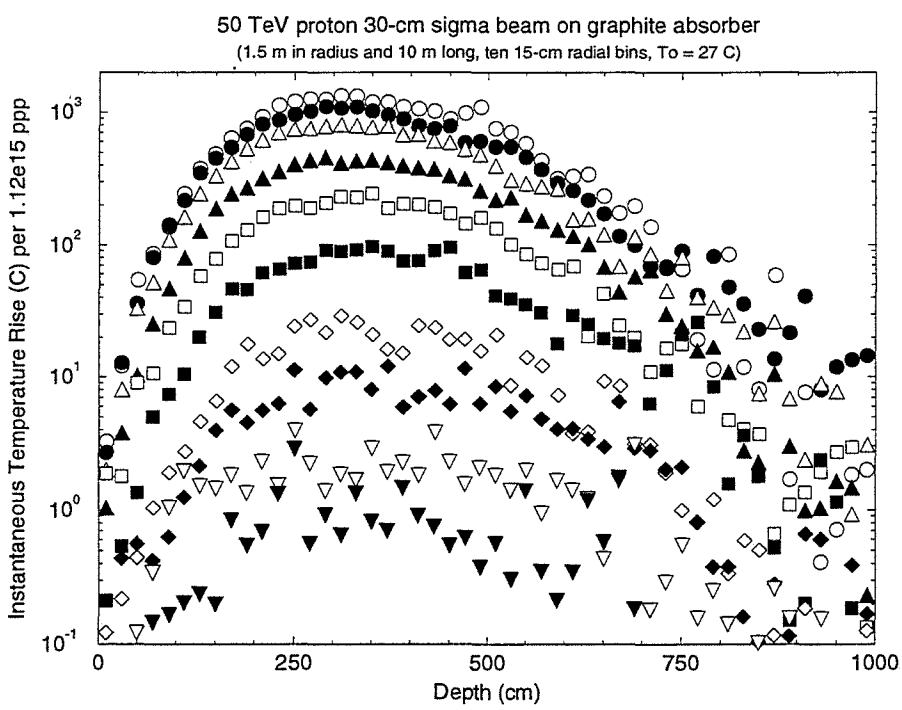

FIGURE 2 Temperature profile in VLHC grahite absorber.

The design goal was to keep the maximum temperature rise at the axis of the graphite core per spill below 1300-1500 deg-C (Tevatron experience and shock-wave considerations). It was found that the graphite would need to be 10 m long and 1.5 m in radius. For a beam spill that is stationary in transverse position, the beam sigma would need to be 30 cm in both x and y for the maximum temperature rise in the core of 1330 deg-C. Expanding the beams to this size with blow-up quadrupoles is out of the question.

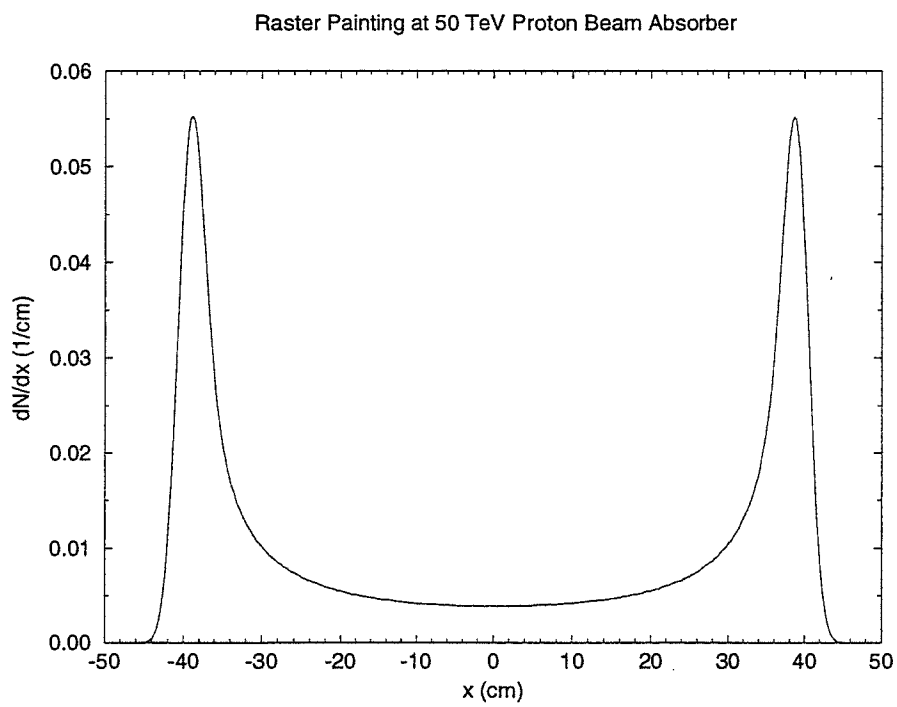

FIGURE 3 Raster painting at VLHC beam absorber.

We immediately switched to the scheme studied by the SSC in which the beam size is effectively enlarged by sweeping the beam across the face of a square absorber in a zig-zag pattern during the 1.8 ms spill time (Fig. 3). A vertical kicker sweeps the beam linearly from y = 40 cm to y = -40 cm, and a horizontal sweeper oscillates back and forth ±40 cm many times during the spill. To keep the frequency of the horizontal sweeper at a reasonable value of 7.5 kHz, the beam sigma needs to be 1.5 cm. This scheme was also simulated with MARS13. In this case the graphite is rectangular, with

dimensions 10×2×2 m. The temperature rise is quite low at the center of the absorber (300 deg-C), but there is a pile-up at x = ±39 cm as the oscillating horizontal sweeper reverses the direction of the sweep, and the temperature reaches 3300 deg-C. In principle, the best graphites survive at such a temperature, but the design goal for conventional pyrolitic graphites is not met. Either the sweep length needs to be increased to ±60 cm or a more complicated sweeping pattern needs to be explored.

Another sweeping scheme conceived by the SSC and LHC is a spiral sweep. A horizontal and a vertical sweeper, 90 deg out of phase, would both oscillate with decaying amplitudes. Of course, the frequency would have to increase as the radius of the spiral decreased in order to keep the temperature rise constant, which is not easy to achieve. A suitable compromise is to limit the inner radius of the spiral to half that of the outer radius and accept a factor two higher temperature rise at the inner radius. A hand calculation indicates that an outer radius of 30 cm would be adequate to keep the temperature below 1500 deg-C. If the beam sigma was 0.5 cm in both planes, the frequency of these sweepers would be 9.7 kHz.

0.4 Air Absorber

A different idea which has been explored is to use a long tunnel of air as the primary core of the absorber. Here the principal problem is that a narrow beam will expand the air to create a partial vacuum, leaving a hole all the way to the end of the tunnel. To keep the air pressure at the center at half an atmosphere, the temperature rise must be limited to twice room temperature, or 300 deg-C. Again, MARS13 was used to simulate this case. It was found that the beam sigma incident on the air must be 1.5 cm and that the air absorber needs to be 5000 to 6000 m long and 1 to 2 m flared in radius. Fig. 4 shows the energy deposition density as a function of the distance along the air core for various radial annuli. Peak energy deposition drops rapidly with beam size (Fig. 5).

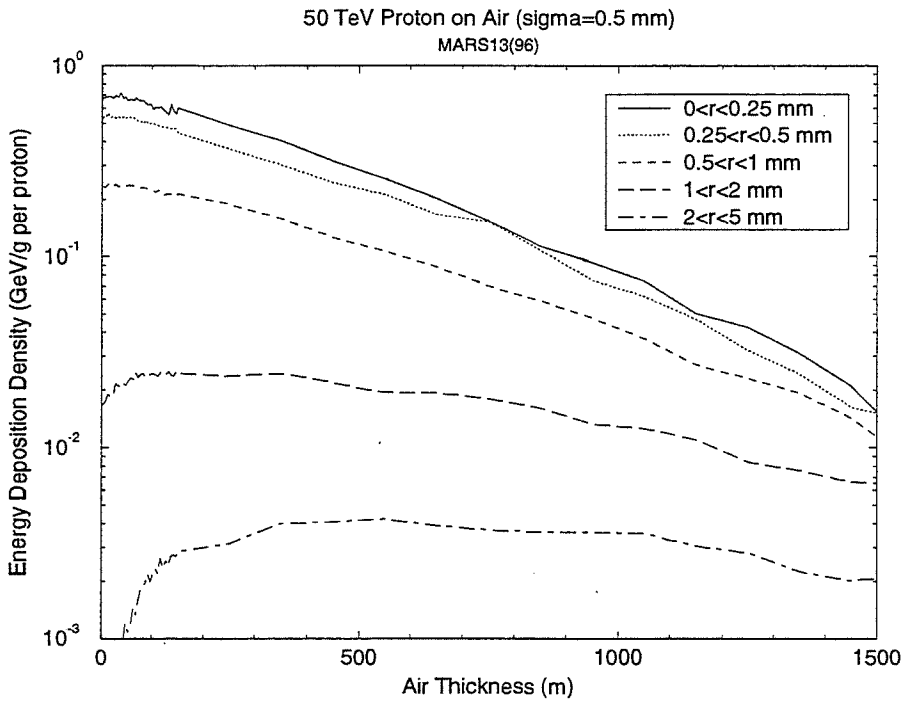

FIGURE 4 Energy deposition as a function of distance in VLHC air absorber.

The air core serves two functions. Some of the beam interacts inelastically with the air and distributes some radioactivity, very dilutely, along the tunnel wall. Secondly, the air multiple scatters the beam until the beam size is large enough to be absorbed on a standard graphite absorber. A graphite absorber is needed at the end of the tunnel of length 5 m and radius 2 m. Radionuclide production in air is mitigated via dilution with an appropriate ventilation scheme. Depending on the site, groundwater activation may or may not be a problem. In the first case it is solved via standard thin concrete or isolated rock layer around the extraction tunnel.

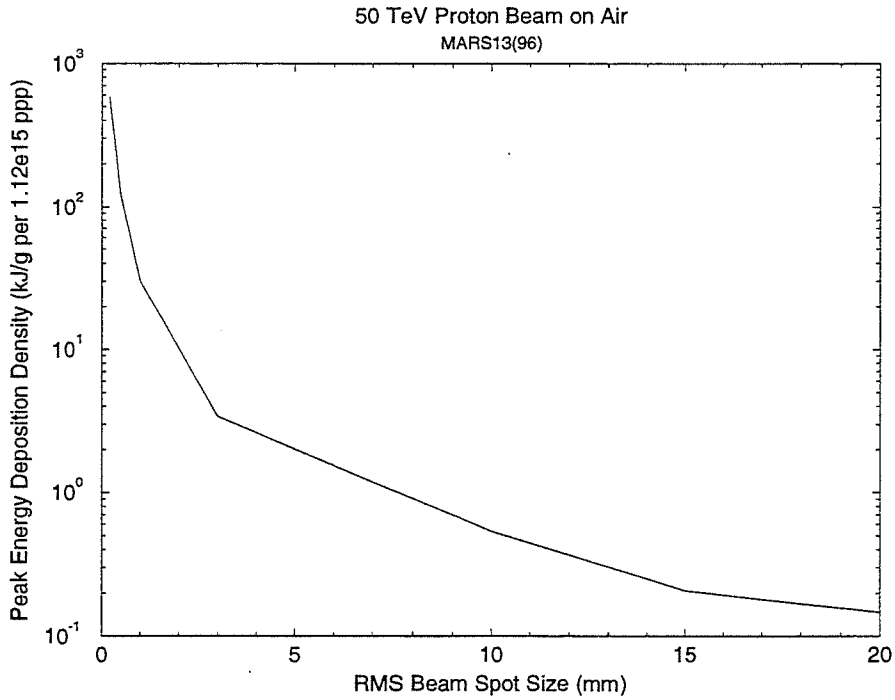

FIGURE 5 Peak energy deposition in air at 50 TeV *vs* beam RMS spot size.

0.5 Vacuum Window

Another thermal consideration which must be kept in mind is that a thin titanium vacuum window in the extracted beam line will melt, just from dE/dx, if the beam sigma is less than 0.5 cm. This condition is automatically met if the first windows encountered by the beams are just before the absorber. The beam sigma must be 1.5 cm for the air core absorber, and the spiral sweep spreads the beam over 30 cm for the graphite absorber.

0.6 Elements to shape the beams

In the above schemes, the beam sigmas need to be enlarged from their values of 0.14 mm at the center of the straight section to 5 mm or 15 mm at the absorber, which must be done with a singlet quadrupole in the extracted line.

0.8 Conclusions

We have shown that it is not difficult to kick the beams out of the tunnel towards absorbers. The minimum requirement is 4 m of fast kicker magnets in each beam, 57 m of Lambertson magnets, 50 m of blow-up quadrupoles, and 3000 m between the center of the straight section and the absorber. Two absorber schemes have been proposed. One uses a graphite core as the principal absorber and requires 37 m of fast sweeper magnets in each line to spread the beams out over the face of the graphite. The other uses air as the principal absorber, does not require fast sweeping, but needs an extra 8000 m of tunnel. If the extra tunnel costs about the same as sweeper magnets (our guestimate), then reliability would indicate that the air absorber is the favored choice. The failure of one of the two sweeper firing circuits would destroy the graphite absorber.

There are only two serious failure modes which would destroy part of the accelerator. The first is the failure of one of the many kickers to discharge during a requested extraction of the beams. This can be accommodated by making the aperture of the extraction line sufficient to tolerate the loss of one kicker. The other is more serious, the firing of one of the many kickers at some random time (this happens routinely in the Tevatron). Composite graphite shadow septa and collimators upstream of all the limiting apertures is the way to protect the machine components against beam-induced destruction. More work is obviously needed to explore all these possibilities.

Transverse Resistive Wall Instability in a Very Large Hadron Collider

Jean-François Ostiguy
Beam Physics Department
Fermilab

Revision 1

Abstract

Recently, the concept of a very large, low field (2T) 50 TeV hadron collider has received some attention. At the Snowmass 1996 meeting, a number of technical issues associated with very large machines have been identified. Two instabilities appear potentially serious: the transverse coupled bunch instability and the transverse mode-coupling single bunch instability (TMCI). In both cases, the instability is driven by the resistive component of the vacuum pipe "wall" impedance, which normally scales like $\rho^{1/2}R^{3/2}b^{-3}$ where ρ is the wall resistivity, R is the machine radius and b is the beam pipe radius. Because the revolution frequency of a very large machine is so low, the beam pipe is not thick enough to contain all the electromagnetic fields induced by the beam. Magnetic field leaking out of the beam tube may have a significant impact on the the wall impedance, in particular in presence of conventional iron pole pieces; reliable estimates must be obtained in that situation.

In this note, we briefly outline standard transverse resistive wall instability theory and discuss the special problems posed by very large machines. We also present numerical computations of the wall impedance at low frequency and compare the results to theoretical predictions. All computations are performed with a low frequency eddy current code since standard accelerator impedance and wakefield codes (e.g. MAFIA) currently do not deal with situations where fields are not confined inside the beam pipe.

Introduction

Recently, the concept of a very large, low field (2T) 50 TeV hadron collider has received some attention. At the Snowmass 1996 meeting, a number of technical issues associated with new generation, very large machines have been identified. Two instabilities appear potentially serious [1]: the transverse coupled bunch instability and the transverse mode-coupling single bunch instability (TMCI). In both cases, the instability is driven by the resistive component of the vacuum pipe wall impedance, which is expected to scale like $\rho^{1/2}R^{3/2}b^{-3}$ where ρ is the wall resistivity and R, b are respectively the machine and the beam pipe radius.

Transverse Resistive Wall Instability in a Very Large Hadron Collider

Jean-François Ostiguy
Beam Physics Department
Fermilab

Revision 1

Abstract

Recently, the concept of a very large, low field (2T) 50 TeV hadron collider has received some attention. At the Snowmass 1996 meeting, a number of technical issues associated with very large machines have been identified. Two instabilities appear potentially serious: the transverse coupled bunch instability and the transverse mode-coupling single bunch instability (TMCI). In both cases, the instability is driven by the resistive component of the vacuum pipe "wall" impedance, which normally scales like $\rho^{1/2}R^{3/2}b^{-3}$ where ρ is the wall resistivity, R is the machine radius and b is the beam pipe radius. Because the revolution frequency of a very large machine is so low, the beam pipe is not thick enough to contain all the electromagnetic fields induced by the beam. Magnetic field leaking out of the beam tube may have a significant impact on the the wall impedance, in particular in presence of conventional iron pole pieces; reliable estimates must be obtained in that situation.

In this note, we briefly outline standard transverse resistive wall instability theory and discuss the special problems posed by very large machines. We also present numerical computations of the wall impedance at low frequency and compare the results to theoretical predictions. All computations are performed with a low frequency eddy current code since standard accelerator impedance and wakefield codes (e.g. MAFIA) currently do not deal with situations where fields are not confined inside the beam pipe.

Introduction

Recently, the concept of a very large, low field (2T) 50 TeV hadron collider has received some attention. At the Snowmass 1996 meeting, a number of technical issues associated with new generation, very large machines have been identified. Two instabilities appear potentially serious [1]: the transverse coupled bunch instability and the transverse mode-coupling single bunch instability (TMCI). In both cases, the instability is driven by the resistive component of the vacuum pipe wall impedance, which is expected to scale like $\rho^{1/2}R^{3/2}b^{-3}$ where ρ is the wall resistivity and R, b are respectively the machine and the beam pipe radius.

For reference, a 50 TeV low field (2T) ring would have a circumference of approximately 600 km, with a corresponding revolution period of 2 ms ($f \simeq 500$ Hz). A 3 TeV injector ring would have a circumference of 30 km and a revolution frequency $f \simeq 3$ kHz. It interesting to note in passing that a 50 TeV collider would probably have to support 100,000 bunches in order to keep the number of interactions per crossing within reasonable limits !

Instability growth rates predictions (such as those made in reference [1]) are based on an established frequency domain formalism used to assess beam stability in circular high energy accelerators. The fundamental underlying assumption is that the *revolution frequency is constant*, or at least, that it does not change significantly on a time scale set by the revolution period. In principle, the formalism imposes no restriction on the magnitude of the predicted growth rates with respect the the rotation frequency. In practice, one often deals with a combination of continuously distributed impedances (e.g. beam pipe wall) and spatially concentrated impedances (e.g. accelerating cavities). To simplify calculations, all impedances along the machine circumference are often lumped together. Clearly, this approximation is valid as long as the predicted growth times remain smaller than a revolution period. When that is not case, the growth rate predictions are clearly not reliable in a absolute sense. Since one is generally concerned primarily by the conditions that render the beam unstable i.e. whether or not the growth rate is positive for a certain impedance, from a practical standpoint it is acceptable to continue to use lumped impedance predictions even when the assumptions under which they are based are not strictly valid.

Assuming a copper or aluminum vacuum tube at room temperature, the predicted growth time for the coupled bunch transverse resistive wall instability in a 50 TeV low field ring is on the order of a third of a turn. Active feedback is considered manageable if the growth rate of the instability is small enough that the damper can act over several turns; if that is not the case, bunch-by-bunch correction is necessary. This requires very large bandwidth electronics that is currently beyond the state-of-the-art. Although some [2] believe that active feedback damping system is technically feasible for the VLHC, it remains vital to minimize the potential for instability as much as possible.

Aluminum and copper are very good conductors, relatively cheap and mechanically easy to deal with; little would be gained by using silver, the best known conductor. One option would be cooling to very low temperatures (< 77) K [1]; this is impractical for machines based on conventional magnet technology. The resistive wall effects can certainly be mitigated by increasing the beam pipe radius; unfortunately, this has a significant impact on magnet size, and ultimately, on overall costs.

For very large machines, an additional factor must be taken into account: the beam pipe may not be thick enough to confine all the low frequency electromagnetic fields induced by the beam inside the pipe. In a machine based on iron-dominated magnet technology, this can have a significant impact on the "wall" impedance because of the proximity of iron pole pieces.

At this preliminary stage, one must be cautious with "standard" results based on approximations that may not be appropriate for very large machines. It is also clear that a

[1] While Al and Cu are not superconducting, their resistivity is considerably lower at low temperatures because it is impurity and imperfection dominated rather than phonon dominated.

reliable way of predicting low frequency impedance must be established and validated. In this note, we briefly outline the standard transverse resistive wall instability theory. We then present numerical calculations of wall impedance at very low frequency and compare the results to theoretical predictions.

Transverse Resistive Wall Instability

The transverse resistive wall instability theory was initially developed by Laslett, Neil and Sessler [3]. The basic mechanism is as follows: a small transverse oscillation is initiated, possibly by noise. This oscillation induces a reaction of the charges inside the vacuum chamber walls; these charges in turn produce alternating electromagnetic fields which act back on the beam. For a highly relativistic beam in a perfectly conducting circular vacuum chamber, the reaction forces are parallel to and essentially in quadrature with the transverse velocity of the beam and there is no instability. Finite conductivity of the vacuum pipe introduces a small force component in phase with the transverse velocity. This component acts on the amplitude of the oscillations and under certain conditions, can lead to instability.

Unbunched Beam

The force on a particle of charge e is given by the Lorentz relation

$$\mathbf{F} = e[\mathbf{E} + c\vec{\beta} \times \mathbf{B}] \tag{1}$$

In the present context, $\mathbf{E}$ and $\mathbf{B}$ are the resultant of the beam self and induced fields. Assume that $\mathbf{E}_1$,$\mathbf{B}_1$ represent respectively the electric and magnetic fields in presence of a perfectly conducting beam pipe and $\mathbf{E}_2$,$\mathbf{B}_2$ the perturbations introduced when the conductivity is large but finite. To a good approximation, the perturbation $\mathbf{E}_2$ is tangent to the wall surface and equal to the product of the unperturbed wall current $\hat{\mathbf{n}} \times \mathbf{H}_1 = \hat{\mathbf{n}} \times (\mathbf{B}_1/\mu)$ and the surface impedance. The (transverse) field $\mathbf{B}_2$ is determined by requiring that consistency with Maxwell's equations be preserved. For small displacements the net *transverse* force on a particle with transverse (vertical) position y has a single component

$$F_y(y,\bar{y}) = e\left\{[E_{1y}(y) - c\beta(B_{1x}(y)] + [-c\beta(B_{2x}(y,\bar{y})]\right\} \tag{2}$$

where $\bar{y}$ is the average transverse position of the beam. The first term in rectangular brackets in (2) represents the beam self-force. For a uniform, round beam at the center of a circular pipe, it is easy to show that

$$e\left[E_{1y}(y) - c\beta B_{1x}(y)\right] = \frac{eE_{1y}(y)}{\gamma^2} \tag{3}$$

$B_{2x}(\bar{y})$, is caused by the environment reaction and scales linearly with the *average* vertical beam displacement $\bar{y}$. E_{2y} is generally small and can usually be neglected. The

expression (3) can be seen as a particular case of the general linear approximation for the force experienced by a particle at position y:

$$F_y(y,\bar{y}) \simeq \left[\frac{\partial F_y}{\partial y}\right]_{\bar{y}=0} y + \left[\frac{\partial F_y}{\partial \bar{y}}\right]_{y=0} \bar{y} \tag{4}$$

In a circular accelerator, frequency and position measurements are usually made at fixed azimuth; it is therefore practical to see both field and transverse position as functions of the time t and azimuth θ. Fourier transforming with respect to θ and t, one can express the transverse force F_y as follows [2]

$$F_y(t,\theta) = \sum_{\ell=-\infty}^{\infty} \int_{-\infty}^{\infty} F_y(\omega,\ell)\, e^{j(\omega t - \ell\theta)}\, d\omega \tag{5}$$

where we have made use of the fact that any instant t, the beam charge distribution around the ring is spatially periodic. Let

$$\theta = \Omega(p)t = \Omega t \tag{6}$$

where Ω is the revolution frequency of particles of momentum p. Note that in the present context, θ represents the azimuthal coordinate around the ring, *not* the azimuthal position of a specific particle. For $\beta \to 1$, we shall see that the effect of the field produced by a point charge on a test particle located at a distance Δs behind it depends exclusively on the distance Δs between the two charges, or equivalently, on the time interval $\Delta t = \Delta s/c$. Under these conditions, it is convenient to introduce the impedance per unit length $Z_\perp(\omega)$

$$Z_\perp = -\frac{F_\perp}{jI(\omega)y} \tag{7}$$

In this expression, $I(\omega)$ is the *longitudinal* beam current and δy is the tranverse beam offset. The definition is formally similar to that of the longitudinal impedance in terms of the *longitudinal* beam current. The factor j appears in the denominator because the *tranverse* "current" is proportional to $\frac{d\Delta y}{dt}$ and the Fourier transform of the time derivative of a function $f(t)$ is $j\omega f(\omega)$. With the above definition, the transverse impedance *per unit length* is, in the frequency domain [3]:

$$Z_\perp(\omega - \ell\Omega) = -\frac{1}{j}\frac{F_y(\omega,\ell)}{\beta c e^2 Y(\omega,\ell)} \tag{8}$$

In the early literature, before the formulation in terms of impedance became popular, the transverse force arising from resistive wall effects is sometimes expressed in terms of the (real) dimensionless parameters U and V which are, clearly, closely related to the impedance:

$$F_y(\omega,\ell) = 2\gamma m_0 \Omega[U(\omega - \ell\Omega) + (1+j)V(\omega - \ell\Omega)]Y(\omega,\ell) \tag{9}$$

[2] We use the convention $F(\omega) = \int_{-\infty}^{\infty} f(t) e^{-j\omega t}\, dt$ and $f(t) = \frac{1}{2\pi}\int_{-\infty}^{\infty} F(\omega) e^{j\omega t}\, d\omega$ for harmonic varying quantities. The literature is unfortunately inconsistent on that point.

[3] Equation is actually a simplification in the sense that the total transverse force depends not only the dipole moment of the beam distribution but also on higher order moments. Higher moment contributions are usually negligible for small transverse displacements and are generally ignored.

Assuming that f is the force induced by coherent motion of the beam, the equation of motion for the transverse position y of a filament beam uniformly populated in betatron phase with particles of momentum p is

$$m_0\gamma\left[\ddot{y}+\omega_\beta^2 y\right]=f(t,\theta(t)) \tag{10}$$

where both y and f are to be regarded as functions of time and azimuth. Assuming periodicity in θ and considering separately the Fourier coefficient of each azimuthal harmonic ℓ yields

$$\left[\omega_\beta^2-(\omega-\ell\Omega)^2\right]Y(\omega,\ell) = \frac{e\beta I Z_\perp}{j\gamma m_0}\bar{Y}(\omega,\ell) \tag{11}$$

$$= \frac{e\beta I Z_\perp}{j\gamma m_0 C_0}\bar{Y}(\omega,\ell) \tag{12}$$

where C_0 is the machine circumference and the frequency ω is measured at fixed azimuth. In equation (12) $Z_\perp$ represents the **total** transverse impedance of the ring.

Averaging over the beam momentum distribution $\psi(p)$ yields a dispersion relation, connecting ω to the spatial frequency ℓ

$$1=\frac{je\beta I Z_\perp}{m_0\gamma C_0}\int_{-\infty}^{\infty}\frac{\psi(p)}{(\omega-\ell\Omega(p))^2-\omega_\beta^2(p)}\,dp \tag{13}$$

For the azimuthal mode ℓ, the impedance is to be evaluated at the frequency $\omega-\ell\Omega$. In general, ω is a complex quantity which depends on the specific character of the distribution $\psi(p)$. To assess stability, a useful tool is the so-called stability diagram, obtained by plotting in the complex impedance plane the boundary curve defined by

$$\mathrm{Re}\{\omega\}=0 \tag{14}$$

In general, the stability boundary defines a closed region of the impedance plane; the beam is stable if the impedance lies inside the region and unstable if it lies outside of it. Expanding (13) in partial fractions, yields

$$1=\frac{je\beta I Z_\perp}{\gamma m_0 C_0}\int_{-\infty}^{\infty}\frac{\psi(p)}{\omega_\beta}\left[\frac{1}{\ell\Omega-\omega_\beta-\omega}-\frac{1}{\ell\Omega+\omega_\beta-\omega}\right]dp \tag{15}$$

In this form, one can clearly distinguish the contribution of two types of modes[4]: the slow wave modes, with frequencies $\omega\simeq\ell\Omega-\omega_\beta$ and the fast wave modes, with frequencies $\omega\simeq\ell\Omega+\omega_\beta$. For a given azimuthal index ℓ, the slow wave and fast wave modes are separated by $2\omega_\beta$. The frequency separation is considerably larger than the betatron frequency spread in the beam; therefore, one can consider the contributions of either type of mode to the integral (15) separately. It is not difficult to show that the

[4]The modes frequencies are the frequencies that satisfy the dispersion equation and make the growth rate $1/\tau=-\mathrm{Im}\{\omega\}=0^+$ denominator in 15 vanish

"fast" modes are always stable for $\mathrm{Re}\{Z_\perp\} > 0$, i.e. $\mathrm{Re}\{\omega\} < 0$. Considering only the slow modes, (15) becomes

$$1 \simeq \frac{je\beta I Z_\perp}{m_0 \gamma C_0 \tilde{\omega}_\beta} \int_{-\infty}^{\infty} \frac{\psi(p)}{\ell\Omega - \omega_\beta - \omega}\, dp \tag{16}$$

When ω_β and ω are both real, this integral has a singularity at $\omega = \ell\Omega - \omega_\beta$ and the integral should be interpreted as the limit of a contour integral. Since the particle momentum is a distribution, not all particles are on resonance exactly at the same frequency; the overall effect is equivalent to damping and is commonly referred to as Landau damping. For the trivially simple case where the momentum distribution is a delta function, one can show that the growth rate $1/\tau$ is

$$\frac{1}{\tau} = \mathrm{Im}\{\omega\} = \frac{e\beta I \,\mathrm{Re}\{Z_\perp\}}{2 m_0 \gamma \omega_\beta C_0} \tag{17}$$

and the beam is unstable if the resistive (real) part of the wall impedance is positive. For a realistic distribution ψ, the beam remains stable even if the wall impedance has a finite resistive component. The stability region can usually roughly be approximated by a half circle. This leads to the stability criterion

$$|Z_\perp| < F_2 \left[\frac{E_0}{e}\right] \left[\frac{8\pi Q_0 \gamma \beta}{I C_0}\right] \left[\frac{\delta p}{p_0}\right] |(\ell - Q_0)\eta - \frac{1}{p_0}\frac{dQ}{dp}| \tag{18}$$

In this expression F_2 is a form factor of order unity which depends on the nature of the distribution $\psi(p)$, E_0 is the rest energy of the reference particle, C_0 is the machine circumference, $Q_0 = \omega_{\beta 0}/\Omega_0$ is the tune of the reference particle and η is the momentum compaction factor.

Bunched Beam

Although the transverse behavior of a bunched beam is in some ways analogous to that of an unbunched beam, there are some important differences. In unbunched beams, momentum compaction and chromaticity introduce Landau damping. When the beam is constrained longitudinally to lie into regions defined by RF buckets, the presence of momentum compaction and finite chromaticity has fundamentally different consequences.

Time-Domain Wakes

We digress briefly to mention that instead of working in the frequency domain to establish dispersion relations relating ω and ℓ, it is sometimes more appropriate to consider a direct description in the time domain. In that context, the fields induced by the passage of a particle are are referred to as wakefields. In general, the calculation of the wake produced by a point charge q moving inside a circular vacuum chamber is a very complicated problem. For a highly relativistic particle circulating in a high conductivity beam pipe, we have seen that simple asymptotic solutions. In general, for particles with $\beta \simeq 1$, one can define a function W such that

$$F_y(s) = \int W(s - s')\lambda(s')ds' \tag{19}$$

where in the context of transverse instability theory, $\lambda(s)$ represents the (*dipole*) line density. Clearly, the wake function and the transverse impedance are, within a possible constant, Fourier transforms of each other.

If the longitudinal distance s between a the test point is larger than

$$s_0 = \left[\frac{b^2}{Z_0\sigma}\right]^{1/3} \tag{20}$$

where Z_0 is the characteristic impedance of vacuum ($\simeq 377\Omega$), one can easily show that the longitudinal electric field at a distance s behind a particle of charge q is

$$E_z = \frac{qc}{4\pi b}\left[\frac{Z_0}{\pi\sigma}\right]^{1/2} s^{-3/2} \tag{21}$$

Similarly, the the transverse (magnetic) field is

$$H_\theta = -\frac{3}{4}\frac{qc}{4\pi b}\left[\frac{1}{Z_0\pi\sigma}\right]^{1/2} rs^{-5/2} \tag{22}$$

The time-domain formulation has the advantage of being general; it is a straightforward matter to write a simulation code based on equations such as (21) and (22). One can then easily deal with the transient behavior of the beam at injection, study asymmetric bunch patterns or transient behavior on the scale of less than a turn.

Rigid Bunch Approximation

In the first approximation, one may neglect internal degrees of freedom and consider bunches as rigid objects. This approach was used by Courant and Sessler in 1966 [4]. First, consider a single bunch. Each time it goes around the ring, the bunch sees the wake left by its previous passage. Clearly, transverse motion stability depends on the change in the phase of the betatron oscillation from turn to turn. If R is the nearest integer to the tune Q, the motion is stable when

$$R + \frac{1}{2} > Q > R \tag{23}$$

and unstable when

$$R > Q > R - \frac{1}{2} \tag{24}$$

For a machine symmetrically filled with M identical bunches, the situation is slightly different. In the linear approximation, the M bunches can be considered as M coupled oscillators. Such a system has M normal modes; for each mode, all bunches oscillate at a unique frequency ω_m, with a relative phase difference $\phi_m = 2\pi m/M$, $m = 0, M-1$. At fixed azimuth, the signal S due to transverse beam motion in mode m is of the form

$$S(\omega) = \sum_{\ell=-\infty}^{\infty} h_m(\omega)\delta(\omega - \ell\Omega - \omega_m) \tag{25}$$

where

$$h_m(\omega) = \mathcal{F}\{h_m(s/c)\} \tag{26}$$

is the Fourier transform of the modal bunch (transverse dipole) distribution. In the context of a bunched beam in a symmetrically filled machine, it is appropriate to let y represent the average transverse position of a *bunch*. Since the net deflecting field produced by a bunch is proportional to $Z_\perp(\omega)h(\omega)$, the net force on a bunch is proportional to $Z_\perp(\omega)|h(\omega)|^2$. One can show that the complex frequency shift for mode m is given by

$$\Delta\omega_m = \frac{1}{1+m}\left[\frac{j}{2\omega_\beta}\right]\left[\frac{e\beta}{\gamma m_0}\right]\left[\frac{I_0}{C_0}\right]\frac{\sum Z_\perp(\omega)|h_m(\omega-\omega_\xi)|^2}{\sum|h_m(\omega-\omega_\xi)|^2} \tag{27}$$

In this expression, ω_ξ represents a real frequency shift caused by chromaticity, I_0 is the beam current in one bunch and $|h_m(\omega)|^2$ is the mode power spectrum. The summations are to be taken over the (discrete) spectra for mode m.

Transverse Coupled Bunch Instability in Very Large Machines

For a beam with M equispaced bunches, the envelope of mode m corresponds roughly to the envelope of the continuous beam mode. However, the discontinuous nature of the mode distribution introduces aliased frequencies in the spectrum over which a summation has to be performed. Consequently, the stability of mode m depends on the impedance at frequencies

$$\omega_{mk} = \omega_m + kM\Omega_0 \quad k = 0, 1, .. \tag{28}$$

Note that this state of affairs is fundamentally different from the case of the continuous beam for which each transverse mode corresponds to a **single** frequency

$$\omega_m = \omega_\beta + m\Omega_0 \tag{29}$$

For a certain coupled bunch mode m, the coupled-bunch mode spectrum exhibits a very low frequency line at

$$\omega = \omega_\beta + m\Omega_0 + kM\Omega_0 = (Q + m + kM)\Omega_0 \simeq q\Omega_0 \tag{30}$$

where q is the fractional part of the tune Q. In a low field 50 TeV ring, $2\pi\Omega_0 \simeq 500$ Hz, and this frequency on the order of a few hundred Hz. This is an unusually low frequency and it is important to understand the resistive wall impedance in the low frequency limit. Nevertheless, it is clear that, to the extent the resistive transverse wall impedance scales roughly like $\omega^{-1/2}$, one can expect its contribution to be very important in a large machine.

The mode spectrum is affected by chromaticity and bunch structure. By carefully controlling either or both, it may be possible to suppress the contribution of most troublesome line. Other lines remain at frequencies that are still relatively low; they may also be unstable.

Finally, contrary to the situation prevailing with a continuous beam, short bunches also interact strongly with the broad-band coupling impedance[5]. This interaction produces a real frequency shift which tends to suppress Landau damping: as a consequence, even a very small growth rate can lead to the eventual destruction of the beam.

It is quite likely that for a very large large machine, a damping system for the transverse coupled bunch instability must cover all the possible collective modes, which is equivalent to saying that each bunch must be individually damped.

Impedance Calculations

Analytical Results

As hinted in the previous section, the resistive wall impedance can be calculated analytically for an infinitely long beam pipe of circular cross section. We recall here some essential steps of this derivation. In the frequency domain, Maxwell's equations in source-free regions become:

$$\left[\nabla^2 + k_0^2\right]\mathbf{H} = 0 \tag{31}$$

$$\left[\nabla^2 + k_0^2\right]\mathbf{E} = 0 \tag{32}$$

where $k_0^2 = \omega^2/c^2$. Assuming translation symmetry, and a $e^{-jk_z z}$ spatial dependence along the z-axis, one can easily show that the longitudinal components E_z and H_z play the role of a potential[6] for TM and TE modes respectively:

$$\left[\nabla_\perp^2 + (k_0^2 - k_z^2)\right]E_z = 0 \tag{33}$$

$$\left[\nabla_\perp^2 + (k_0^2 - k_z^2)\right]H_z = 0 \tag{34}$$

Now, the only field components that, on average, can produce a net beam deflection travel at the beam velocity βc i.e. k_z must satisfy the condition:

$$k_z = \omega/\beta c \tag{35}$$

and one has

$$k_0^2 - k_z^2 = \frac{\omega^2}{c^2}\left[1 - 1/\beta^2\right] = \frac{k_0^2}{\gamma^2} \tag{36}$$

For $\gamma \to \infty$,

$$\left[\nabla_\perp^2 + \frac{k_0^2}{\gamma^2}\right] H_z \simeq \nabla_\perp^2 H_z = 0 \tag{37}$$

[5]Typically, the integrated effect of various impedances such as small discontinuities such as vacuum bellows is accounted for by introducing a broadband impedance, basically a resonator with $Q \simeq 1$ with center frequency equal to the beam pipe cutoff frequency.

[6]That is to say, once E_z and H_z are known, the transverse components E_x, E_y, H_x, H_y can be obtained from Maxwell's equations.

and similarly for E_z. Thus, in the relativistic limit, both E_z and H_z satisfy Laplace's equation in transverse coordinates. Separating the angular and radial dependence in cylindrical coordinates, one finds that the field produced by individual Fourier components of infinitely thin radial sheets of beam charge and current densities can be analyzed separately. The $m = 0$ case, which corresponds to excitation by an azimuthally uniform ring of charge of spatial frequency k_z produces only a longitudinal electric field. The $m > 0$ excitations produce magnetic field and are generally responsible for the transverse forces. In practice, the $m = 1$ contribution corresponding to a simple $\cos\theta$ azimuthal distribution is dominant and the effect of the $m > 1$ components are neglected. One thus consider an infinitely thin ring beam of radius a over which the charge is deposited with a $\cos\theta$ distribution and matches the fields (solutions of the homogeneous Laplace equation) both at the beam interface and on the beam pipe surface. This is done by first assuming an perfectly conducting beam pipe. When the conductivity σ is large and finite there is a tangential electric field which is connected to the surface current density by a complex surface impedance Z_m

$$\mathbf{E}_{2z} = Z_m \mathbf{J}_z = Z_m(\mathbf{n} \times \mathbf{H}_{1\theta}) \tag{38}$$

where

$$Z_m = \frac{1+j}{\sigma\delta} \tag{39}$$

and

$$\delta = \left[\frac{\omega}{2\mu_0\sigma}\right]^{1/2} \tag{40}$$

is the skin depth. The field E_{2z} is a small perturbation; to preserve consistency with Maxwell's equations a small magnetic field correction B_{2y} is also required. We note that B_{2y} has a component which is in quadrature with the unperturbed magnetic magnetic field. Essentially, the perturbation represents the effect of lossy eddy currents induced in the beam pipe.

As mentioned before, the transverse coupling impedance is defined as follows [5]:

$$Z_\perp(\omega) = j\frac{1}{e\beta I_0 y}\int \langle F_\perp \rangle ds \tag{41}$$

Historically, the factor j has been introduced in (20) to make $Z_\perp$ play a role similar to $Z_\parallel$ in the longitudinal instability theory. After some manipulations, one can recast the expression (3) of the preceding section into an expression for the transverse coupling impedance of a circular resistive vacuum pipe

$$Z_\perp = Z_{\perp\mathrm{S.C.}} + Z_{\perp\mathrm{R.W.}} = jRZ_0\left[\frac{1}{\beta^2\gamma^2}\left(\frac{1}{a^2} - \frac{1}{b^2}\right) - (1+j)\frac{\delta(\omega)}{b^3}\right] \tag{42}$$

where R,Z_0 and I_0 are respectively the machine radius, the characteristic impedance of vacuum and the beam current; a and b are the vacuum chamber and beam radii. The term in γ^2 in (21) is due to the beam self-field and is is usually considered separately. To fix ideas, consider now a low field VLHC ring with a circumference of 600 km and

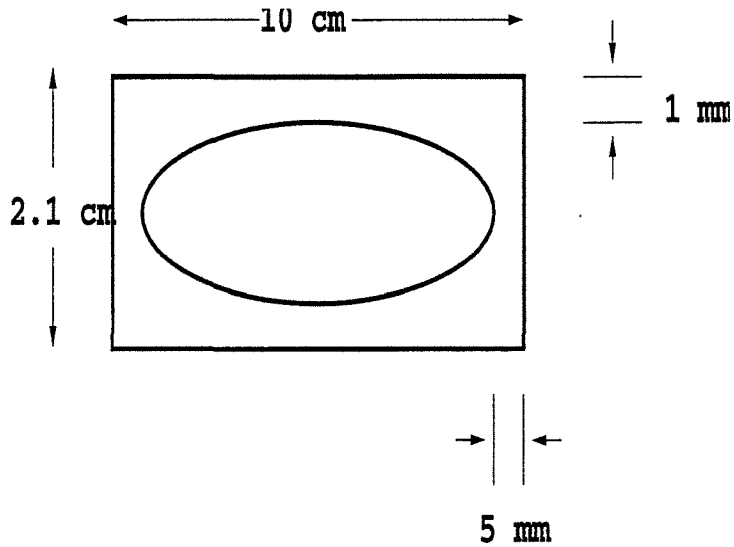

Figure 1: *Beam pipe geometry. The horizontal and vertical thicknesses are 5 mm and 1 mm respectively.*

an aluminum beam pipe ($\sigma = 3.5 \times 10^7$ [Ω-m^{-1} of inner radius $b = 0.9$ cm. With the frequency $f = \omega/2\pi$ expressed in kHz, one finds

$$Z_\perp(\omega) \simeq (1+j)0.20 \cdot R\sqrt{\frac{1}{f}} \ [\mathrm{M}\Omega/\mathrm{m}] \tag{43}$$

Numerical Computations

To obtain impedance estimates for more realistic beam pipe geometries it is necessary to resort to numerical methods. The transverse resistive wall impedance is primarily due to the magnetic field produced by the eddy currents induced in the beam pipe. Most established codes used to compute impedance assume that the fields are confined inside accelerator structures and consequently cannot deal very well with the situation prevailing at very low frequency when the fields leak out of the beam tube and wander inside neighboring magnet poles. We have therefore attempted to use a conventional low frequency eddy current code to determine the impedance. This type of code neglects the displacement current and solves a diffusion equation for the vector potential. As we shall see, as long as the code limitations are understood, it is possible to obtain useful results. We consider the geometry illustrated in Figure 1 which approximates the currently favored geometry. In lieu of a true $\cos\theta$ spatial current distribution, we use two currents circulating in opposite directions separated by a distance δ. In addition to the dipole component, this choice introduces higher order multipoles in the excitation but the relative contribution to the induced currents is very small. The results obtained with a beam current of ± 1A and a separation $\Delta = 1$ cm are shown in Figure (2). The

corresponding eddy current distributions (at 1 kHz) are shown in Figure (3). All calculations were made using a frequency domain solver; the magnetic field plots represent the component of the field in quadrature with the excitation. This field is proportional to both the real and imaginary part of the impedance $Z_\perp(\omega)$. At 1 kHz, the calculated impedance in the vertical plane is (using equation (41)) for a machine of radius R is

$$Z_\perp(1kHz) \simeq (1+j)\cdot 0.276R[\mathrm{M}\Omega] \tag{44}$$

which is about 30 % higher than the value predicted (see equation 43).

At frequencies above a few KHz, the impedance behaves as $1/\sqrt{\omega}$, as expected. Below 1 kHz, the magnetic field leaks out of the chamber and the impedance gradually goes to zero. This is most likely is an underestimation of reality since the presence of magnet poles above and below the beam pipe has been accounted for through a simple boundary condition. A better estimate would require including the effect of lossy pole pieces of finite permeability. At this point, the important observation is that the resistive wall impedance of a finite thickness beam tube does not appear to scale as $1/\sqrt{(\omega)}$ as $\omega \rightarrow 0$ and may not be as large as anticipated on the basis of equation (42).

Conclusion

The work presented in this note is preliminary. The results demonstrate that a simple low frequency electromagnetics code can be used to obtain good estimates of the low frequency transverse impedance in situations where the wall thickness is smaller than the skin depth. In principle, the influence of iron poles could be taken into account by introducing a lossy permeability. Using time domain representation, it should also be possible to devise a numerical simulation of the transverse resistive wall instability and of possible damping schemes in a very large machine.

References

[1] J.T. Rogers, "Collective Effects and Impedances in the RLHC(s)", in Proceedings of the 1996 Snowmass meeting.

[2] John Marriner, "A Damper to Suppress Low Frequency Transverse Instabilities in the VLHC ", VLHC Summer Studies, Fermilab August 1997.

[3] J. Laslett, V.K. Neil and A.M. Sessler, "Transverse instabilities of intense coasting beams in particle accelerators" Rev. Sci. Instr. **36**, 4 (1965) p 436-448

[4] E.D. Courant and A.M. Sessler, "Transverse Coherent Resistive Instabilities of Azimuthally Bunched Beams in Particle Accelerators", *Re. sci. Instrum.*, **37**, 1579

[5] B. Zotter and F. Sacherer, "Transverse Instabilities of Relativistic Particle Beams in Accelerators and Storage Rings", CERN 77-13

[6] J.D. Lawson, "The Physics of Charged-Particle Beams", Oxford, 1988

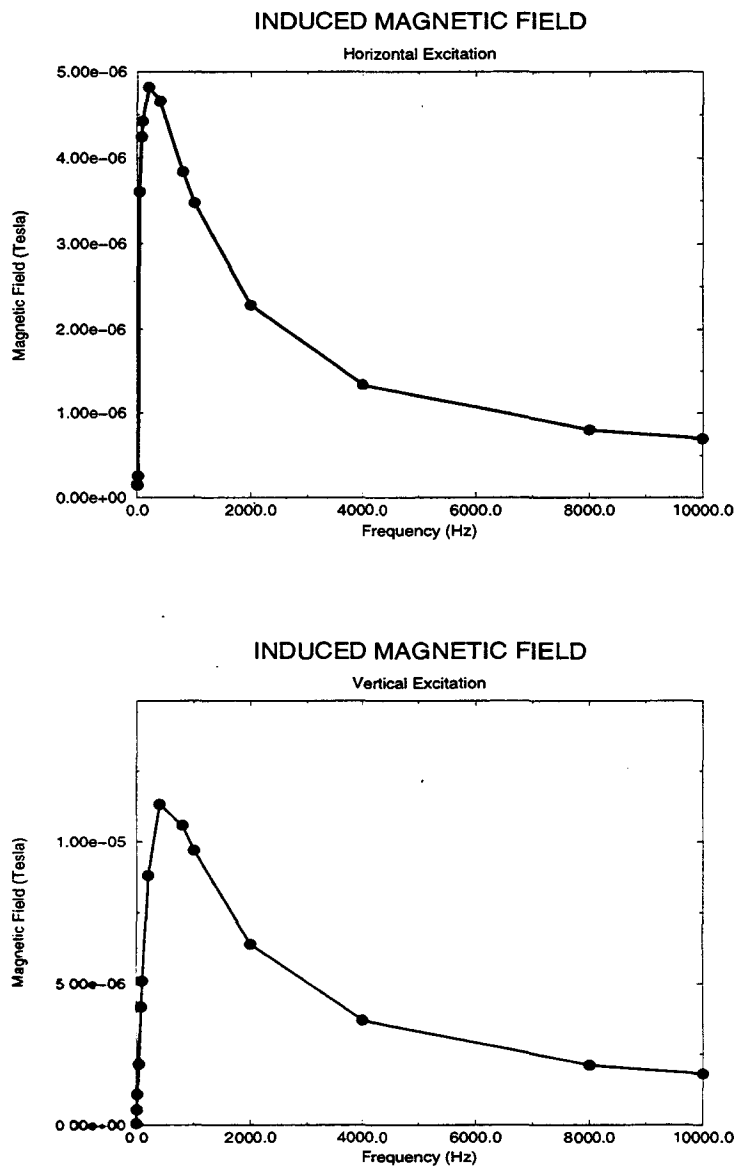

Figure 2: *Top: calculated deflecting magnetic field for a horizontal* ($\cos\theta$) *dipole excitation. Bottom: calculated deflecting magnetic field for a vertical* ($\sin\theta$) *dipole excitation.*

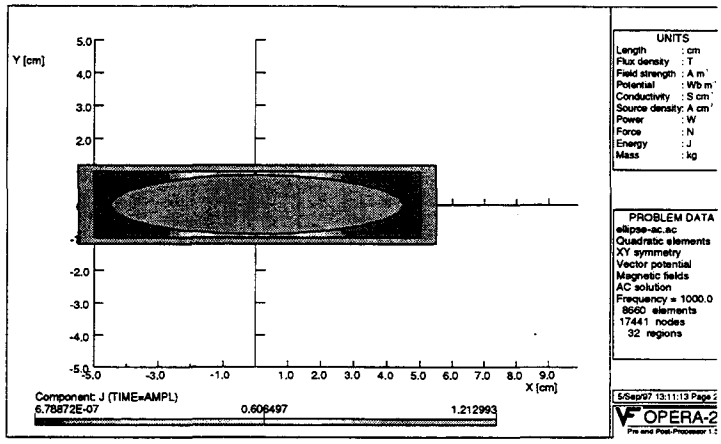

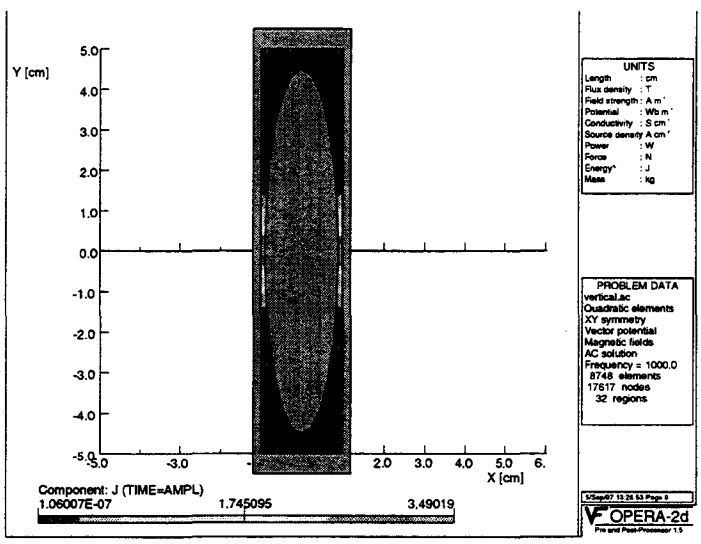

Figure 3: *Top: eddy current distribution at 1 KHz for a horizontal beam displacement. The vacuum pipe is Al with* $\sigma = 3.5 \times 10^7 [\Omega - \mathrm{m}]^{-1}$. *Bottom: eddy current distribution at 1 Khz for a vertical beam displacement. The vacuum pipe is Al with* $\sigma = 3.5 \times 10^7 [\Omega - \mathrm{m}]^{-1}$.

[7] J. Gareyte, "Collective Phenomena and Instabilities", in Advances of Accelerator Physics and Technologies, Herwig Shopper Ed., World Scientific, 1993 "The Physics of Charged-Particle Beams", Oxford, 1988

Appendix: Eddy Currents at Very Low Frequency

In this appendix, we derive a classical solution for the eddy currents induced near the surface of a high conductivity material. We assume that the displacement current is negligible, that is

$$\nabla \times \mathbf{H} = \mathbf{J} + \frac{\partial \mathbf{D}}{\partial t} \simeq \mathbf{J} \tag{45}$$

Using the subscript c to denote the fields inside the conductors one has,

$$\nabla \times \mathbf{H}_c = \sigma \mathbf{E}_c + \frac{\partial \mathbf{D}_c}{\partial t} \simeq \sigma \mathbf{E}_c \tag{46}$$

$$\nabla \times \mathbf{E}_c = -\frac{\partial \mathbf{B}_c}{\partial t} \tag{47}$$

therefore

$$\mathbf{E}_c \simeq \frac{1}{\sigma} \nabla \times \mathbf{H}_c \tag{48}$$

$$\mathbf{H}_c \simeq \frac{1}{j\omega\mu_0} \nabla \times \mathbf{E}_c \tag{49}$$

With $\hat{\mathbf{n}}$ a unit normal vector pointing outside the conductor and ξ a coordinate defined along the direction perpendicular to the surface and positively increasing inside the conductor, one can neglect all spatial variations parallel to the conductor surface and write

$$\nabla \simeq -\hat{\mathbf{n}} \frac{\partial}{\partial \xi} \tag{50}$$

and

$$\mathbf{E}_c \simeq -\frac{1}{\sigma} \hat{\mathbf{n}} \times \frac{\partial \mathbf{H}_c}{\partial \xi} \tag{51}$$

$$\mathbf{H}_c \simeq \frac{1}{j\omega\mu} \hat{\mathbf{n}} \times \frac{\partial \mathbf{E}_c}{\partial \xi} \tag{52}$$

Differentiating (51) and substituting (52) one gets

$$\frac{\partial^2}{\partial \xi^2} (\hat{\mathbf{n}} \times \mathbf{H}_c) - j \frac{2}{\delta^2} (\hat{\mathbf{n}} \times \mathbf{H}_c) \simeq 0 \tag{53}$$

$$(\hat{\mathbf{n}} \cdot \mathbf{H}_c) \simeq 0 \tag{54}$$

The solution for $\mathbf{H}_c$ is

$$\mathbf{H}_c = \mathbf{H}_{\parallel} e^{-\xi/\delta} e^{-j\xi/\delta} \tag{55}$$

The corresponding electric field

$$\mathbf{E}_c = \frac{(1+j)}{\sigma\delta}(\hat{\mathbf{n}} \times \mathbf{H}_{\|})e^{-\xi/\delta}e^{-j\xi/\delta} \tag{56}$$

where

$$\delta = \left[\frac{\omega}{2\mu_0\sigma}\right]^{1/2} \tag{57}$$

is the skin depth.

SLAC/AAS–91
August 1997
(AP)

Electron-Cloud Instability in the VLHC[1]

Frank Zimmermann
Stanford Linear Accelerator Center, Stanford, CA 94309

Abstract

Over a few bunch passages photoemission and secondary emission could generate a quasi-stationary electron-cloud in the VLHC beam pipe, giving rise to a multi-bunch instability. In this paper, we report preliminary simulation results of the electron cloud build-up and its response to a beam displacement. The estimated instability rise time is about 3–4 s in both transverse planes.

1 Introduction

Recent simulation studies for the Large Hadron Collider (LHC) predict an electron-cloud instability with a rise time of about 25 ms horizontally and 130 ms vertically, at top energy [1]. This instability arises due to a combination of photoemission and secondary emission from the vacuum chamber wall, by which, for each passing bunch train, an electron cloud builds up in the beam pipe. Interaction with this electron cloud can amplify a small perturbation in the orbit of the individual bunches, which results in a multi-bunch instability. Electron-cloud instabilities of this type have been studied both experimentally and theoretically for several positron storage rings, for example, the KEK photon factory [2, 3], BEPC at IHEP in Bejing [4], and the PEP-II B factory [5, 6, 7]. Although beam-induced multipacting was observed with an aluminum-chamber prototype in the ISR [9], the LHC will be the first proton storage ring with significant synchrotron radiation, and, thus, the first proton ring which should encounter a photoelectron-induced instability [1, 8].

Since the electron-cloud instability appears to be potentially significant for the LHC, it could also be important for the Very Large Hadron Collider (VLHC). Parameters for the LHC and the low-field version of the VLHC are compared in Table 1. The VLHC design contemplates the use of a (warm) aluminum vacuum chamber. While the secondary emission yield of aluminum is much higher than that of the LHC copper beam screen, which could increase the charge density of the electron cloud and, thus, aggravate its effect, the higher beam energy (increased stiffness of the beam and higher critical photon energy) and the reduced charge per bunch in the VLHC will weaken the instability. Another difference is the much flatter geometry of the vacuum chamber in the VLHC, which may change the electron-cloud dynamics, since the secondary emission yield depends strongly

[1]Work supported by the US Department of Energy under contract DE–AC03–76SF00515.

on the angle of incidence. To arrive at a more quantitative comparison, we have simulated the build-up of the electron cloud in a bending magnet of the VLHC, as well as its response to a transversely displaced bunch and the resulting deflection of the following bunch. From this deflection in turn, the effective wake field and the instability rise time can be estimated.

storage ring	LHC	VLHC
beam energy E (TeV)	7	50
number of particles / bunch N_b	10^{11}	10^{10}
beam current I (A)	0.54	0.09
h. r.m.s. beam size σ_x (mm)	0.303	0.089
v. r.m.s. beam size σ_y (mm)	0.303	0.089
r.m.s. bunch length σ_z (cm)	7.7	4.3
bunch spacing L_{sep} (m)	7.48	5.2
bend length l_b (m)	14.2	250
bend field B (T)	8.4	2
bending radius ρ (km)	2.78	83.3
circumference C (km)	26.66	551
vacuum screen half height h (mm)	18.5	9
vacuum screen half width w (mm)	23	20
critical photon energy (eV)	44	500
hor./vert. tune Q	63	247
chamber/beam-screen material	Cu*	Al
chamber/beam-screen temperature	4 K	300 K

Table 1: Comparison of parameters for the LHC [10] and the low-field VLHC [11];
* possibly with TiN or TiZr coating [12, 13].

2 Simulation

Simulations of the electron-cloud instability were carried out with the same program as used for the LHC studies. For a description of the underlying physics model and for details of its implementation, the interested reader may consult Ref. [1]. We point out that, as for the simulations in Ref. [1], the photoelectrons are launched with an initial uniform distribution around the vacuum-chamber aperture, which is a good approximation, if the photon reflectivity of the beam pipe is considerably larger than 50%. The reflectivity will most likely be that high, unless it is reduced by a special coating. We further assume that on average the number of photoelectrons is approximately equal to the number of emitted photons, *i.e.*, we assume an effective photoemission yield (including conversion after reflection) close to unity. Since the chamber wall could be coated to reduce the photoemission, we have simulated how sensitive the instability rise time is to the number of primary photoelectrons. We have also studied the dependence on the secondary-emission yield. For aluminum or, more precisely, for aluminum oxide, the secondary-emission yield is very high. Values of δ_{max} (the maximum yield at perpendicular incidence) quoted in the literature vary between about 2.6 and 3.5. The yield could be drastically reduced

with a titanium nitride coating, as it is applied to the aluminum vacuum chamber of the PEP-II Low Energy Ring.

Since at the VLHC the maximum number of secondary electrons is most likely generated by primary electrons which have come very close to the beam, care must be taken to model the motion of such electrons as accurately as possible. To obtain a precise result, the minimum number of tracking steps during a single bunch passage must be chosen larger than [14]

$$n_{\text{step}} \approx \frac{5\sqrt{N_b r_e \sigma_z}}{\sigma_x} \tag{1}$$

where N_b denotes the bunch population, r_e the classical electron radius, σ_z the rms bunch length and σ_x $(= \sigma_y)$ the rms transverse beam size. Inserting the VLHC parameters into Eq. (1), we find $n_{\text{step}} \approx 60$. To keep the computation time within acceptable bounds, we had to choose a slightly smaller number of steps per bunch, $n_{\text{step}} \approx 30$, which should still assure a reasonable accuracy. The error can be estimated from the variation of the results over different random seeds. For this number of steps, it is of the order of 10–20%.

Figure 1 presents a typical simulation result for the electron-cloud build-up inside a bending magnet. The charge increase as a function of time is shown for two different secondary-emission yields. As can be seen, in both cases the charge density saturates after the passage of less than 10 bunches. For these parameters the neutralization density (at which the number of electrons in the beam pipe equals the time-averaged number of protons) amounts to a total electron charge of about 5×10^{11} e per bend, which is roughly a factor of 2 higher than the saturation values observed in Fig. 1.

In Fig. 2, the transverse macroparticle distribution after the passage of 20 bunches is depicted for two different secondary-emission yields δ_{max}. For both cases, we notice a vertical stripe of increased electron density near the center of the beam pipe. In these two pictures, it is difficult to discern significant differences for the two secondary-emission yields. The situation becomes clearer, when, instead of the macroelectron density, we display the charge distributions of the macroelectrons. The projected horizontal and vertical charge distributions are shown in Fig. 3. For the higher secondary emission yield (bottom picture), a narrow stripe of much enhanced electron density is visible around the center of the beam pipe. We can explain the origin of this stripe by the higher electron energies and the consequently greater secondary-emission yield in this region. If the maximum yield is modest or low, such as $\delta_{max} = 1.5$ (top picture), the secondary emission is less important, and the electron distribution, which is now dominated by the primary photoelectrons, is more uniform.

To estimate the effective wake function W_1, we performed simulations for 20 different random seeds. For each random seed, we computed the average of the kicks for a positive and a negative offset—correcting for the relative sign of kick and offset—, to further reduce the statistical fluctuation of the result. Simulation results for a variety of conditions are summarized in Table 2.

Lowering the maximum secondary-emission yield δ_{max} from 3.5 to 1.5 does not significantly affect the vertical wakefield. By contrast, for the same change of δ_{max}, the horizontal wakefield reverses its sign! The large sensitivity of the horizontal wake to the secondary emission yield appears to have the same origin as the difference in the two horizontal density projections of Fig. 3. A possible explanation is the following.

If a bunch is displaced horizontally, the electrons closer to the displaced bunch are more strongly accelerated by the beam field than the electrons on the other side of the

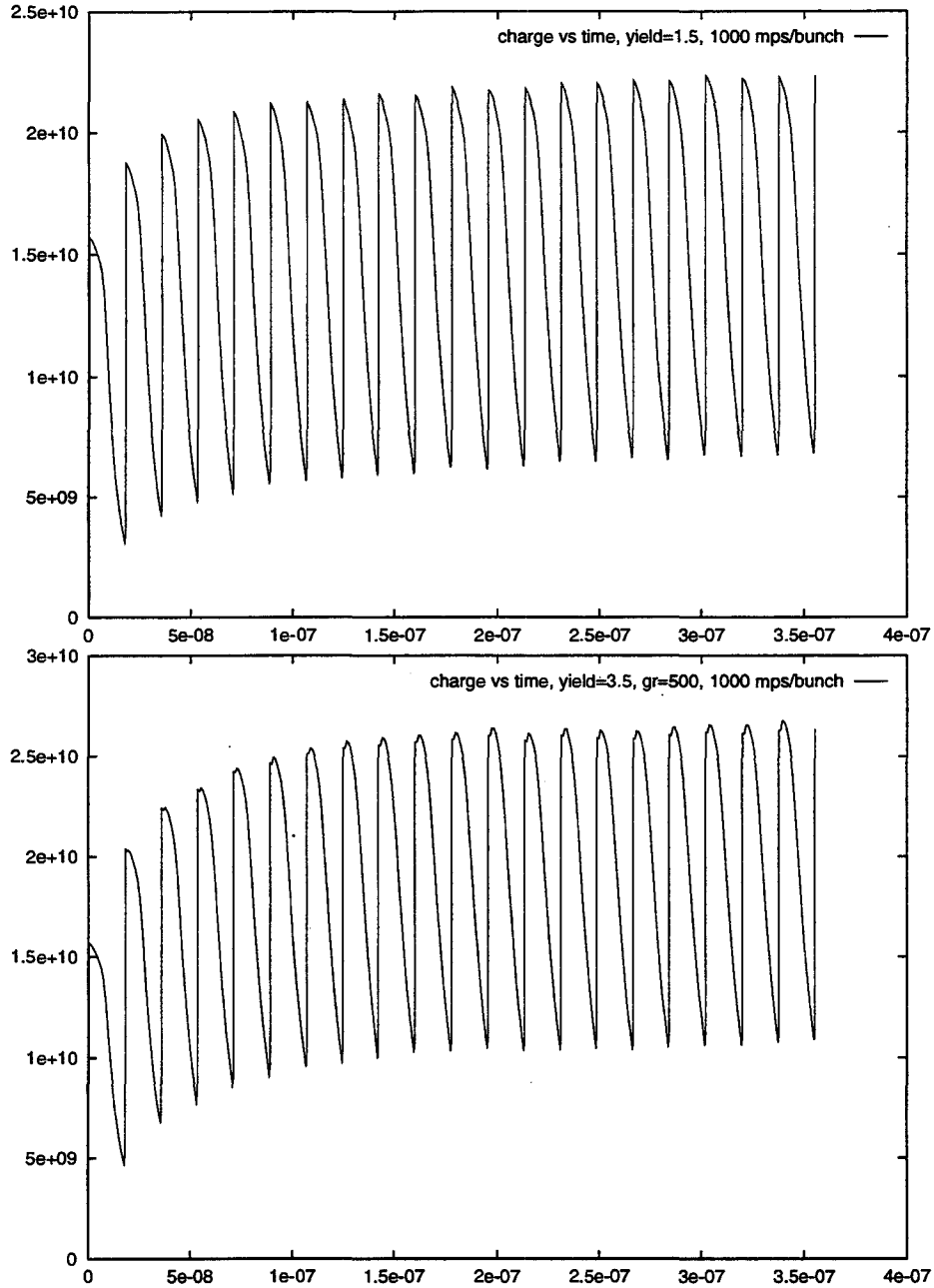

Figure 1: Charge of the electron cloud (in units of e) accumulated inside a bending magnet as a function of time (in s), for two different values of the maximum yield δ_{max}; top: $\delta_{max} = 1.5$; bottom: $\delta_{max} = 3.5$. The total time span corresponds to 21 bunch passages, which are reflected in the sawtooth-like evolution pattern. In this simulation, 1000 macroparticles per bunch were launched, and the grid size for the space-charge calculation was 500 points.

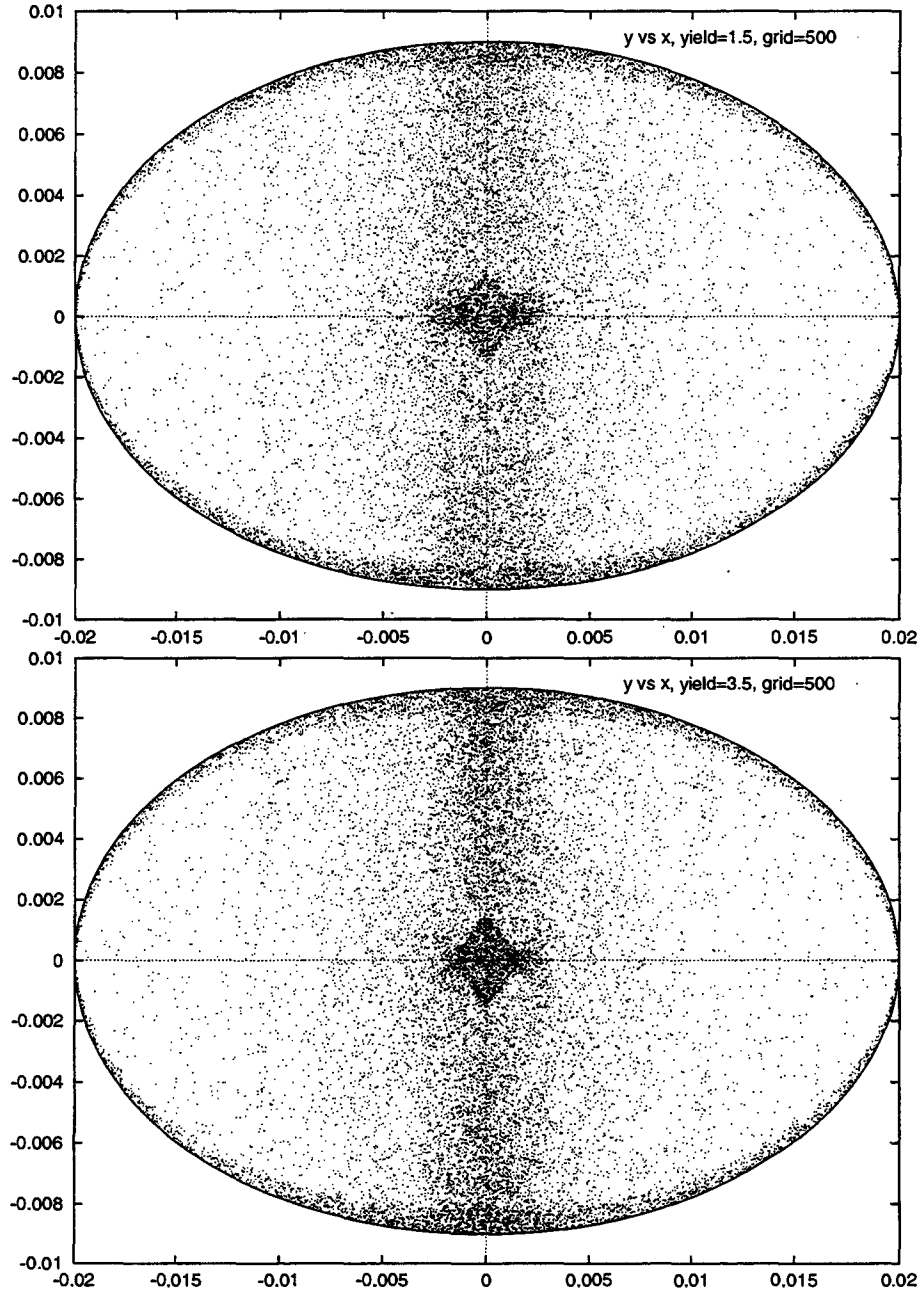

Figure 2: Transverse distribution of macroelectrons after 20 bunches for a maximum secondary emission yield δ_{max} of 1.5 (top) and 3.5 (bottom). Horizontal and vertical dimensions are given in units of m.

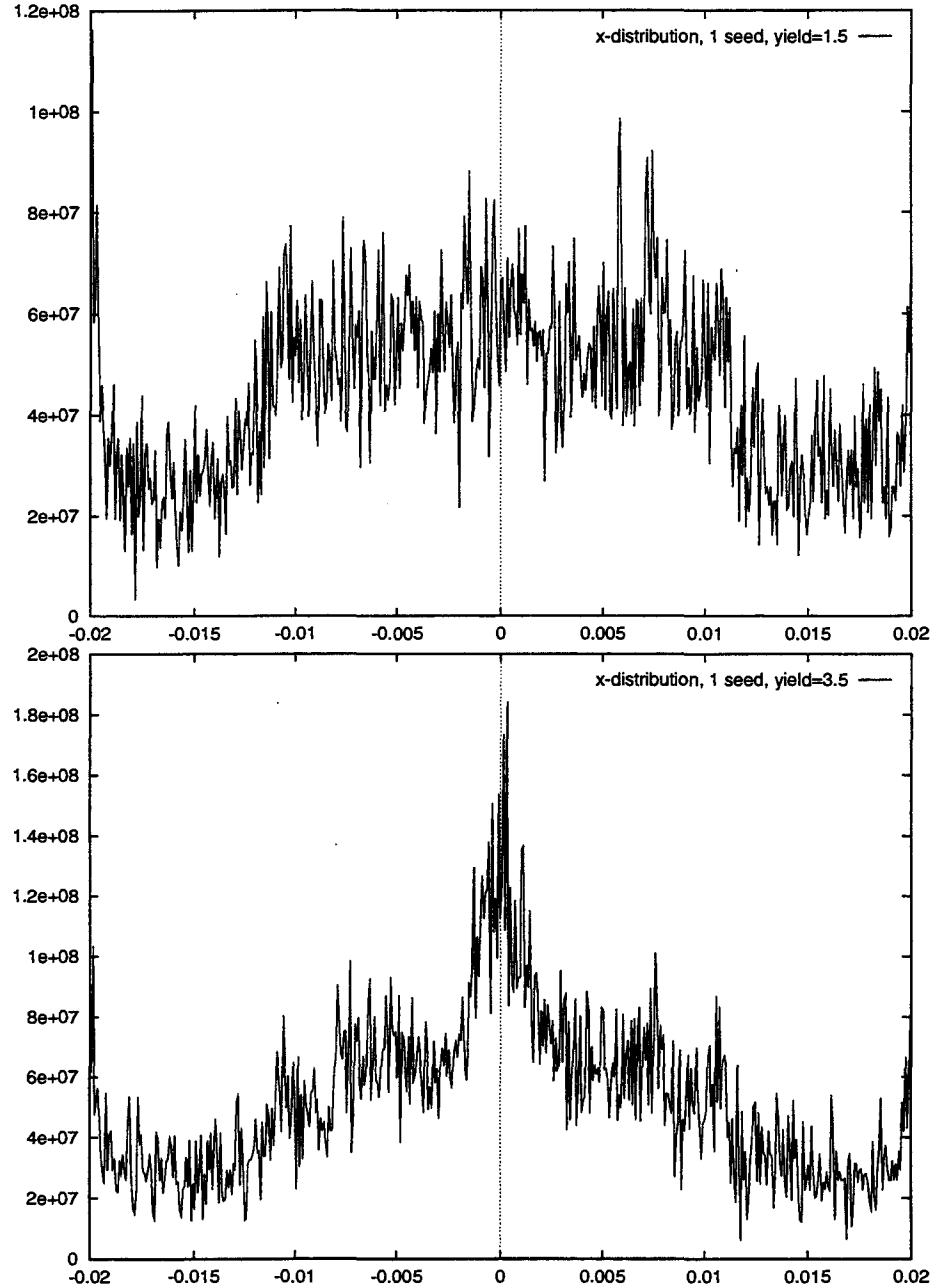

Figure 3: Projected horizontal electron charge density after 20 bunches, as obtained for one random seed, and a yield of $\delta_{max} = 1.5$ (top) and $\delta_{max} = 3.5$ (bottom). The horizontal coordinate is given in units of meters; the vertical coordinate is the charge (in units of e) per bending magnet, per bin and per grid point. The total number of grid points is 500, and 1000 macroparticles per bunch (and per seed) were used.

vacuum chamber. For a large secondary emission yield, these higher-energetic electrons generate a lot of secondaries. When the following bunch passes by (which is assumed to be on the design orbit at the center of the beam pipe), it will be deflected by these secondary electrons in the same direction in which the previous bunch was displaced. This means that the wakefield has a positive sign. On the other hand, when the secondary emission yield is low, the primary electrons closer to the displaced bunch (which gain a higher energy and accordingly move faster than those on the other side), because of their larger speed have a higher probability to be lost before the next bunch arrives, but, for a reduced yield δ_{max}, they do not generate as many secondaries. The next bunch then interacts with an electron cloud whose centroid charge is on the side opposite from the displaced bunch. Therefore, in this case the effective wakefield is negative.

To demonstrate the correctness of this interpretation, Fig. 4 shows horizontal projections of the electron charge distribution just prior to the arrival of the 22nd bunch after the 21st bunch was displaced horizontally by 5 mm. Depicted are simulation results for three different values of the secondary emission yield. It is obvious that the charge centroid shifts from the left to the right, as the emission yield increases, which is consistent with the observed sign reversal of the horizontal wakefield.

δ_{max}	mps./b.	section	Δy (Δx)	$W_{1,y}$ (10^6 m^{-2})	$W_{1,x}$ (10^6 m^{-2})	comment
3.5	1000	bend	0.3 cm	9.4 ± 1.9	8.9 ± 2.2	—
2.5	1000	bend	0.3 cm	8.8 ± 1.2	-2.2 ± 1.3	—
1.5	1000	bend	0.3 cm	8.1 ± 0.9	-14.6 ± 1.8	—
2.5	1000	bend	0.3 cm	4.5 ± 0.7	-2.9 ± 0.8	$\eta_{pe}^{eff} = 0.25$

Table 2: Effective bunch-to-bunch dipole wake function after 20 bunches, extracted from the simulation, for various secondary emission yields, macroparticle numbers, transverse offsets, charges per bunch, and effective photoemission yields. The comment $\eta_{pe}^{eff} = 0.25$ refers to a reduction of the photoemission probability by a factor of 4, compared with the nominal case.

Reducing the number of photoelectrons emitted per photon by a factor of 4 results in a 50% smaller vertical wakefield, while the horizontal wakefield remains essentially unchanged (in Table 2 this case is indicated by the comment '$\eta_{pe}^{eff} = 0.25$').

From Table 2, the integrated dipole wake functions $W_{1,x}(L_{sep})$ and $W_{1,y}(L_{sep})$ at a distance equal to the bunch spacing are about 8–9$\times 10^6$ m^{-2} and 9–(−15) $\times$ 10^6 m^{-2}, respectively, for the nominal photoemission yield. Assuming that the wakefield decays rapidly and only affects the next bunch, we can use the estimate [15]

$$\tau \approx \frac{4\pi\gamma Q}{N_b r_p c W_1(L_{sep})}, \tag{2}$$

where Q is the betatron tune, to find an instability rise time of about 3–4 s for both the horizontal and the vertical plane. The vertical instability rise time doubles, when the photoemission yield is reduced by a factor of 4, while the horizontal rise time appears to be less sensitive.

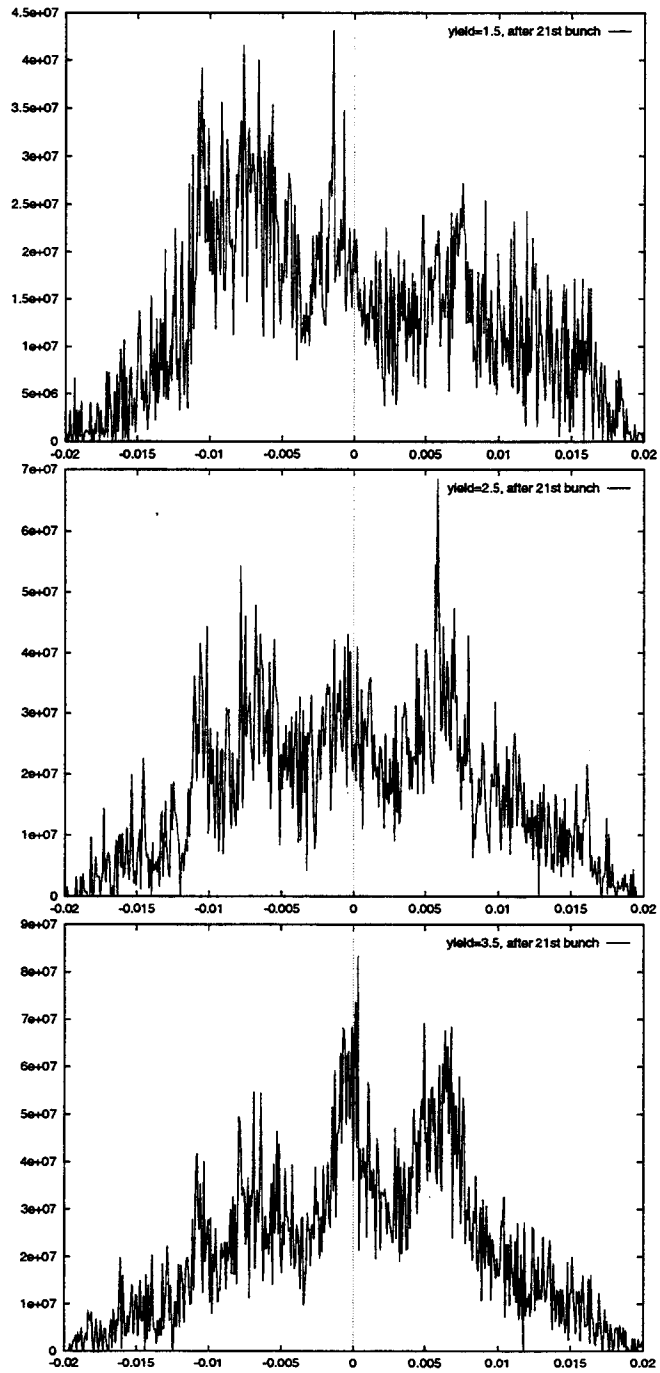

Figure 4: Projected horizontal electron charge density just prior to the arrival of the 22nd bunch, when the 21st bunch was displaced by 5 mm. Shown are pictures for three different secondary emission yields: $\delta_{max} = 1.5$ (top), $\delta_{max} = 2.5$ (center), $\delta_{max} = 3.5$ (bottom). The horizontal coordinate is in units of meters; the vertical coordinate is the charge (in units of e) per bending magnet, per bin and per grid point. The total number of grid points is 500, and 1000 macroparticles per bunch (and per seed) were used.

3 Conclusions

The rise time of the electron-cloud instability in the VLHC was estimated to be of the order of 3–4 s. The instability appears to be equally strong in both transverse planes. This is different from the LHC case, where the horizontal wakefield was found to be a factor of 5 larger than the vertical [1]. The difference can be attributed to the different vacuum-chamber aspect ratio and the different beam current.

In the VLHC, the effective vertical wakefield is fairly independent of the assumed secondary emission yield δ_{max}, whereas the horizontal wakefield reverses its sign at a yield value δ_{max} slightly above 2.5. This sign reversal is caused by a change of the relative importance of photoemission and secondary emission and by the accompanying change in the response of the electron cloud to horizontal bunch displacements.

Finally, our simulation results suggest that a moderate reduction of the photoemission yield, *e.g.*, by special coatings, is unlikely to significantly suppress the instability.

Acknowledgements

I would like to thank Ernie Malamud and Jim Holt for suggesting this study. F. Ruggiero, M. Furman, O. Gröbner and S. Heifets deserve my thanks for many helpful discussions on the electron-cloud instability. The work reported here was strongly influenced by similar simulation studies which M. Furman has recently performed for PEP-II.

References

[1] F. Zimmermann, "A Simulation Study of Electron-Cloud Instability and Beam-Induced Multipacting in the LHC", CERN LHC Project Report 95 and SLAC-PUB- (1997).

[2] M. Izawa et al., Phys. Rev. Lett., Vol. 74 No. 8 (1995).

[3] K. Ohmi, Phys. Rev. Lett., Vol. 75, No. 8 (1995).

[4] S. Kurokawa, private communication (1997).

[5] M. Furman and G. Lambertson, talk for PEP-II Machine Advisory Committee and updates, January 1997 (1997).

[6] S.A. Heifets, "Transverse Instability Driven by Trapped Electrons", SLAC/AP-95-101 (1995).

[7] W. Stoeffl, private communication (1994).

[8] A.V. Burov and N.S. Dikansky, "Electron-Cloud Instabilities", Novosibirsk, presented at MBI97, Tsukuba, (1997).

[9] O. Gröbner, 10th Int. Conference on High Energy Accelerators, Protvino (1977).

[10] The Large Hadron Collider, Conceptual Design, CERN/AC/95-05 (1995); note that the dimensions of the beam screen have been slightly increased to the values quoted, since this report was written.

[11] E. Malamud, private communication (1997).

[12] C. Benvenuti, private communication (1997).

[13] O. Brüning, private communication (1997).

[14] J.S. Berg, "Energy Gain in an Electron Cloud During the Passage of a Bunch", CERN Project Note 97 (1997).

[15] A. Chao, "Physics of Collective Beam Instabilities in High Energy Accelerators", Wiley, p. 208 (1995).

BEAM STABILITY ISSUES OF 3 TeV LOW-FIELD COLLIDER

King-Yuen Ng

Fermi National Accelerator Laboratory, P.O. Box 500, Batavia, IL 60510*

(August, 1997)

I. INTRODUCTION

We analyze the stability issues of the 3 TeV low-field collider. Some relevant properties of the collider are listed in Table I. In the table, the rms bunch length of $\sigma_\ell = 0.50$ m and bunch area of $A = 1.50$ eV-s at injection are extraction values from the Main Injector. At extraction of this 3 TeV ring, we assume the bunch area to be the same, but the rf voltage has been cranked up to $V_{\rm rf} = 4.00$ MV.

II. MICROWAVE INSTABILITIES

Both longitudinal and transverse microwave instabilities have growth rates much faster than a synchrotron period. They are driven by broad-band impedances centered at frequency f_r, corresponding to a wavelength less than the length of the bunch. Therefore, we take $f_r \gtrsim \sigma_\tau^{-1}$, where σ_τ is the rms length of the bunch. The limit for longitudinal microwave stability is

$$\left|\frac{Z_0^{\|}}{n}\right| = \frac{2\pi E|\eta|\sigma_E^2}{eI_{\rm pk}}, \tag{2.1}$$

which equals 7.12 and 1.01 Ohms at injection and extraction. In the above, E is the total energy and σ_E the fractional energy spread. A longitudinal impedance budget of

*Operated by the Universities Research Association, Inc., under contract with the U.S. Department of Energy.

Table I: Properties of the 3 TeV low-field ring.

	Injection	Extraction
Circumference C (km)	34.00	34.00
Kinetic Energy (GeV)	150.00	3000.00
Gamma γ	160.868	3198.37
Revolution frequency f_0 (Hz)	8817.25	8817.42
Number of proton per bunch N	2.70×10^{11}	2.70×10^{11}
Number of bunches M	790	790
Rf harmonic h	6020	6020
Rms bunch length σ_ℓ (m)	0.5000	0.5000
σ_τ (ns)	1.6679	0.6186
Average current per bunch I_b (amp)	3.814×10^{-4}	3.814×10^{-4}
Peak current $I_{\rm pk}$ (amp)	10.35	27.90
Bunch area A (eV-s)	1.50	1.50
Rms energy spread σ_E	3.161×10^{-4}	4.287×10^{-5}
Normalized 95% emittance (π m)	1.50×10^{-5}	1.50×10^{-5}
Betatron tune ν_β	~ 50	~ 50
Bunch area A (eV-s)	1.50	1.50
Rms energy spread σ_E	3.161×10^{-4}	4.287×10^{-5}
Transition gamma γ_t	35.0	35.0
Slippage factor η	7.777×10^{-4}	8.162×10^{-4}
Synchrotron tune ν_s	2.661×10^{-3}	1.021×10^{-3}
Rf Voltage $V_{\rm rf}$ (MV)	1.434	4.000
Beam pipe radius b (cm)	0.90	0.90

less than 1 Ohm is reasonable for such a ring. Thus longitudinal microwave instability should not be a problem.

The limit for transverse longitudinal microwave instability is

$$\left|Z_1^{\perp}\right| = \frac{4\sqrt{2\pi}|\eta|E\sigma_E n_r}{\langle\beta\rangle I_{\rm pk}}, \tag{2.2}$$

where the average betatron function $\langle\beta\rangle$ is taken as R/ν_β and $n_r = f_r/f_0$ is the revolution harmonic of the driving broad-band impedance, $f_0 = \omega_0/(2\pi)$ being the revolution frequency. We obtain the limits $|Z_1^{\perp}| = 22.6$ and 63.9 MOhm/m. One source of impedance is the resistive wall. According to Eq. (3.2) below, the resistive wall of the beam pipe contributes, respectively, $|Z_1^{\perp}| = 13.2$ and 8.06 MOhm/m at injection and extraction for the the frequency $f_r = \sigma_\tau^{-1}$. However, with all the the bellows shielded, it should not be difficult to maintain a transverse impedance budget for this below these stability limits.. Thus, transverse microwave instability should not be a problem.

III. COUPLED-BUNCH INSTABILITIES

Coupled-bunch instabilities are driven by narrow resonances, mostly from the higher-order modes of the rf cavities. Without any knowledge of these cavities, it will be hard to make any estimation of the instabilities. However, there is a transverse coupled-bunch instability driven by the resistivity of the beam-pipe wall, which can be studied easily.

The beam pipe is of inner radius $b = 0.90$ cm. It is made of one inner layer of pure aluminum having 1 mm thickness with resistivity $\rho = 2.65 \times 10^{-8}$ Ohm-m, and an outer layer of a harder alloy having slightly higher resistivity. The skin depth at one revolution harmonic is

$$\delta_1 = \sqrt{\frac{\rho c}{Z_0\omega_0}} = 0.873 \text{ mm}, \tag{3.1}$$

where c is the velocity of light and Z_0 is the impedance of free space. As will be shown below, if we assume a residual betatron tune of $[\nu_\beta] = 0.4$, the lowest tune-line

that causes an instability is at the frequency of $f_{\min} = -0.6 f_0 = -5290$ Hz. There, the skin depth will be 1.13 mm, which is roughly the thickness of the aluminum layer of the beam pipe. Thus, we can assume that no electromagnetic fields will leak out from the beam pipe.

The resistive-wall impedance can be written as

$$\left(Z_1^{\perp}\right)_{\text{wall}}(\omega) = [1 - i\,\text{sgn}(\omega)]\frac{R\delta_1}{b^3}\sqrt{\frac{\omega_0}{|\omega|}}\,. \tag{3.2}$$

This formula is correct when (1) the skin depth is less than the wall thickness, which we have demonstrated to be roughly true, (2)

$$\sqrt{\omega} \gg \frac{1}{b}\sqrt{\frac{2\rho c}{Z_0}}\,, \tag{3.3}$$

or frequency $f \gg 82.9$ Hz, which is very well satisfied, and (3)

$$\omega^{3/2} \ll \frac{2c}{b}\sqrt{\frac{cZ_0}{2\rho}}\,, \tag{3.4}$$

or $f \ll 3.5 \times 10^{12}$ Hz, which is very much larger than the bunch frequency and even the cutoff frequency of the beam pipe. By the way, Eq. (3.3) can also be written as pipe radius very much larger than skin depth.

There are $M = 790$ bunches. If they are situated symmetrically in the accelerator ring, there will be M transverse coupled-bunch modes driven by the resistive wall. The growth rate of the sth mode is given by

$$\tau_s^{-1} = -\frac{ecMI_b}{4\pi E\nu}\sum_k \mathcal{R}e\, Z_1^{\perp}[(Mk + s + \nu_\beta)\omega_0]F\,, \tag{3.5}$$

where the form factor F is close to unity for low frequencies. Since there are M bunches, for each mode the betatron lines are separated by M revolution harmonics. According to Eq. (3.2), The transverse impedance due to the resistive wall falls off as $|\omega|^{-1/2}$. Therefore, the most dangerous mode is the one where one betatron line has a negative frequency closest to zero. If we assume the residual betatron tune to be $[\nu_\beta| = 0.4$, that line has the frequency of $f_{\min} = -0.6 f_0 = -5290$ Hz. Retaining only that term in the summation in Eq. (3.5), the most dangerous growth rates

are, respectively, 3287 and 165.3 s^{-1} at injection and extraction. The corresponding growth times are 2.68 and 53.3 turns.

Let us investigate whether the fast growth rates can be lowered by running the machine at a positive chromaticity. This amounts to shifting the bunch spectrum towards the positive-frequency side, so that the $n = -0.6$ betatron line only overlaps with the tail of the bunch spectrum. However, the bunch rms frequency spread is $\sigma_f = (2\pi\sigma_\tau)^{-1} = 95.4$ and 257.3 MHz for the two energies. Therefore, to have a significant effect, the chromaticities required will be roughly $\xi = \sigma_f/f_0 = 1 \times 10^4$ and 2.9×10^4 units, for injection and extraction. This is, of course, not practical at all. The main reason is the large size of the ring resulting in too low a revolution frequency f_0.

Another way to reduce the growth rates is to install octupoles so that there will be an amplitude dependent tune spread. We want each bunch to have so much tune spread that coherency will be lost during the growth time. Roughly the required tune spreads will be ~ 0.37 and ~ 0.018 for the two energies. Obviously, the tune spread at injection is too large to be acceptable. The last resort is a fast active damper.

IV. MODE COUPLING INSTABILITIES

For impedances with wavelengths longer than the bunch length, bunch instabilities occur when two stable modes collide. Longitudinal mode-coupling instability will be self-stabilized by the lengthening of the bunch, and is therefore not as important. Transverse mode-coupling instability will lead to beam breakup. Here, we concentrate on the transverse modes. When mode 0 shifts by $\Delta\nu_s \sim -\nu_s$, it collides with mode -1 and an instability occurs. The threshold is given by

$$\Delta\nu_s = -\frac{ieI_b\langle\beta\rangle\omega_0}{4\pi E}\int_{-\infty}^{\infty} Z_1^{\perp}(\omega)e^{-\omega^2\sigma_\tau^2}d\omega \sim -\nu_s\,. \tag{4.1}$$

Due to the symmetry properties of $Z_1^{\perp}$, it is only the reactive part which contributes

to this instability. If we define an effective inductive transverse impedance

$$\left(Z_1^{\perp}\right)_{\text{eff}} = \frac{\int_{-\infty}^{\infty} -\mathcal{I}m\, Z_1^{\perp}(\omega) e^{-\omega^2\sigma_\tau^2} d\omega}{\int_{-\infty}^{\infty} e^{-\omega^2\sigma_\tau^2} d\omega}, \tag{4.2}$$

Then instability will not occur if

$$\left(Z_1^{\perp}\right)_{\text{eff}} \lesssim \frac{4\sqrt{\pi}\nu_s E\sigma_\tau\omega_0}{eI_b\langle\beta\rangle}. \tag{4.3}$$

These limits are, respectively, 6.37 and 18.03 MOhms/m at injection and extraction. For a broad-band impedance that resonates at a frequency much higher than the bunch spectrum, the integral can be approximated and we obtain the threshold $Z_1^{\perp}|_{\text{eff}} = -\mathcal{I}m\, Z_1^{\perp}(0)$. For the resistive wall, using the transverse impedance given by Eq. (3.2), we obtain

$$\left(Z_1^{\perp}\right)_{\text{eff}} = -\mathcal{I}m\left(Z_1^{\perp}\right)_{\text{wall}}(\omega_0)\Gamma(\tfrac{1}{4})\sqrt{\frac{\omega_0\sigma_\tau}{\pi}} = \begin{cases} 48.0 \text{ MOhm/m} & \text{Injection} \\ 29.2 \text{ MOhm/m} & \text{Extraction}. \end{cases} \tag{4.4}$$

We see that these values exceed the stability limits.

A Damper
to Suppress Low Frequency Transverse Instabilites
in the VLHC

John Marriner
September 3, 1997

Introduction

The 1996 Snowmass summer study highlighted the lowest frequency transverse coupled bunch instability as an important consideration for the design of a low field (<2 T) VLHC (Very Large Hadron Collider).[1] The growth rate was estimated to be 1/3 of the revolution period. This instability is routinely suppressed with electronic feedback* at operating machines such as the Main Ring and Tevatron, but was thought to be "beyond the state of the art"[2] for the VLHC– presumably because the calculated growth time was shorter than the revolution period. The purpose of this paper is to describe a feedback system (a "damper") using straight-forward techniques on a very modest scale that would suppress the instability.

Should We Believe the Growth Rate Estimate?

The growth rate is calculated assuming that thecollective motion is the same as the single particle motion plus a perturbation. The effect of the perturbation is evaluated by averaging over the motion. It seems that this procedure can hardly be valid when the instability grows by e^3 in a single turn. Nevertheless, it is plausible that the answer is at least roughly correct: one can observe similar growth rates (of the order of 1000 $\sec^{-1}$) in the Tevatron and other FNAL machines. These growth rates only seem short when compared to the very long revolution period of the VLHC. For the purposes of this paper, I will assume that we are required to achieve a damping time of 1/3 of a revolution period

The Issue

The main issue is whether the resistive wall instability dictates the aperture required. The resistive wall impedance depends on the pipe radius (b) and mode frequency (f) as follows:

$$Z_\perp \propto \frac{1}{b^3\sqrt{f}}.$$

The impedance can be drastically reduced by increasing the beam pipe aperture. However, the cost of increasing the aperture is significant and it would be desirable to have the aperture as small as possible.

---

* The dependence of the growth rate on the chromaticity can be and is also used to control the instability.

What Bandwidth is Required?

The growth time is assumed to be about 1 msec for the lowest mode. Higher order modes will be unstable with growth rates proportional to $f^{-1/2}$ and will be Landau damped when the growth rate is comparable to the synchrotron frequency (~1 Hz). Assuming 100 Hz for the lowest unstable line, lines are unstable up to 100 MHz (this is almost all the lines). Let us consider only the fastest growing modes (those below 100 kHz) and leave the others to a "conventional" bunch-by-bunch damper with a single turn delay.

System Concept

A signal is derived from a "difference" pickup, *i.e.*, a pickup that is sensitive to the product of the beam current and its transverse position. The signal is amplified and transmitted downstream to a point 90° advanced in betatron phase. The signal is further amplified and applied to a kicker to provide the negative feedback required to stabilize the beam. The fact that the signal arrives late and is applied to succeeding bunches doesn't matter at these low frequencies (because the phase error is small).

Pickup

I assume that a capacitive pickup is used to derive a signal proportional to the beam intensity times displacement. The pickup is made of two striplines terminated by an open circuit at one end and a high impedance amplifier at the other. The signal voltage is given by:

$$V_p = S i_b Z_0 \frac{2\Delta x}{g}$$

With a beam current (i_b)=4 A, a characteristic impedance (Z_0)=50 Ω, an electrode gap (g)=3cm, a sensitivity factor (S)=0.8, and a displacement (Δx)=0.1 mm, one obtains V_p=1 V.

Kicker

I assume we want to kick a reasonable fraction of the 0.1 mm displacement at the kicker. A displacement of Δx at the pickup is equivalent to an angular displacement at the kicker of

$$\theta_k = \frac{\Delta x}{\sqrt{\beta_p \beta_k}} = 231 \text{ nrad}$$

when $\Delta x = 0.1$ mm, $\beta_p = 250$ m,

and $\beta_k = 750$ m.

A stripline kicker will provide a deflection of

$$\Delta\theta = 2\sqrt{2}\frac{SVl}{gE}$$

$$V = \sqrt{PZ_0}$$

For a sensitivity factor (S)=0.8, length (l)=10 m, electrode gap(g)=3 cm, final amplifier power (P)=2000 W, characteristic impedance (Z_0)=50 Ω, and E=3 TeV one finds $\Delta\theta$=80 nrad. I consider this to be an adequate kick, but a larger kick could be obtained by using a longer kicker or by making a magnetic (ferrite loaded) kicker. Both options decrease the system bandwidth, but it is only of practical concern for a slow rise-time magnet kicker. The 10 m long kicker does not need to be a continous object. For example, ten 1-m long kickers connected in series could perform the same function.

System Gain

The critical feature of the damper is the gain. We require a damping time of 1/3 of a turn or a damping rate of about 3. A total of 10 systems distributed around the ring, each with a damping rate of 1/3 would provide the necesary feedback. With the pickup and kicker structures described previously, an electronic gain of about 300 (50 dB) is required.

Beam Heating Rate

The beam heating rate resulting from a broadband noise spectrum is:

$$\begin{aligned}\frac{d\varepsilon}{dt} &= 24\pi\beta_k f_0 \frac{Z_0 S^2 l^2 P}{g^2(E/e)} \\ &= 24\pi \bullet 750 \bullet 464 \frac{50 \bullet 0.8^2 \bullet 10^2 P}{0.03^2 \bullet \left(3\times10^{12}\right)^2} \\ &= 6.6\times10^{-14}\pi P \text{ m - rad/(W - sec)}\end{aligned}$$

where I have chosen to evaluate the heating at the injection energy of 3 TeV. Converting to normalized emittance and somewhat more convenient units

$$\frac{d\varepsilon}{dt} = 0.76\pi \text{ mm - mrad/(W - hr)}$$

The maximum total damper power level that could be tolerated appears to be in the range of 0.1 to 1 W. Ten damper units running at a full power of 2000 W would result in excessive emittance growth, but a 5 nV/$\sqrt{\text{Hz}}$ preamp at this gain (300) and bandwith (1 MHz) generates less that 1 μW–well below the maximum tolerable level. I conclude that the emittance growth will be negligible provided that an effort is made to produce a low noise system.

System Power

The required damping rate determines the system gain. In an ideal system no power is required because the beam is not oscillating. A practical system requires power to amplify the undesired signals at the input of the amplifier. These signals could include:

- Static closed orbit distortion caused by steering errors.
- Dynamic closed orbit distortion caused by power supply ripple and ground motion.
- Turn by turn oscillations following injection.
- Amplifier Thermal Noise.

These extraneous signals affect the damping only if they reduce the system gain by saturating the feedback amplifier. With a unit power amplifier of 2000 W and a gain of 300, the maximum effective orbit offset that can be tolerated about 0.1 mm. The closed orbit distortion can be suppressed by a factor of 10 (probably more in a slowly cycling machine like the VLHC) by electronically nulling the damping pickup. Thus, the tolerance on the closed orbit at the damper pickup is the fairly comfortable value of 1 mm. If necessary, real-time feedback from the damper pickup to the orbit correction system could be used.

The analysis of power supply ripple and ground motion is well beyond the scope of this note, but it seems reasonable to assume that it is much less than the 1 mm closed orbit error. The electronic pickup nulling circuit will be effective for nulling low frequency motion (such as ground motion and motion at the synchrotron frequency), but probably not be effective for power supply ripple at multiples of 60 Hz.

A maximum injection oscillation of 0.1 mm could be tolerated by the damper system with no degradation in performance (neglecting any closed orbit error). I don't know whether this tolerance will be difficult to achieve, but it is clear that it must be achieved to obtain a beam size of 10π mm-mrad (the rms beam size of a 10π mm-mrad at β=250 m is 0.36 mm). Even if the emittance requirement is relaxed somewhat, the damper system still has some margin assuming that the beam is injected in short batches. Only the most recently batch will saturate the amplifier: the damper will still work as long as the batch length is short compared to the distance required for the instability to grow by a power of *e*.

It is important to note that the damper system power that comes from the motion of the beam does not normally result in emittance growth. In fact, the system will have the beneficial effect of reducing emittance growth from these other noise sources. The amount of reduction depends on the ratio of feedback system gain (damping in 1/3 of a turn) to the decoherence time of the beam, which depends on the spread in synchrotron and betatron tunes. The decoherence time has not been estimated, but it seems likely that it would be considerably greater than one turn.

Bandwidth

The main limitation of the bandwidth of the system described above is the transit time delay between pickup and kicker. The pickup to kicker distance must be about 1000 m to get 90° phase advance between pickup and kicker. The signal could be transmitted with "foam" coaxial cable, which has a beta greater than 0.8. The difference in delay between the beam and the signal is therefore about 200 m at the speed of light plus an estimated electronics delay of 50 nsec or about 700 nsec total. The maximum frequency consistent with this delay is about 1/8 × (1/700 nsec) = 179 kHz. This bandwidth meets the requirements for this system (100 KHz), but it could be extended by using an air-dielectric type cable.

Concluding Remarks

It appears to be straight-forward to damp low frequency instabilties in the VLHC. The system described damps any type of transverse, dipole, coupled bunch instability provided that the bunch-to-bunch phase advance is small enough to be included in the system bandwidth. Single bunch instabilities, such as transverse mode coupling instabilities, and high-frequency coupled bunch modes would not be damped by this type of system.

The system is not particularly challenging in any respect. It is fairly easy to provide stronger feedback if necessary by increasing the gain (more systems, more power, more electronic gain, stronger kickers, more bandwidth, etc.). The technique is not speculative and should not be controversial. A similar system was used to damp the resistive wall instability in the Main Ring (but only the lowest band). The parameters of the proposed system (power, gain, etc.) are similar to or less challenging than systems already in use.

---

[1] G. Dugan, P. Limon, and M. Syphers, "Really Large Hadron Collider Working Group Summary," *New Directions for High-Energy Physics, Proceedings of the 1996 DPF/DPB Summer Study on High-Energy Physics, Snowmass '96.* This document is available from Stanford Linear Accelerator Center's World Wide Web site, http://www.slac.stanford.edu/a.

[2] J. Rogers, "Collective Effects and Impedances in the RLHC(s)," *New Directions for High-Energy Physics, Proceedings of the 1996 DPF/DPB Summer Study on High-Energy Physics, Snowmass '96.* This document is available from Stanford Linear Accelerator Center's World Wide Web site, http://www.slac.stanford.edu/a.

"Pipetron" Beam Dynamics with Noise

V. D. Shiltsev

Fermi National Accelerator Laboratory

P.O. Box 500, Batavia, Illinois 60510

October 14, 1996

Abstract

Extra-large hadron collider – "Pipetron" – at 100 TeV energy range is currently under consideration. In this article we study the Pipetron transverse and longitudinal beam dynamics under influence of external noises. The major effects are growths of transverse and longitudinal emittances of the beam caused by noisy forces which vary over the revolution period or synchrotron oscillation period, respectively; and closed orbit distortions induced by slow drift of magnet positions. Based on analytical consideration of these phenomena, we estimate tolerable levels of these noises and compare them with available experimental data. Although it is concluded that transverse and, probably, longitudinal feedback systems are necessary for the emittances preservation, and sophisticated beam-based orbit correction methods should be used at the Pipetron, we observe no unreasonable requirements which present an impenetrable barrier to the project.

Contents

1 Introduction **3**

2 Transverse Emittance Growth **4**
- 2.1 Effect of Transverse Kicks 4
- 2.2 Measured Ground Motion 6
- 2.3 Feedback System 12
- 2.4 RF Phase Noise 14

3 Longitudinal Emittance Growth **15**
- 3.1 RF Noise Effect 15
- 3.2 Transverse Kicks Effect 17

4 Closed Orbit Distortions **17**
- 4.1 Alignment Tolerances 17
- 4.2 Slow Ground Motion 18
- 4.3 Correction System 20

5 Discussion **21**

6 Conclusions **23**

1 Introduction

Several proposals of the post-LHC large colliders with 30–100 TeV beam energy and $10^{33} - -10^{35}\ s^{-1}cm^{-2}$ have been considered in recent years. Two approaches can be distinguished in the trend – namely, smaller circumference ring with high magnetic field dipoles based on high-T_c technology [1], and presumably lower cost option of a micro-tunnel low-field machine with consequently large circumference [2]. The later – often referred as "Pipetron" (or "MegaCollider") – is a subject of this article. Table 1 shows relevant parameters of the collider [3].

Table 1: "Pipetron"- MegaCollider parameters

Proton Energy,	E_p, TeV	100
Circumference,	C, km	1000
Luminosity,	L, $s^{-1}cm^{-2}$	10^{35}
Intensity,	N_p/bunch	$4.1 \cdot 10^{10}$
No. of Bunches,	N_b	25000
RMS emittance,	ϵ_n, $10^{-6}\,m$	1
Long. emittance (rms),	A, eV·sec	0.3
Bunch length (rms),	σ_s, cm	10
Mom.spread (rms),	$\Delta P/P$	10^{-5}
Rev. frequency,	f_0, Hz	300
Interaction focus	β^*, cm	10
IP size	σ_{IP}, μm	1
Beam-beam tune shift	ξ_p	0.005

The collider ring consists of thousands of magnetic elements, and their field imperfections can seriously affect proper machine operation. It is known [5] that depending on the frequency band one can distinguish two mechanisms of beam perturbations in circular accelerator. Slow processes (with respect to revolution period) produce a distortion of the closed orbit of the beam. At higher frequencies (comparable with the revolution frequency), noises cause direct emittance growth. The revolution frequency of the Pipetron is much lower than in any other existing or ever planned accelerator, so, because numerous natural noises rapidly grow with frequency decrease, the noise may produce dramatic effect on the beam dynamics

of the Pipetron. This article is devoted to major effects in beam dynamics due to external noise. Besides this Introduction, the paper consists of four chapters devoted to transverse emittance growth, longitudinal emittance growth, closed orbit drifts, and comparison of the Pipetron tolerances with those of the LHC and the SSC. The final chapter summarizes major conclusions.

2 Transverse Emittance Growth

2.1 Effect of Transverse Kicks

Transverse kicks. The primary sources which lead to emittance growth in large hadron colliders are quadrupoles (quad) jitter and high-frequency variations of the bending magnetic field in dipoles. Both sources produce angular kicks and excite coherent betatron oscillations. After some time (which is about 1200 turns in the case of the Pipetron – see below in the section devoted to a feedback system) filamentation or dilution process due to tune spread within the beam transforms the coherent oscillations into the emittance increase. If there is no damping of the excited coherent motion, then the latter as whole "smears" to the beam phase space volume. In the simplest case, when the kick amplitude $\Delta\theta$ varies randomly after the revolution time $1/f_0$ and its variance is $\delta\theta^2$, one can estimate the transverse emittance growth as:

$$\frac{d\epsilon_n}{dt} = \frac{1}{2} f_0 \gamma \sum_i^{all\,kicks} \Delta\theta_i^2 \beta_i = \frac{1}{2} f_0 \gamma \delta\theta^2 < \beta > N \qquad (1)$$

where $< \beta >$ is the average beta function, $\gamma = E_p/mc^2$ is relativistic factor, and N is the number of elements which produce uncorrelated kicks. Two major sources of the dipole kicks are fluctuations δB of the bending dipole magnetic field B_0 which give horizontal kick of $\delta\theta = \theta_0(\delta B/B_0)$ ($\theta_0 = 2\pi/N_d$ is bending angle in each dipole, N_d is total number of dipoles); and transverse quadrupole magnets displacements δX which lead to kick of $\delta\theta = \delta X/F$, where F is the quadrupole focusing length. For a ring which consists mostly of FODO focusing structure with half cell length of L (approximately equal to dipole magnet length) and the phase advance per cell of μ one can rewrite the emittance growth rate equation [1]:

$$\frac{d\epsilon_n}{dt} = 2 f_0 \gamma \frac{\delta X^2 N_q}{L} tg(\mu/2) = 2c\gamma \frac{\delta X^2}{L^2} tg(\mu/2) = \gamma \frac{\delta X^2}{c} N_q^2 2 tg(\mu/2), \qquad (2)$$

where N_q is total number of quads, c is the speed of light. Similarly, uncorrelated field fluctuations in dipoles result into mostly horizontal emittance growth rate – while (2) stands for both vertical and horizontal emittances – equal to:

[1] following Ref. [4], we take into account FODO equation $\sum_i \beta_i/F_i^2 = 4tg(\mu/2)N_q/L$

$$\frac{d\epsilon_n}{dt} = \frac{\pi f_0 \gamma L}{\nu} \frac{\delta B^2}{B_0^2} = \frac{\pi c \gamma}{N_d \nu} \frac{\delta B^2}{B_0^2}, \tag{3}$$

$\nu = C/(2\pi\nu)$ is the tune.

It is interesting to note, that "vibrational" emittance growth (2) is proportional to factor of $N_q^2 tg(\mu/2) \propto N_q \nu = \Phi$, while dipole field effect (3) is proportional to Φ^{-1}. The value of Φ is proportional to ν if the half-cell length value L is fixed, or grows as ν^2 if the phase advance per cell μ is constant. Therefore, the two contributions to the emittance growth rate (2,3) perform exactly opposite dependencies on the machine tune.

In general case, when external noise is not "white" (exactly random in time) and can be described by power spectral density $S_{\delta\theta}(f)$ [2] which depends on frequency f, the emittance growth rate is calculated in [5]:

$$\frac{d\epsilon_n}{dt} = \gamma f_0^2 \sum_i \Big(\beta_i Sum_i(\nu)\Big) \tag{4}$$

where

$$Sum_i(\nu) = \sum_{n=-\infty}^{\infty} S_{\delta\theta}\Big(f_0|\nu - n|\Big) \tag{5}$$

is the sum of power spectral densities of angular kicks produced by the i-th source at frequencies of $f_0|\nu - n|$, n is integer, the lowest of them is fractional part of the tune times revolution frequency $f_1 = \Delta\nu f_0$ (β_i is the beta function at the i-th magnet). The dimension of $Sum(f)$ is 1/Hz, so the dimension of the emittance growth rate is meters/sec. Note, that we assume that kick sources are uncorrelated.

Beam lifetime and acceptable emittance growth. Let us constrain that external noise should lead to less than 10% emittance increase while the beam circulates in the accelerator. Characteristic beam lifetime τ in Pipetron has to be chosen to optimize integrated luminosity. Several time constants play role in that. First of all, these are longitudinal and transverse *emittance* growth times due to intrabeam scattering, which are equal to (see, e.g. [6]):

$$\tau_{\|}^{IBS} \approx \frac{4\epsilon_n^2 A \nu_x d}{\pi L_c m_p c^2 N_p r_p^2}, \quad d^2 = 1/(1 + \frac{\sigma_x^2}{D_x^2(\Delta P/P)^2}) \approx \frac{cA\nu_s}{\epsilon_x E_p \nu_x}, \tag{6}$$

and

$$\tau_x^{IBS} \approx \tau_{\|}^{IBS}/d^2, \quad L_c = \ln \frac{\gamma^{1/4}\nu_x^{1/4}\epsilon_x^{3/4}}{R^{1/4} r_p^{1/2}} \tag{7}$$

[2] see definitions of the power spectral density in the next section concerning ground vibration noise

where $r_p = 1.53 \cdot 10^{-18}$m is proton's classical radius, $R = C/2\pi$ is the ring radius , and ν_x is the horizontal betatron tune. Taking for definiteness $\nu_x \approx 500$ (see below) one gets $\tau_{||}^{IBS} \approx 6$ hrs, and $\tau_x^{IBS} \approx 500$ hrs. The luminosity "burn-up" time $\tau_L = N_p N_b/(L\sigma_{pp}) \approx 28$ hours ($\sigma_{pp} \approx 100$ mb is total pp cross section at 100 TeV). Transverse damping time τ_D due to synchrotron radiation of protons in Pipetron is about 42 hours, that is too small for the radiation to play any significant role in beam dynamics.

Comparing these temporal values one can choose the Pipetron cycle time of about $\tau_c = 5$ hours and get the constraint on the noise-induced emittance growth:

$$\frac{d\epsilon_n}{dt} \leq 0.1\frac{\epsilon_n}{\tau_c} = 5.6 \cdot 10^{-12}\, m/s. \tag{8}$$

Tolerances. Taking into consideration 500-m long FODO cell (i.e. $L = 250$m) focusing structure with $\mu = 90^o$ phase advance per cell [3] one can estimate the tune $\nu \simeq 500$, total number of focusing quadrupoles as $N_q = 4000$ and about the same number of dipoles N_d. Now, the acceptable transverse emittance growth rate requires:

- single quadrupole transverse vibration spectral density of power is limited by the value of:

$$\sum_n S_{\delta X}(f_0|\nu - n|) \approx S_{\delta X}(f_0\Delta\nu) \leq 2 \cdot 10^{-11}\, \frac{\mu m^2}{Hz} = 20\, \frac{pm^2}{Hz},$$

  where $\Delta\nu$ is fractional part of ν. Approximation sign reflects that spectrum of vibrations falls fast with frequency increase (see below).

- or the rms amplitude of turn-to-turn jitter of each quadrupole (white noise in frequency band f_0 [3]):

$$\delta X_{rms} \leq 0.76 \cdot 10^{-10}\, m = 0.76 \cdot 10^{-4}\, \mu m = 0.76\, \dot{A}.$$

- and a tolerable level of bending magnetic field fluctuations to its mean value B_0 in the dipole:

$$\left(\delta B/B_0\right)_{rms} \leq 3.4 \cdot 10^{-10}.$$

2.2 Measured Ground Motion

Let us make a comparison of the above calculated constraints with experimental data. First of all, one should consider the ground motion because it is ambient,always existing and non-controlled noise. Technological near-by equipment can increase

[3] note, that transition between "white noise" formula (1) to "color noise" one (5) corresponds to substitution $\delta X^2 \Leftrightarrow f_0 S_X(\Delta\nu f_0)$

natural vibrations level by several orders of magnitude. In addition, accelerator environment contains many other sources which can produce angular kicks and, therefore, initiate the emittance growth (see, e.g. Tevatron experience in [23]). In recent years a number of thorough experimental investigations of ground vibrations have been done for future colliders (see review in [7]). Below we outline some results.

As most of disturbances are *noises*, then statistical spectral analysis defines the *power spectral density* $S_x(f)$ (PSD) of noise process $x(t)$ at frequency $f \geq 0$ as:

$$S_x(f) = \lim_{T\to\infty} \frac{2}{T} \left| \int_0^T x(t) \quad e^{-i2\pi f t} dt \right|^2 . \tag{9}$$

The dimension of the PSD is *power in unit frequency band*, e.g. m^2/Hz for the PSD of displacement. PSD relates to the *rms value of signal* $\sigma_{rms}(f_1, f_2)$ in the frequency band from f_1 to f_2 as $\sigma^2_{rms}(f_1, f_2) = \int_{f_1}^{f_2} S_x(f)df$, e.g. below we note integrated rms amplitude that corresponds to $f_2 = \infty$. The *spectrum of coherence* $C(f)$ of two signals $x(t), y(t)$ is defined as:

$$C(f) = \left| \frac{\langle X(f)Y^*(f)\rangle}{\sqrt{\langle X(f)X^*(f)\rangle\langle Y(f)Y^*(f)\rangle}} \right| , \tag{10}$$

here $< \ldots. >$ means averaging over different measurements and $X(f), Y(f)$ are Fourier transformations of x, y. The coherence does not exceed 1.0 and is equal to 0 for completely uncorrelated signals.

Fig.1 compares the value of $S_x(f)(2\pi f)^2$ in units of $(\mu m/s)^2/Hz$ [4] for the US Geological Survey "New Low Noise Model" [8] – a minimum of the PSD observed by geophysicists worldwide – and data from accelerator facilities of HERA [9], KEK [10], CERN [12], SLAC[14], and FNAL [15]. These PSDs of velocity indicate that: 1) accelerators are essentially "noisy" places; 2) ground vibrations above 1 Hz are strongly determined by cultural noises – they manifest themselves as numerous peaks in Fig.1; 3) even among accelerator sites the difference is very large, that gives a hint for the Pipetron builders.

[4] i.e. the PSD of velocity $v = 2\pi f x$. The ground velocity spectra plots are looking much better than the PSDs of displacement x which look very tilted because of strong reduction of noises at higher frequencies.

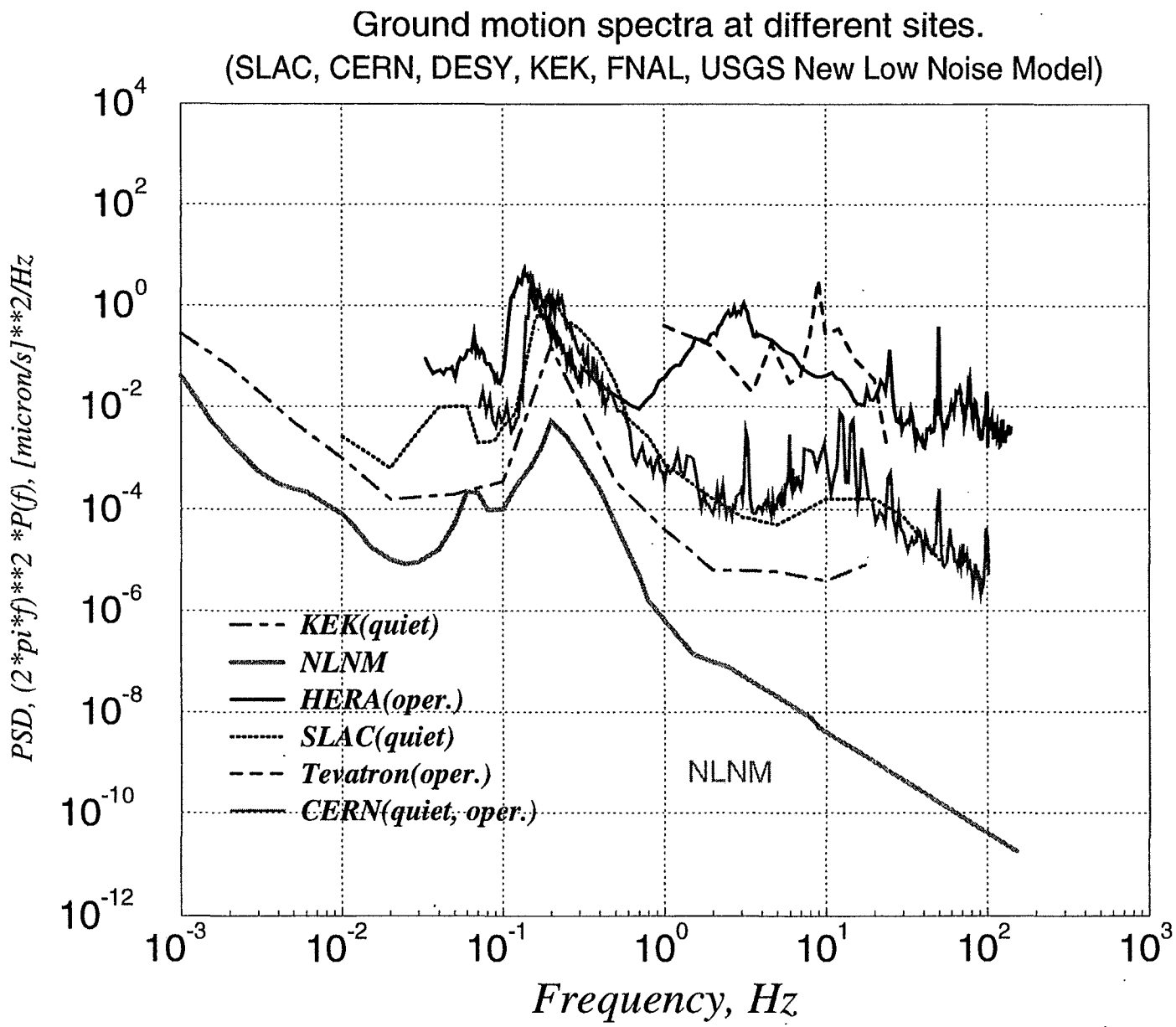
Ground motion spectra at different sites.
(SLAC, CERN, DESY, KEK, FNAL, USGS New Low Noise Model)
PSD, (2*pi*f)**2 *P(f), [micron/s]**2/Hz
Frequency, Hz
KEK(quiet)
NLNM
HERA(oper.)
SLAC(quiet)
Tevatron(oper.)
CERN(quiet, oper.)
NLNM

There is a "rule of thumb" [7] that says that the rms amplitude of the vibration at frequency f and above is equal to $r.m.s.X = B/f[Hz]$ (here B is a constant) which corresponds to the PSD of $S_x(f) = 2B^2/f^3$. Within a factor of 4 this rule usually fits well the accelerators-averaged vibration amplitudes above 1 Hz under "quiet" conditions. Fig.2 presents the values of $rmsX(f) = \int_f^\infty S_x(f)df$ calculated for several spectra from Fig.1 – namely, for SLAC, CERN, HERA, and FNAL data. The measurement of tunnel floor vibration amplitude made in the Tevatron tunnel at FNAL covers frequencies of 1–25 Hz and can be approximated by the "rule of thumb" with $B = 100$ nm. Although there is no data on FNAL site vibrations at higher frequencies, we will use the fit predictions above 25 Hz as well. From Fig.2 one can see that almost the same coefficient B is applicable for the HERA tunnel amplitudes, while ground motion amplitudes in tunnels of SLC(SLAC) and TT2A(CERN) are about 10-20 times smaller.

Below 1 Hz the ground motion amplitude is about 0.3-1 μm due to remarkable phenomena of "7-second hum". This hum is waves produced by oceans – see a broad peak around 0.14 Hz in Fig.1 – with wavelength of about $\lambda \simeq 30$ km. It produces negligible effect on Pipetron, because λ is much bigger than typical betatron wavelength $2\pi\beta \simeq 2$ km.

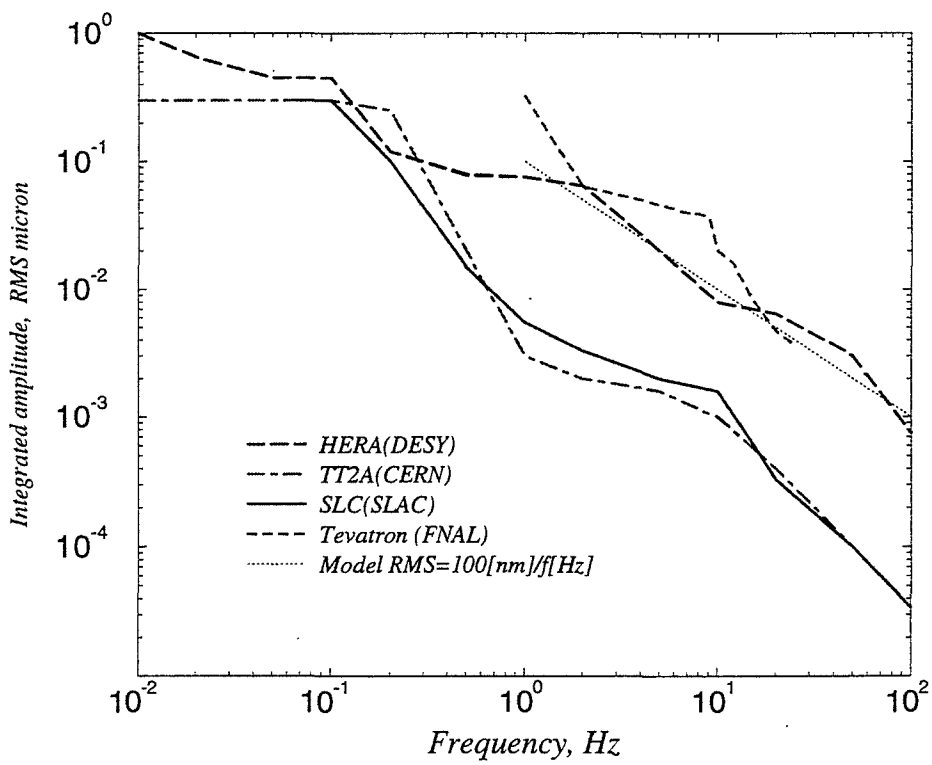

Figure 2: RMS amplitude above f vs. f.

Thorough investigations of spatial characteristics of the fast ground motion have shown that above 1-4 Hz the correlation significantly drops at dozens of meters of distance between points. Fig.3 shows the spectrum of coherence between vibrations of two quadrupoles distanced by 60m at the APS(ANL) [13]. The coherence falls with increasing distance L between observation points, and sometimes a 2-D random waves model prediction of $C(f) = |J_0(2\pi f L/v)|$ with $v = 200 - 500$m/s fits well to the experimental data [14]. For the FODO lattice with distance between quads $L = 250$ one may treat motion of magnets as uncorrelated at frequencies above 1 Hz.

Table 2 compares requirements for the Pipetron with three particular tunes $\Delta\nu = 0.18,\ 0.31$ and 0.45 and experimental data. Note that corresponding frequencies $f_1 = f_0\Delta\nu$ are equal to 54 Hz, 93 Hz, and 135 Hz.

Table 2: PSD of Ground Motion (in $(pm)^2/Hz$) at Three Frequencies

$\Delta\nu$	0.18	0.31	0.45
f_1	54 Hz	93 Hz	135 Hz
Pipetron tolerance	**20**	**20**	**20**
NLNM	0.02	$2{\cdot}10^{-3}$	$2{\cdot}10^{-4}$
SLAC (quiet)	100	-	-
DESY (tunnel)	10^5	7000	1700
SSC (quiet) [11]	10^4	100	20
CERN (tunnel)	300	20	-
"Rule of thumb"	**1.3**$\cdot 10^5$	**2.5**$\cdot 10^4$	**8000**

One can see that none of the accelerator data shows vibrations which are less than the Pipetron requirements, although PSDs at higher frequencies (say $f_1 = 135$ Hz) are much less than at lower frequency of 54 Hz, and, therefore, larger $\Delta\nu$ – closer to half integer resonance – are preferable from this point of view. At $\Delta\nu = 0.18$ one needs the vibration power reduction factor of $R = 10 - 10^4$.

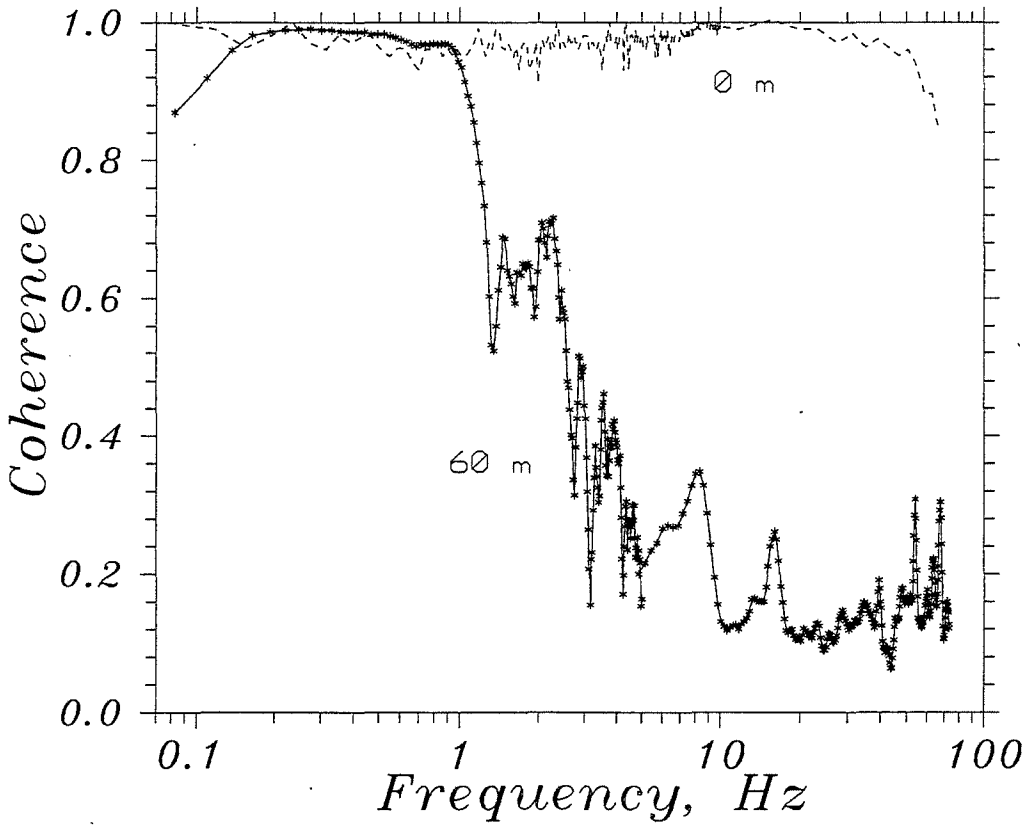

Figure 3: Coherence spectra at the APS (ANL).

Before discussion on the feedback system which can effectively counteract the emittance growth, we'd like to make three comments: firstly, there are ways to reduce quadrupole vibrations with active mechanical stabilization of the magnets or passive dampers which isolate magnets from sources of vibrations (ground, cryogenic/electrical systems, etc.). The active stabilization of magnetic elements - besides its probable high cost for the really large accelerator – doesn't seem to be applicable for damping at frequencies above 20-30 Hz (see e.g. [16]). In opposite, the passive isolation works better at higher frequencies, although its capability is quite limited (characteristic damping of 10-20dB [17]), but it leads to certain degradation of low-frequency stability and does not cure vibrations produced inside the magnet.

Secondly, requirement on the magnet motions is somewhat easy in the combined function lattice. Indeed, from 1, one can see that if the characteristic length over which mechanical motion of the dipole+quadrupole in one magnet can be considered as coherent is equal to l_c, than the emittance growth rate is $r = l_c/L$ times less than (1) [5]. At frequencies about 50-100 Hz and above one can roughly estimate $l_c \sim 10$

[5]indeed, the number of coherently vibrating sub-quads with length l_c is proportional to $N_c \propto 1/r$ while the kick produced by each of them is r times weaker $\Delta\theta_c \propto r$, thus the total effect in the emittance growth is proportional to the product of N_c and $\Delta\theta_c^2$ that is $\propto (1/r) * r^2 = r$.

m, so, as $L = 250$ m, we obtain $r \simeq 1/25$ and, consequently, 5 times larger tolerance on the ground motion *amplitude*. Unfortunately, variations in the PSD of ground motion are at least hundred times larger than r, thus, the combined function lattice can not solve the whole problem.

Thirdly, we have not enough experimental data to answer the question: "Is it possible to reduce dipole field fluctuations at 50-150 Hz down to the level of $3{\cdot}10^{-9}$?". At these frequencies the skin depth even in copper is about 1 cm, thus, no reasonable vacuum chamber can effectively reduce field variation due to current ripple. Another important and unanswered question is spatial coherence of the current ripple: correlated field changes over the ring can lead to substantial increase as well as decrease of the emittance growth. To avoid confusion, we should note, that in contrast to a wideband noise, the main components of the ripple are usually concentrated at several well-defined frequencies (multiples and subharmonics of 60 Hz in the USA), and one can significantly reduce their detrimental influence by detuning $f_1 = \Delta\nu f_0$ away from these frequencies.

2.3 Feedback System

Emittance evolution. A transverse feedback frequency allows one to suppress the emittance growth caused by excitation of the betatron oscillations by external noise kicks simply by damping the coherent beam motion which otherwise goes directly to the beam phase space increase. It is obvious that the oscillations should be damped much faster then they decohere. The system monitors the dipole offset X of the beam centroid and tries to correct it by dipole kicks θ which are proportional to the offset, applied a quarter of the betatron oscillation downstream. We operate with dimensionless amplification factor g of the system (gain) which is equal to:

$$g = \frac{\theta\sqrt{\beta_1\beta_2}}{X}, \tag{11}$$

where β_1 and β_2 are the beta-functions at the positions of the pick up and the kicker electrodes respectively. In the limit of $g \ll 1$ the decrement due to the feedback is equal to $\frac{1}{2}f_0 g$, i.e. the amplitude of the betatron oscillations being reduced $1/e$ times after $2/g$ revolution periods. Theory of the feedback (see e.g. [5]) gives the transverse emittance evolution formula:

$$\frac{d\epsilon_n}{dt} = \Big(\frac{4\pi\delta\nu_{rms}}{g}\Big)^2\Big[\Big(\frac{d\epsilon_n}{dt}\Big)_0 + \frac{\gamma f_0 g^2}{2\beta_1}X^2_{noise}\Big], \quad g \gg 4\pi\delta\nu_{rms}, \tag{12}$$

where emittance growth rate without feedback $(d\epsilon_n/dt)_0$ is given by (1,4), X_{noise} is the rms noise of the system (presented as equivalent input noise at the pick-up position), and $\delta\nu_{rms}$ is the rms tune spread within a beam.

Sources of decoherence. The decoherence of betatron oscillations is caused by several kinds of the tune spread [18, 19, 20]:

- rms tune spread due to nonlinear fields is about

$$\delta\nu_{NL,O} = \sigma^2(d\nu/da^2) \simeq \nu\frac{\epsilon_n < \beta >^2}{\gamma} b_3 = 10^{-6},$$

  due to systematic error octupole component of $b_3 = 10^{-6}\ cm^{-3}$ [3], and about twice larger due to sextupoles used for chromaticity correction $b_2 \approx \nu/(< \beta >< D_x >) = 2.5 \cdot 10^{-4}\ cm^{-2}$:

$$\delta\nu_{NL,S} \simeq \frac{\epsilon_n < \beta >^3}{2\gamma\nu} b_2^2 = \nu\frac{\epsilon_n < \beta >}{2\gamma < D_x >^2} \approx 2 \cdot 10^{-6},$$

- tune spread due to residual chromaticity and momentum spread

$$\delta\nu_{CR} \approx 2\nu_s\Big(\frac{\eta(\Delta P/P)}{2\nu_s}\Big)^2 \simeq 10^{-5}$$

  if the chromaticity η is compensated down to 5, and the synchrotron tune is $\nu_s = 2.4 \cdot 10^{-4}$;

- major source of the tune spread (and, consequently, decoherence) is nonlinear beam-beam force which results in the rms tune spread of [20]

$$\delta\nu_{BB} \approx 0.167\xi = 8.4 \cdot 10^{-4}.$$

The decoherence takes place over about $N_{decoher} \approx 1/\delta\nu_{BB} \approx 1200$ turns.

Ultimate gain and emittance growth reduction. Computer simulations [4, 21] and analytical consideration of the feedback system [22] resulted in maximum useful gain factor $g_{max} \simeq 0.3$ – there found no reduction of the emittance growth rate with further increase of g because of higher-(than dipole)-order kicks effect, the system noise contribution grows, while the coherent tune shift due to feedback becomes too large, and affects multibunch beam stability in presence of resistive wall impedance.

Therefore, maximum reduction factor $R_{max} = (g_{max}/4\pi\Delta\nu_{BB})^2$ is about 800 for the Pipetron design parameter of $\xi = 0.005$, while the minimum practical gain which still can lead to the damping is about $4\pi\delta\nu_{BB} \approx 0.01$. Note, that DESY and SSC ground motion powers – see Table 2 – at $f_1 = 0.18 f_0$ are beyond the extreme feedback capability.

As it is seen from (12), feedback noise also leads to emittance growth and its relative contribution grows as $\propto g^2$. Taking the beta function at the pick-up $\beta_1 =$ 500m we get limit on the rms noise amplitude:

$$X_{noise} \ll X_{noise}^{max} = \Big[\frac{2\beta_1(d\epsilon_n/dt)_0}{f_0(4\pi\delta\nu_{BB})^2\gamma}\Big]^{1/2} \approx 1.4\,\mu m. \tag{13}$$

Thermal noise at room temperature T for a pick-up with half-aperture b can be estimated as:

$$X_{th} = \frac{b}{f_0 N_p N_b e}\sqrt{\frac{4kT\Delta f}{Z}} \approx 0.5[nm]\sqrt{\Delta f[kHz]}, \tag{14}$$

here k is Boltzmann constant; pick-up impedance was chosen $Z = 50$ Ohm. For a narrow band system with $\Delta f \sim 10$ kHz, the noise is about 1.6nm, while for a bunch-by-bunch feedback system $\Delta f = 10$MHz and $X_{th} = 0.05\,\mu$m. We see, that, in principle, thermal noise limit is well below the necessary accuracy of 1.4 μm (see (13)).

Power of the output amplifier of the system depends on maximum noise amplitude of the proton beam oscillations. The rms coherent oscillation amplitude can be estimated as $\delta X_{rms} \approx \sqrt{N_{decoher} N_q B/f_1} \approx 2\,\mu$m. Taking the "safety " factor of 5 we get $\delta X_{max} = 5\cdot\delta X_{rms} = 10\,\mu$m maximum amplitude, and the necessary angular kick of about $2\cdot 10^{-9}$ rad – we assume $\beta_2 = 500$ m at the kicker. Such a corrector with a length of $l_k = 1$m, and an aperture $b = 1$cm will require a certain amount of energy δW of electric (or magnetic) field E:

$$\delta W = \frac{E^2}{8\pi}\pi l_k b^2 \simeq \delta X_{max}^2[\mu m]b^2[cm]/l_k[cm]\cdot 5[mJ] = 5[mJ]. \tag{15}$$

Again, for a narrow band feedback system with Δf=10 kHz, it yields the power of $P = \delta W\Delta f$= 50 W, while for a bunch-by-bunch system one needs 50 kW amplifier.

2.4 RF Phase Noise

Basic equation of the longitudinal particle motion describes particle motion under impact of the RF phase error $\Delta\phi$:

$$\Big(\frac{\Delta p}{p}\Big)_{n+1} = \Big(\frac{\Delta p}{p}\Big)_n - \frac{eV_0}{E_p}\phi_n,$$

$$\phi_{n+1} = \phi_n + 2\pi h\Big(\frac{\Delta p}{p}\Big)_n + \Delta\phi_n, \tag{16}$$

here V_0 stands for the RF voltage, hapmonics number $h = f_{RF}/f_0$, p is particle momentum. Turn-to-turn jitter of the RF phase results in fast momentum variation $(\Delta p/p) = (eV_0/E_p)\Delta\phi$ which leads to an instant change of the horizontal orbit of $\Delta X = D_x(\Delta p/p)$, where D_x is the dispersion function at the RF cavities. It is

equivalent to beam displacement and – again, after decoherence process – causes the emittance growth of:

$$\frac{d\epsilon_n}{dt} = \frac{1}{2}\gamma H \delta\phi^2 f_0 \frac{eV_0}{E_p}, \tag{17}$$

where the invariant $H = (D_x^2 + [\beta_x D_x' - \beta_x' D_x/2]^2)/\beta_x$. The energy gain of 100 TeV over τ_R =0.5 hour requires 185 MeV per turn energy increase, thus, taking an overvoltage factor of 2 we need $eV_0 = 370$ MeV. Taking (in the worst case) $H = 1$ cm at the RF system position, one gets that 10% emittance increase during the ramp time occurs with the rms turn-by-turn RF phase jitter $\delta\phi \equiv \sqrt{f_0 \sum_n S_\phi(f_0|\nu - n|)} \simeq$ 5 mrad. Note, that frequencies of interest are still of about f_1 and f_0, i.e. of the order of hundred(s) of Hz. The measured one phase noise at the Tevatron is less than 0.04 in 100 Hz frequency band [23], i.e. more than 100 times less than the tolerance. There is no need of high voltage RF at the collision energy at the Pipetron, and, say, $eV_0 = 20$ MeV should be enough, that yields in easier tolerances on the phase stability of $\delta\phi \simeq 30$ mrad. Thus, the RF phase jitter does not seem to be a real problem for the transverse emittance degradation.

As it is seen from (16), fast variation of the voltage δV also can initiate the effect, and the tolerance on the amplitude can be derived from the phase tolerance as $(\Delta V/V_0) \approx \Delta\phi_s \simeq 0.03$, where $\phi_s = \sigma_s/\lambda_{RF} \approx 0.15$. This requirement also seems to be quite easy to fulfil.

3 Longitudinal Emittance Growth

3.1 RF Noise Effect

The RF phase errors at frequencies of the order of synchrotron one $f_s = \nu_s f_0$ and higher lead to the longitudinal emittance growth of:

$$\frac{dA}{dt} = \frac{eV_0}{f_{RF}} \frac{d\phi^2}{dt}. \tag{18}$$

The synchrotron oscillations phase grows under impact of noise as

$$\frac{d\phi^2}{dt} = \pi\omega_s^2 S_\phi(\omega_s) = 2\pi f_0^2 \nu_s^2 S_\phi(f_0\nu_s)$$

, where $\omega_s = 2\pi\nu_s f_0 > 0$, S_ϕ is the PSD of the phase noise [6] (see e.g. Appendix C in [21]).

The synchrotron frequency

$$f_0\nu_s = f_0\sqrt{\alpha h e V_0/(2\pi E_p)} = 0.017[Hz]\sqrt{V_0[MV]/(E_p/100TeV)}$$

[6]here the PSD in $\omega = 2\pi f$ domain relates to f domain PSD as $S(\omega) = S(f)/(2\pi)$. Extended analytical consideration of the longitudinal emittance growth can be found in e.g. [24, 25].

varies from 3.1 Hz at the beginning of the ramp [7] (E_p=2 TeV, $V_0 = 370$ MV, $\nu_s \approx 0.01$) to 0.33 Hz at the end of the ramp at 100 TeV ($\nu_s \approx 0.0011$), and then it is about 0.076 Hz during the collision time with $V_0 = 20$ MeV The latter frequency corresponds to the synchrotron tune of $\nu_s = 2.5 \cdot 10^{-4}$ which comes from single bunch stability threshold of the transverse mode-coupling instability:

$$\nu_s = \frac{16\sqrt{\pi}(E_p/e)\sigma_s}{2I_s R \mathrm{Im} < Z_\perp \beta >}, \tag{19}$$

where $I_s = 2\,\mu$A is DC single bunch current, and transverse impedance comes mostly from resistive walls $\mathrm{Im} Z_\perp = 377\Omega(R\delta/b^3) \simeq 240\,M\Omega$/m (the skin depth δ for 10-cm long bunch in Al chamber is about 4 μm).

If one requires less than 10% emittance increase during half an hour of ramp time τ_R, than the tolerance on the phase jitter PSD in $f_{RF} = 450$ MHz RF system is:

$$S_\phi(\omega_s) = \frac{0.1 A f_{RF}}{\tau_R(eV_0)\pi\omega_s^2} \approx \frac{6.4 \cdot 10^{-6}}{\omega_s^2}. \tag{20}$$

Measurements with the SSC RF system HP8662 synthesizer [24] shows that in frequency band of 1-100 Hz the PSD of phase noise can be approximated by

$$S_\phi(\omega_s) = \frac{1.3 \cdot 10^{-5}}{\omega^{2.65}}, \tag{21}$$

that is twice the tolerance (20) at frequencies about 1 Hz.

Equivalent rms phase jitter tolerance is $\delta\phi \simeq \sqrt{\omega_s S_\phi(\omega_s)} \approx 0.3$ mrad at $f_s = 3$ Hz.

The same 10% tolerance for 5 hours of the collision operation with $eV_0 = 20$ MeV gives:

$$S_\phi(\omega_s) \approx \frac{1.2 \cdot 10^{-5}}{\omega_s^2}. \tag{22}$$

that is very close to the measured PSD.

Having these numbers one can conclude that with some improvement of the RF phase stability with respect to the SSC synthesizer, no longitudinal feedback will probably be required. If the feedback will be implemented it should be not so sophisticated as transverse one – it should not be fast and have a large gain, because the process of the synchrotron oscillations decoherence takes hundreds of thousands of turns in the Pipetron. Tolerance on the RF voltage stability δV also does not seem tough – it can be estimated as $(\delta V/V_0) \sim (\delta\phi/\phi_s) \simeq 0.2\%$ where we take acceptable phase jitter of 0.3 mrad, and the bunch phase area of $\phi_s = \sigma_s f_{RF}/c \approx 150$ mrad.

[7] here we take the momentum compaction factor of $\alpha \approx 1/\nu_x^2 \approx 4 \cdot 10^{-6}$

3.2 Transverse Kicks Effect

Another possible source of the RF phase errors is the change of the circumference due to non-zero dispersion function D_x at the position of dipole kick [25], produced e.g. by displaced quadrupole magnet $\theta = \Delta X/F$:

$$\Delta\phi = 2\pi h D_x \theta = 2\pi h D_x \Delta X/F.$$

For the whole ring of N_q quadrupoles randomly moving at frequencies about f_s with rms amplitude of δX, it results in rms phase error:

$$\delta\phi = \frac{h < D_x > \sqrt{N_q}\delta X}{FR} \approx \frac{h\sqrt{N_q}\delta X}{\nu_x^2 F}. \tag{23}$$

Combining (23) and (20), and taking $h = 1.5 \cdot 10^6$, $\nu_x \approx 500$, $F \simeq 200$ m and $N_q = 4000$ we get the tolerable PSD of ground motion [8]:

$$S_X(f_s = \nu_s f_0) = \frac{2.8 \cdot 10^5}{f_s^2}\,[\mu m^2/Hz],$$

or about 300 μm rms amplitude in 3 Hz frequency band.

As it is seen from Fig.1, the power of the ground noise at all probable synchrotron frequencies of 0.7–3 Hz is some 10000 times smaller, therefore the quadrupole motion effect is negligible. [9]

Quite similar consideration of the dipole field variation effect results in tolerance on the field stability of about $(\delta B/B) \simeq 0.1\%$ rms in 3 Hz frequency band. Unfortunately, we have no available experimental data on the field stability, but the tolerance we got should not be severe.

4 Closed Orbit Distortions

4.1 Alignment Tolerances

The rms closed orbit distortion dX_{COD} is proportional to the rms error dX of quads alignment, and if these errors are not correlated, then in the FODO lattice we can get:

$$dX_{COD}^2 = \frac{\beta dX^2}{4sin^2(\pi\nu)} \sum_i \frac{\beta_i}{F_i^2} = \frac{\beta N_q tg(\mu/2) dX^2}{Lsin^2(\pi\nu)}. \tag{24}$$

[8] in f domain

[9] the PSDs in Fig.1 are for *absolute* movements, i.e. those measured at one point by use of velocitymeter seismic probe with further integration. Relative displacement is even smaller – see next Section on ground drifts.

Let us take the "safety criteria", i.e. ratio of maximum allowable COD to the rms one, equal to 5 [10], then for maximum COD of dX_{COD}^{max}=1 cm (this is about half aperture of the vacuum chamber) at the focusing lenses where $\beta_F = 765$ m ($L = 250$ m, $\mu = 90^o$) we get requirement on the rms alignment error of $dX \approx 15\,\mu$m (there was used the value of tune $\Delta\nu = 0.31$). This value sets a challenging task, its solution needs the most sophisticated alignment techniques and two questions arise in this connection: 1) temporal stability of the magnets positions; and 2) applicability of the beam-based alignment.

4.2 Slow Ground Motion

Numerous data on uncorrelated slow ground motion support an idea of "space-time ground diffusion". An empirical rule that describes the diffusion – so called "the ATL law" [26] – states the rms of relative displacement dX (in any direction) of two points located at a distance L grows with time interval T:

$$< dX^2 >= ATL, \tag{25}$$

where A is site dependent coefficient of the order of $10^{-5\pm1}\ \mu m^2/(s \cdot m)$. As long as the diffusion coefficient A is very small, the ground wandering presents only a tiny, but important contribution to the total ground motion which can be several orders of magnitude larger but well correlated in space and time at very low frequencies, systematic, unidirectional, and, therefore, sometimes predictable. The PSD of ATL diffusion is equal to

$$S_{ATL}(f) = AL/(2\pi^2 f^2). \tag{26}$$

The ground diffusion should cause corresponding COD diffusion in accelerators with rms value equal to [27]:

$$\langle dX_{COD}^2 \rangle = \frac{\beta ATC(\beta_F + \beta_D)}{8F_0^2 \sin^2(\pi\nu)}, \tag{27}$$

here C is the accelerator circumference, F_0 is the focal length of each quadrupole in $FODO$ lattice, ν is the tune of the machine, β is the beta-function at the point of observation. For most of practical estimations of the rms orbit distortion amplitude averaged over the ring, the formula $COD \simeq 2\sqrt{ATC}$ can be used. It clearly shows that the diffusive orbit drift is not very sensitive to the focusing lattice type (only the circumference C plays role), in particular, there is almost no difference between the combined- and separated-function lattices responses on the ATL-like diffusion.

[10] Let us remark that probably this factor of 5 will not be enough in the Pipetron with its challenging tolerances, because recent accelerator alignment studies at SLAC and Japan [28, 29] show that due to both human and natural factors, the alignment errors statistics is far from Gaussian, it is rather power-law-like, it often has no finite variance value and demonstrates significant probability to have many-sigma outliers.

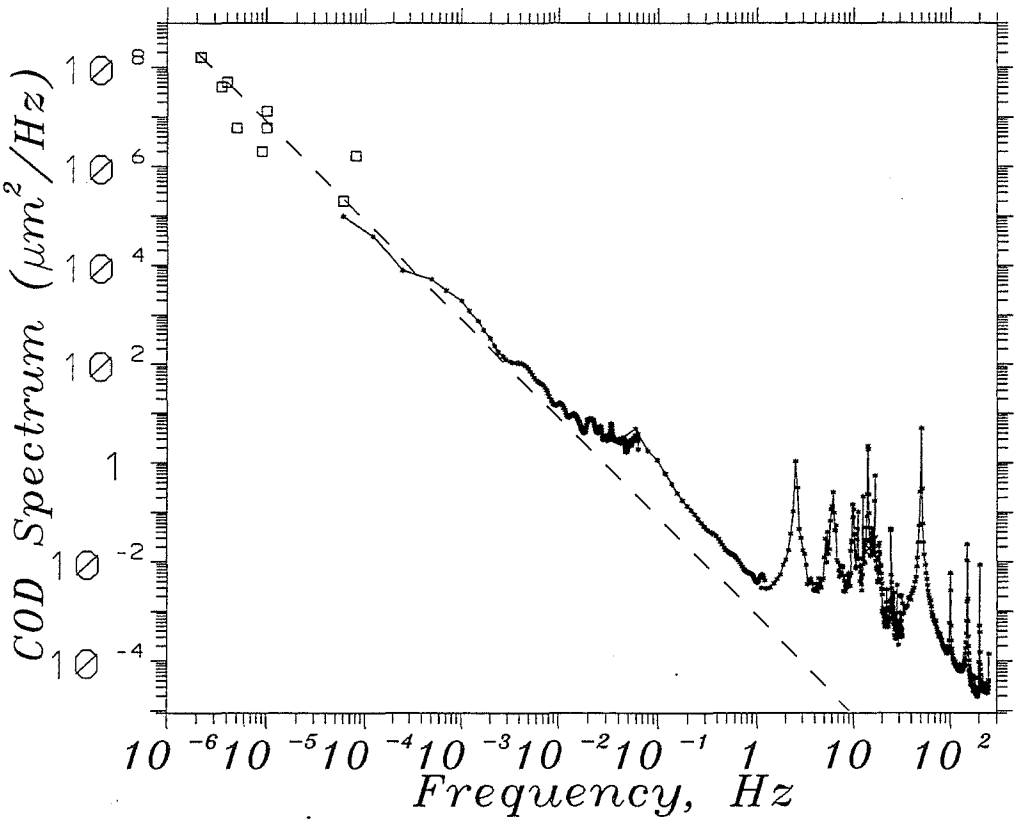

Figure 4: Spectrum of vertical orbit drifts at HERA-p normalized on β =1m. Dashed line is for the ATL model prediction.

Fig.4 presents the PSD of the HERA$-p$ vertical orbit (scaled for $\beta = 1$ m) which clearly demonstrates "diffusion-like" behavior of the COD at frequencies below 0.1 Hz – the dashed line is for $S_{COD}(f) = 8 \cdot 10^{-4}/f^2$ $[\mu m^2/Hz]$ which is in agreement with the ATL law with $A = 3.8 \cdot 10^{-5}$ $\mu m^2/(s \cdot m)$ (see formula (26) above). Peaks above 2 Hz are due to technological equipment. The squares at lower frequencies represent the Fourier spectra of proton orbit in 131 BPMs from different fills of the storage ring [30]. Solid line is for data from a low noise BPM [9]. The motion of quads was checked to be the only candidate that can explain these drifts. It was stressed in [30], that having completely different magnet lattice, the HERA electron ring orbit also performs "random-walk-like" diffusion with comparable coefficient A.

Review of the ground diffusion observations [31] points out that the diffusion coefficient A depends on tunnel depth and type of rock. [11] The question of the limits

[11] Linear Collider study group at KEK reported indication of significant (15 times in the coefficient A) seasonal variations of the diffusion in the 300-m-deep Sazare mine (Japan, green schist) [32] and they also observed 5 time larger A in a dynamite-dug tunnel in welded tuff with respect to drilled tunnel in granite (i.e. the tunnel construction method probably makes a difference) [33].

of applicability of the ATL law is still open – available data cover T from minutes to dozen years, L from meters to dozens km.

Let us scale the HERA-p orbit data from Fig.4 to the Pipetron with use of Eq.(27) (i.e one should replace $\beta_F + \beta_D$ from 94.2 m at HERA to 1000 m at the Pipetron, C from 6.3 km to 1000 km, F_0 from 16.8 m to 177 m, and $\Delta\nu$ from 0.298 to 0.31) then we obtain rms COD at $\beta_{max} = 850$ m equal to:

$$dX_{COD} \approx 800[\mu m]\sqrt{T[hrs]}. \tag{28}$$

Again, requiring "safe" rms COD of 2 mm, we get T=6.3 hours mean time between necessary realignments to initial "smooth" orbit.

If one intends to have a stable and deep tunnel comparable with the LEP one where it was found $A \approx 5 \cdot 10^{-6}\ \mu m^2/(s \cdot m)$, then the corresponding orbit drift is $dX_{COD} \approx 800[\mu m]\sqrt{T[hrs]}$ and the period of necessary repetition of the Pipetron alignments is about 2 days. It does not seem to be an easy task to do it mechanically, even with use of robots, especially taking into account 15 μm precision of the procedure. "Beam-based alignment" technique looks as the most appropriate for that.

4.3 Correction System

"Beam-based alignment" assumes an extensive use of BPM readings in order to utilize information about beam distortions for the "golden" orbit maintenance. In circular accelerators this method (also named "K-modulation") is based on a fact that if the strength of a single quadrupole $K = Gl/Pc$ in the ring is changed by dK, the resulted difference in closed orbit is proportional to the original offset of the beam in the quadrupole – see Fig.5.

From the measured difference orbit the offset can be determined, yielding either the quad offset to eliminate or the offset between quadrupole axis and BPM adjacent to the quad for global correction. The method is widely used now at many accelerators, e.g. in HERA-e all of 148 quads were equipped with switches in order to vary the strength of magnets individually, that allows to align the ring within 0.05 mm error in less than 24 hours [34].

For the Pipetron, the tolerance on quads alignment of $dX = 15\,\mu$m yields in beam displacement in the next downstream quadrupole position (where we assume the BPM) of the order of $dXL/F(dK/K) \simeq 1\,\mu$m if the modulation depth is about $dK/K = 0.05$. Taking several measurements or/and with use of phase-lock technique one can distinguish such displacement with BPM resolution of the order of $\Delta_{BPM} \simeq 5\,\mu$m.

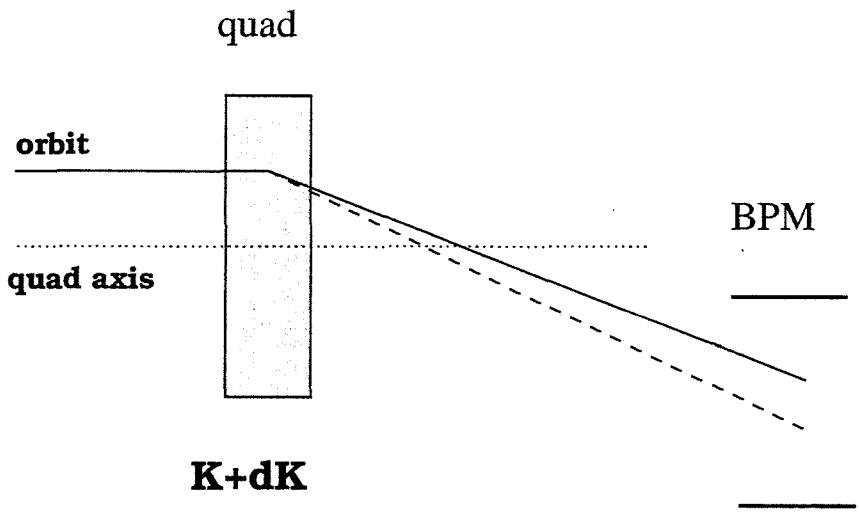

Figure 5: Principle of the beam-based alignment.

Let us calculate necessary strength of correctors assuming two correctors per cell, geologically stable tunnel (deep, in the hard rock) which can be characterized by the ground diffusion coefficient $A = 5 \cdot 10^{-6}\ \mu m^2/m/s$ (close to LEP tunnel data [31]) and requiring that no mechanical realignment will be necessary within T=10 years period. Accordingly to the ATL law (25) it gives $\sqrt{ATL} \approx 630\ \mu$m rms relative quads displacement($L = 250$m), or (factor of 5) about dX_{max} =3.2 mm of maximum displacement. Thus, the maximum angle to correct is $dX_{max}/L \simeq 13\ \mu$rad, or about 4.3 Tm of the corrector strength at 100 TeV.

5 Discussion

Table 3 compares tolerances for hadron colliders of LHC(CERN), SSC and the Pipetron. There are two major effects which limit collider performance. The first is the transverse emittance growth due to fast (turn-to-turn) dipole angular kicks $\delta\theta$ produced by bending field fluctuations in dipole magnets $\Delta B/B$ or by fast motion of quadrupoles σ_q. The 10% emittance increase requirement $d\epsilon_n/dt < 0.1\epsilon_n/\tau_C$, where τ_C is the collision regime duration, sets a limit on the turn-by-turn jitter amplitude which looks extremely tough – of the order of the atomic size! Comparison with results of measurements shows that for all three colliders the effect may have severe consequences, although the Pipetron is the most troublesome case.

Other figures in Table 3 are for the rms quad-to-quad alignment tolerances in order to keep the rms orbit dX_{COD} within 5 mm, and the estimated time after which cumulative drifts due to ground diffusion will cause these distortions $T_c \approx dX^2_{COD}/(4AC)$ (we take here $A = 10^{-5}\ \mu m^2/(s \cdot m)$). One can see that the SSC and the Pipetron

have to be realigned very often – or, another solution, to have strong and numerous correctors.

Table 3: Stability of Hadron Colliders

Parameter	LHC	SSC	Pipetron
Energy E, TeV	7	20	100
Circumference C km	26.7	87.1	1000
Emittance ϵ_n, μm	4	1	1
L-lifetime τ_C, hrs	10	20	5
$\Delta\nu f_0$, Hz	3100	760	54-135
Quads jitter σ_q, nm	0.05	0.03	0.008
Measured jitter, nm	0.01-0.1	0.2	0.1-50
$\Delta B/B$, 10^{-10}	~ 4	~ 2	$\approx$3.4
Align. error, μm	100	60	40
Realign. time, T_c	~1.5 yr.	~6 mos.	~2 weeks

Preceding consideration has shown that natural and man-made vibrations at Pipetron can lead to dangerous transverse emittance growth rate (high-frequency part of spectrum) and closed orbit distortions (at lower frequencies). At the early stage of the project, "on-site" ground motion measurements are necessary to conclude
1) are the measured vibrations dangerous for the Pipetron beam dynamics?
2) (if - presumably - yes) what are necessary parameters of the beam emittance preservation feedback system (gain, noise, bandwidth, power) and strength of dipole orbit correctors?

For that it seems reasonable to investigate experimentally following topics:

- amplitudes of vibrations, their spectra in 0.01–300 Hz band,
- correlation of vibrations at distances of 0...500 m,
- amplitudes in a tunnel (Tevatron or test tunnel) vs. surface ones,
- influence of weather (thunderstorm, wind, rain, temperature changes),
- ground motion at FNAL and at other probable site(s),
- influence of traffic, other high frequency cultural noise,
- impact of quarry blasts, remote and local earthquakes,
- mechanical resonances of the magnet prototype,
- emittance growth modeling with seismometers "on-line" (as in [35]),

- relative drifts of tunnel floor over long periods of time (days–months) at distances from dozen meters to a kilometer.

Besides these items, the Pipetron emittance growth rate estimations call for measurements of:

- the RF system phase and amplitude noises in frequency band of 0.01–500 Hz,
- periodical ripple and random noise in magnitude of dipole magnetic field in 0.01–500 Hz band,
- spatial correlation of the bending magnetic field jitter along 250-m long dipole magnet.

6 Conclusions

In this article we have studied impact of external noises on the Pipetron proton collider transverse and longitudinal beam dynamics. General conclusion is that there are several rather tough requirements on the noise amplitudes but they can be fulfilled.
In more detail, we found that:

Acceptable transverse emittance growth rate (less than 10% over the beam lifetime) requires less than 0.076 nm turn-to-turn uncorrelated jitter of the quadrupole positions and less than $3.4 \cdot 10^{-10}$ field strength fluctuations in dipole magnets. Analysis of up-to-date ground motion measurements worldwide shows that these tolerances are too tight for actual accelerator tunnels. The emittance growth due to ground motion is smaller for larger fractional part of the betatron tune, and we suggest to have $\Delta\nu$ (or $1 - \Delta\nu$) as big as 0.3-0.45. There is a certain need in a feedback system to damp betatron oscillations and reduce the growth. Decoherence due to beam-beam interaction in the Pipetron is too fast, and limits the maximum transverse emittance growth rate reduction factor by the value of about 800. We also found that thermal noise in the feedback BPM will not limit the system performance, and estimated necessary power of system with the 10 MHz frequency band to be about 50 kW. It is noted that combined function magnetic structure of the collider is preferable as it eases the tolerances.

Estimates based on the Tevatron and the SSC RF systems phase errors measurements, show that the RF phase jitter in Pipetron will not cause any significant transverse emittance growths, while only several-fold improvement in the phase stabilization at low frequencies will allow to avoid longitudinal feedback system as well. Low frequency quadrupole movements will not cause the bunch lengthening due to synchrobetatron coupling with non-zero dispersion in the ring.

Maximum distortions of the proton closed orbit of the order of the vacuum chamber size were found to occur with some 15 μm rms relative quad to quad misalignment which is – accordingly to the HERA-p observations and the "ATL law" – to be accumulated during 6 hours of operation. To counteract the effect the beam-based alignment technique must be implemented, that requires some 5μm BPM accuracy, and 4.5 Tm corrector strength, but in return will allow to avoid mechanical realignment with use of robots over 10 years time periods.

Finally, we emphasize an importance of "on-site" ground motion studies and magnet vibrations measurements, as well as necessity of data on long-term tunnel movements, the RF phase and amplitude stability, and dipole field jitter.

Acknowledgments

I acknowledge valuable comments and useful discussions with Bill Foster, David Neuffer, David Finley, Pat Colestock, Ernest Malamud (FNAL) and Gennady Stupakov(SLAC).

References

[1] S.Peggs *et.al*, "Lattice Optimization for a Really Large Hadron Collider", *Proc EPAC'96*, Barcelona, Spain (1996).

[2] E.Malamud and G.W.Foster, "New Technologies for a Future Superconducting Proton Collider", FERMILAB-Conf-96/145 (June 1996);
G.W.Foster and E.Malamud, "Low-Cost Hadron Colliders at Fermilab: A Discussion Paper", FERMILAB-TM-1976 (June 1996);
see also the project information at *http://www-ap.fnal.gov/PIPE/.*

[3] D.Neuffer, "Discussion of parameters, lattices and Beam Stability for the MegaCollider", FERMILAB-TM-1964 (March, 1995).

[4] V.Lebedev, V.Parkhomchuk, V.Shiltsev, A.Skrinsky, "Suppresion of Emittance Growth Caused by Mechanical Vibrations of Magnetic Elements in Presence of Beam-Beam Effects in the SSC", Preprint INP 91-120, Novosibirsk (1991).

[5] V.Lebedev, V.Parkhomchuk, V.Shiltsev, G.Stupakov, "Emittance Growth due to Noise and Its Suppression with the Feedback System in Large Hadron Colliders", *Particle Accelerators*, Vol.44, No.3-4, p.147 (1994).

[6] L.R.Evans, "Beam Effects in Hadron Colliders", in *AIP Conference Proceedings*, No. 127, p.244, (1985).

[7] V.Shiltsev, "Alignment and Stability of Future Machines", *Proc. of EPAC'96*, Barcelona, Spain (1996).

[8] J.Peterson, USGS Open-File Report 93-322, Albuquerque, NM (1993).

[9] V.Shiltsev,et.al, DESY-HERA-95-06; *Proc. of 1995 IEEE PAC*, Dallas, p.2078, p.3424.

[10] S.Takeda, M.Yoshioka, KEK-Preprint 95-209 (1996).

[11] V.D.Shiltsev, in *AIP Conf. Proc. 326*, pp.560-589 (1995).

[12] V.Jouravlev,et.al, CERN-SL/93-53 and CLIC-Note-217 (1993).

[13] V.D.Shiltsev,*Proc. 1995 IEEE PAC*, Dallas, p.2126.

[14] *Ground Motion: Theory and Measurements*, Appendix C of NLC ZDR, SLAC-R-0485 (1996).

[15] C.D.Moore, "Vibrational Analysis of Tevatron Quadrupoles", FNAL-TM-1959, and *Proc. of IV Int. Workshop on Accel. Alignment, Tsukuba, Japan*, KEK Proceedings 95-12 (1995), p.119.

[16] N.Ishihara,et.al, KEK 89-88 (1989);
V.Shiltsev, A.Kolmagorov, in *Proc. of Linear Colliders'91 Workshop*, Protvino (1991);
C.Montag, DESY 96-053 (1996).

[17] G.Decker,*et.al*,,"Reduction of Open-Loop Low Frequency Beam Motion at the APS", *Proc. 1995 IEEE PAC*, Dallas (1995), p.303;
D.Mangra (APS/ANL), private communication on damping pads for the APS girder.

[18] R.E.Meller, *et.al*, "Decoherence of Kicked Beams", SSC-N-369 (1987).

[19] W.Chou, J.O.Peterson, "the SSC Transverse feedback System", SSCL-623, 1993.

[20] G.Stupakov, V.Parkhomchuk, V.Shiltsev, "Decoherence of a Gaussian Beam Due to Beam-Beam Interaction", SSCL-Preprint-495 (1993).

[21] V.Lebedev, "Computer Simulation of the Emittance Growth due to Noise in Large Hadron Colliders", *Particle Accelerators*, (1994), vol.44, p.165.

[22] V.Parkhomchuk, V.Shiltsev, "Is Transverse Feedback Necessary for the SSC Emittance Preservation?", SSCL-622 (1993).

[23] S.R.Mane, G.Jackson, "Studies and Calculations of Transverse Emittance Growth in High Energy Proton Storage Rings", *Proc. 1989 IEEE PAC*, Chicago (1989), p.1801.

[24] H.-J.Shih, *et.al,* "Longitudinal Beam Dynamics with RF Noise", *Particle Accelerators*, Vol.43(3) (1994), p.159.

[25] M.Syphers, *et.al,* "Experimental Simulation of Ground Motion Effects", *Proc. 1993 IEEE PAC*, Washington (1993), p.420.

[26] B.A.Baklakov,et.al, Preprint INP 91-15, Novosibirsk;
Proc. of 1991 IEEE PAC, San-Francisco, p.3273;
Sov. Tech. Phys., v.38 (1993), p.894.

[27] V.Parkhomchuk, V.Shiltsev, G.Stupakov,"Slow Ground Motion and Operation of Large Colliders", *Particle Accelerators*, v.46 (1994), p.241.

[28] R.Pitthan, "Realignment: It Is the Tunnel Floor Which Moves, Isn't It?", *Proc. of IV Int. Work. on Accel. Alignment*, KEK Proceedings 95-12 (1995), p.382.

[29] V.Shiltsev, comment on 17-years Sazare mine (Japan) hydrostatic level measurements, private communication at *IV Int. Work. on Accel. Alignment.*

[30] R.Brinkmann and J.Rossbach, *Nucl. Instr. Meth.*, v. A350 (1994), N.1-2, p.8.

[31] V.Shiltsev, "Space-Time Ground Diffusion: The ATL law for Accelerators", *Proc. of IV Int. Work. on Accel. Alignment*, KEK Proceedings 95-12 (1995), p.352.

[32] S.Takeda, *et.al*, "Slow Ground Motion and Alignment System", *Proc. of 1994 EPAC*, London (1994), p.2564, and KEK Preprint 94-48 (1994).

[33] S.Takeda, *et.al*, "Slow Ground Motion and Large Future Accelerator", *Proc. of 1996 EPAC*, Barcelona (1996), and KEK Preprint 96-38 (1994).

[34] M.Boge and R.Brinkmann, "Optimization of Electron Spin Polarization by application of a Beam-based Alignment Technique in the HERA Electron Ring", *Proc. of IV Int. Work. on Accel. Alignment*, KEK Proceedings 95-12 (1995), p.412.

[35] V.D.Shiltsev, V.V.Parkhomchuk, "Real-Time Modeling of Transverse Emittance Growth Due to Ground Motion", SSCL-639 (1993).

External Noise Issues in VLHC

Vladimir Shiltsev, BD/LUG

August 5, 1997

1 Introduction

There are several proposals of the "beyond-LHC" large colliders with 30–100 TeV beam energy and luminosity of $10^{33} - 10^{35}\ s^{-1}cm^{-2}$. During 1997 Summer Studies we focused on beam dynamics issues in the Very Large Hadron Collider (VLHC). Many sources of noises which are of interest for the VLHC operation are considered in Ref.[1] and there is shown that the effects of transverse and longitudinal emittance growths due to RF noise and longitudinal emittance increase due to ground motion most probably will be negligible, and they are out of consideration in this paper. The issues of real importance are transverse emittance growth due to dipole field ripple and quadrupole jitter, emittance preservation with a feedback system for damping of the coherent oscillations, orbit oscillations, long-term dynamical alignment and orbit correction scenario.

This paper contains explanations and estimates of the effects. Tolerances are calculated three machines: 50 TeV collider with 12.5T magnetic field dipoles [2], low-field option of superferric 2T magnet machine with larger circumference, 50 TeV "Pipetron" [3], and 3 TeV injector ring with low-field magnets. Some of input parameters can be found in the "pink book" of Snowmass'96 reports [4], others were taken from the VLHC Summer Studies contributions by E.Malamud and S.Mishra. The rest of the paper contains brief explanation of the numbers presented in Table 1.

The accelerators under consideration are large, they consist of thousands of magnetic elements, the field imperfections of those can seriously affect proper machine operation. Depending on the frequency band one can distinguish two mechanisms of beam perturbations in circular accelerator. Slow processes (with respect to revolution period) produce a distortion of the closed orbit of the beam. At higher frequencies (comparable with the revolution frequency), noises cause direct emittance growth.

Table 1: External Noise Tolerances in VLHC

Parameter		Low-Field	High-field	Injector	Comments
Proton Energy,	E_p, TeV	50	50	50	50
Dipole field,	B, T	2.0	12.5	2.0	
Circumference,	C, km	551.2	104.0	34.0	
Rev.frequency	f_0, Hz	544	2885	8824	$f_0 = c/C$
Tune (phase/cell),	$\nu\ (\mu)$	215.82 (90)	52.82 (90)	33.18 (90)	
f_1=$\Delta\nu f_0$,	Hz	98	520	1588	
Number of cells,	N_c	1100	208	198	
Number of quads,	N_q	2200	416	396	
Number of dipoles,	N_d	2200	416	348	
Beam-beam tune shift,	ξ_p	0.006	0.001	-	
RMS emittance,	ϵ_n, $10^{-6}\,m$	1	1	1	
Beam-time,	τ, hrs	5	2.6	0.1	
Emm. growth rate,	$d\epsilon_n/dt$, μm/hr	0.02	0.04	1	$0.1\epsilon_n/\tau$
Dipole fluct.,	$\delta B/B$, 10^{-10}	2.3	0.7	10.3	
Quad jitter,	δX, A	1.05	1.5	115	1 A=0.1 nm
δX comb.function,	δX_{cf}, A	3.0	4.3	200	$L_{coh} = 30$ m
PSD of quad vibr.,	$S_x(f_1)$, pm^2/Hz	20	8	15000	
Expected PSD,	$\frac{pm^2}{Hz}$	180	0.2	0.003	$\delta X = \frac{0.3[\mu m]}{f^{3/2}}$
Max. PSD,	pm^2/Hz	25000	1000	4	$\delta X = \frac{0.1[\mu m]}{f}$
Max FB reduction,	R	240	32000	-	
FB input noise,	δX_{FB}, μm	0.8	5	-	
FB power,	P_{FB}, kW	5	5	-	$\Delta f = 1$ MHz
Orbit oscillations,	δ/σ	0.14	0.06	0.025	
Init. alignment,	Δ_{rms}, μm	10	20	50	quad-to-quad
RMS orbit,	COD, mm	$0.2\sqrt{T}$	$0.09\sqrt{T}$	$0.05\sqrt{T}$	$T[hrs]$
Max orbit,	COD_{max}, mm	$1\sqrt{T}$	$0.45\sqrt{T}$	$0.25\sqrt{T}$	max=5 r.m.s.
Realign intervals,	T, days	4	21	67	
Max. corrector,	$T \cdot m$	0.67	0.67	0.07	T=1 yr no

2 Transverse Emittance Growth

2.1 Effect of Transverse Kicks

The primary sources which lead to emittance growth in large hadron colliders are quadrupoles (quad) jitter and high-frequency variations of the bending magnetic field in dipoles. Both sources produce angular kicks and excite coherent betatron oscillations. After decoherence time (determined mostly by beam-beam non-linearities,

$N_{decoh} = 1200$ turns) filamentation or dilution process due to tune spread within the beam transforms the coherent oscillations into the emittance increase. If the kick amplitude $\Delta\theta$ varies randomly from turn to turn with variance of $\delta\theta^2$, one can estimate the transverse emittance growth as:

$$\frac{d\epsilon_n}{dt} = \frac{1}{2} f_0 \gamma \sum_i^{all\,kicks} \Delta\theta_i^2 \beta_i = \frac{1}{2} f_0 \gamma \delta\theta^2 < \beta > N \tag{1}$$

where $< \beta >$ is the average beta function, γ is relativistic factor, and N is the number of elements which produce uncorrelated kicks. Two major sources of the dipole kicks are fluctuations δB of the bending dipole magnetic field B_0 which give horizontal kick of $\delta\theta = \theta_0(\delta B/B_0)$ ($\theta_0 = 2\pi/N_d$ is bending angle in each dipole, N_d is total number of dipoles); and transverse quadrupole magnets displacements δX (e.g. due to ground motion) which lead to kick of $\delta\theta = \delta X/F$, where F is the quadrupole focusing length.

Non-"white" noise can be described by frequency-dependent power spectral density(PSD) $S_{\delta\theta}(f)$, and causes the emittance growth with rate of [5]:

$$\frac{d\epsilon_n}{dt} = \gamma f_0^2 \sum_i \Big(\beta_i \sum_{n=-\infty}^{\infty} S_{\delta\theta}(f_0|\nu - n|)\Big), \tag{2}$$

which consists of the sum of PSDs of angular kicks produced by the i-th source at frequencies of $f_0|\nu - n|$, n is integer, the lowest of them is fractional part of the tune times revolution frequency f_1 =Min $(\Delta\nu, (1 - \Delta\nu))f_0$.

Beam lifetime in the Pipetron is about $\tau = 5$ hours (determined mostly by longitudinal intrabeam scattering [1] $\tau_{\parallel}^{IBS} \approx 6$ hrs, while synchrotron radiation transverse damping time is about 42 hours). The characteristic time interval of 2.6 hours in the high-field VLHC option is set by the synchrotron radiation. For 3TeV low-field injector we take the beam life-time of 6 min - it is about duration of the acceleration from the Main Injector energy of 150 GeV to 3 TeV.

We require that the external noise lead to less than 10% emittance increase while the beam circulates in the accelerator. Then we get tolerable the noise-induced emittance growth rate of

$$\frac{d\epsilon_n}{dt} \leq 0.1 \frac{\epsilon_n}{\tau} \tag{3}$$

(see data in Table 1).

This acceptable transverse emittance growth rate requires for the "Pipetron":
a) the PSD of single quadrupole transverse vibration is limited by the value of $\sum_n S_{\delta X}(f_0|\nu - n|) \approx S_{\delta X}(f_0\Delta\nu) \leq 2 \cdot 10^{-11}\,\frac{\mu m^2}{Hz} = 20\,\frac{pm^2}{Hz}$, where $\Delta\nu$ is fractional part of ν;
b) or the rms amplitude of turn-to-turn jitter of each quadrupole (white noise in frequency band f_0) $\delta X_{rms} \leq 1 \cdot 10^{-10}$m; [1]

[1] quadrupole turn-to-turn jitter tolerance in the combined function lattice is about 3 times larger. Indeed, if we consider $L = 250$m long quadrupole as 9 quadrupoles each about $L_{coher} = 30$m long

c) and a tolerable level of bending magnetic field fluctuations to its mean value B_0 in the dipole: $\left(\delta B/B_0\right)_{rms} \leq 2.3 \cdot 10^{-10}$. [2] See the numbers for other machines in Table 1.

2.2 Measured Ground Motion

Let us make a comparison of the above calculated constraints with experimental data on ground motion. Fig.1 presents PSDs of ground velocity $S_x(f)(2\pi f)^2$ in units of $(\mu m/s)^2/Hz$ for the USGS "New Low Noise Model" – a minimum of the PSD observed by geophysicists worldwide – and data from accelerator facilities of HERA, KEK, CERN, SLAC, and FNAL (see references in [1]). These spectra indicate that: 1) accelerators are essentially "noisy" places; 2) ground vibrations above 1 Hz are strongly determined by cultural noises – they manifest themselves as numerous peaks in Fig.1; 3) even among accelerator sites the difference is very large, that calls for extensive experimental studies of the seismic vibrations at FNAL.

Below 1 Hz the ground motion amplitude is about 0.3-1 μm due to remarkable phenomena of "7-second hum". This hum is waves produced by oceans – see a broad peak around 0.14 Hz in Fig.1 – with wavelength of about $\lambda \simeq 30$ km. It produces negligible effect on Pipetron, because λ is much bigger than typical betatron wavelength $2\pi\beta \simeq 2$ km. Investigations of spatial characteristics of the fast ground motion have shown that above 1-4 Hz the correlation significantly drops at dozens of meters of distance between points.

Table 2 compares requirements for the Pipetron with three particular tunes $\Delta\nu = 0.10$, 0.18 and 0.24 and available experimental data.

Table 2: PSD of Ground Motion (in $(pm)^2/Hz$)

$\Delta\nu$	0.10	0.18	0.24
$f_1 = \Delta\nu f_0$	54 Hz	98 Hz	135 Hz
Pipetron tolerance	**20**	**20**	**20**
SLAC (quiet)	100	-	-
DESY (tunnel)	10^5	7000	1700
CERN (tunnel)	300	20	-

One can see that none of the accelerator data shows vibrations which are less than the Pipetron requirements, although PSDs at higher frequencies (say $f_1 = 135$ Hz) are much less than at lower frequency of 54 Hz, and, therefore, larger $\Delta\nu$ – closer to half integer resonance – are preferable from this point of view. At $\Delta\nu = 0.18$ one needs the vibration power reduction factor of $R \simeq 10 - 1000$ (see Table 1). For other machine estimates we assumed that there is a "rule of thumb" which says that rms amplitude of the vibrations X above some frequency f is equal

(i.e. each nine times weaker) which move independently, then we get that for the same amplitude of the vibrations, the increase of the emittance will be 9 times less.

[2] one again, we emphasize that this tolerance assumes variation of the total integrated field of 250m long dipole.

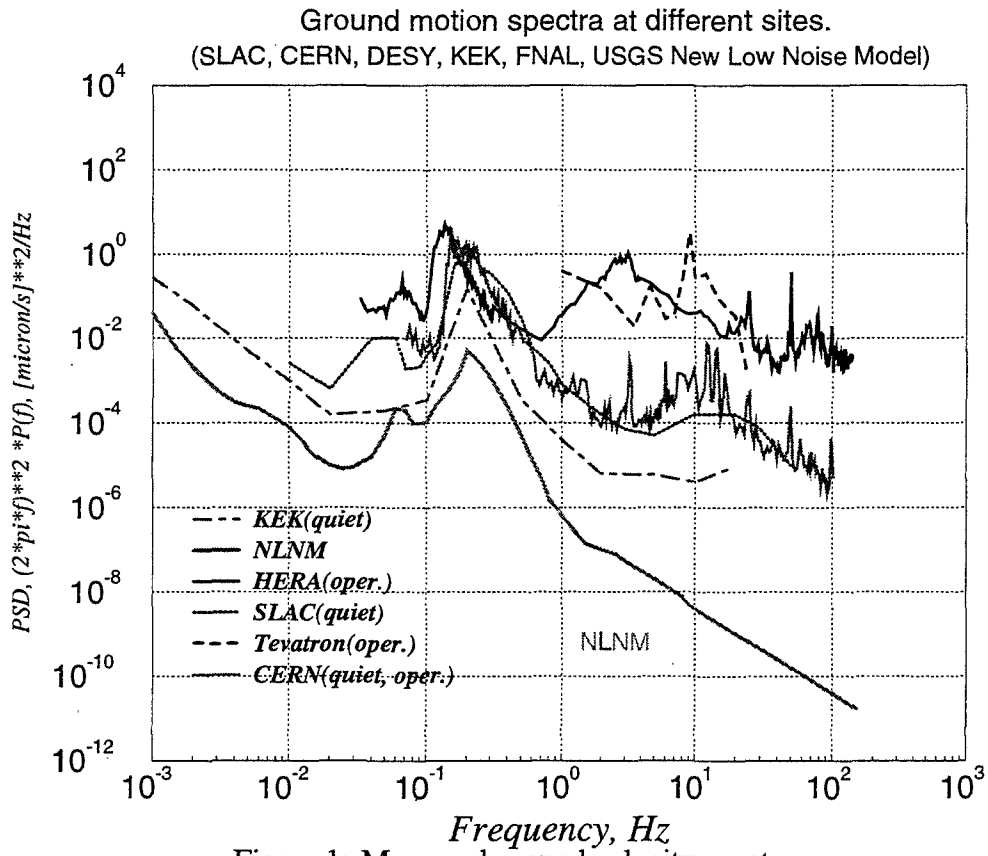

Figure 1: Measured ground velocity spectra.

to $r.m.s.\,X = B/f[Hz]$ (here B is a constant) which corresponds to the PSD of $S_x(f) = 2B^2/f^3$. Within a factor of 4 this rule usually fits well the accelerators-averaged vibration amplitudes above 1 Hz under "quiet" conditions. Fig.2 presents the values of $rmsX(f) = \int_f^\infty S_x(f)df$ calculated for several spectra from Fig.1 – namely, for SLAC, CERN, HERA, and FNAL data. The measurement of tunnel floor vibration amplitude made in the Tevatron tunnel at FNAL covers frequencies of 1–25 Hz and can be approximated by the "rule of thumb" with $B = 100$ nm. Although there is no data on FNAL site vibrations at high frequencies, we will use the fit predictions above 25 Hz as well. From Fig.2 one can see that the same coefficient B is applicable for the HERA tunnel amplitudes, while ground motion in tunnels of SLC(SLAC) and TT2A(CERN) are about 10-20 times smaller. This "rule of thumb" was used for maximum estimates of the PSD of ground vibrations at high frequencies. As the "quiet" PSD we took $r.m.s.\,X = 0.3[\mu m]/f^{3/2}[Hz]$. Both expectations are quoted in Table 1.

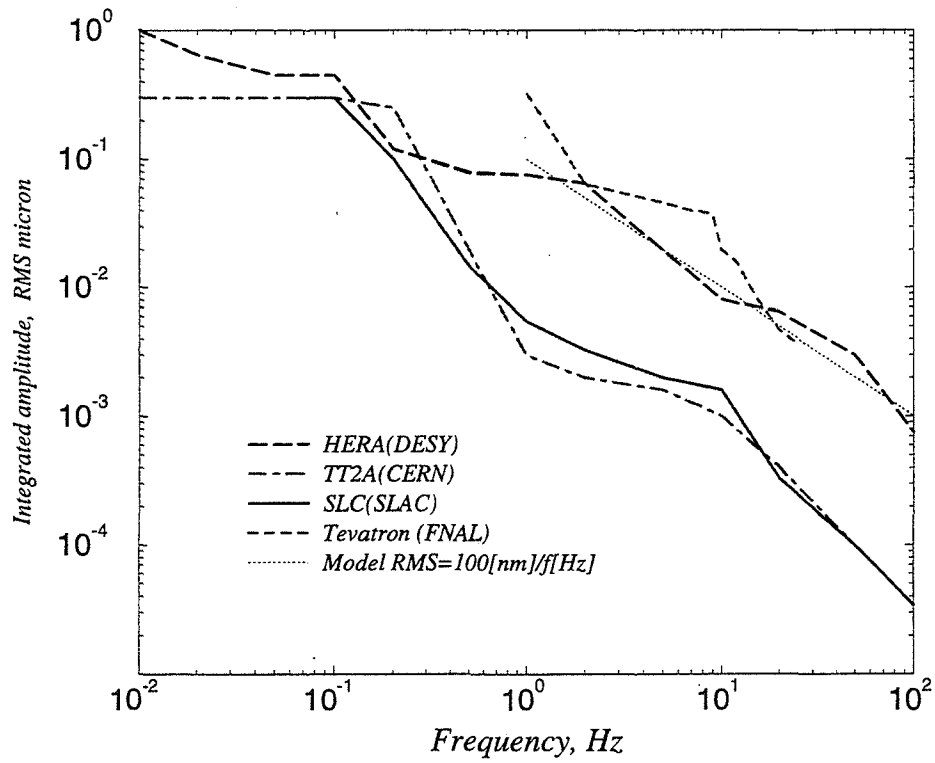

Figure 2: RMS amplitude above f vs. f.

We have no experimental data on dipole field fluctuations at 50-150 Hz and mechanical resonances in long dipoles and quadrupoles which may drastically increase the emittance growth.

2.3 Feedback System

A transverse feedback frequency allows one to suppress the emittance growth caused by excitation of the betatron oscillations simply by damping the coherent beam motion faster then they decohere. The system monitors the dipole offset X of the beam centroid and tries to correct it by dipole kicks θ which are proportional to the offset, applied a quarter of the betatron oscillation downstream. We operate with dimensionless amplification factor g of the system (gain) which is equal to $g = \frac{\theta\sqrt{\beta_1\beta_2}}{X}$, where β_1 and β_2 are the beta-functions at the positions of the pick up and the kicker electrodes respectively. In the limit of $g \ll 1$ the decrement due to the feedback is equal to $\frac{1}{2}f_0 g$, i.e. the amplitude of the betatron oscillations being reduced $1/e$ times after $2/g$ revolution periods. Theory of the feedback (see e.g. [5]) gives the transverse emittance evolution formula:

$$\frac{d\epsilon_n}{dt} = \Big(\frac{4\pi\delta\nu_{rms}}{g}\Big)^2\Big[\Big(\frac{d\epsilon_n}{dt}\Big)_0 + \frac{\gamma f_0 g^2}{2\beta_1}X^2_{noise}\Big], \tag{4}$$

$g \gg 4\pi\delta\nu_{rms}$, where emittance growth rate without feedback $(d\epsilon_n/dt)_0$ is given by (1), X_{noise} is the rms noise of the system (presented as equivalent input noise at the pick-up position), and $\delta\nu_{rms}$ is the rms tune spread within a beam.

Major source of the tune spread (and, consequently, decoherence) is nonlinear beam-beam force which results in the rms tune spread of $\delta\nu_{BB} \approx 0.167\xi \approx 0.001$.

Analytical consideration of the feedback system resulted in maximum useful gain factor $g_{max} \simeq 0.3$ – there is no reduction of the emittance growth rate with further increase of g because of higher-(than dipole)-order kicks effect, the system noise contribution grows, while the coherent tune shift due to feedback becomes too large, and affects multibunch beam stability in presence of resistive wall impedance.

Therefore, maximum reduction factor $R_{max} = (g_{max}/4\pi\Delta\nu_{BB})^2$ is about 240 for the Pipetron design parameter of $\xi = 0.006$, while the minimum practical gain which still can lead to the damping is about $4\pi\delta\nu_{BB} \approx 0.01$. For the high-field option of the VLHC with smaller ξ, the maximum reduction factor R can reach $3{\cdot}10^4$.

As it is seen from (2.3), feedback noise also leads to emittance growth and its relative contribution grows as $\propto g^2$. Taking the beta function at the pick-up $\beta_1 =$ 500m we get limit on the rms noise amplitude:

$$X_{noise} \ll \Big[\frac{2\beta_1(d\epsilon_n/dt)_0}{f_0(4\pi\delta\nu_{BB})^2\gamma}\Big]^{1/2} \approx 1.0\,\mu m. \tag{5}$$

Power of the output amplifier of the system depends on maximum noise amplitude of the proton beam oscillations and is estimated to be about 50 kW for a bunch-by-bunch system[1].

3 Closed Orbit Distortions

3.1 Alignment Tolerances

The rms closed orbit distortion dX_{COD} is proportional to the rms error dX of quads alignment, and if these errors are not correlated, then in the FODO lattice we can get:

$$dX^2_{COD} = \frac{\beta dX^2}{4sin^2(\pi\nu)}\sum_i \frac{\beta_i}{F_i^2} = \frac{\beta N_q tg(\mu/2)dX^2}{Lsin^2(\pi\nu)}. \tag{6}$$

Let us take the "safety criteria", i.e. ratio of maximum allowable COD to the rms one, equal to 5, then for maximum COD of dX^{max}_{COD}=1 cm (this is about half aperture of the vacuum chamber) at the focusing lenses where $\beta_F = 765$ m ($L = 250$ m, $\mu = 90^o$) we get requirement on the rms alignment error of $dX \approx 10\,\mu$m (here we take $\Delta\nu = 0.18$). The same estimate for the quad-to-quad alignment in the high-field VLHC gives 20μm and 50μm for the 3TeV injector (see Table 1). These values set a challenging task, and the solution needs the most sophisticated alignment

techniques and two questions arise in this connection: 1) temporal stability of the magnets positions; and 2) applicability of the beam-based alignment.

3.2 Slow Ground Motion

Numerous data on uncorrelated slow ground motion support an idea of "space-time ground diffusion". An empirical rule that describes the diffusion – so called "the ATL law" [8] – states the rms of relative displacement dX (in any direction) of two points located at a distance L grows with time interval $T < dX^2 >= ATL$, where A is site dependent coefficient of the order of $10^{-5\pm1}\,\mu m^2/(s \cdot m)$.

The ground diffusion should cause corresponding closed orbit diffusion (COD) in accelerators [3] with rms value over the ring approximately equal to $\langle dX^2_{COD}\rangle \simeq 2\sqrt{ATC}$. It clearly shows that the diffusive orbit drift is not very sensitive to the focusing lattice type (only the circumference C plays role), in particular, there is almost no difference between the combined- and separated-function lattices responses on the ATL-like diffusion.

We applied the ATL law predictions with $A \approx 5 \cdot 10^{-5}\,\mu m^2/(s \cdot m)$ (close to what was observed at LEP) to the VLHC (see [1]) and obtained the rms COD – see Table 1. Maximum COD is taken to be five times the rms COD, e.g. for the low-field option $dX^{max}_{COD} \approx 1[mm]\sqrt{T[hrs]}$. Requirement of "safe" max COD of 10 mm yields in T=4 days of mean time between necessary realignments to an initial "smooth" orbit of the low-field VLHC. It does not seem to be an easy task to do it mechanically, even with use of robots, especially taking into account 15 μm precision of the procedure. "Beam-based alignment" technique looks as an appropriate method but requires numerous (of the order of the number of quads) correctors with about 1 Tm maximum strength.

4 Conclusion. R&D plans.

Preceding consideration shows that natural and man-made vibrations at the VLHC can lead to dangerous transverse emittance growth rate (high-frequency part of spectrum) and closed orbit distortions (at low frequencies). Being comparable, the tolerances on quadrupole turn-to-turn vibrations are somewhat less stringent at the high-field option. For the dipole field fluctuations the relation is opposite. 3TeV injector seems free of troubles with the transverse emittance growth. Longitudinal emittance in all the machines is almost independent on the external noises [1]. The transverse feedback system can drastically reduce the transverse emittance increase.

Wandering of the parts of the tunnel can be a major problem for the orbit stability in all the considered accelerators (the conclusion is based on the other places' data). Sophisticated alignment methods are necessary to keep the VLHC and 3TeV

[3] observed in HERA [9]

injector beams on a "golden orbit".

The VLHC R&D on the external noise issues.

- In Aug.-Oct. 1997 we are going to carry out "on-site" ground motion studies and magnet vibrations measurements in frequency band 0.05-150 Hz. It will answer the question of the ground motion contribution to the transverse emittance growth.
- Other important contribution can be the dipole field jitter. It definitely must be measured.
- There is real need in experimental data on long-term tunnel movements which will determine the long-term orbit stability and the correction scenario. Experiments with 30-300 m long hydrostatic levels in a similar to the VLHC tunnel can shed the light on the issue.

References

[1] V. Shiltsev, "Pipetron Beam Dynamics with Noise", FERMILAB-TM-1987 (1996).

[2] S.Peggs *et.al*, *Proc EPAC'96*, Barcelona, p377.

[3] G.W.Foster, E.Malamud, FERMILAB-TM-1976 (1996)

[4] E.Malamud, ed., "The Pipetron, A Low-Field Approach to a Very Large Hadron Collider", selected reports submitted to the Proceedings of Snowmass'96.

[5] V.Lebedev, *et.al*, *Part. Accel.*, Vol.44, No.3-4, p.147 (1994).

[6] H.-J.Shih, *et.al*, *Part. Accel.*, Vol.43(3) (1994), p.159.

[7] M.Syphers, *et.al*, *Proc. 1993 IEEE PAC*, Washington, p.420.

[8] V.Parkhomchuk*et.al*, *Part. Accel.*, v.46 (1994), p.241.

[9] R.Brinkmann, J.Rossbach, *Nucl. Instr. Meth.*, v. A350 (1994), N.1-2, p.8.

Transverse Mode Coupling Instability in the VLHC

V.V. Danilov, V.D. Shiltsev

Fermi National Accelerator Laboratory

P.O. Box 500, Batavia, Illinois 60510

January 9, 1998

Abstract

We present the results of calculation of transverse mode coupling instability (TMCI) thresholds for Very Large Hadron Collider (VLHC). The estimates are done with use of conventional approach and more sophisticated mode dynamics analysis. We found the RF system parameters which allows to get appropriate TMCI threshold number of particles per bunch and attain high luminosity of the collider. Alternative ways to raise the threshold are briefly discussed.

1 Introduction

The Very Large Hadron Collider(VLHC) [1] will have large circumference, that leads to domination of transverse instabilities in beam dynamics problems [2, 3]. Consideration done by J.Rogers [2] concludes that dominant single bunch effect is the transverse mode coupling instability(TMCI) driven by a broadband impedance. We redo estimates of the impedance budget and the TMCI threshold using conventional approach and discuss observations at the Tevatron in Section 2. As most of the impedance comes from resistive wall fields which are not constant over longitudinal coordinate in a bunch s, then more sophisticated analysis is done in Section 3 with means of the method developed in [5]. We study dependence of the beam eigenfrequencies versus current and modes coupling in the VLHC low-field option. In Section 4 we consider possible ways to increase the threshold in the VLHC.

2 Rough estimates

Basically, the TMCI (or "strong head-tail instability ") appears due to defocusing effect of the wake fields induced by the head of the bunch on the bunch tail particles. In the presence of synchrotron motion, there is a permanent exchange of head and tail particles that helps to avoid the instability. The instability was observed at many electron storage rings which usually tend to increase the synchrotron tune ν_s in order to stabilize the TMCI. To date there is no solid evidence of the "strong-head tail" instability in proton machines [4]. Nonetheless, it is expected the proton TMCI will be important at injection into the SPS, when it works with LHC parameters and in the VLHC. We have to note that for existing proton accelerators, stabilizing processes other than the synchrotron mixing can play important role, for example, incoherent tune spread due to direct space charge and/or broad-band impedance, or other sources of possible Landau damping. They are not yet analyzed properly, and, therefore, it is not clear will they distort the picture of the TMCI at the VLHC or not.

After these precautions, we start with routine analysis of the mode coupling phenomena.

The transverse mode-coupling instability leads to fast beam break-up, and, therefore, sets strong constraint on a broad band transverse impedance $Z_\perp$. The threshold number of particles per bunch N_p can be estimated as [6]:

$$N_p^{th} = \frac{32\pi^{3/2}(E/e)\sigma_s\nu_s}{3ec\mathrm{Im} < Z_\perp\beta_\perp >} \tag{1}$$

where brackets $< .... >$ mean averaging with the beta-function at locations of the impedance sources.

As it was pointed out in [2], transverse broad band impedance in the low-field VLHC is dominated by resistive wall impedance. The latter can be estimated for round vacuum chamber with radius a as:

$$Z_\perp(\omega) = (1-i)\frac{Z_0\delta R}{a^3}, \tag{2}$$

where R is the radius of the machine, $Z_0 = 377\Omega$ is the vacuum impedance, $\delta = c/\sqrt{2\pi\sigma\omega}$ is the skin depth at frequency ω.

As the impedance depends on frequency, its' effective value integrated over the bunch spectrum is used[1]:

$$Z_\perp = \frac{\sum_n Z_\perp(\omega = n\omega_0)e^{-(n\omega_0\sigma_s/c)^2}}{\sum_n e^{-(n\omega_0\sigma_s/c)^2}}. \tag{3}$$

where $\omega_0 = c/R$ and σ_s is the rms bunch length. Using (2, 3) one finds that

$$Z_\perp^{RW} = \frac{\Gamma(1/4)}{\sqrt{\pi}}Z_\perp(\omega = c/\sigma_s) = 2.05Z_\perp(\omega = c/\sigma_s). \tag{4}$$

For $\sigma_s = 10$ cm long bunches in Al vacuum chamber with conductivity of $\sigma = 3.2\cdot 10^{17}c^{-1}$ the skin depth at $\omega = c/\sigma_s = 3$ GHz is about 3.86 μm.

For other than round vacuum chambers, a geometry factor can be introduced. For example, it is equal to $R_G \approx 0.84$ for elliptical vacuum chamber with minor half-aperture a two times less than the major one [7], i.e.

$$\mathrm{Im}Z_\perp^{eff} \approx 2.05\cdot 0.84\frac{Z_0R\delta(\omega = c/\sigma_s)}{a^3} = 1.72\frac{Z_0R\delta(\omega = c/\sigma_s)}{a^3}. \tag{5}$$

Additional wide-band impedance of the ring can be estimated as a sum of impedances of its components, such as bellows, BPMs, kickers, vacuum ports, tapers, etc. Most of these elements are discontinuities having resonant frequencies much higher the frequencies within the bunch spectrum, and, therefore, they give rise to a mostly inductive impedance. At this stage of the VLHC ring design we restrict ourselves with rough estimate, based on assumption that for every half FODO cell length of $L = 250$m, there are some discontinuities like aperture increase $\Delta = 0.5$mm and total length of about $g = 10$cm, then

$$\mathrm{Im}Z_\perp = \left(\frac{Z}{n}\right)\cdot\frac{2R}{a^2} = -\frac{2R}{a^2}\cdot\frac{Z_0g\Delta}{2\pi Ra}\times N_{elements},\ N_{elements} = 2\pi R/L. \tag{6}$$

Resulting impedance budgets for low-field and high-field options of the VLHC (some parameters are taken from [2]), 3 TeV low-field injector with $C = 34$ km (with $L \simeq 86$m) and for the LHC [8] are presented in Table 1.

[1] as will discuss in the next section, this is the point of some uncertainty in the impedance estimates

Table 1 also presents the threshold bunch population for these machines at their injection energies where the TMCI is expected to be more dangerous.

For the low-field option of the VLHC the bunch intensity threshold determined by the TMCI (mostly due to resistive walls) is equal to:

$$N_{th} \approx 3.87 \cdot 10^{10} \cdot \sqrt{\frac{\sigma_s}{10\mathrm{cm}}} \cdot \frac{E}{3\mathrm{TeV}} \cdot \frac{\nu_s}{0.01} \cdot (\frac{a}{0.9\mathrm{cm}})^3 \cdot \frac{550\mathrm{km}}{C} \cdot \frac{320\mathrm{m}}{<\beta>}. \tag{7}$$

For example, one can expect that due to 4 times smaller beta-function and seven times longer bunch length, the threshold in 3 TeV ring build with the same low-field magnet technology will be about 10 times the threshold of the 50 TeV collider ring as long as acceleration ratio (top energy divided by injection energy) and ν_s are the same for both rings.

It is useful to apply the above consideration to the Tevatron ring (see also Table 1). Assuming stainless steel *round* vacuum chamber with $a = 3.5$cm, resistivity of $\rho = 7.4 \cdot 10^{-7}\ \Omega m$, the rms bunch length of about 0.5 m and synchrotron tune 0.002 at the injection energy of 150 GeV, $<\beta> \approx 50$ m, one gets

$$N_{th}^{TeV} \approx 4.6 \cdot 10^{12}, \tag{8}$$

that corresponds to effective resistive wall broadband impedance of about 0.8 MΩ/m. Detailed estimate of the impedance made by K.Y.Ng [9] gives total transverse impedance about 3-4 times larger. There are some experimental evidences of the longitudinal broadband impedance as large as $(Z/n)^{TeV} \sim 10\Omega$ [10]. From that one can estimate the transverse broadband impedance as $Z_\perp = 2R(Z/n)/a^2 = 10\, M\Omega/\mathrm{m}$ [2]. For the given spread of the impedance of (3-10) MΩ/m we get the threshold bunch populations of $N_{th}^{TeV} = (3.7 - 12) \cdot 10^{11}$. Particle production at the Tevatron limits maximum bunch population at the Tevatron at the level of about $3 \cdot 10^{11}$, and that probably explains why the TMCI was not observed at the Tevatron. As we mentioned at the beginning of this Section, there is other factor which may play role and increase the TMCI threshold - the spread of betatron tunes within the bunch. Such a spread takes place along the bunch (due to direct space-charge or/and broad-band impedance) as well as across the bunch (due to direct space charge, octupole magnets, beam-beam interaction, etc.) It is not clear now which of the spreads may lead to more effective stabilization. Recent numerical studies [11] of the TMCI with direct space charge tune shift δQ_{sc} have shown that the threshold grows approximately as $\mathcal{R} = 1 + \Delta Q_{sc}/\nu_s$. For the Tevatron at injection

$$\Delta Q_{sc} = \frac{N_p r_p R}{2\sqrt{2\pi}\sigma_s \epsilon_N \gamma^2} \approx 0.001,$$

(here $\epsilon_N \approx 4 \cdot 10^{-6}$ m is the rms normalized emittance, $r_p = 1.53 \cdot 10^{-18}$m is the proton classical radius, and we took $N_p = 3 \cdot 10^{11}$) that may give additional 50% of the threshold increase. The direct space charge tune shift and tune spread are negligible at high energies (e.g. for all machines we considered above except 3TeV low-field injector ring with 150 GeV injection energy at from the Main Injector). It would be of interest to observe the TMCI at the Tevatron, for example, by increasing the transverse broad-band impedance of the ring and to study the tune shift and the coupling of the transverse modes.

[2] in the estimate we used $a = 4.5$ cm, i.e. somewhat larger than for the vacuum chamber, because the aperture is larger in the Tevatron injection and abort kickers which are though to contribute significantly into the broad-band impedance.

Table 1: Broadband Impedance Model and Threshold Bunch Intensities (L-F is for low-field VLHC option, H-F - high-field option, 3TI - 3 TeV low-field VLHC injector ring, TEV is for the Tevatron)

Parameter		L-F	H-F	3TI	LHC	TEV
Circumference	C, km	554	102	34	26.7	6.3
Top beam energy	E, TeV	50	50	3	7	1
Injection energy	E_i, TeV	3	3	0.15	0.45	0.15
Bunch length (inj.)	σ_s, m	0.06	0.029	0.43	0.13	~0.5
Long. emittance (inj.)	A_{rms}, eV·s	0.3	0.04	0.2	0.13	~0.5
Synchr. tune	ν_s	0.01	0.01	0.01	0.005	0.002
Beam pipe half-size	a, cm	0.9	1.9*	0.9	1.9*	3.5
$<\beta>$	m	320	255	82	71	50
Resistive wall (inj.)	$\mathrm{Im}Z_\perp$, MΩ/m	235	0.7	38.5	0.35	0.8
Bellows, BPMS, etc.	$\mathrm{Im}Z_\perp$, MΩ/m	18	7.3**	1.2	5.65	2-9
Total transverse	$\mathrm{Im}Z_\perp$, MΩ/m	253	8.0	39.7	6.0	3-10
Total longitudinal	Z/n, Ω	0.14	0.034**	0.15	0.14	2-10
TMCI threshold (inj.)	$N_p/10^{11}$, Eq.(1)	0.27	5.5	2.5	5.4	3.7-12
RW threshold (inj.)	$N_p^{RW}/10^{11}$, Eq.(10)	0.21	n/a	1.8	n/a	n/a

*- effective radius of square beam screen (3.4 cm side length) for the resistive wall estimates.
**- from [2].

3 Mode coupling simulations

As most of the impedance comes from the resistive wall fields which are not constant over the bunch longitudinal coordinate s. The transverse wake-function is given by [12]:

$$W(s) = -\frac{2C}{\pi a^3}\sqrt{\frac{c}{\sigma s}}, \tag{9}$$

One can see, that the wake field has a singularity $\propto 1/\sqrt{s}$. The method developed in [5] suggests more correct treatment of the problem other than the averaging over the bunch spectrum. In fact such averaging should be performed over different modes of transverse motion.

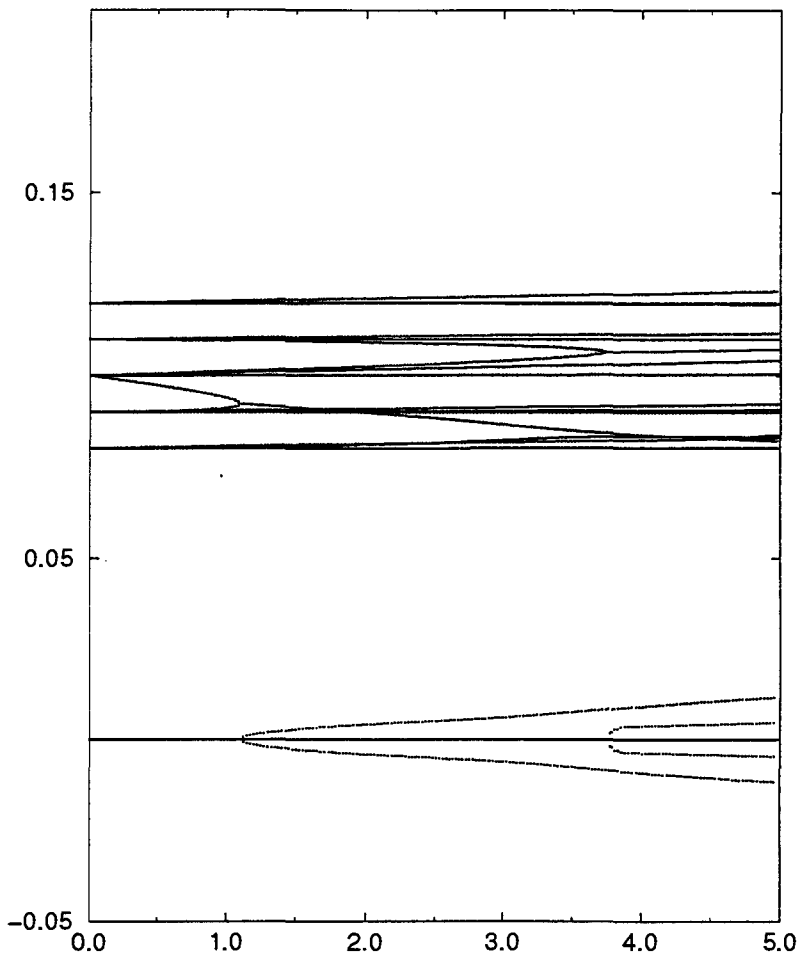

Figure 1: Eigentunes (vertical axis) versus number of protons per bunch (horizontal axis). The fractional part of the betatron tune is 0.1; upper lines present real part, and lower ones - imaginary part of eigentunes.

In our simulations, the bunch is divided into 4 radial and 5 azimuthal parts, so it is possible to see the behavior of the first 4 radial and 5 azimuthal modes. It gives about few percent deviation from the exact threshold current value for the first (0,+1,-1) modes coupling (see details in [5]). The integrated wake kick Eq.(9) is applied one over the revolution period, that is a good approximation while the tune shifts due to impedance and synchrotron tune are much less than 1. The rest of the lattice is presented as a linear transform matrix. Total transformation matrices including the kick are different for different modes. Eigenvalues (eigentunes) of these modes can calculated numerically.

In Fig.(1) one can see the eigentunes versus number of protons per bunch. The parameters used in this simulation are $< \beta >= 600$m, $\nu_s = 0.01$, $\sigma_s = 0.1$m, $E = 3$TeV, $C = 550$km. The fractional part of the betatron tune is equal to $\nu_\beta = 0.1$. We found that being far from low-order resonances, the tune is not significant for the threshold estimations. There is a number of "radial" eigentunes with zero "azimuthal" number around the betatron frequency at $\nu_\beta \pm \nu_s$, $\pm 2\nu_s$. All these modes for small current have zero oscillations of the dipole momentum over the angle in synchrotron phase space, and they have different dependence on the dipole momentum over the synchrotron amplitude ("radius" in synchrotron phase space). For each synchrotron sideband, there are several

higher "azimuthal" modes, whose tunes for small current are different from the betatron tune on a particular integer number of synchrotron tunes. This number means the eigenmode variation numbers over the angle in the synchrotron phase space. As in the case of "zero" azimuthal modes, there are a lot of "radial" modes for every azimuthal number.

With chosen parameters, the first merging of some "zero" radial mode and some "-1" radial mode occurs for the number of protons in bunch equal to $1.2 \cdot 10^{10}$. The next merging occurs for approximately triple current ("0" radial and "+1" radial modes). In both cases a pair of the modes with equal real parts of the tune and with opposite imaginary parts of the tune appears; this, evidently, gives unstable motion of the bunch.

Let us take into account the reduction factor of $R_G = 0.84$ due to the beam pipe ellipticity, and present the threshold obtained in the same form as Eq.(7):

$$N_{th} \approx 2.7 \cdot 10^{10} \cdot \sqrt{\frac{\sigma_s}{.1\mathrm{m}}} \cdot \frac{E}{3\mathrm{TeV}} \cdot \frac{\nu_s}{0.01} \cdot (\frac{a}{0.9\mathrm{cm}})^3 \cdot \frac{550\mathrm{km}}{C} \cdot \frac{320\mathrm{m}}{<\beta>}, \tag{10}$$

This value is about 0.7 times the value we got with straightforward estimates above. Again, worrisome intensity limitation in the VLHC occurs at the injection energy.

4 Luminosity and safety factor.

Now we can estimate luminosity of the low-field VLHC under assumption that the number of particles per bunch N_p remains the same during the acceleration, normalized transverse emittance $\epsilon_n = 2.5mm \cdot mrad$ (or 95% emittance of 15π mm·mrad), beta-function at the interaction point of $\beta^* = 10$cm, revolution frequency $f_0 = 0.5$ kHz, and the collision energy of 50 TeV ($\gamma_p = 5.1 \cdot 10^4$):

$$\mathcal{L} = f_0 N_b \frac{N_p^2 \gamma_p}{4\pi\epsilon_n \beta^*} \mathcal{F}(\frac{\sigma_s}{\beta^*}), \tag{11}$$

where the geometrical luminosity reduction factor for round beams is $\mathcal{F}(x) = \mathcal{L}(\sigma_s)/\mathcal{L}(0) = \sqrt{\pi} x e^{x^2} \mathrm{erfc}(x)$, $x \equiv \beta^*/\sigma_s$. For 7 cm rms bunch length it leads to $\mathcal{F} \approx 0.82$ and one gets the luminosity of

$$\mathcal{L}/10^{34}[s^{-1}cm^{-2}] = 0.73 \cdot \frac{N_b}{10^5} \cdot \left(\frac{N_p}{10^{10}}\right)^2. \tag{12}$$

Number of interactions per crossing due to inelastic interaction of protons with 132mb cross section is about

$$n_{int} = 28 \cdot (\mathcal{L}/10^{34}) \cdot \frac{10^5}{N_b}. \tag{13}$$

One can see, from this formula, that, for the same luminosity,larger number of bunches is preferable in order to decrease the number of particles per bunch and n_{int}. The same preference occurs for the parameter of the beam-beam interaction:

$$\xi = \frac{r_p n_p}{4\pi\epsilon_n} \approx 0.0005 \cdot \frac{N_p}{10^{10}}, \tag{14}$$

although the bunch intensity limitation due to the TMCI at the injection appears well before beam-beam effects would be of importance.

Let us choose for definiteness the frequency of the RF accelerating cavities to be $f_{RF} = 500$ MHz[3], it is equal to $h = 9 \cdot 10^5$ harmonics of the revolution frequency. If one fills every 9th bucket then number of bunches is $N_b = 10^5$ and bunch spacing is 18 ns.

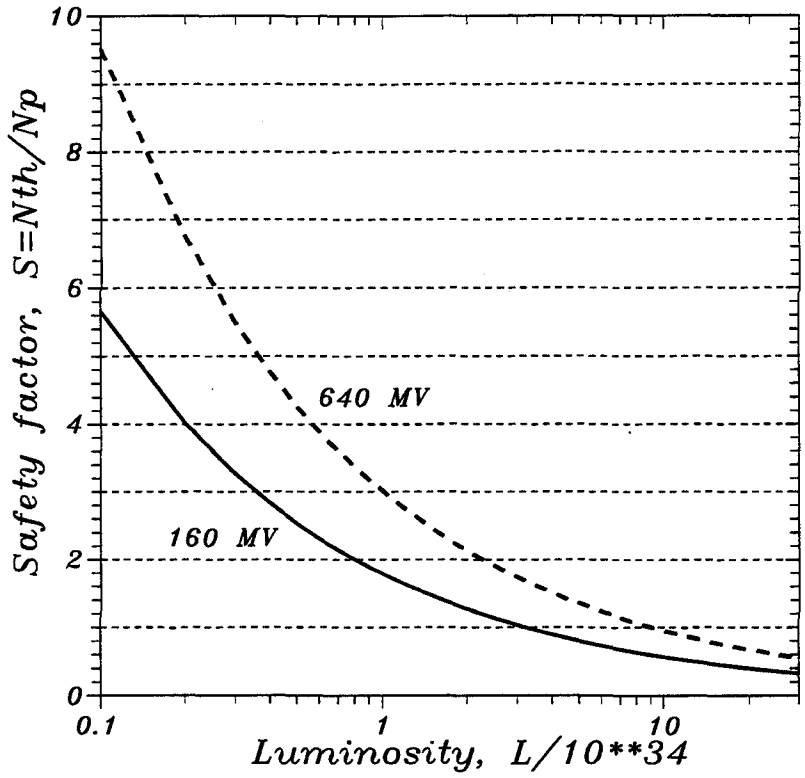

Figure 2: Safety factor $S = N_{th}/N_p$ vs luminosity. RF voltage at injection is 160 MV (solid line) and 640 MV (dashed line).

Other parameters of the collider are as follow: the half FODO cell length $L = 250$ m, betatron phase advance per cell $\psi = 90^o$, average beta-function $< \beta >= 318$ m, tune of the 554km-long machine is about $\nu \approx 275$ that yields a momentum compaction factor $\alpha \approx 1/\nu_x^2 = 1.3 \cdot 10^{-5}$.

In order to have synchrotron tune at the injection (at 3 TeV) of

$$\nu_s = \sqrt{\frac{\alpha h e V_0}{2\pi E_{inj}}} = 0.01,$$

one needs to have the total RF voltage of $V_0 = 160$ MV. That value correspond to some 10 minutes ramp of the proton energy from 3 TeV to 50 TeV. With $V_0 = 640$ MV RF voltage, the ramp is four times faster and the synchrotron tune is 0.02.

Using all parameters presented above and Equation (10), we can calculate a *safety factor* of $S = N_{th}/N_p$ versus luminosity (see Fig.2):

$$S = \frac{1.79}{\sqrt{\mathcal{L}/10^{34}}} \quad at\ V_0 = 160\,MV,$$

[3]powerful DC klystrons are available for such frequency at present time, both normal- and super-conducting RF technology at this frequency is well developed for electron-positron storage rings

and

$$S = \frac{3.01}{\sqrt{\mathcal{L}/10^{34}}} \quad at\ V_0 = 640 MV.$$

For example, the safety factor of $S = 2$ corresponds to $\mathcal{L} = 8 \cdot 10^{33}\, s^{-1} cm^{-2}$ with $V_0 = 160$ MV and $\mathcal{L} = 2.26 \cdot 10^{34}\, s^{-1} cm^{-2}$ with $V_0 = 640$ MV at the injection.

The scaling of the safety factor S for fixed luminosity is:

$$S \propto a^3 f_{RF}^{7/8} V_0^{3/8} < \beta >^{1/4} A^{1/4}.$$

Thus, the most attractive ways are to increase the dipole magnet aperture or the RF frequency. Unfortunately, there is not too much freedom to vary these parameters, and therefore, it would be very useful to consider other ways of improvement.

5 Ways to increase the TMCI threshold.

There were several attempts in the past to increase the TMCI threshold with use of a feedback system. A resistive feedback doubles the threshold in PEP (see [13] and references therein) and in VEPP-4M storage rings [14]. Sophisticated reactive feedback (oscillator-like) was tested at LEP (CERN) and raised the threshold by 5% [15]. The conventional feedback at LEP didn't help for several reasons. Due to noises (or due to some other reasons) it didn't work in essentially resistive variant, but for reactive regime of work the "-1" mode became unstable. The calculations also gave the instability of "+1" azimuthal mode for near-threshold current.

The difference for situation with the TMCI at LEP in comparison with the other machines is its large synchrotron tune and large impedance between pickup and kicker. The VLHC parameters are closer to the VEPP-4M parameters, then to the LEP ones due to the fact, that their synchrotron tunes are of the same order. So, it can be assumed, that conventional feedback has to help at VLHC, as it does at the VEPP-4M collider. Special variants of feedbacks may also help to damp the TMCI [5].

One more opportunity to counteract effectively the TMCI was considered recently in Ref.[16]. Introduction of a correlated tune spread from head to tail of the bunch using RF quadrupoles has shown significant increase of the threshold if the spread is several times the synchrotron tune ν_s. The idea is similar to the BNS-damping in linear electron-positron colliders [17] which was experimentally proven as an effective way to counteract beam brake-up in SLAC Linear Collider.

Acknowledgments

We sincerely acknowledge useful comments of Gerry Jackson, John Marriner and Glenn Goderre on the Tevatron parameters and the TMCI experience at hadron machines. We thank K.Y.Ng for providing us with the Tevatron broad band impedance estimates.

References

[1] G.W.Foster, E.Malamud, "Low-Cost Hadron Colliders at Fermilab", FNAL TM-1976 (1996).

[2] J.Rogers, "Collective Effects and Impedances in the RLHC(s)", *Proc. of the DPF/DPB Summer Study on New Directions for High Energy Physics Snowmass '96.*

[3] W.Chou, J.Griffin, "Impedance Scaling and Impedance Control", FERMILAB-Conf-97-197, and *Proc. 1997 Part. Accel. Conf.*, Vancouver (1997).

[4] see S.Peggs, "Summary of the Beam Dynamics Group", in *Proc. Work. on Collective Effects in Large Hadron Colliders*, CERN (1994), *Particle Accelerators*, vol.50 (1995), p.19.

[5] V.V.Danilov and E.A.Perevedentsev, "Feedback System for Elimination of the Transverse Mode Coupling Instability", NIM A, 391 (1997) p.77-92.

[6] see, e.g. *PEP-II: An Asymmetric B-Factory*, Conceptual Design Report, SLAC-418, LBL-PUB-5379 (June 1993).

[7] L.Palumbo, V.Vaccaro, M.Zobov, "Wake Fields and Impedances" LNF-94/041 (1994) and *CERN Accelerator School, 5th Advanced Course*, CERN 95-06 (1995), p.331.

[8] F.Ruggiero, "Single Beam Collective Effects in the LHC", CERN SL/95-09 (AP), LHC Note 313 (1995).

[9] K.Y.Ng, "Beam Stability Issues of the Tevatron", *Report presented at the Fermilab III Technical Advisory Committee Second Meeting* (July 1995).

[10] G.Jackson, private communication (1998).

[11] M.Blaskiewicz, "Effects of Incoherent Space Charge Forces on the Fast Head-Tail Instability", *Proc. 1997 IEEE PAC*, Vancouver (1997).

[12] A.W.Chao, "Physics of Collective Beam Instabilities in High Energy Accelerators", John Wiley & Sons, Inc., 1993

[13] S.Mayers, "Stabilization of the Fast Head-Tail Instability by Feedback", *Proc. 1987 IEEE PAC*, Washington DC (1987), p.503.

[14] M.M.Karliner, *et al.*,"Feedback System for Elimination of the Fast Head-Tail Instability at Storage Ring VEPP-4M", *Proc. 1996 European Particle Accelerator Conference*, Barcelona (1996).

[15] L.Arnaudon, *et al.*, "First Test with a New Transverse Reactive Feedback System", CERN SL-MD Note 158 (1994)

[16] V.V.Danilov, "On Possibility to Increase the TMCI Threshold by RF Quadrupole", FNAL TM-2033 (1997).

[17] V.Balakin, A.Novokhatsky, V.Smirnov, "VLEPP: Transverse Beam Dynamics", *Proc. of 12th Int. Conf. on High-Energy Accelerators*, Fermilab (1983), p.119.

Synchrotron Radiation in the VLHC

T. K. Kroc, FNAL, Batavia, USA

Introduction

This report describes the calculations of the synchrotron radiation produced in the VLHC. Four cases were looked at using the combinations of low and high energy rings (3 TeV and 50 Tev) and low and high field magnets (2.125 T and 12.5 T). The amount of radiated power is calculated. A simple heat transfer calculation is made for the tunnel environment. Similar calculations are performed for electron machines housed in the same tunnels as the low field (large circumference) options.

Calculations and Assumptions

Spreadsheet 1 shows all the calculations that went into determining the synchrotron radiated power. We start by calculating the size of the rings including packing factor and 4km of straights for injection, extraction, and experimental halls. Then we calculate the number of protons the rings can hold. This assumes that every sixth bucket is filled. For the 3 TeV ring it is assumed that the 53 MHz Tev RF is reused. For the 50 TeV ring 360 MHz was used as is done in Table 1 of Dugan, Limon, and Syphers report in the "pink" book. The radiated power is calculated as [1]

$$P = \frac{1}{6\pi\epsilon_0}\frac{e^4}{m^4c^2}B^2E^2$$

The highest power density is 2 W/m for the high energy high field ring. The highest energy of the photons produced is 1 keV. These are stopped within 1 mm of the inside surface of the aluminum vacuum chamber.

Heat Transfer Considerations

An attempt to calculate the temperature increase due to this heat load was done in 2 ways. First we assumed a line heat source in an infinite medium [2]

$$\Delta T = \frac{q}{4\pi\kappa}Ei\left(-\frac{r^2}{4\kappa t}\right)$$

with $q = \frac{Q}{\rho c}$ and $\kappa = \frac{K}{\rho c}$. Q is the heat load, 2W/m. K is the thermal conductivity of rock, taken to be 2 W/m °C. ρ is the density, 2500 kg/m^2, and c is the specific heat, 850 J/kg °C, of rock. Ei is the exponential integral.

Because of the assumption of an infinite medium, this never reaches an equilibrium. However, after 20 days of continuous operation the temperature at the tunnel wall has only risen 1.2 degrees. This method does not take into account the finite radius of the tunnel.

The second attempt assumed a cylindrical geometry with finite inner and outer radius.

$$\Delta T = \frac{q\, ln(r_o/r_i)}{2\pi K}$$

The outer radius was taken to be the depth of the tunnel, 120m. This analysis gives a temperature rise of .7 degrees.

Electron Ring Calculations

When one contemplates installing an electron ring in these tunnels, things change dramatically. The details are shown in spreadsheet 2. Here the size of the rings is carried over from the proton spreadsheet. The strength of the magnets are adjusted to match the size of the ring. The energy losses range from 40 to 190 MW per ring.

Electron Ring Heat Loss

Heat flow calculations, similar to those conducted for the proton rings, were done for the electron rings. In the case of the 500 km ring, the power density of 1300 W/m leads to steady state temperatures of 400 degrees C or more.

References

[1] D. A. Edwards & M. J. Syphers, An Introduction to the Physics of High Energy Accelerators, (John Wiley & sons, New York,1993), p. 271.

[2] H. S. Carslaw & J. C. Jaeger, Conduction of Heat in Solids, 2nd ed., (Oxford University Press, New York,1959, reprint 1992), pp. 261-262.

	A	B	C	D	E	G	H	I	J
1						**Spreadsheet 1**			
2	Planck/2pi	6.58E-16	eV-sec						
3	proton charge	1.60E-19	Coul						
4	proton mass	1.67E-27	Kg						
5	proton rest ener.	938.23	MeV						
6	speed of light	3.00E+08	m/s			**Add. Straight**			
7	permittivity	8.85E-12	farad/m				High Field	Low Field	
8	Tev -> Joule	1.60E-07				High Energy	4.00	4.00	Km
9						Low Energy	4.00	4.00	Km
10	power constant	0.21							
11						**Total Accel**			
12							High Field	Low Field	
13		High	Low			High Energy	108.72	522.74	Km
14	Field	12.50	2.125	Tesla		Low Energy	10.28	35.12	Km
15									
16		TeV	Joules	Gamma		**# of Bunches**	1/6 buckets filled		
17	High Energy	50.00	8.01E-06	53291.72			High Field	Low Field	
18	Low Energy	3.00	4.81E-07	3197.50		High Energy	21758.46	104616.87	
19						Low Energy	302.98	1034.90	
20									
21	**Radius of Curv**					**Protons/Bunch**	from pink book		
22		High Field	Low Field				High Field	Low Field	
23	High Energy	13.33	78.43	Km		High Energy	5.00E+09	9.40E+09	
24	Low Energy	0.80	4.71	Km		Low Energy	5.00E+09	9.40E+09	
25									
26	**Circum of Magnets**					**Total Protons**			
27		High Field	Low Field				High Field	Low Field	
28	High Energy	83.78	492.80	Km		High Energy	1.08E+14	9.83E+14	
29	Low Energy	5.03	29.57	Km		Low Energy	1.51E+12	9.73E+12	
30									
31	**Packing Factor**					**Current**			
32		High Field	Low Field				High Field	Low Field	
33	High Energy	0.80	0.95			High Energy	0.05	0.09	amps
34	Low Energy	0.80	0.95			Low Energy	0.01	0.01	amps
35									
36	**Total Arc**								
37		High Field	Low Field						
38	High Energy	104.72	518.74	Km					
39	Low Energy	6.28	31.12	Km					

	A	B	C	D	G	H	I	J
40					**Spreadsheet 1 (cont.)**			
41		High Energy	Low Energy					
42	RF freq	360.00	53.00	Mhz				
43	RF wave	0.83	5.66	m				
44	RF period	2.78E-09	1.89E-08	sec	**Power/m**	in arcs only		
45	400 ns space	144.00	21.20	RF buckets		High Field	Low Field	
46	20 ns space	7.20	1.06	Rf buckets	High Energy	2.183	0.115	W/m
47					Low Energy	0.002	0.000	W/m
48								
49	**Revolution Freq**	for whole ring			**Energy Loss/rev**			
50		High Field	Low Field			High Field	Low Field	
51	High Energy	2757.55	573.52	rev/sec	High Energy	4.756	0.661	Mev/turn
52	Low Energy	29154.39	8535.44	rev/sec	Low Energy	1.620	0.160	Kev/turn
53								
54	**Angular Freq**	arcs only			**Peak Sync Rad Photon Energy**			
55		High Field	Low Field			High Field	Low Field	
56	High Energy	3578.60	608.36	/sec	High Energy	1120.06	190.41	eV
57	Low Energy	59643.31	10139.36	/sec	Low Energy	4.03	0.69	eV
58								
59	**Power/particle**				**Critical Photon Energy**			
60		High Field	Low Field			High Field	Low Field	
61	High Energy	2.10E-09	6.07E-11	W/part	High Energy	534.79	90.91	eV
62	Low Energy	7.56E-12	2.19E-13	W/part	Low Energy	1.93	0.33	eV
63								
64	**Power/ring**				**Mean Photon Energy**			
65		High Field	Low Field			High Field	Low Field	
66	High Energy	2.29E+05	5.97E+04	W	High Energy	164.67	27.99	eV
67	Low Energy	1.15E+01	2.13E+00	W	Low Energy	0.59	0.10	eV
68								

	A	B	C		F	G	H	I
1					**Spreadsheet 2**			
2	Planck/2pi	6.58E-16	eV-sec					
3	electron charge	1.60E-19	Coul					
4	electron mass	9.11E-31	Kg					
5	electron rest ene	0.51	MeV		**Total Accel**			
6	speed of light	3.00E+08	m/s		High Energy	522.74	Km	
7	permittivity	8.85E-12	farad/m		Low Energy	35.12	Km	
8	Tev -> Joule	1.60E-07						
9					**# of Bunches**	from pink book		
10	power constant	2.37E+12			High Energy	512.00		
11					Low Energy	34.44		
12	**Field**							
13	High Energy	0.0106	Tesla		**Electrons/Bunch**	from pink book		
14	Low Energy	0.0581	Tesla		High Energy	8.61E+11		
15					Low Energy	8.61E+11		
16		High Energy	Low Energy					
17	TeV	0.250	0.082		**Total Electrons**			
18	Joules	4.01E-08	1.31E-08		High Energy	4.41E+14		
19	Gamma	489236.79	160469.67		Low Energy	2.96E+13		
20								
21	**Radius of Curv**	from proton ring			**Current**			
22	High Energy	78.43	Km		High Energy	0.04	amps	
23	Low Energy	4.71	Km		Low Energy	0.04	amps	
24								
25	**Circum of Magnets**							
26	High Energy	492.80	Km					
27	Low Energy	29.57	Km					
28						High Energy	Low Energy	
29	**Packing Factor**				RF freq (Mhz)	351.70	351.70	
30	High Energy	0 95			RF wave (m)	0.85	0.85	
31	Low Energy	0 95			RF period (sec)	2.84E-09	2.84E-09	
32								
33	**Total Arc**				**Revolution Freq**	for whole ring		
34	High Energy	518.73561	Km		High Energy	573.52	rev/sec	
35	Low Energy	31.12412	Km		Low Energy	8535.44	rev/sec	
36								
37	**Add. Straight**				**Angular Freq**	arcs only		
38	High Energy	4.00	Km		High Energy	608.36	/sec	
39	Low Energy	4.00	Km		Low Energy	10139.37	/sec	

	A	B	C	F	G	H	I
40				**Spreadsheet 2 (cont.)**			
41							
42	**Power/particle**			**Peak Sync Rad Photon Energy**			
43	High Energy	4.29E-07	W/part	High Energy	147.32	keV	
44	Low Energy	1.38E-06	W/part	Low Energy	86.64	keV	
45							
46	**Power/ring**			**Critical Photon Energy**			
47	High Energy	188.93	MW	High Energy	70.34	keV	
48	Low Energy	40.85	MW	Low Energy	41.37	keV	
49							
50	**Power/m**	in arcs only		**Mean Photon Energy**			
51	High Energy	364.220	W/m	High Energy	21.66	keV	
52	Low Energy	1.313	kW/m	Low Energy	12.74	keV	
53							
54	**Energy Loss/rev**			**Bunch Spacing**			
55	High Energy	4.665	Gev/turn	High Energy	1.02	Km/bunch	
56	Low Energy	1.008	Gev/turn	Low Energy	1.02		
57							
58				**Bunch Spacing**			
59				High Energy	1197.71	Wavelengths/bunch	
60				Low Energy	1200.00		
61							
62							
63							
64							
65							
66							
67							
68							
69							
70							
71							
72							
73							
74							
75							
76							
77							
78							

Section 3: ACCELERATOR SYSTEMS

G. W. Foster — Status Report on the Transmission Line Magnet

G. W. Foster — Local Alignment of the Transmission Line Magnet

G. W. Foster — Permanent Magnet for the Transfer Lines from the Main Injector to the 3 TeV VLHC Injector

G. W. Foster et al. — Design and operation of an experimental "Double-C" Transmission Line Magnet

M. McAshan — Cryogenic System for the 3 TeV Injector Study

T. Anderson — Examination of the Proposed VLHC Vacuum System

A. Hahn — Instrumentation: Beam Intensity and Longitudinal Measurements

J. Crisp — Position Monitors for the 3 TeV High Energy Booster

H. Glass et al. — High Field Magnet R&D for VLHC

R. Goodwin et al. — Thoughts on Controls/Instrumentation for 3 TeV Booster and VLHC

STATUS REPORT ON THE TRANSMISSION LINE MAGNET

G.W. Foster,
Fermi National Accelerator Laboratory, PO Box 500 Batavia IL 60510
September 29, 1997

Abstract

The current status of the design of the "Double-C" transmission line magnet is reviewed. Technical notes describing prototype results, design changes, and performance calculations are cited. Open design issues, the ongoing R&D efforts, and plans for the next round of prototypes are discussed.

1 INTRODUCTION

A cross section of the Transmission Line Magnet [1] design is shown in figure 1. It is a 2-in-1 warm-iron superferric magnet is built around a 75kA superconducting transmission line. The current is returned in the cryogenic distribution lines located in a structural tube underneath the magnet. Steel yokes above and below the transmission line concentrate the magnetic flux in a pair of gaps which provide opposite bend fields in the twin apertures needed for P-P collisions. The pole tips are shaped to provide the alternating gradient necessary to focus the beams, thereby eliminating quadrupoles and allowing the magnet to be continuous in long lengths. All vacuum hardware, instrumentation, and cryogenics are pre-assembled and tested in the factory. The length of the magnet assembly is ~250m (four half-cells).

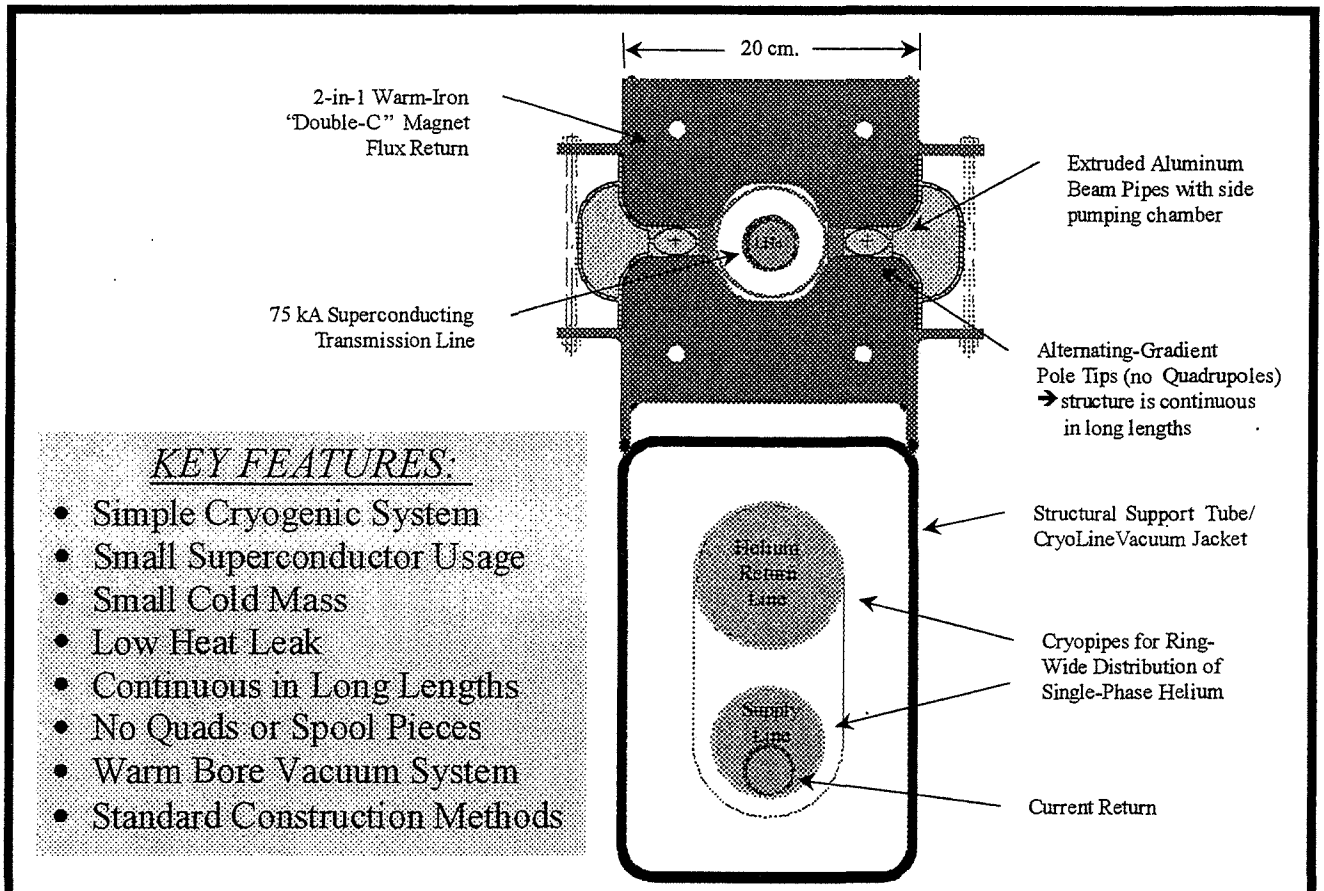

Figure 1 - Transmission Line Magnet

This design is believed to address all mechanical, cryogenic, electrical and beam dynamics constraints for both the 50x50 TeV VLHC and the 3 TeV injector. A 2m long model magnet built to test various aspects of the assembly procedures is shown in Fig. 2. We are currently ordering parts for the next (~50m long) prototype based on this design.

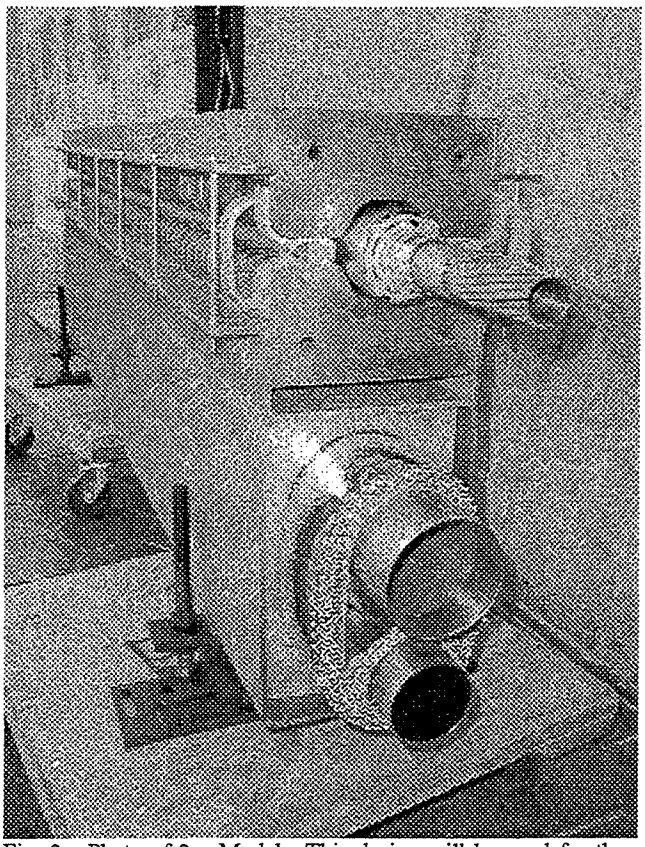

Fig. 2 - Photo of 2m Model. This design will be used for the 50m prototype.

A table of parameters for the transmission line magnet is given in Table 1.

Magnet Type	Warm Iron, Warm Bore
Magnet Topology	Double-C, 2-in-1
Operating Range	0.1T → 2T
Drive Conductor	Single turn, 75 kA Superconducting Transmission line
Focusing	Alternating-Gradient Combined Function (no quads or spool pieces)
Normalized Gradient	5%/cm for a typical lattice
Magnet Aperture	3cm x 2cm (H x V)
Good-Field Aperture ($\lvert\delta By/Bo\rvert < 10^{-4}$)	2cm round at injection 1cm round at 2T
Iron Dimensions	20cm x 20cm
Transmission Line	7.5cm diam x 250m length
Inductance	2.3uH/m (low currents) 1.9uH/m ($2E_S/I^2$ at 75kA)
Iron Yoke	Laminated Low-carbon Steel

Table 1. – Transmission Line Magnet Parameters

2 FIRST PROTOTYPE SYSTEM

A short prototype system (Fig. 3) was built and operated under the guidance of Peter Mazur, stewardship of Cosmore Sylvester, and with instrumentation built by Phil Schlabach. A paper [2] on results from the first test run of the prototype system was presented at the 1997 PAC (Particle Accelerator Conference) and is included in these design notes. The system included a 5m loop of superconducting transmission line, a current transformer, and a double-C magnet iron yoke 1m long. The current transformer was used to excite a large circulating current in the superconducting loop. This approach was used because it avoids the expense of large superconducting current leads. The system worked as expected, with the magnetic and electrical behavior of the current transformer, flux reversing switch, and double-C magnet behaving as calculated [3].

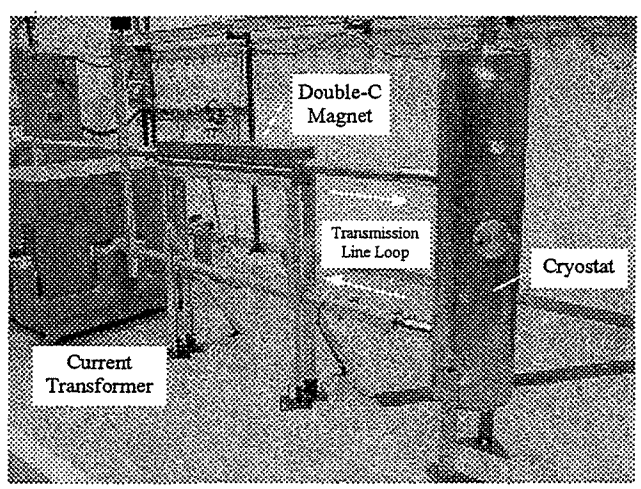

Fig. 3 – Photograph of the first prototype transmission line magnet.

The superconducting transmission line conductor quenched at a somewhat lower current than expected (43kA vs. 50kA design). The cause of this is believed to be that the conductor bundle (7 loops of leftover SSC cable) was essentially unconstrained in sections of the transmission line cryopipe. In subsequent designs the conductor will be continuously soldered to a monolithic copper stabilizer and this should be avoided.

3 MAGNETIC DESIGN

The magnetic design of the double-C magnet is essentially unchanged from the Snowmass [4] design. See Fig. 4. Field lines circulating around the transmission line are concentrated into the beam gaps by the iron pole tips. Saturation of the steel limits the field in the gaps to 2T at 75kA drive current and 2.2T at 100kA.

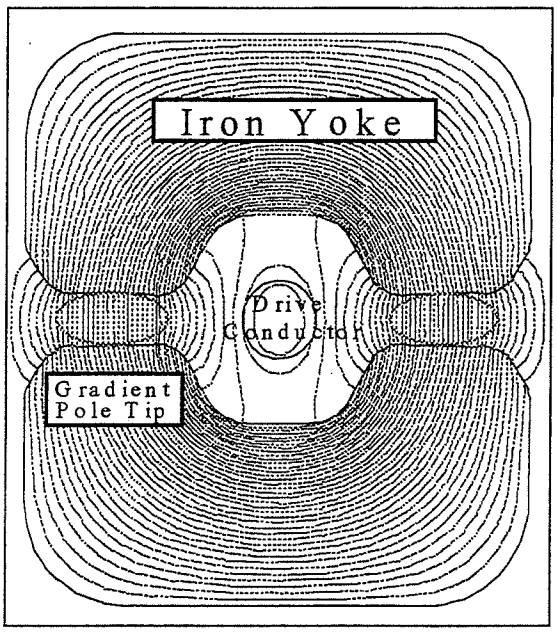

Fig. 4 – Magnetic field map of the transmission line magnet generated by POISSON. The small field gradient (~5%/cm) is visible in the pole tip shape.

The design features a "crenellated" pole tip [5] to mitigate saturation effects up to ~2 Tesla. This technique (Fig. 5) reduces the average density of the iron in the low-field regions of the pole tip, so that the pole saturates evenly. This preserves the field quality at much higher excitations (perhaps as high as 2.2T, see Fig. 6) than would be possible in an all-iron magnet.

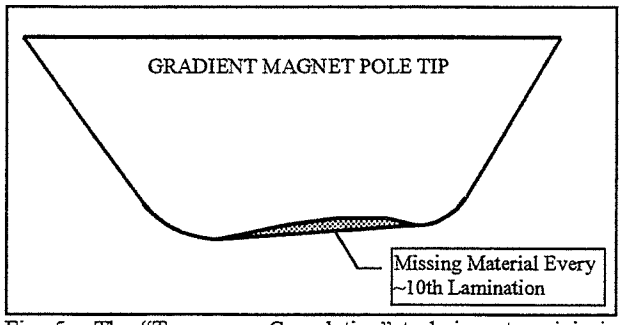

Fig. 5 - The "Transverse Crenelation" technique to minimize field shape changes from saturation.

The 2m laminated iron model in Fig. 2 has been constructed with one of its bores crenellated and the other without. This will be used for magnetic testing to verify the crenellation concept.

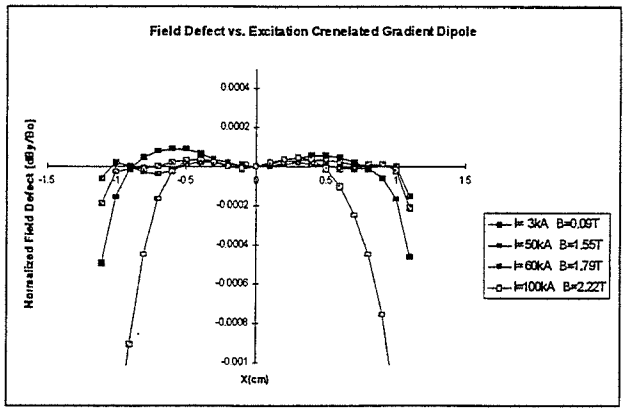

Fig. 6 - POISSON calculation of normalized field defect vs. horizontal position at different excitation currents for the crenelated pole tip design. The uncorrected field defect is below $\pm 10^{-4}$ across the ±1 cm aperture for fields up to 1.8T. The goal of the R&D program is to demonstrate a design with acceptable field quality above 2T.

A "Double-C" iron test stand[6] with a drive conductor using water-cooled copper coils is being built by A. Makarov of the FNAL Technical Division to allow rapid turnaround of magnetic measurements. See Fig. 7. This will allow optimization of the pole tip shape, crenellation patterns, as well as the study of various correction strategies.

The magnetic measurement systems to be used on the transmission line magnets will also be developed on this test stand. The leading candidate is a stretched-wire system using support arms that reach into the gap of the C-Magnet. A rotating coil becomes difficult due to the scaling of pickup coil tolerances vs. coil aperture. Arrays of Hall probes are also being considered. A key issue is the presence or absence of the beam pipe as the long magnet assemblies are measured.

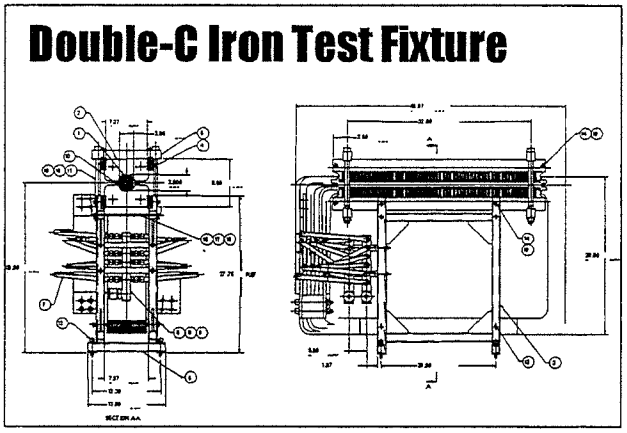

Fig. 7 – Design of the water-cooled copper test stand for optimizing the Double-C iron shape and developing appropriate measurement techniques. The fixture is electrically interchangeable with the Main Injector Dipole test stand at Fermilab's Magnet Test Facility. The coil is capable of putting 100kA-turns through a 3" diameter hole and driving the Double-C iron yoke far into saturation.

Another significant ongoing effort is to quantify the effects of variations in steel properties on the performance of the magnet. B-H data using the full production run of magnet iron for the Fermilab Main Injector is being used. Production trimming techniques to compensate for variations in strength and saturation properties of the magnet iron are being investigated numerically in POISSON.

Another area of work involves the alignment tolerances and decentering forces of the transmission line drive conductor. The present design requires alignment of the drive conductor within ~0.5mm of the magnet center[7]. This is felt to be doable, but we may change our mind after building and measuring the conductor centering in the first long prototype.

Preliminary magnetic designs exist for the 2-in-1 Lambertson [8] for beam extraction and abort. These magnets will be powered from the transmission line current so that they track the arc magnets and the beam energy. No separate power supplies or LCW connections are needed. Similar designs for the beam separation dipoles and straight-section quads will be developed.

The presence of the nearby iron in the structural support tube does not cause difficulties. This iron saturates completely at a very low excitation currents (well below injection energy) and does not contribute significantly to the stored energy or inductance at high field. The main detrimental effect of the iron support tube is to create an anomalous high inductance at low excitation currents. This makes it difficult to measure the electrical parameters of prototype magnets, and increases the size of the current transformer needed to drive long prototype magnets.

Two minor design changes are contemplated. Firstly, the gradient of the magnet will be reduced from ~5%/cm to 3%/cm to correspond to the lattice design for the 3 TeV injector[9]. This simplifies the design slightly. The second possible change is to increase the inner diameter of the iron by 1-2cm to allow additional insulation space for the transmission line vacuum jacket. This increases the iron cost somewhat but may prove cost-effective when cryogenics costs are factored in. It also reduces the conductor forces and loosens assembly tolerances on the centering of the conductor.

4 MAGNET APERTURE

Various concerns have been expressed regarding the sufficiency of the (2cm x 3cm) magnet gap of the proposed design. These include concerns over beam instabilities at injection energy, closed orbit distortions, magnet alignment and tunnel settling, the need for additional working aperture for beam injection and extraction, the need for additional horizontal aperture to perform resonant extraction for fixed-target operations, and the possibility of Pbar-P collisions in a single aperture.

Each of these items has been addressed, and the magnet aperture of the existing design is sufficient. (Pbar-P will require a separate set of magnets due, among other things, to limitations from the long range beam-beam tune shift). A companion note[10] discusses aperture requirements in more detail.

The two beam instability issues have been resolved as follows. The damper system to control the resistive wall (RW) coupled-bunch instability has been described by Marriner[11]. The damper system relies on proven technology, is not expensive, and does not require a 1-turn delay or across-the-ring signal transmission. Such a system has already been successfully demonstrated in the Fermilab Main Ring. The second (TCMI) instability is more conjectural since it has never actually been seen in a hadron machine. Like the RW instability, it is only a potential problem at injection energy into the large ring, and only for the high-luminosity ($L > 10^{34}$) scenarios. If it does become a problem, a straightforward workaround (due to Malamud[12]) is to inject and accelerate the charge in a number of high frequency RF buckets, then coalesce the beams into their final intense bunches at full energy. This reduces the bunch current at injection to a level below the TMCI thresholds. This type of coalescing is routinely done in FNAL collider operations and is an essential ingredient in achieving high luminosities in the Tevatron. Therefore, beam instabilities are not a problem for the 2cm aperture.

Magnetic field quality (dynamic aperture) at injection should not be a difficulty assuming that the normal field quality obtained in iron-dominated magnets is achieved. A properly designed iron magnet operating at 1 kG (the VLHC injection field) will typically have a dynamic aperture larger that the physical aperture of the magnet [13]. In other words the good-field region of iron magnets goes all the way up to the pole tip. This is in contrast to standard (conductor dominated cosΘ) superconducting magnets, in which the coil must be located a couple of cm outside of the good field region to

maintain adequate field quality. Thus the good-field area (roughly defined by the area in which the total field defect exceeds 10^{-4} of the bend field) of the Transmission Line Magnet significantly exceeds that of (for example) the LHC dipoles at injection energy.

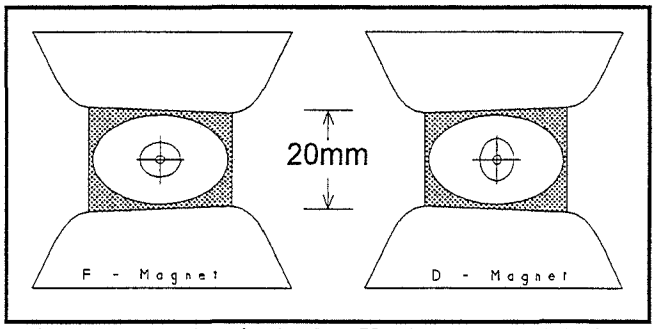

Fig. 8 - Beam Sizes in the 3 TeV Injector. The 95% beam envelopes for 15π beams (roughly the current FNAL collider emittances) are shown. The large ellipses show the beam envelope at injection energy (150 GeV). The small ellipses show the beam size at flattop (3000 GeV). The left and right pictures indicate the beam envelopes in the in the vicinity of focussing and defocusing half-cell locations. Lattice functions are β min =130m, β max = 200m, Dx = 6m. Beam sizes - 150 GeV: Rmin=3.5mm, Rmax=4.3mm; 3000 GeV: Rmin=0.8mm, Rmax=1.0mm. The magnet gap is 20mm x 30mm (h x v) and the beam pipe aperture is 18mm x 27mm. Beam sizes in the 50 TeV machine are roughly 2x smaller.

The physical aperture of the beam pipe is also a concern. The current beam pipe has an excess radial aperture of ~5mm (see Fig. 8 and Table 2). Here the excess radial aperture is the nominal aperture outside of the 95% beam envelope, for beams at injection energy, with the current emittances used in the Fermilab collider (15π in FNAL units). The situation improves when the beam is accelerated. It improves when one gets away from the β-max values encountered at each BPM. It improves if one considers the 50x50TeV machine where the beam sizes are ~2x smaller. It will improve further if (as expected) the emittance of the FNAL injector continues to decrease. The issue is then what aperture losses are anticipated from closed orbit distortions, magnet misalignments, etc.

	Horizontal	Vertical
15π 95% beam size @β-max, dP/P=.01%	± 4.4mm	± 4.3mm
Closed orbit distortion	± 0.5mm	± 0.5mm
Injection Steering Errs	± 1mm	± 1mm
BPM Offsets	± 0.1mm	± 0.1mm
Magnet Straightness	± 0.5mm	± 0.5mm
Magnet Settling (between realignments)	±1.0mm	±0.5mm
TOTAL	± 7.5mm	± 6.9mm
Available Aperture	± 10mm	± 9mm

Table 2 – Aperture at injection into the 3 TeV machine.

The 3 TeV machine does not need extra aperture for allowing kicked beams to propagate off-center through the arcs. (Several machines at FNAL do this). This is because it has zero-dispersion straight sections with enough length to contain both the kicker and Lambertson. It does not need helical orbits for Pbar-P since this would be done using two sets of magnets. Thus only on-axis orbits need to be considered in the arc magnets.

Closed orbit distortions are largely an issue of corrector strength, beam position monitors, and software. We assume that adequate corrector strength will be available to control orbit errors at injection. In the Tevatron, closed orbit distortions are generally kept under 1-2mm, which is adequate given the physical aperture of the machine. At LEP (where beam centering in the quads is more important due to radiation damping) they do ~0.1mm [17]. DESY does 0.05mm [14]. We assume in table 2 that a closed orbit distortion of 0.5mm will be achieved.

The aperture allowance for injection steering errors has been considered. Here the issue is the short-term reproducibility of the beam transfer kicks, since the injection orbit can be verified immediately before filling via low intensity pilot shots. The reproducibility of the injection orbit is currently <0.1mm for the Tevatron [15]. (It is worth noting that the warm-iron magnet should not be as sensitive to quenching from a mis-steered pilot shots as the Tevatron or other cold-bore machines.) Thus the allowance of 1mm in table 2 seems reasonable.

Beam Position Monitor (BPM) offsets will contribute to the aperture budget. Gross errors in BPM centering can be verified *in situ* with aperture scans which scrape either side of the aperture in the vicinity of each BPM. Again, the warm-iron magnet should tolerate aperture scans better than cold-bore superconducting magnets. The 0.1mm allowance in table 2 corresponds to ½% position accuracy in the BPM readout.

Kinks in the magnet bore will reduce the available aperture. The assembly tolerances are discussed in ref 16. The straightness tolerance (R&D goal for the 50m prototype) is ±0.5mm. Survey of the magnet bore is straightforward since the position of the aperture can be surveyed to ±0.25mm at any place along the length of the magnet via fiducial notches on the warm iron laminations. Alignment feet allow the magnet bore to be re-centered on the beam every 6m along its length. Between the supports, the magnet assembly must be straight to the required tolerances. It should also be noted that the straightness tolerance only applies to the bore in the vicinity of the focussing BPM in each coordinate, and is relaxed at other points nearer the beam waist.

Tunnel settling will be another source of kinks in the magnets that develop over time. Tunnel deformations with a distance scale longer than the BPM/corrector spacing can be compensated for by reprogramming the correctors or moving magnets. Tunnel deformations between the BPM's will reduce aperture and must be corrected for by periodically realigning the magnets. Current thinking is to have a semi-automated mechanism

which regularly surveys and realigns the magnets them so that they are straight between the BPM's. The tunnel settling straightness tolerances in Table 2 reflect estimates based on the random movement of quadrupoles in the SPS tunnel [17] over a 2-year period between alignments. See Ref. 16.

Resonant extraction aperture requirements for fixed-target operations from the 3 TeV injector have been calculated by Marriner[18]. This does not affect aperture requirements at injection since extraction takes place at flat top; however it often gets mentioned as a possible reason to need a bigger beam pipe. Optimized resonant extraction involves spreading out the beam in whatever horizontal aperture is available. Only the horizontal physical aperture is relevant rather than the good-field aperture since the high-amplitude resonant particles in the beam are lost after only a few turns. Vertical aperture requirements are not increased. The beam is extracted at a localized high-beta insert in a straight section in order to make the septum width (measured in beam sigmas) as small as possible. Assuming a 1:4 ratio between the β-functions in the arcs and the extraction septum, Marriner calculates that acceptable extraction efficiencies of 99% can be obtained. If necessary, this extraction efficiency could be increased further by increasing β at the extraction septum. Thus the current beam pipe dimensions are sufficient for high-efficiency resonant extraction should this be desired.

Another possible concern is that the lower energy beams of the 3 TeV injector may require a somewhat larger aperture than the 50 TeV VLHC itself. This would prohibit a common magnet design for both machines. For lattices under consideration[19], the betatron beam sizes in the injector are roughly 2x smaller in the 50 TeV VLHC. However the injector benefits from a number of mitigating factors, including the feasibility of stronger beam orbit correctors, a more favorable situation with respect to beam instabilities, a smaller dwell time at injection, and the relative ease of survey and alignment. Thus the present design appears suitable for both.

5 MECHANICAL DESIGN

A significant design change since Snowmass is the switch from extruded steel to laminated iron half-cores. This is an important decision since ~2/3 of the magnet cost is in the iron yokes. This change was driven by several factors. Firstly, the 3 TeV injector may have a ramping time as short as 10 seconds, and the eddy-current-induced field defect from a solid iron pole tip would require strong correctors[20]. A second factor was that implementing the crenellations in the pole tip is much easier in a laminated magnet than in an extruded magnet, and does not require special tooling. A third consideration is that we were able to obtain very attractive pricing for assembled, stacked, and crenellated half-cores from the same vendors who produced the Main Injector magnets.

For the 50 TeV machine we expect that the extruded/cold drawn steel yokes will be significantly less expensive. Eddy currents are not a problem for the 1000 second ramp time of the 50 TeV machine. Extruded steel pole tips were used successfully for quadrupole production for Fermilab's Recycler Ring, and gradient magnet pole tips have been produced for the Recycler which meet the required ±0.0002" tolerances on the pole tip shape. The learning curve on the extrusion/cold draw process was steep. We feel however that it is expedient to adopt a conventional baseline design using traditional stacked and welded laminations for the cost estimate as well as the next round of prototypes.

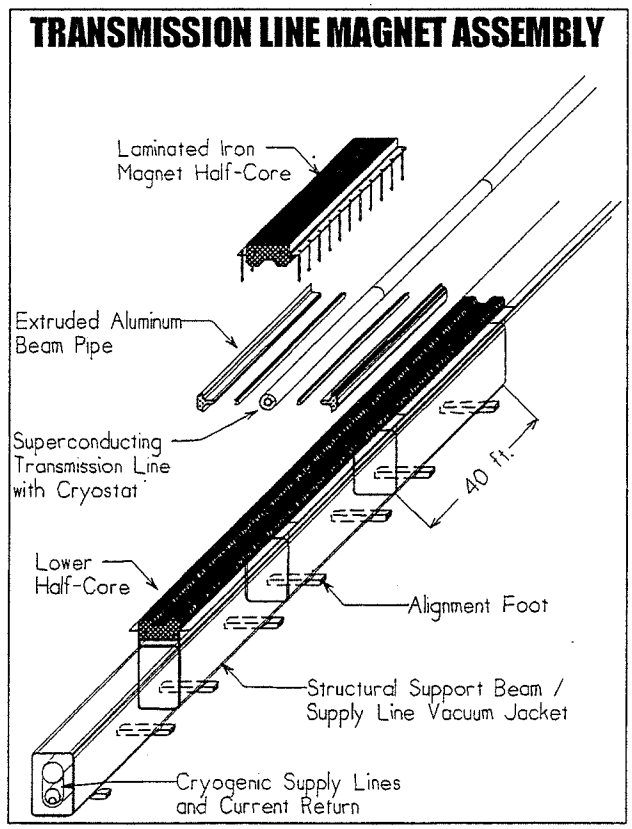

Fig. 9 – Transmission Line Magnet Assembly.

A structural support beam [see Fig. 9] is required to support the laminated iron structure. This support beam also serves as the vacuum jacket of the cryogenic distribution lines. The combined structure is rigid enough that supports every 6m (20') are sufficient to align the structure. Support and alignment tolerances in the Transmission Line Magnet assembly are discussed in Ref. 21.

Thermal expansion forces on the support beam are a significant engineering issue. The current plan is to mechanically connect the support beams between magnets. It thus becomes a continuous mechanical element analogous to continuously welded railroad rails (which go 100's of km between cities without thermal relief). However these longitudinal forces must be periodically anchored to the rock (e.g. at the ends of the magnets) to prevent fault conditions from damaging long

lengths of magnets. Maintaining transverse alignment tolerances in the presence of these longitudinal forces will require engineering attention and prototype work.

The mechanical stability of the transmission line cryopipe is another significant engineering issue. The challenge is to support the cryopipe with the lowest possible heat leak in the presence of decentering magnetic forces. (Although there are no magnetic forces on the drive conductor when it is at its nominal center position, there is a decentering "negative spring constant" which means that the drive conductor will be attracted to the top or bottom of the iron yoke when it becomes vertically off center). The situation is analyzed in Ref 28.

6 MAGNET ASSEMBLY

A baseline magnet assembly plan has been defined which makes maximum use of products from commercial vendors while maintaining final assembly and Q/A under control of Fermilab. The goal is to minimize on-site infrastructure and tooling costs. The situation should be similar to the case of Main Injector magnets, in which 95% of the value added came from outside vendors and only 5% of the costs were from on-site assembly and Q/A.

Major components are pieced together from commercially produced 40-foot lengths: the pre-assembled laminated half-cores, the structural support tube, the Invar transmission line cryopipe, vacuum jacket, and the cryogenic transfer lines. The choice of 40-foot lengths allows truck shipment to the final assembly site.

This approach is similar to the construction of the ~8km of cryogenic transfer lines for the Fermilab Tevatron. The construction of the cryo transfer lines (which were pieced together from long lengths at an on-site factory) was completed quickly and at a cost that was dominated by the parts cost. They have operated for 13 years without failure.

The superconductor and copper stabilizer must be continuous for the full length of the magnet. This is accomplished by commercially fabricating the copper stabilizer and superconducting strand into strips 10cm x 3mm x 250m long. The strip is transported on 750ft, 1500-lb. reels to FNAL where a final roll-forming operation converts the strip into a helical coil.

7 TRANSMISSION LINE DESIGN

Considerable progress has been made at arriving at a baseline design (

Fig. 10) which satisfies all known requirements while relying as much as possible on normal commercial processes.

Design constraints include carrying the 75kA current with adequate margin, handling thermal contraction, quench protection, hydraulic impedance, manufacturability, splicing, heat leak, conductor centering, and control of conductor forces. A cross section of the transmission line conductor is shown in Fig. 12.

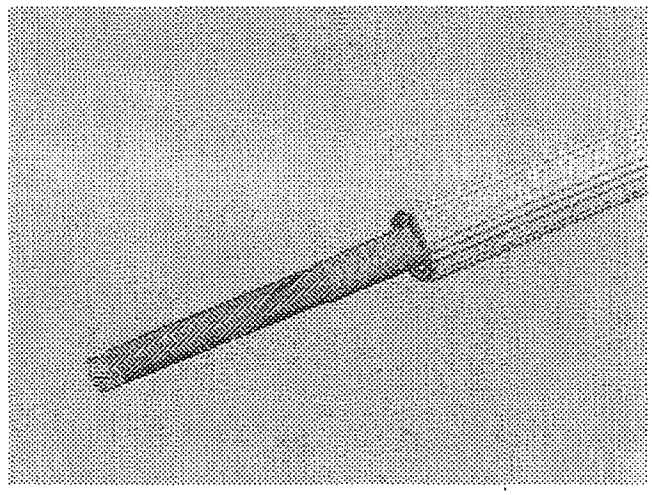

Fig. 10 – CAD rendering of the superconducting transmission line. From left to right: superconducting NbTi strand, helically slit copper stabilizer, invar cryopipe, G-10 cold-mass support "spider", and aluminized-mylar superinsulation. Not shown: stainless steel vacuum jacket and vacuum breaks

The superconductor consists of 18 strands of 2mm diameter copper-stabilized NbTi with a Cu:SC ratio of 1.3:1. The conductor operates in essentially a self-field of 0.8 Tesla, even when there is 2T on the pole tips (see Fig. 4). Fine filaments are not required since persistent current effects are unimportant in an iron-dominated magnet. The operating current is 75kA at an operating temperature of 7K. Enough superconductor is included to operate at 100kA if the cryogenic system operates with 6°K peak temperature in the drive conductor.

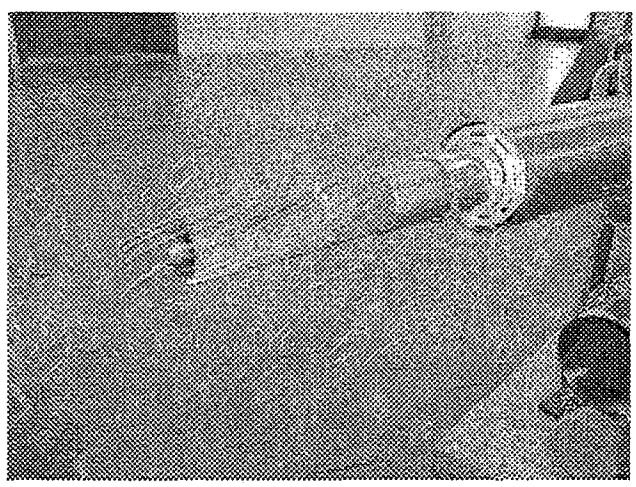

Figure 11 – Photograph of transmission line conductor at end of 2m model magnet. From left to right: NbTi superconducting strand, helically-slit copper stabilizer, Invar cryogenic pipe, vacuum superinsulation, G-10 support "spider", 304 Stainless Steel vacuum jacket, and body of transmission line magnet.

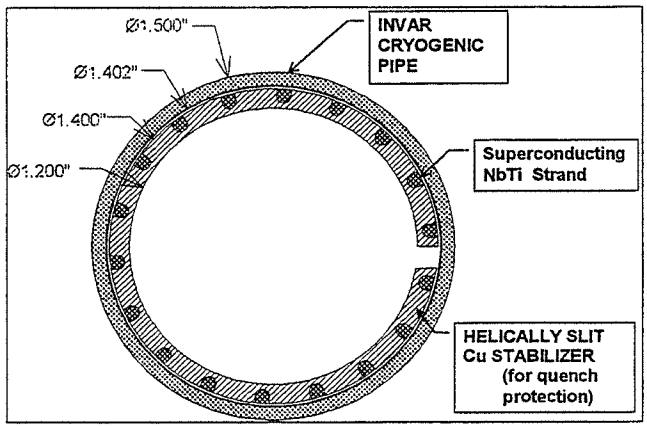

Fig. 12 - Transmission Line Drive Conductor

Operating Current	75kA
Operating Temperature	4.5-6.5K
Operating Field	0.8 Tesla
Superconductor	2mm NbTi Strands
Number of Strands	18 strands at 20°Spacing
Strand Diameter	2 mm
Copper: SC ratio	1.3:1
Cryopipe	1.5" Drawn Tube
Material	36% Nickel Steel (Invar)
OD/ID/Wall	1.5" / 1.402" / 0.049"
Manufacture	Assembled (orbital welded) at FNAL from 40ft lengths
Copper Stabilizer	Helical Slit copper tube
OD / ID / Wall	1.400" / 1.200" / 0.100"
Alloy	OFHC
RRR	55 (min, after cold work)
Helix Pitch	3-5 turns/meter
Strand Attachment	Soldered to stabilizer

Table 3 – Transmission Line Conductor Parameters

8 INVAR CRYOPIPE

The Invar cryopipe of the transmission line drive conductor solves several problems in the design of the drive conductor. The main benefit of Invar[22] is that its low thermal contraction to cryogenic temperatures (approximately 1/7 of 304 stainless steel) eliminates the need for cryogenic bellows. This permits a compact design and a lower heat leak. It also minimizes or eliminates abrasion problems on the drive conductor and support spiders.

In its planned use, the Invar cryopipe will be physically constrained at the vacuum breaks at the ends of the transmission line segments. Under these circumstances cold Invar goes into modest tension (7 kPSI stress) which is well below its yield point (120 kPSI at cryogenic temperatures). In the Invar can then be thermally cycled repeatedly to cryogenic temperatures without damage.

There are however several potential concerns in our application of Invar. Firstly, Invar is reputed to be difficult to weld, although problems occur mainly in connections to dissimilar steels. We must ensure that our welding procedures produce welds that survive repeated thermal cycling, under tension, without loss of reliability. Secondly, adequate dimensional stability of the Invar should be verified after repeated thermal cycles. There is mention in the literature that Invar changes length slightly for some period following cold work. Finally, Invar it is not a true stainless steel and it can rust.

For these reasons, as well as to gain experience in handling Invar before committing to a prototype, we are arranging the simple test setup in Fig. 13. A 50m length of Invar piping with a large number of girth welds will be clamped on either end, then thermally cycled by flushing alternately with liquid nitrogen and room temperature nitrogen. Warm strain gauges will monitor the forces from thermal contraction. The leak-tightness and length of the pipe will be checked before and after hundreds of thermal cycles.

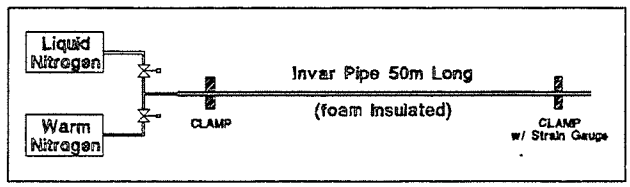

Fig. 13 – Invar Cryopipe test setup.

Invar is ferromagnetic (B_{SAT} ~0.8T) and will fully saturate at low currents in the drive conductor (below injection energy). It is not believed that this will cause any difficulties.

9 HELICAL COPPER STABILIZER

The superconductor/copper stabilizer structure has a helical slit (see

Fig. 10). This serves three purposes. Firstly, it avoids mechanical damage during cryogenic cool down. The slit provides a "springiness" which, if not present, would cause excessive stress and yielding in the copper. This cold work would mechanically and electrically degrade the copper and superconductor. Secondly, the helical structure allows the copper/superconductor structure to be shipped in strip form on reels to FNAL, then formed into the helically slit pipe in a single roll forming operation. This minimizes the on-site labor content of the transmission line and allows the use of commercial processing for the copper fabrication, plating, and soldering of the superconducting strand. Thirdly, the helical slit provides a structure that can be shrunken radially by twisting it up (like a rubber band). This permits an assembly procedure in which a long section of copper helix is twisted up to reduce its radius. Forty-foot sections of Invar pipe are then slid over the copper

structure and welded into a continuous length, and finally the torsion on the copper is released so that it fits snugly into each section of Invar pipe. This assembly procedure is being tested on dummy copper helix and stainless pipe sections.

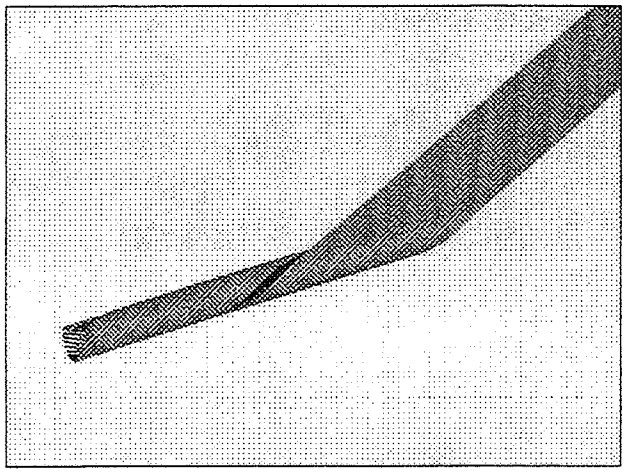

Figure 14 – Roll forming operation which converts the copper strip containing the superconducting strand into a helically-slit pipe. The strip arrives on reels from a commercial vendor and is roll-formed on site. The helical twist is necessary so that the pipe can sustain cool down to cryogenic temperatures without damage.

A finite element analysis [23] of the thermal stresses of the copper helical structure was made. The total force necessary to constrain the copper to a fixed length on cool down was calculated. This force was found to vary roughly as 11000kgf/N^3, where N is the number of helix twists per meter. Choosing N=4 twists per meter gives a tension of 690kgf. This is less than the thermal tension on the Invar pipe (~750 kgf).

To verify the calculations, a mechanical sample of the helical copper structure was prepared and tested in the Instron machine at the FNAL Materials Testing Laboratory. The sample was 1m long with a helix pitch of 2 turns/meter. The elastic modulus agreed within 20% with the finite-element analysis.

There are several unresolved issues in the transmission line conductor design. The electrical insulator that isolates the transmission line from the rest of the magnet can be warm or cold, inside or outside the cryopipe and/or vacuum shell. The copper stabilizer may be a monolithic helical pipe or a series of interlocking but mechanically independent pieces. The helix pitch of the conductor is not yet set and will depend on further calculations and experience with the long prototypes. These issues are more in the nature of cost optimizations rather than fundamental questions about the feasibility of the design.

10 AUTOMATIC WELDING

We have tested Fermilab's automatic orbital welders for use in assembly of the cryogenic piping. The performance is excellent on both Invar and stainless steel. The weld on the transmission line cryopipe can apparently take place directly over the copper/superconductor structure without damaging it. This success is significant because it opens up a number of convenient options for manufacturing and splicing the transmission line conductor.

Fermilab also owns larger orbital welders for sectioning together the structural support beam and cryostats. These will be used building the 50m prototype.

11 TRANSMISSION LINE SPLICE

The ability to make simple and reliable *in situ* splices in the transmission line is essential. The procedure is as follows. First, the magnets are moved into position and the two ends of the transmission line conductor are brought together. It is not necessary that transmission line ends line up exactly, and a gap of 1-2" between the copper pipe stabilizers is allowable. The ends of the copper structure are modified so that each corresponding pair of strands of superconductor can lay alongside each other in a common channel in the copper. The strands are laid alongside each other and soldered using a clamping fixture analogous to the soldering fixture developed for Tevatron cables. Next, a pair of copper half-pipe sections are clam-shelled and soldered around the joint. This provides the electrical continuity of the copper stabilizer necessary for quench protection of the splice. A telescoping section of Invar cryopipe is then orbitally welded over the splice. This joint is leak checked using methods developed by Mazur [24] for externally leak checking a pipe-to-pipe weld joint. The final step is to weld together and pump out the vacuum jacket, again using telescoping sections, orbital welders, and external leak checking.

A strand overlap distance of ~30cm is required to achieve 0.1 nΩ resistance in the splice. This corresponds to I^2R losses of 1W at 100kA. This length was estimated from joint resistance measurements of measurements of solder splices in SSC cables [25]. The actual joint resistance will be measured from the decay time of the current in the superconducting loop in the next prototype. If necessary, the splice overlap region can be increased to reduce the joint resistance, or additional superconductor can be added in the splice region.

Vacuum breaks are required at each end of the transmission line for the splicing scheme described above. This has the advantage that the vacuum integrity of long lengths of transmission line can be pre-tested in the factory, and the segments can be shipped into the tunnel already pumped down. An overall length of 1.5m and a heat leak of 1W are estimated for each of the two vacuum breaks.

12 MAGNET LENGTH

The optimum magnet length is still under consideration. The driving considerations are the cost and complexity of the magnet ends, the electrical power dissipation at resistive cryogenic joints, the layout of

cabling and instrumentation on the magnet assembly, and the desire to minimize the work performed in the tunnel. All of these considerations argue for longer magnets. The arguments for a larger number of shorter magnets include the cost and complexities of handling long magnets and the cost of long assembly buildings.

The 50m prototype will provide several key inputs into this optimization. These include the electrical resistance which can be obtained at the transmission line splice, the heat leak that can be obtained at the vacuum breaks in the cryostat, and the ease or difficulty of dealing with long segments of iron. At present a magnet length of 250m (four half-cells) is contemplated.

13 EDDY CURRENT LOSSES

An area of concern which had not been addressed as of Snowmass was that of AC power dissipation due to eddy currents in the transmission line superconductor. This is of concern principally for the rapid cycling 3 TeV injector, which might also see duty as a continuously ramped fixed-target machine. A calculation has recently been performed [26] which indicates an average power dissipation of 50mW/meter for a very aggressive ramping scenario (10 second ramp time to 3 TeV, 40 second cycle time). This compares to the 100mW/meter anticipated for the heat leak into the transmission line cryostat, and does not appear to be a problem.

Field quality defects from conductor eddy currents and persistent current loops in the superconductor are not a problem for the superferric design. They are typically a major problem for conductor dominated superconducting magnets.

14 CRYOGENIC SYSTEM DESIGN

The cryogenic system has matured considerably since the work at Snowmass [27]. Work has focussed on the design of the 3 TeV injector system based on conventional NbTi conductor operating at 6-7°K. (The 50x50 TeV cryo system essentially replicates a very similar system).

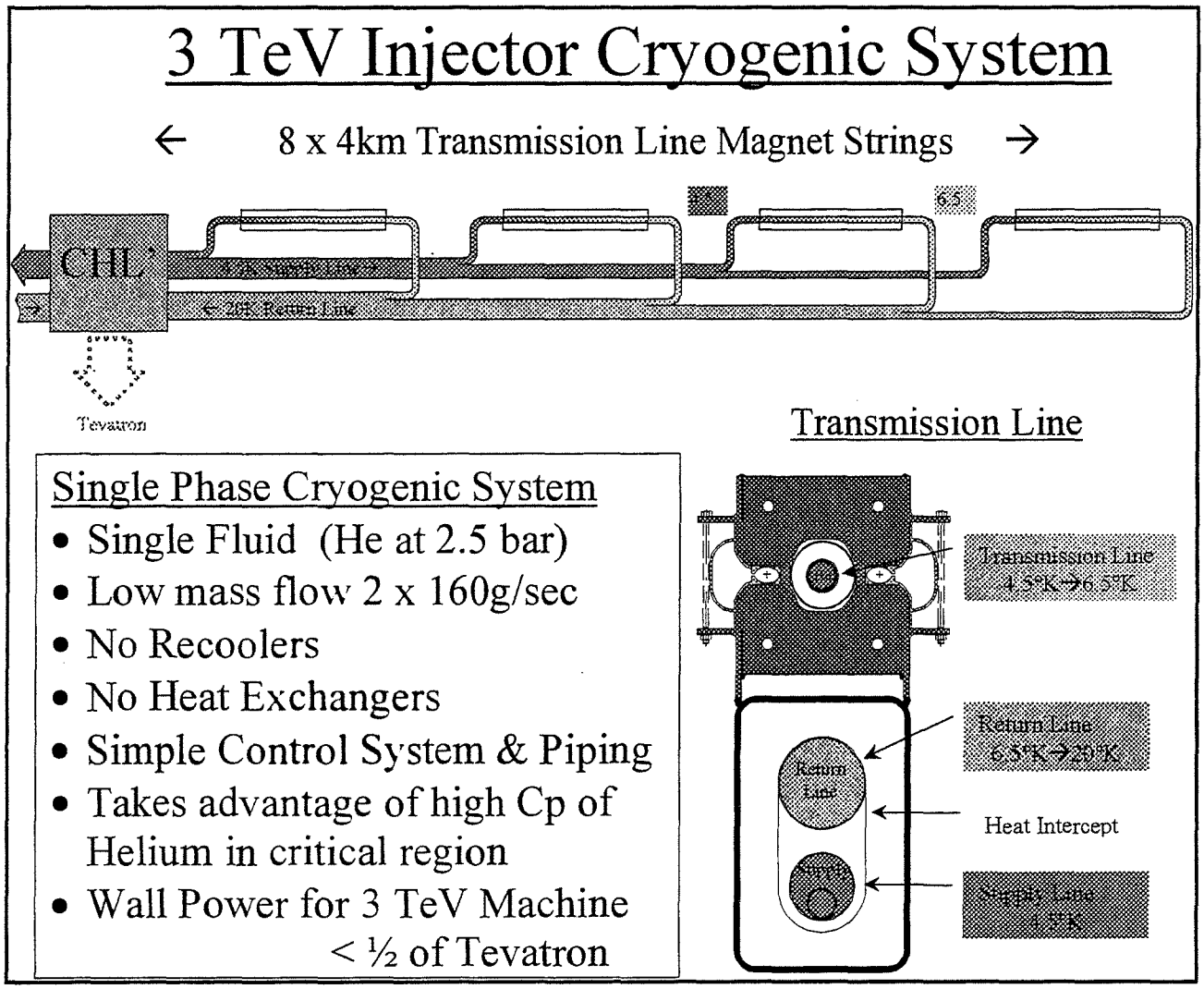

Fig. 15 – Cryogenic system for 3 TeV Injector. The 50x50 TeV cryosystem replicates this structure with 40km loops.

The cryogenic system is described more fully in the paper by McAshan [28]. It is a single-phase system with no recoolers or heat exchangers. A very simple control system is possible – of order 12 remotely operated valves for the 3 TeV cryogenic system. The system could be run from (a modified version of) the existing Fermilab Central Helium Liquifier (CHL) or a new cryo plant could be built. A very low power consumption system is possible if R&D goals for transmission line heat leak are achieved.

15 SUPERCONDUCTOR COSTS AND CHOICE OF OPERATING TEMPERATURE

The choice of operating temperature is a well-known tradeoff between superconductor costs and high-field performance (which favor a low operating temperature) and cryogenic complexity, capital and operating costs (which favor a high operating temperature). In many cases the operating field at the conductor has been pushed as hard as technologically feasible. Conductor costs have traditionally accounted for ~1/3 of total superconducting magnet costs. Thus historically this tradeoff has been resolved in favor of more costly and complex cryogenics systems and a lower operating temperature.

The situation for the VLHC is quite different. Firstly, the superconductor costs for 4.5K operation of the transmission line magnets represents only ~5% of the total cost of the magnets. There are several reasons for this. The iron-dominated design requires fewer ampere-turns per Tesla than a conductor-dominated (cosine-theta) magnet. The conductor itself operates at a low field (0.8T) so that a very high current density can be achieved. There has been almost an order-of-magnitude increase[29] in the current-carrying capability of NbTi conductors (at low field) since the time of the Tevatron. The transmission line magnet does not require the micron-sized filaments needed by cosΘ magnets, which lowers processing costs.

Secondly, the Carnot efficiency of refrigeration rises with operating temperature. This is directly reflected in electrical operating costs. The best predictor of cryo plant costs is the ideal wall power consumption of the system, so that these also scale with the Carnot efficiency.

Thirdly, a number of technological simplifications occur as the operating temperature is raised. At temperatures above 1.8K the complexities of a superfluid helium system are avoided. At temperatures above ~5K the recoolers and heat exchangers used in the Tevatron, SSC, etc. disappear. Thus there is considerable opportunity to trade increases in superconductor costs for decreases in cryogenic capital and operating costs by raising the temperature.

There are three components to the transmission line conductor costs: the transmission line conductor, the current return conductor, and the copper stabilizer.

The amount of transmission line conductor required scales inversely with the current density (Jc) in the conductor. At the temperature and operating field under consideration, Jc goes linearly to zero at ~8.8K. Thus for example raising the operating temperature from 4.4K to 6.6K will double the amount of transmission line conductor required. This raises conductor costs by about $400K/TeV.

The current return superconductor resides in the LHe supply line, which will operate at 4.5-5K in any scenario. Thus the return current (which represents half of the Ampere-meters in the magnet) does not scale significantly with operating temperature.

The copper stabilizer is far less expensive ($5/lb vs. $85/lb for the superconductor). The amount of copper stabilizer required is determined by quench protection and is essentially independent of temperature.

Our present understanding is that the single-phase cryo system operating at a peak temperature of 6-7K, using conventional NbTi conductor, is by a significant margin the lowest cost system for the transmission line magnet. This is discussed in more detail in Ref. 28.

16 THE RELEVANCE OF HIGH-TEMPERATURE SUPERCONDUCTORS AND Nb_3Sn

High-Tc Superconductors (HTS) have been considered and tentatively rejected for use in the VLHC. The main difficulty is that the projected conductor costs are far too high -- even if the R&D goals for superconductor production costs are met. The 5-year R&D targets for HTS are $10/kA-m (corresponding to $15M/TeV) which would more than double the magnet costs. Cryogenic system savings would not come close to covering this cost increase, even if the cryogenic system operated at 77K and was essentially free. In addition, there is a technical problem involving the DC power dissipation due to flux creep in HTS materials when operating near their rated J_C, which causes an unacceptably large cryogenic heat load. The result is that High Tc conductors must be operated at only about half of their rated quench current, thereby doubling the conductor costs. Another technical problem is that there is no known way of bypassing the quench current from the HTS material, aside from using the powder-in-tube conductors which contain an unaffordable amount of silver. In conclusion, it will require a major improvement in the technology, beyond what is hoped for in the short-term HTS R&D programs, before HTS conductor becomes economical for the transmission line magnet.

The situation for Nb_3Sn conductors is similar. A Nb_3Sn conductor could be operated at temperatures as high as 10-11°K, which results in substantial cryogenic savings. Because of this, there have already been extensive efforts commercialize the conductor for low field applications such as MRI. However the costs in large volume are roughly ten times the cost of NbTi. These represent mature production costs for volumes of conductor in excess of what is needed for the VLHC injector. Thus these efforts have largely failed to make

Nb_3Sn cost-effective for MRI despite its cryogenic advantages, and it will take an unanticipated breakthrough to make Nb_3Sn cost-competitive for the VLHC.

By far the most important development in superconductor for the transmission line magnet has already taken place, namely the order-of-magnitude increase in current density per dollar of conventional NbTi for low field applications. This was driven by the commercial interest in low-field (1-2T) applications such as MRI magnets. Continued development of NbTi conductors, particularly the commercialization of Artificial Pinning Center (APC) conductors[29], will no doubt continue to bring costs down. However conductor costs are already a sufficiently small part of the overall magnet costs (~$1-2M/TeV depending on operating temperature) that further conductor development is not required.

CRYOGENIC DISTRIBUTION LINES

A reference design has been adopted that is consistent with McAshan's parameters for the 3 TeV Injector cryo system[28]. The design of the distribution lines is more straightforward than that of the transmission line because of the absence of large conductor forces and the larger radial space available for superinsulation and radiation shields. A cross section is shown in Fig. 16. The supply and return flows (both single phase supercritical He at 2-3 bar) are carried in 3" and 4" OD stainless tubing.

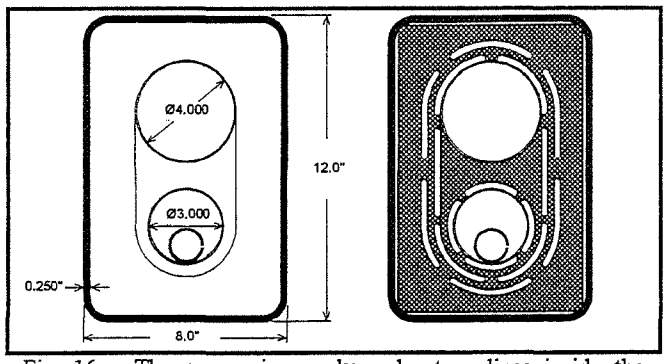

Fig. 16 – The cryogenic supply and return lines inside the structural support beam/vacuum jacket. The 3" LHe supply line contains the current return. A thermal shield connected the 4" return line protects the supply line from radiative heat loads. A 3cm thick blanket of superinsulation (not shown) is wrapped around the cold mass. The G-10 support "spider" built for the 2m prototype is shown at right. Other support geometries (such as slings or support posts) are also under consideration.

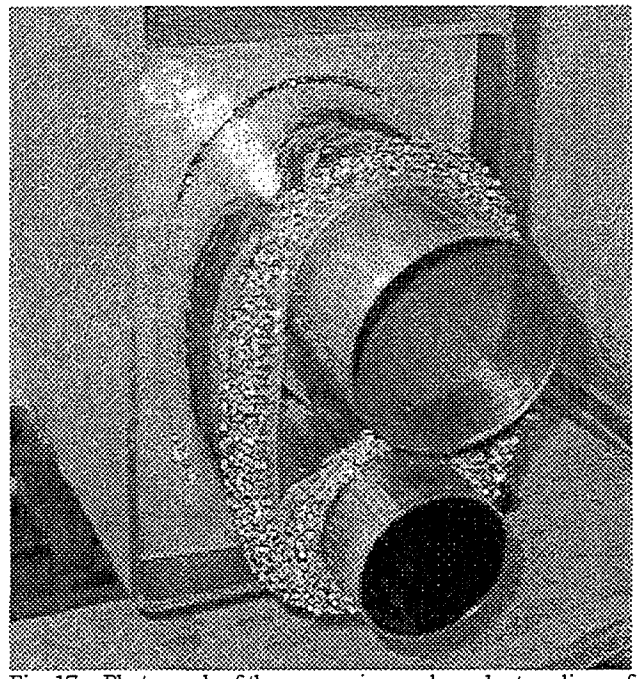

Fig. 17 – Photograph of the cryogenic supply and return lines of the 2m prototype. Dimpled aluminized Mylar is wrapped around the 2-pipe package as well as the smaller 3" supply line.

The cryo distribution lines are a conventional all-welded system with bellows and flow liners (Fig. 18) every 40ft to handle thermal contraction. The design and manufacture of these cryogenic lines are similar to others used at Fermilab for years[30].

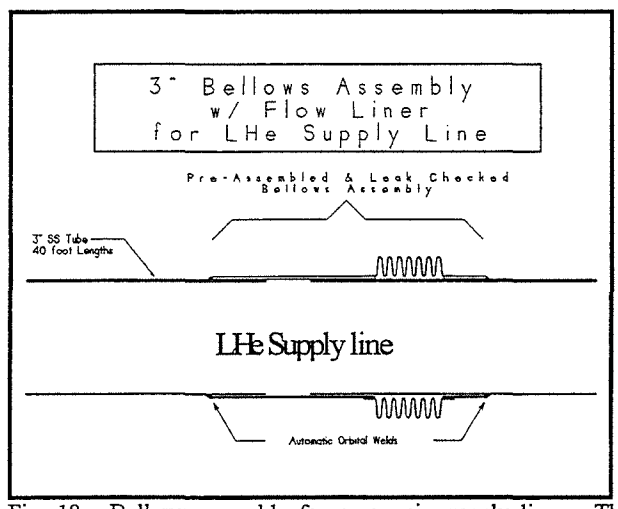

Fig. 18 - Bellows assembly for cryogenic supply lines. The bellows allows for thermal contraction of each 40ft length of pipe. The tubes are supported in a semi-rigid coaxial telescoping geometry. A relatively smooth inner bore maintains low hydraulic impedance. A useful feature of this design is that does not require exactly cut lengths of 40ft tubing.

The supply line is shielded by an aluminum heat intercept which is in thermal contact with the return line. Thus ambient heat is intercepted into the return line instead of the supply line, and the delivery temperature of cryogens to the magnet string is not strongly affected by

variations in the effectiveness of the superinsulation on the cryogenic lines. This also ensures a maximum temperature below 5K in the current return conductor carried in the supply line.

A design variation under consideration is to cool the shield with a separate gaseous-He cooling line operating in the 30-80K range. This would reduce operating costs and insulation requirements but increase the number of pipes to three and increase overall system complexity.

Alternate materials are being considered for the cryogenic transfer lines. These include corrugated stainless or aluminum piping, and Invar. These materials have the potential for eliminating bellows from the cryogenic lines. At present it appears that the conventional (welded stainless pipe + bellows) approach is the lowest cost.

In the present design the cryo line vacuum jacket also functions as the support beam for the magnet assembly. An alternative is to place the cryo distribution lines in a separate mechanical pipe. This has the benefit of de-coupling the installation and maintenance of the cryo line from the rest of the magnet, and perhaps allowing somewhat longer lengths of cryogenic line to be installed in single pieces. The fluid flows interconnect only every ~4km (see Fig. 15). The present approach has the advantage of holding the return conductors in a reproducible location, and making all conductor-to-conductor forces self-contained inside the magnet assembly.

Also under consideration is replacing the rectangular structural tube with a round pipe. Round pipe (as opposed to rectangular structural tube) comes with an implied warrantee of not leaking. It can be obtained in the certified clean, oil-free condition that is needed for a vacuum jacket. It is more straightforward for automatic equipment to weld and inspect. The twist tolerance for rectangular tube is not an issue with round piping. The arguments against a round vacuum jacket are that it needs more wall thickness than a rectangular tube to achieve the same structural stiffness, and that the overall assembly looks sort of peculiar.

17 HEAT LEAK TESTS

One of the most cost-effective R&D activities on the transmission line magnet is the demonstration of low heat leaks in a manufacturable structure. Using generic costs for superinsulation performance (heat leak ~1 W/m^2) and cryo plant costs (~$1k per watt at 4.5K Carnot equivalent), we find that cryogenic plant costs are roughly half of magnet costs. If a lower heat leak can be demonstrated this goes almost directly into reduced cryo plant operating and equipment costs.

We have performed preliminary tests of a promising new superinsulation material[31] using large-crystal aluminum to achieve ultra low infrared emissivity. These tests used the superinsulation test stand developed at Fermilab for SSC tests[32].

We are designing a dedicated superinsulation test fixture to measure and optimize the performance of insulation and support structures in a transfer line geometry. This system will rely on measuring the rate of LHe boil-off to determine the heat flux leaking into a sample of transmission line. See Fig. 19.

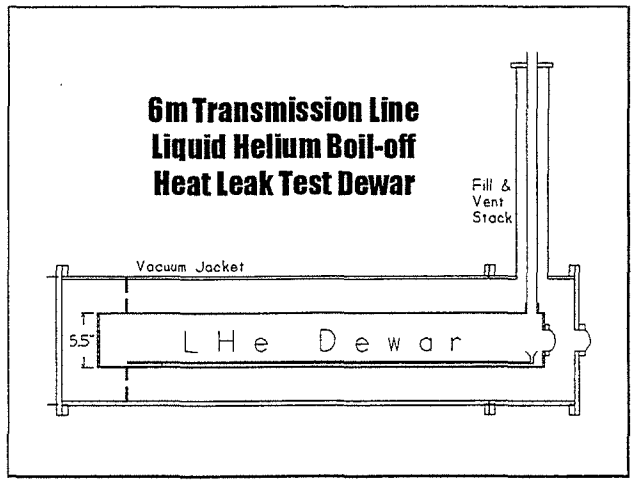

Fig. 19 – Test Dewar to measure heat leak of transmission line using LHe boil-off rate.

The boil-off approach has been chosen because it can reasonably be extended to long prototype magnet assemblies. The initial tests will concentrate on the 4" diameter lines for the cryo distribution pipes which dominate the heat leak. Our goal is to reproduce the best published results[33] of ~0.3 W/m^2 with an insulation and support design compatible with mass production of transmission line.

18 POWER SUPPLY AND QUENCH PROTECTION

The power supply and quench protection system for the 3 TeV machine (Fig. 20) is almost identical to one half-sector of the 50 TeV machine described by Koepke et. al. [34].

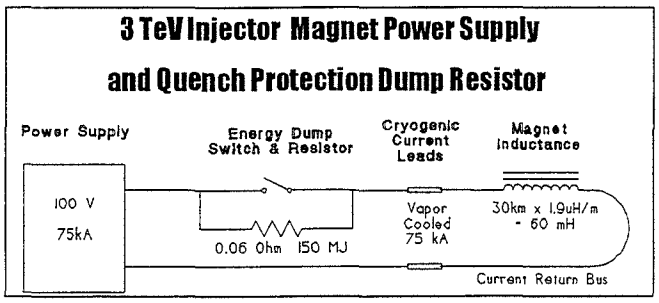

Fig. 20 – Power Supply and Dump Circuit for 3 TeV Injector.

The VLHC power supply is greatly simplified by the low inductance of the 1-turn magnet. This enables the entire magnet string to be treated as a two-terminal device (a single lumped inductance). In contrast, the Tevatron is

something like a 12-Terminal device, with non-negligible distributed capacitance.

The power supply and dump circuit are located in a service building upstairs. They are connected to the magnets by a length of superconducting transmission line carried inside the cryogenic transfer lines. There are no remote power supply buildings. Among other benefits, this reduces the number of possible entry points for power supply noise which could affect beam emittance growth.

The power supply voltage depends on the ramp time chosen, which depends on the physics mission of the machine. The 100V supply in Fig. 20 will provide a 40-second ramp time for the 3 TeV machine. For this ramp rate 7.5MVA are required or about 1/12 of the Main Injector. Steady-state power dissipation at full current comes primarily from voltage drops in the power supply output filter, copper bus work, dump switch, and current leads and is estimated to be 1.5 MW.

A dump time constant of 1 second has been chosen. This corresponds to a maximum voltage of ±2kV to ground during a full-current dump. Longer dump times reduce this voltage but require more copper stabilizer in the transmission line drive conductor.

The dump switch is based on the Tevatron dump switch. As in the Tevatron, the switch will consist of two switches in series: an electronic switch which opens immediately, and a electromechanical switch which opens a few milliseconds later and serves as a fail-safe backup for the electronic switch.

The design of the electronic switch for the 3 TeV dump is simplified by the use of Gate-Turn-Off (GTO) SCR's which were not available at the time of the Tevatron. The design will become even easier when MOS-Controlled Thyristors (MCT's) become available with appropriate voltage and power ratings. These eliminate the obnoxiously large drive currents required to turn off GTO's.

The dump resistor itself is an appropriately scaled length of stainless steel. A thermal mass of 1 Ton is required for a 375°C rise in temperature from a full current quench.

The 75kA cryogenic current leads are larger than those used for HEP magnets but are comparable to leads developed for Superconducting Magnet Energy Storage (SMES) applications [35]. The development of High-Tc leads will be useful but not essential reduction in the operating costs since there are only one set of power supply leads in the machine.

19 ELECTRICAL TRANSMISSION LINE MODES

Treating the entire string of transmission line magnets as a single lumped inductance requires that the electrical propagation delay through the magnet chain be small compared to the start and stop times of the ramp. To evaluate this, a SPICE simulation[36] of the transmission line and current return system was performed. Mutual and self-inductances and capacitances were estimated from the transmission line geometry, and a subcircuit was developed representing a unit length of transmission line. Only a single dissipative source was included, namely the eddy-current losses in the stainless vacuum jacket of the transmission line.

The result of the SPICE simulations was that the transmission line magnet string for the 3 TeV machine can be treated as a single lumped inductance up to frequencies of ~500Hz. At this frequency the first transmission line resonance appeared, with a Q of ~10. By comparison, a similar simulation for one sector of the Tevatron magnets correctly predicts the first transmission line resonance at ~70Hz. The conclusion is that transmission line effects should be negligible for the frequency components present in a 10 second (or longer) ramp times under discussion for the 3 TeV machine.

20 VACUUM SYSTEM

The vacuum system of the transmission line magnet is an extruded-aluminum system similar to many electron machines. Primary pumping is provided by Non-Evaporable Getter (NEG) strips located in a high-conductance antechamber (see figs. 1,2). Lumped sputter-ion pumps are required every ~100m to pump methane and noble gasses (which are not pumped by the NEG strip). The design is reviewed in the Snowmass proceedings [37].

A custom aluminum extrusion and a vacuum test system are being built by our Japanese collaborators at KEK this fall. Their industrial partner is Ishikawajima-Harima Heavy Industries (IHI) who were responsible for fabricating the aluminum vacuum system for the SPring-8 light source. IHI has performed a finite-element analysis and several design optimizations are being made. Support for a continuation and expansion of this collaboration has been applied for as part of the US-Japan accord.

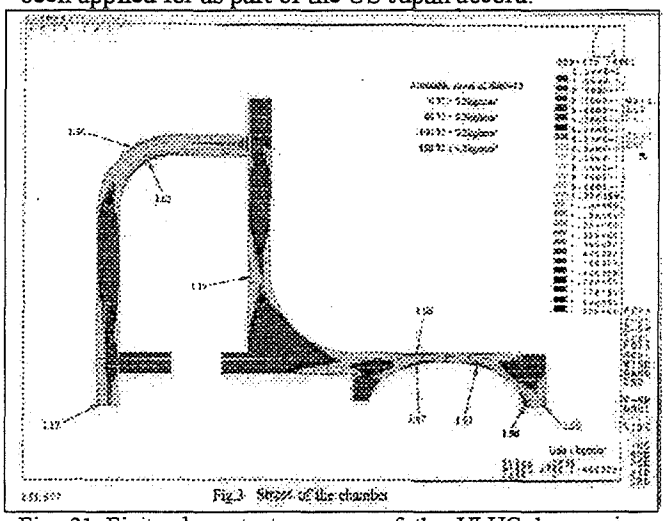

Fig. 21 Finite-element stress map of the VLHC beam pipe extrusion performed by IHI. Yielding of the Aluminum is an issue because of the elevated bakeout temperature, the use of high-purity aluminum, and the desire for as thin an extrusion wall as possible in the region immediately above the beam.

An attractive scheme for installing and supporting the long lengths of NEG strip in the vacuum chamber has been developed. The NEG strip will be double insulated

and supported by a silica-coated aluminum U-channel. This technique should allow the NEG strip to be pulled down the 65m free length of extruded beam pipe between BPM/Pump assemblies. The outgassing rate of the silica coating is low and the insulation and mechanical properties are excellent.

Two extremely useful developments in the NEG strips have occurred of the last couple of years. The first development is that the SAES patent on NEG strip has expired, resulting in increased competition and a dramatic drop in price[38]. The second development is that lower activation temperature getters have been demonstrated[39]. This simplifies the getter strip regeneration procedures.

A bellows-free vacuum system [40] is planned and must survive modest bakeout temperatures of ~85°C. Finite element analyses [41] indicate that the longitudinal stress in the aluminum stays below allowable limits provided the compressive load is appropriately transferred to the magnet and support beam.

21 INSTRUMENTATION

The low-field VLHC contains two classes of instrumentation: the "once per turn" instrumentation, and the equipment that is distributed repetitively around the circumference. The "once per turn" instrumentation for the 3 TeV machine is discussed by A. Hahn in Ref. 42. Essentially everything can be copied (or recycled) from the Tevatron. This equipment will be housed in the on-site straight section and its installation and maintenance will be similar to existing operations.

The instrumentation distributed around the ring is discussed and enumerated in [43]. This equipment dominates the electronics costs. An important feature of the VLHC design concept is that this instrumentation, which occurs in "lumps" every half- cell (~65m for the 3 TeV machine, longer for the 50x50 TeV machine), is to be integrated into the long length magnets. Instrumentation is pre-assembled, cabled, and tested before the magnet is transported into the tunnel. The only tunnel installation jobs are the electrical connections at the ends of the magnets for power distribution and the fiber optic network links. This minimizes the requirements for and costs of tunnel infrastructure around the circumference.

An aluminum-shelled beam position monitor (Fig. 23) with an aperture appropriate to the transmission line magnet has been built by our Japanese collaborators. It is a split-tube device with the inner electrodes plated onto a ceramic shell. This is being tested at FNAL to determine if the electrical parameters, beam impedance, and linearity (response map) are suitable.

The device fits inside a slightly enlarged magnet gap (with about 2/3 the nominal bend field) in modified section of steel 15cm long. Thus the loss in dipole filling factor from the BPM's will be only ~5cm. The sputter-ion vacuum pumps, NEG activation feed-throughs, and pump out ports will be housed in a "unit chamber" at each BPM location. These vacuum connections will not interrupt the bend field.

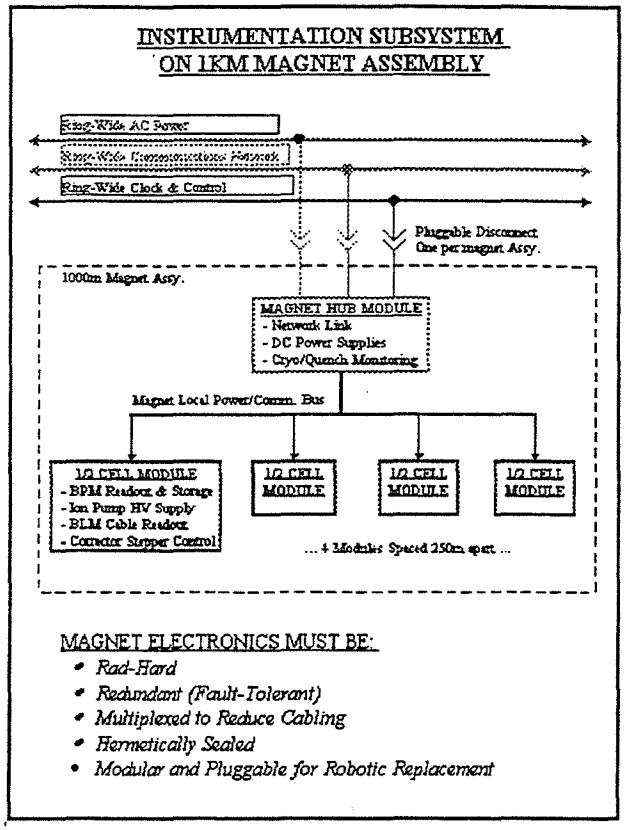

Figure 22 – Schematic instrumentation layout on the transmission line magnet. Instrumentation is lumped at each half-cell location (shown here for 250m half-cell spacing for the 100 TeV machine). The instrmentation is multiplexed onto a small number of ring-wide digital links, which can be in either a "star" or "ring" topology. The instrumentation "lumps" are discussed in Ref. 43.

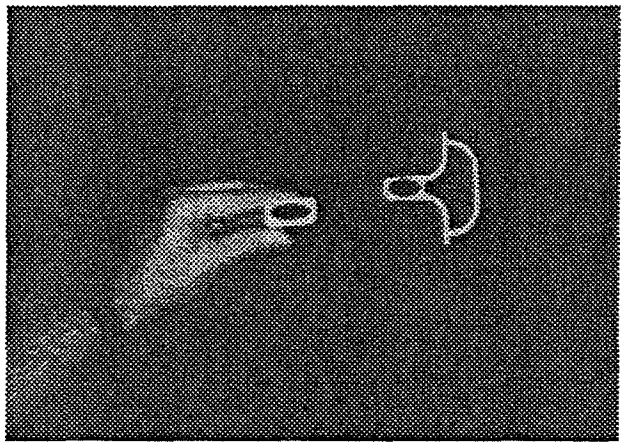

Fig. 23 – Photograph of the aluminum shelled split-tube BPM and an aluminum beam pipe test section.

Beam-loss monitors are needed which span the length of the transmission line magnet. Tevatron-style ionization chambers work well, are radiation resistant, hermetically sealed and require no maintenance.

However a large number of these would be required to span the 75m between half-cells without the possibility of blind spots. Cable-style loss monitors provide continuous coverage but require gas flow because of the plastic shell. The best of both worlds should be attainable with a gas-filled rigid coax cable with a solid aluminum shell as the outer conductor. This rigid coax will be installed and transported as part of the long magnet assembly. We will perform tests to determine if such a rigid-coax BLM can be adequately sealed and thereby maintain an indefinite service life.

22 THE NEXT PROTOTYPE

Design work and parts ordering has begun on the next ~50m long prototype magnet[44]. The goal is to realistically test a complete magnet assembly, i.e. one which simultaneously meets all design constraints involving conductor performance, thermal contraction, magnetic forces, alignment, conductor splicing, and vacuum breaks at the magnet ends. At present we are not adding to this list the crenellated iron shape which will provide the ultimate field quality; this is being pursued in parallel on the iron test stand. When the iron shape is fully developed then the iron structure on the prototype can be easily replaced.

Three methods of driving the prototype 75kA transmission line were considered. The system components are being designed to 100kA capability to provide adequate design margin and the ability to drive the iron deep into saturation.

The first method considered was to use a pair of 100kA current leads and a 100kA power supply. The system would look very much like the final power supply configuration in Fig. 20. This would however cost of order $1M and many man-months of design work. It would require a direct connection to the Fermilab's Central Helium Liquefier (which will not be running in the next 12 months) and would require a substantial support crew. It has the advantages that the power supply & leads would be usable for arbitrarily long string tests and (depending on the voltage and required ramp rate) could be usable as the ramping supply and current leads for the 3 TeV injector. These supplies would allow us to "beat up" on the magnet by ramping continuously, etc.

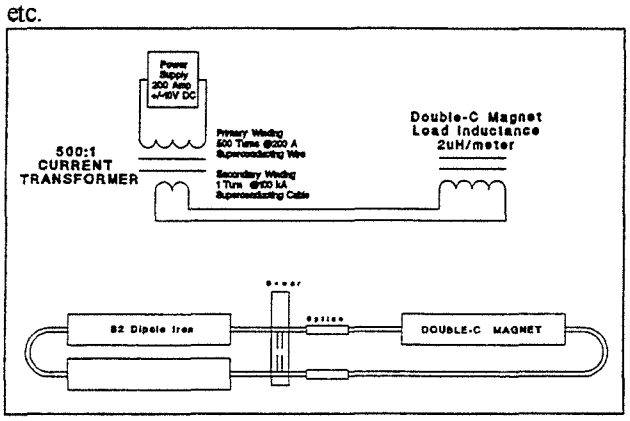

Figure 24 – An alternative considered for driving the next transmission line prototype. The current transformer approach of the first prototype would be scaled up using B2 magnets leftover from the Main Ring as the transformer cores. The primary winding would be 500 turns of superconducting strand wire in a shared cryostat with the transmission line.

A second method considered was to scale up the existing current transformer setup, but make a primary winding using superconducting strand at modest current (e.g. 500 turns at 200 Amps). Existing magnet cores (B1's or B2's from the Fermilab Main Ring) would be used as the transformer cores. The advantage of this approach is that the system can remain Dewar-based since no high current (and high Helium consumption) leads are needed. A further advantage is that a small rack-mounted 200 Amp power supply is sufficient to charge the magnet. A disadvantage of the system is that a rapid ramp rate cannot be achieved since the voltage on the primary becomes prohibitive. Quench protection of the multi-turn primary winding is also an issue.

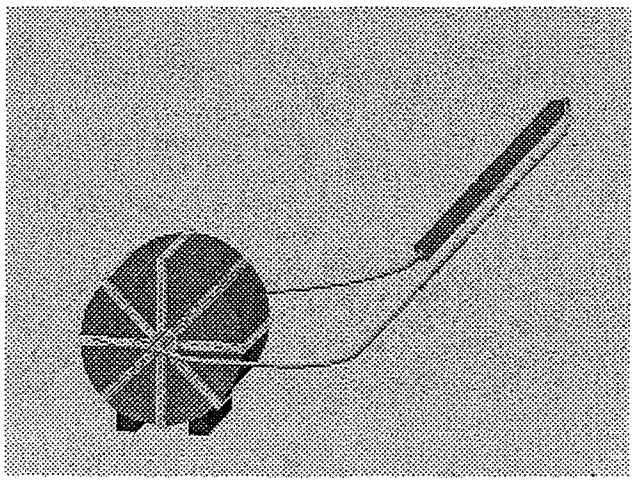

Fig. 25 – Use of a surplus fixed-target analysis toroid magnet as the drive transformer to power the next (50m) prototype magnet. This is a direct scale-up of the technique used in the first prototype. The system will be set up in the MP8 tunnel upstream of the MP9 Permanent Magnet Factory.

The third (favored) method considered was to scale up the existing current transformer setup, with more Ampere-turns on a water-cooled-copper primary and more iron in the transformer core. A breakthrough was made with Jim Volk's suggestion that an existing analysis toroid from a fixed-target experiment could serve as both the transformer core and primary winding for the flux transformer. See Fig. 25. The superconducting transmission line would be looped through the toroid, and the 100kA current would be excited when the toroid was energized. The total magnetic flux (volt-seconds in the transformer core) of an existing (MW9) toroid would be sufficient to power a 50m test magnet. This system will be limited to a ramping time of 10-20 seconds due to the solid iron core of the toroidal transformer.

The cryogenic system for the 50m prototype will benefit from several lessons learned from the first prototype. These include the need for a more mechanically robust conductor, the desirability of designing vessels in diameters below 6" so that piping codes (instead of pressure-vessel codes) apply, and the desirability of forced flow and controlled venting of warm gas during cool-down.

The convective "bubble-pump" approach used in the short transmission line prototype will not work for the 50m magnet. The current plans are to attempt the simplest possible LHe transfer scheme, which is to force-flow single phase liquid from a Dewar into one end of the loop and to discharge 90%gas/10% liquid out the other end of the loop. The transfer rate will be regulated to control the level of liquid in a vertical phase separator column at the end of the loop. There is some possibility that this simple system may become vapor-locked. In this case it will be necessary to install an inline pump to recover and recycle the liquid from the phase separation column, and pump it back into the head of the transmission line. Such a pump will be necessary in any case when we convert the transmission line test to single-phase (supercritical fluid) operation to study the behavior of the conductor at elevated temperatures.

REFERENCES

[1] 'The Pipetron, a Low-Field Approach to a Very Large Hadron Collider' [The Pink Book], selected reports submitted to the Proceedings of the DPF/DPB Summer Study on New Directions in High-Energy Physics (Snowmass '96), compiled by Ernie Malamud (malamud@fnal.gov) Jan 1997. Current project information can be found at http:://www-AP.fnal.gov/PIPE and ../VLHC

[2] G. W. Foster, P. O. Mazur, T. Peterson, C.D. Sylvester, P. Schlabach, "Design and Operation of an Experimental "Double-C" Transmission Line Magnet", presented at PAC '97.

[3] "Magnetic Calculations for the Transmission Line Magnet and Current Transformer Test Setup", G.W. Foster, FNAL Tech. Div. Note #TD-97-014.

[4] G. W. Foster, 'Magnetic Calculations for the Pipetron Transmission Line Magnet', in Ref. 1.

[5] The crenelation technique was described by R.R. Wilson in the 1982 Snowmass proceedings. He describes it as "an old idea". Stan Snowdon evaluated it numerically and wrote a 1983 Fermilab TM on the subject. As far as I can tell it has never been tried experimentally.

[6] A. Makarov, Design notes for the water-cooled copper Double-C magnet test stand. FNAL Tech. Div. Drawing #.

[7] "Magnetic Forces on the Transmission Line Drive Conductor", G.W. Foster (in preparation). Mechanical support and rigidity issues are addressed in M. McAshan's writeup on the 3 TeV Cryosystem.

[8] "A 2-in-1 Lambertson Magnet for VLHC beam Transfers", G.W. Foster Aug 1997.

[9] S. Mishra, "Lattice Design for the 3 TeV Low Field Injector", contribution to the FNAL 1997 VLHC summer study.

[10] G. W. Foster, "Aperture Requirements for the Low Field VLHC and Injector", contribution to the FNAL 1997 VLHC summer study (in preparation).

[11] J. Marriner, "A Damper to Suppress Low Frequency Transverse Instabilities in the VLHC", contribution to the FNAL 1997 VLHC summer study.

[12] TMCI note (in preparation).

[13] Examples of this are the CESR magnets and the (calculated) performance of the FNAL Main Injector and Recycler magnets. The acceptance of these machines is limited by the vertical physical aperture, not the field quality of the iron magnets.

[14] V. Shiltsev, "Pipetron Beam Dynamics with Noise", contribution to the FNAL 1997 VLHC summer study

[15] G. P. Jackson private communication.

[16] "Local Alignment Tolerances in the Transmission Line Magnet", G.W. Foster, contribution to the FNAL 1997 VLHC summer study.

[17] T. Murphy, "Alignment of the 3 TeV VLHC Injector", contribution to the FNAL 1997 VLHC summer study.

[18] "Slow Extraction from the 3 TeV Injector to the VLHC", J.Marriner, contribution to the FNAL 1997 VLHC summer study.

[19] S. Mishra, "Lattice Design for the 50x50 TeV Low Field VLHC.

[20] Zhijing Tang, "ANSYS Calculation of the Eddy Current Field Defects in the VLHC Transmission Line Conductor", presentation to the VLHC low field magnet design group, 1996.

[21] "Local Alignment Tolerances in Transmission Line Magnet Assembly", G. W. Foster, contribution to the FNAL 1997 VLHC summer study.

[22] Invar is a trade name for 36% Nickel steel, available from Carpenter Technologies (formerly Carpenter Steel) and a number of other vendors.

[23] Tom Moreland (a FNAL Beams Division Engineering co-op student) is writing his term report on thermal contraction issues in the drive conductor.

[24] The external leak-checking technique developed by P.O. Mazur of Fermilab involves a disposable rubber seal which makes the clamshell leak-checking possible.

[25] M. Kuchnir, measurements of SC splice resistances in IEEE magnetics last year.

[26] "Eddy Current Power Loss in the VLHC Transmission Line Conductor", Iouri Terechkine Sept. 1997.

[27] M. McAshan, P.O. Mazur, "Cryogenic Systems for the Low Field RLHC Study Cases", in Ref. 1.

[28] M. McAshan, "Cryogenic Systems for the 3 TeV Injector Study".

[29] D. Larbelestier and P. J. Lee, "New Developments in Niobium Titanium Superconductors", proceedings of the 1995 Particle Accelerator Conference (Dallas).

[30] P-West Transfer Lines at FNAL use this bellows arrangement.
[31] Dr. H. Ishimaru of KEK provided us with samples of large grain size aluminized Kapton for these tests.
[32] "Design and Calibration of a Test Facility for MLI Performance Measurements Below 80K", W. Boroski et. al., FNAL, Proc. CEC/ICMC Conf. Huntsville AL. June 1991.
[33] T. Ohmori et. al., "Multilayer Insulation with Aluminized Dimpled Polyester Film" (Solenoid Cryostat for the Venus experiment at KEK) in Proc. 11th Intl. Cryogenic Engr. Conf., Berlin, April 1986. Somewhat better results are reported in R.J. Stochl, et. al. "Variable Density MLI Test Results" , Adv. Cryo. Engr. 41a, Plenum 1996.
[34] K. Koepke, A Zlobin, G.W. Foster, "Power Circuit and Quench Protection for the Pipetron Transmission Line Magnet", in Ref. 1.
[35] There are a set of 65-kA current leads in a test setup at the University of Wisconsin, for example.
[36] Dan Wolff of FNAL performed the SPICE simulations under the direction of Karl Koepke. I have copies of his notes and intend to scan them in and put them on our Web server.
[37] William C. Turner, "Beam Tube Vacuum in Low Field and High Field Very Large Hadron Colliders", in Ref. 1, also LBNL-39482, UC-414.
[38] Currrent pricing for NEG strip in large quantity is between $10-$20/m. W. Chou tells us that the Advanced Photon Source at ANL previously paid $120/m.
[39] Benvenuti et. al, recent CERN preprint.
[40] H. Ishimaru, "Conceptual Design for a Very Low Cost Aluminum Alloy Vacuum Chamber in a High Energy Low-Field Collider", in Ref. 1.
[41] H. Ishimaru, presentation to the VLHC low field magnet working group.
[42] A. Hahn, "Single point beam insrumentation for the 3 TeV Injector", contribution to the FNAL 1997 VLHC summer study.
[43] B. Goodwin, P. Lucas, E. McRory, M. Shea, "Controls and Instrumentation for the 3 TeV Booster to the VLHC", contribution to the FNAL 1997 VLHC summer study.
[44] "Design Parameters for the Next Transmission Line Magnet Prototype" , G. W. Foster (in preparation).

LOCAL ALIGNMENT OF THE TRANSMISSION LINE MAGNET

G.W. Foster
Fermi National Accelerator Laboratory, PO Box 500 Batavia IL 60510
September 28, 1997

Abstract

The transverse alignment strategy of the "Double-C" transmission line magnet over "short" distance scales (between the BPM's) is described.

1 INTRODUCTION

The alignment of transmission line magnets[1] for the VLHC/Injector[2] divides naturally into two distance scales. The *Global* alignment of the machines can be thought of as establishing the Beam Position Monitors (BPM's) at their nominal coordinates. The BPM's occur every ½ cell (~ 65m). The initial global alignment will be accomplished with normal survey techniques, and will eventually be replaced by beam-based alignment using the BPM's themselves during machine commissioning.

The subject of this note is the *Local* alignment of the transmission line magnet. Basically this means ensuring that the magnets are straight (or more precisely follow their nominal curvature) in the span between the BPM's. This is necessary to prevent loss of aperture due to 'kinks' in the magnets.

2 ALIGNMENT TOLERANCES

The R&D target for the straightness of the bore of the transmission line magnet, after alignment in the tunnel, is ±0.5 mm. This is also the alignment goal for the 50m prototype magnet. The meaning of this tolerance is that if the beam is centered perfectly at two successive BPM's, then the available radial aperture will be reduced by at most 0.5mm due to misalignments and kinks in the magnet.

Aperture requirements are discussed in Ref. 3. The nominal physical aperture of the magnets exceeds the beam envelope by 5mm. See Fig 1. The 0.5mm local alignment tolerance means that 10% of the surplus aperture of the 3 TeV injector will be lost from magnet kinks.

The modulation of the beam envelope means that in principle the alignment tolerance could be loosened away from the β-max locations in each cell. Thus the 0.5mm tolerance only needs to be held in the horizontal (vertical) coordinate only within a 10-20m of the BPM at a horizontally (vertically) focussing location. The alignment tolerance could gradually loosen to as much as ±2 mm in the vicinity of the beam waists which occur at the defocusing BPM in each coordinate. See Fig. 1. However, if one allows the magnet to be out of alignment by this amount, then the effects on beam steering (closed orbit distortion) due to off-center propagation in the combined-function magnet will be significant[4]. Thus we do not plan to take advantage of this looser tolerance, and our goal is to hold the tighter 0.5mm tolerance throughout the length of the magnet.

We note that this extra radial aperture may prove useful by permitting beam orbit correction by deliberately decentering the gradient magnet the magnet in the vicinity of the beam waist. This allows correction of closed-orbit errors (via "quad steering" in the gradient magnets) without suffering loss of aperture.

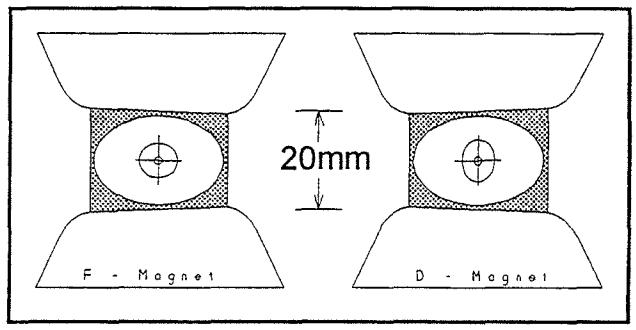

Fig. 1 - Beam Sizes in the 3 TeV Injector (from Ref. 3) -. The 95% beam envelopes for 15π beams (roughly the current FNAL collider emittances) are shown. The large ellipses show the beam envelope at injection energy (150 GeV). The small ellipses show the beam size at flattop (3000 GeV). Beam sizes in the 50 TeV machine are roughly 2x smaller. The left and right pictures indicate the beam envelopes in the in the vicinity of focussing and defocusing half-cell locations. Lattice functions are β min =130m, β max = 200m, Dx = 6m. Beam sizes - 150 GeV: Rmin=3.5mm, Rmax=4.3mm; 3000 GeV: Rmin=0.8mm, Rmax=1.0mm. The magnet gap is 20mm x 30mm (h x v) and the beam pipe aperture is 18mm x 27mm.

3 SURVEY

The first question is, "how do you know where the bore of the magnet is?" This is nontrivial issue for cold bore magnets. For the warm-iron design of the transmission line magnet, the position of the magnet gap at any point along its length can be known within 0.1mm from the position of survey notches on the magnet laminations. The position of the beam pipe extrusion, which will be clamped between the iron pole tips, will be known implicitly to the same precision.

The tunnel is very straight. Therefore there is always a line-of-sight between the BPM fiducials (or survey monuments) at adjacent half-cells. Thus the position of two BPM's and all of the intervening magnet laminations can be surveyed with a single optical setup. It should be possible to know the straightness of the magnet within ±0.25mm over the span between BPM's.

There may be issues in propagating a laser beam or line-of-sight straight to the required accuracy over the 65m half-cell. If necessary, the laser beam could be propagated in a vacuum pipe or helium bag.

4 DISTANCE SCALES

The straightness of the magnet must be addressed on several distance scales. See Figs. 2 and 3.

1) On a length scale <0.3m, the magnets are straight due to the rigidity of the laminated half-cores. The laminated cores are stacked on precise fixtures and contain longitudinal stiffening members (angle iron). A precisely machined aluminum spacer sets the magnet gap and ensures the relative alignment of the top and bottom half-cores.

2) On the length scale 0.3m-6m, the laminated cores are flexible and the magnet is aligned using welded connections to the structural tube that supports the magnet. The connections are made via skip welds every 30cm between the iron half-cores and the support beam (see Fig. 2). The half-cores are fixtured precisely in place as the welds are made, and the weld procedures will be designed to preserve that alignment. At the time that the welds are made, the support beam is in its relaxed state and is supported by alignment feet on the factory floor. The support beam is preloaded to pre-compensate for the sag (~2mm) of the magnet in the 6m between supports.

3) On distance scales 6m-75m, the structural tube is flexible and the magnet is aligned by adjusting the individual alignment feet. The process in 2) above guarantees a magnet that is straight when the magnet is supported with the feet in the nominal position on the factory floor. When the coordinates of the adjusters are reestablished in the tunnel, the magnet will again be straight.

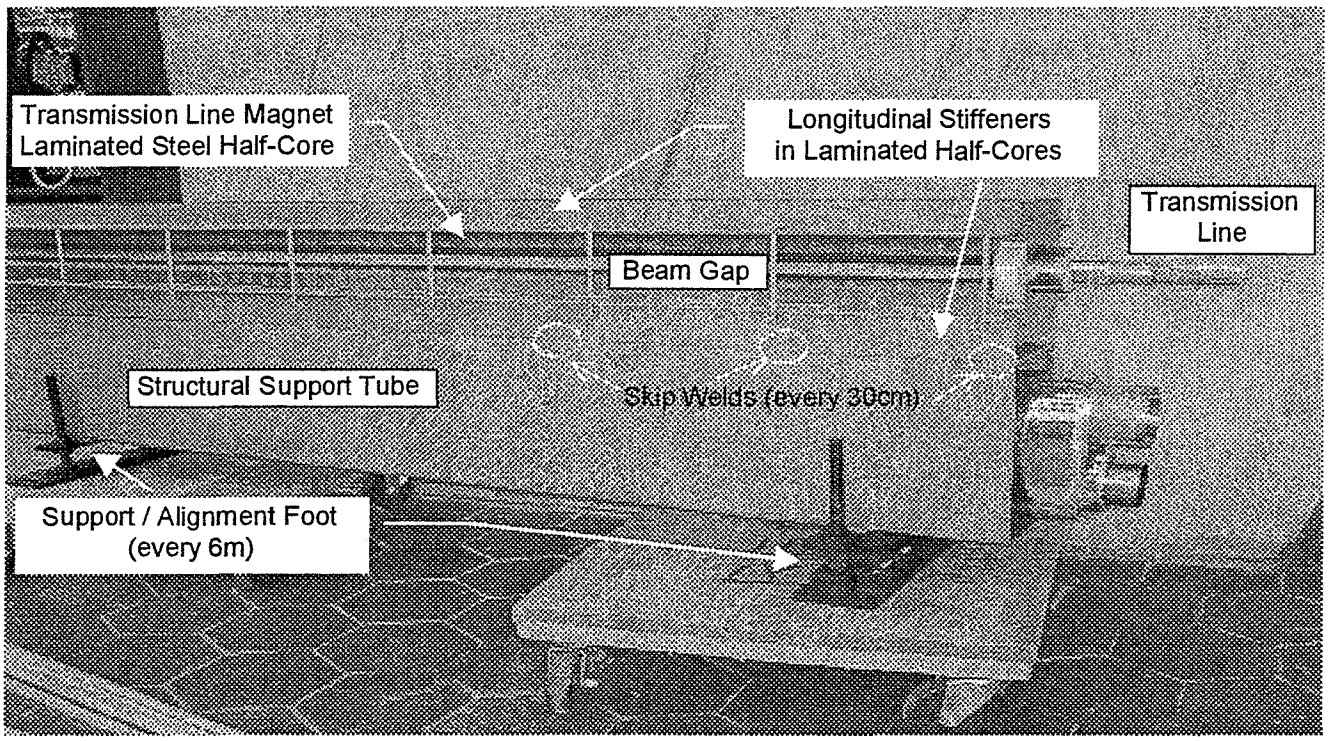

Fig. 2 – Components relevant to the alignment of the transmisssion line magnet.

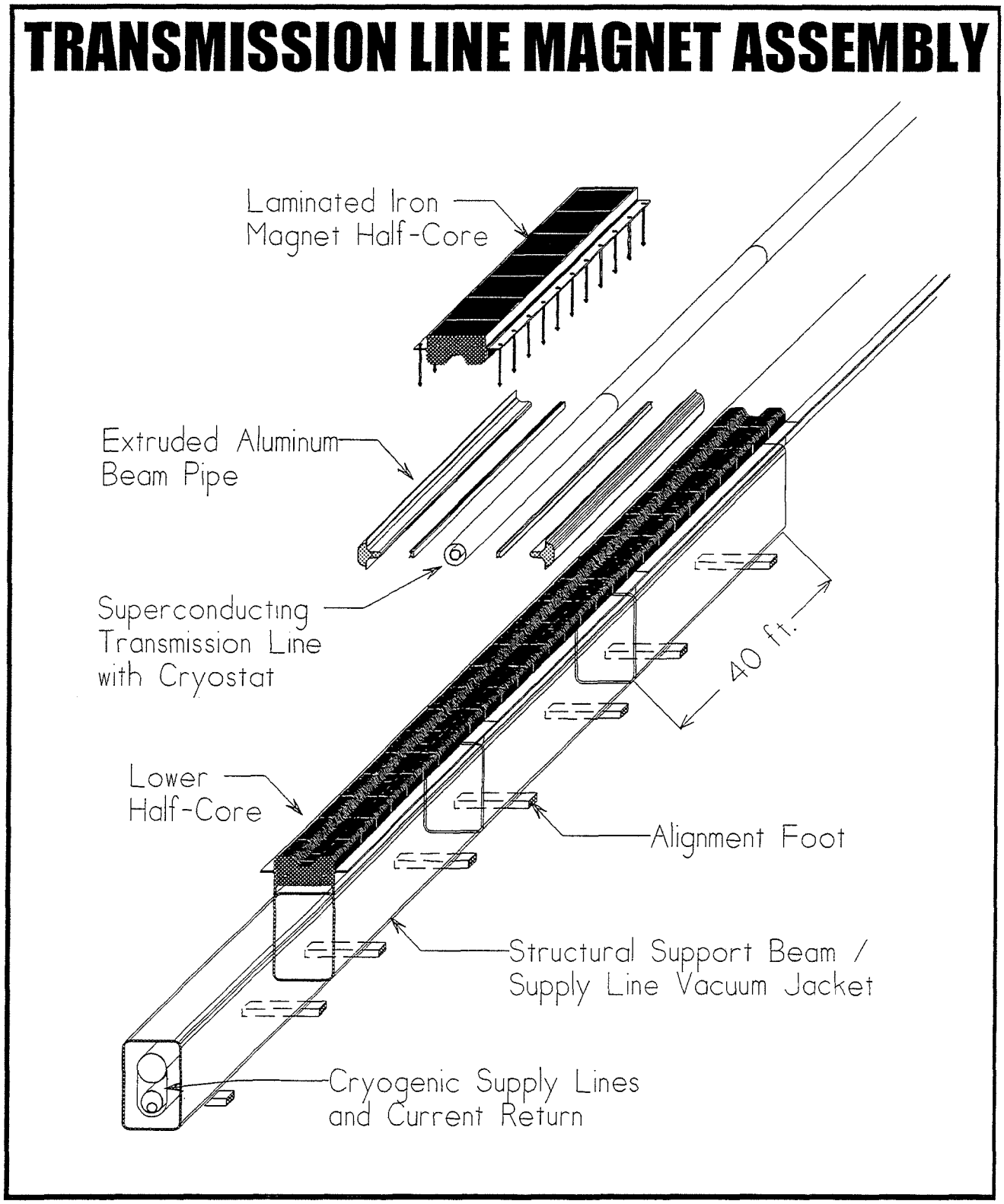

Fig. 3 - Assembly sequence for the transmission line magnet.

5 ALIGNMENT DECAY

Once established, the local alignment will decay over time due to motion of the tunnel floor. As before, the time dependent misalignment of the magnets can be decomposed into a component which is coherent over the half-cell (this drives closed-orbit distortions) and a part ("magnet kinks") which cause aperture reduction.

In bedrock tunnels such as the SPS [5] the RMS quad displacements grew at about 0.02mm per year horizontally and by 0.05mm/year vertically. One can (hopefully pessimistically) assume that all of this RMS is incoherent and will result in magnet kinks. Thus one can expect worst-case (5σ) kinks in the magnets which are equal to the initial ± 0.5mm assembly tolerance after about 2 years of operation. Whether or not this results in any aperture loss depends on where in the cell the kink occurs as discussed in section 2. In any case this sets the time scale for how often the magnets need be resurveyed (1-2 years) and how often one expects to remove a kink in a magnet anywhere in the ring to preserve the physical aperture (2-5 years). Magnet moves to preserve or correct the closed-orbit distortions will be more frequent occurrences.

6 AUTOMATION OF ALIGNMENT

In the 3 TeV injector there are 10 alignment fixtures in each half-cell, and a total of 5000 adjusters (15,000 alignment bolts) in the entire machine. Whenever a BPM is re-centered on the beam, in principle all 20 alignment fixtures on either side of the BPM should be realigned. This is a simple, repetitive procedure that cries out for an automated solution. This might take the form of an "alignment robot" which contains a conventional laser tracker and a motorized socket wrench for adjusting the magnet stands. Similar survey robots are already in use commercially for microtunneling of curved underground pipelines [6].

An advantage of this "robot" (actually a remotely operated servomechanism) is that beam-based alignment could take place by moving magnets in beam-on conditions. Survey and realignment and of the machine could take place on a continuing basis without need for dedicated downtime. The alignment robot might also find other uses, e.g. it could carry a PIN beam loss monitor to accurately localize beam losses.

7 STEPPING MOTORS

An alternative which is lower-tech but more flexible is to provide individual stepping motor controls on each magnet adjuster. If a cost of $200/motor ($600/adjuster) could be attained, the 5,000 adjusters for the 3 TeV machine would cost $3M. Considered as beam-steering correctors, these would have considerable excess strength and overlapping capabilities. Thus a sizeable fraction of the adjusters could be broken without affecting the ability to establish an acceptable closed orbit. The stepping motor approach does not eliminate the need for a survey robot since it is still necessary to know where to move the magnets.

REFERENCES

[1] "Status Report on the Transmission Line Magnet", G. W. Foster, contribution to the the FNAL 1997 VLHC summer study.

[2] "The Pipetron, a Low-Field Approach to a Very Large Hadron Collider' [The Pink Book], selected reports submitted to the Proceedings of the DPF/DPB Summer Study on New Directions in High-Energy Physics (Snowmass '96), compiled by Ernie Malamud (malamud@fnal.gov) Jan 1997. Current project information can be found at http:://www-AP.fnal.gov/VLHC

[3] "Aperture Requirements for the Low Field VLHC and Injector", G. W. Foster, contribution to the FNAL 1997 VLHC summer study.

[4] "Pipetron Beam Dynamics with Noise", V. Shiltsev, contribution to the FNAL 1997 VLHC summer study.

[5] "Alignment Issues for the 3 TeV Ring", C.T. Murphy, contribution to the FNAL 1997 VLHC summer study.

[6] DYWIDAG (a large German tunneling concern) advertises robot theodelites for tunneling applications. Iseki Inc. in Japan uses remote-control survey devices with alignment lasers to microtunnel around corners.

PERMANENT MAGNETS FOR THE TRANSFER LINES FROM THE MAIN INJECTOR TO THE 3 TeV VLHC INJECTOR

G.W. Foster
Fermi National Accelerator Laboratory, PO Box 500 Batavia IL 60510
September 28, 1997

Abstract

The parameters and preliminary designs for permanent magnet dipoles and quadrupoles suitable for use in the 150 GeV transfer lines from the Main Injector to the 3 TeV injector to the VLHC are described. The designs are based on the permanent magnets for the 8 GeV line and Recycler. The magnets use strontium ferrite permanent magnet material and temperature compensation alloy in the magnetic circuit. This is a companion to the note [1] by Bieniosek et. al. who describe the optics and geometry of the of the transport lines.

1 INTRODUCTION

The 150 GeV transfer lines from the Main Injector to the 3 TeV VLHC injector are essentially straight FODO channels 3km long. The beams are transported down at a 4% grade through the transfer line enclosures into the 3 TeV tunnel locate 450' underground. It is proposed to use permanent magnets based on the technology developed for the 8 GeV Line/Recycler for beam transport.

At either end of the line a 40mr (20 Tesla-m) vertical deflection is required. It is likely that additional horizontal bends will be required to match details of the final footprints of the tunnel. It is proposed to accomplish most of these bends with 0.6 Tesla permanent magnet dipoles. The remainder of the bends will be accomplished with vertically deflecting electromagnets (to pitch the beam downwards coming out of the Main Injector) and by the vertical kick from the injection Lambertson (in the 3 TeV tunnel).

The transfer line enclosure will also be used to transport the transmission line magnets railway-style down from the surface assembly building into the tunnel. An option under consideration is that most of one of the transport lines could be shared with the NUMI tunnel. More details are given in Ref. 1.

2 WHY PERMANENT MAGNETS?

The advantages of permanent magnets are that they avoid the cost and complexity of power supplies, power cabling, safety interlocks, LCW distribution piping, valves, and interconnections. Their main disadvantages are that the transfer line can be run over a smaller range of beam energy than a line built with electromagnets, and that certain types of beam line tuning experiments (e.g. tests of quad steering) are not possible. Since there seems to be no advantage to running the transport line at any energy different than the 150 GeV nominal top energy of the Main Injector, permanent magnets seem appropriate.

3 MAGNET APERTURE

The optical design for the transfer line adopts the *ansatz* that the 3 TeV ring and 150 GeV transfer lines have identical optics, i.e. 60-degree cells and a β-max of 200m. Thus the beam size in the transport line is identical to the circulating beam size at injection in the 3 TeV ring. Aperture requirements should in principle be identical. However we chose the minimum aperture of transport line magnets to be somewhat larger (2.5cm x 3cm vs. 2x2cm for the 3 TeV arc magnets). This seems reasonable in view of the fact that the beam transport enclosure passes through a variety of ground conditions on its way down to the bedrock of the 3 TeV machine.

A larger beam pipe than this may be desired for vacuum conductance reasons. We discuss designs below for 3½" beam pipe, 1¾" beam pipe, and 1" beam pipe.

As a side comment, it may be desirable to have explicit collimators to limit the beam size that might accidentally be introduced into the 3 TeV Injector and 150 GeV transfer line. This may be necessary since the aperture for circulating beam at flat top in the Main Injector is in excess of 1000π. Attractive places to scrape the beams are as they pass through the Main Injector abort (MI-40 line) and near the NUMI target station (MI60/NuMI line). This would ensure that no non-transportable beam halo (or badly mis-extracted beam) could be transmitted into the 3 TeV machine or transfer line.

4 QUADUPOLE PARAMETERS

The 60-degree cells for the 150 GeV transfer lines have a quad spacing of ~50m and require an integrated quad strength of 10 Tesla. Three design options were considered:

1) A stretched version of the 8 GeV/Recycler quadrupole[2] 3.5m in length and weighing about 1200lbs. This design permits a 3½" beam pipe to pass through.

2) By scaling down the previous design by a factor of two in all dimensions, the same integrated gradient is obtained and the magnet weights 1/8 as much. This permits a 1¾" beam pipe.
3) A "minimum aperture" design (Fig. 1) which barely exceeds the minimum aperture requirements discussed above. This design permits a 1" round beam pipe to pass through, or a larger elliptical pipe.

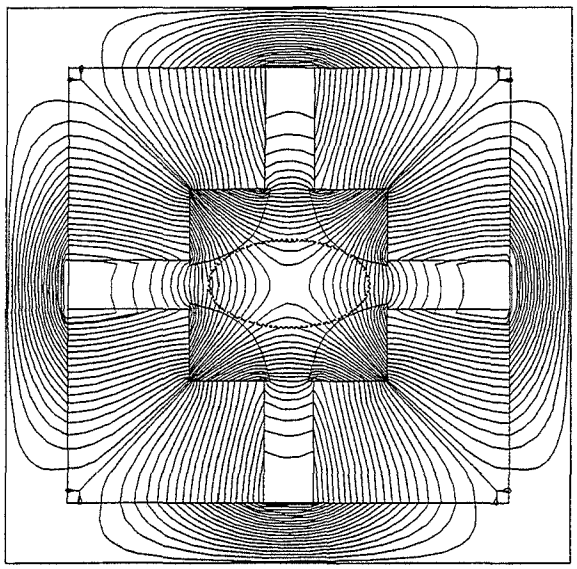

Fig. 1 – POISSON field map of the "Minimum Aperture" quadrupole design. Overall dimensions are 4.6" x 4.6" x 24" and the weight is approximately 90 lbs.

The three quadrupole design options are summarized in Table 1. At present I favor the intermediate option labeled "½ Scale Recycler". A fourth, attractive option which has not been developed is to scale down all dimensions of the Recycler design except the thickness of the ferrite brick (which would remain 1"). This would result in a magnet ~1.5m long which would fit around a 2" beam pipe.

	Stretched Recycler	½ Scale Recycler	Minimum Aperture
Beam Pipe Diameter	3.5"	1.75"	1"
Gradient	3 T/m	6 T/m	20 T/m
Magnetic Length	3.3m	1.7m	0.5m
Length Overall	140"	70"	24"
Height, Width	8"	4."	4.6"
Weight	1200 lbs.	150 lbs.	90 lbs.

Table 1 - Mechanical parameters for different quadrupole designs discussed in the text.

5 DIPOLE PARAMETERS

Bend dipoles with smaller apertures and somewhat stronger bend fields are straightforward extensions of the "Double-Double Dipole" permanent magnet design of the 8 GeV line[2]. In order to concentrate the flux from a larger volume of ferrite, the aspect ratio of the pole tip must be increased (see fig. 2). In principle this approach can be extended to obtain dipole fields >0.6T. However, it becomes very inefficient and subjects the ferrite near the magnet gap to large demagnetizing forces.

An option has been chosen in the dipole design is to place the temperature compensator alloy in the magnet gap, on either side of the beam pipe. This results in a more compact and efficient design but results in multipole defects that depend (weakly) on the operating temperature [3]. This is acceptable for a transfer line.

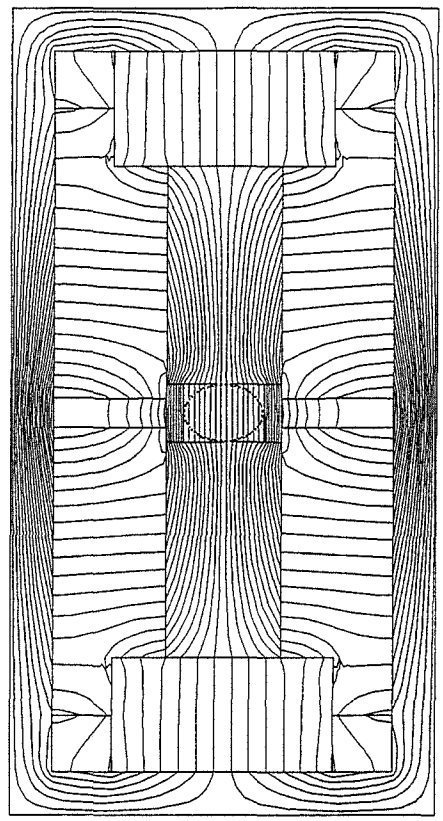

Fig. 2 – POISSON field map of the permanent magnet dipole for the 150 GeV transfer line to the 3 TeV injector.

Bend Field	0.6 Tesla
Magnet Gap	1" x 1.5"
Elliptical Beam Pipe	1.5" x 1"
Temperature Compensator	In Magnet Gap
Overall Dimensions	7.5" x 13.5"
Length	Up to 4m

Table 2 - Permanent Magnet Dipole parameters.

6 ROUGH COST ESTIMATE

The permanent magnets are very similar in design and production quantity to those for the Recycler and 8 GeV Line. Sixty-four Recycler quadrupoles were built at a cost about $3k each (dominated by labor cost). The two permanent magnet transfer lines require a total of 120 quads of comparable design, so a reasonable guess at their cost might be $360k. The dipole design is comparable to the "double-double" dipole design for the 8 GeV line, which cost $11k (dominated by M&S). Roughly 20 of these are required for both transfer lines, so that the total cost of permanent magnets for the line should be in the vicinity of $600k.

REFERENCES

[1] "Beam Transfer Lines for a VLHC", F. Bieniosek, N. Gelfand, D. E. Johnson, A. D. Russell, M.J. Yang, contribution to FNAL 1997 VLHC summer study.

[2] The 8 GeV line permanent magnets are described in the Fermilab Main Injector Technical Design Handbook.

[3] H. Glass, presentation on the temperature dependence of field multipoles in the Double-Double Dipole to the Main Injector Magnet Physics (MIMP) group, 1995.

VLHC Injector 150 GeV Transfer Line
Permanent Magnet Quad
(Minimum Aperture Design)

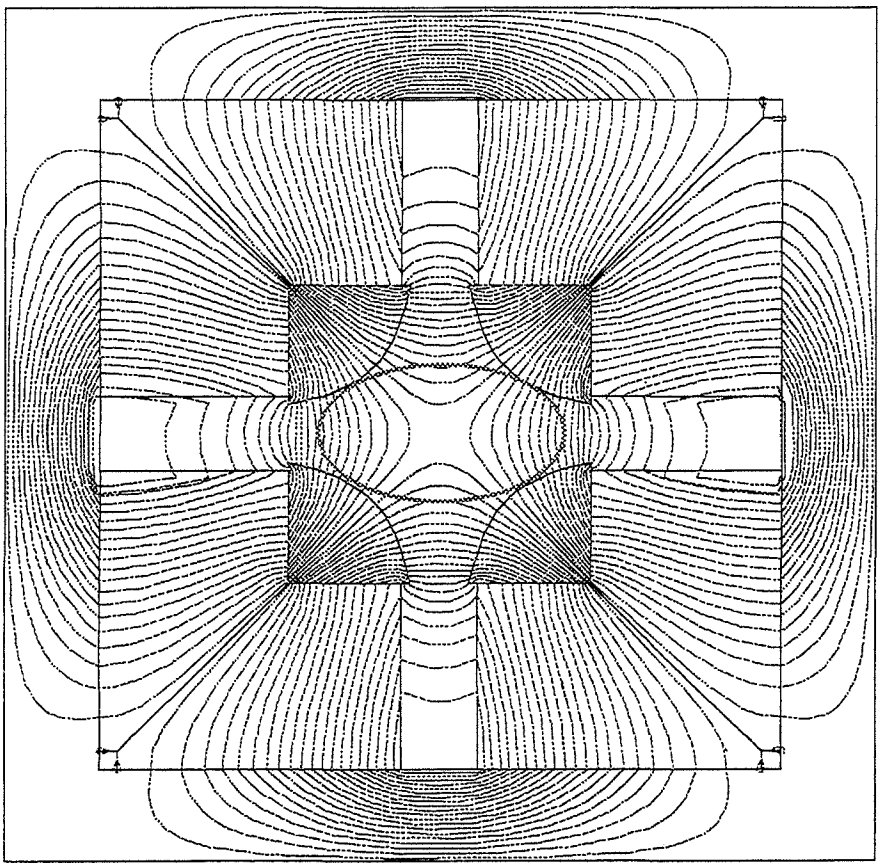

Gradient: 20 Tesla/m

Magnetic Length: 0.5m

Pole Tip Diameter: 1”

Elliptical Beam Pipe: ~ 1.3” x 0.9”

Overall Dimensions 4.6” x 4.6” x 24”

VLHC Injector Transfer Line
Permanent Magnet Dipole

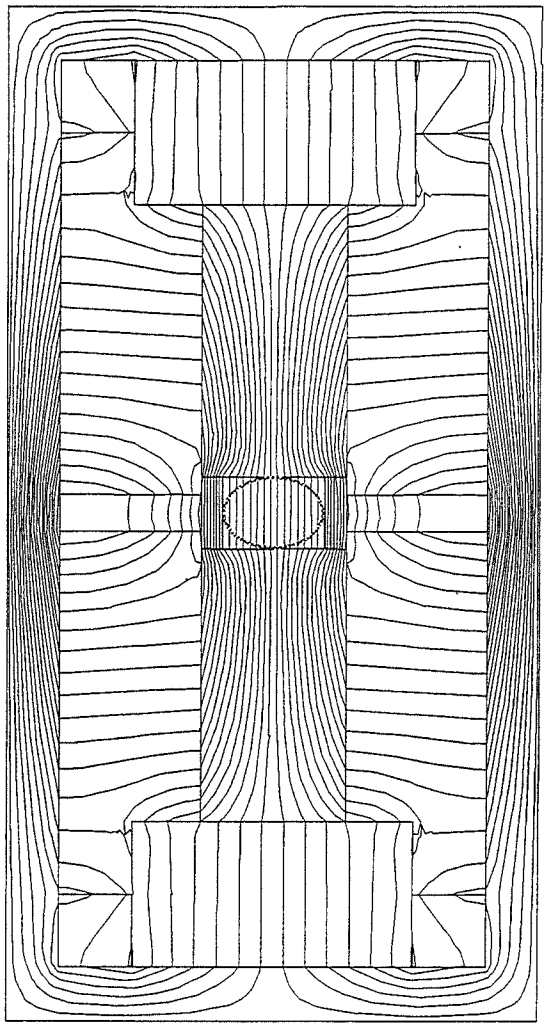

Bend Field: 0.6 Tesla
Magnet Gap: 1" x 1.5"
Elliptical Beam Pipe: 1.5" x 1"
Temperature Compensator in Gap
Overall Dimensions 7.5" x 13.5"
Length: up to 4m

DESIGN AND OPERATION OF AN EXPERIMENTAL "DOUBLE-C" TRANSMISSION LINE MAGNET

G.W. Foster, P.O. Mazur, T. Peterson, C.D. Sylvester, P. Schlabach,
Fermi National Accelerator Laboratory, PO Box 500 Batavia IL 60510

Abstract

The "Double-C" transmission line magnet is a warm-iron warm-bore single turn 2-in-1 superferric magnet designed to provide a significant reduction in magnet costs for future hadron colliders. Construction and first operational tests of a prototype magnet system are described.

1 INTRODUCTION

The transmission line magnet development program[1] has the goal of demonstrating a magnet with construction and operating costs (per Tesla-meter) which are an order of magnitude below current (cosine theta) superconducting magnets.

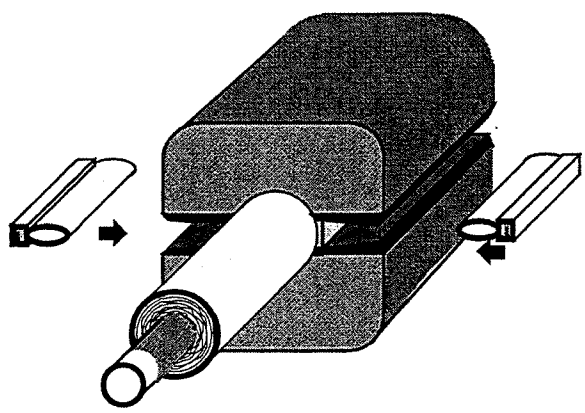

1.1 Transmission Line Magnet Design

Fig. 1 - The Transmission Line Magnet is a single-turn warm iron superferric magnet built around a superconducting 75kA DC transmisssion line.

A "Double-C" magnet yoke placed around the transmission line provides twin gaps with opposite bend fields for two counter-rotating proton beams. Alternating gradients of the iron pole tips eliminate quadrupoles and most costs associated with magnet ends. The current is returned in a cryogen distribution line located nearby.

Other design features include:

- Crenelated iron pole tips[2] which maintain acceptable field quality up to ~2 Tesla in an alternating-gradient design.
- An peak operating field at the conductor of ~0.8T. This translates to a very high current density and/or a high allowable operating temperature. Superconductor costs (for today's NbTi conductors operated at 7K) are in the range of $1M/TeV.
- A very simple and low heat leak cryogenic structure[3] from the transmission-line geometry. This translates into low cryogenic operating costs.
- A small cold mass (0.7kG/m or ~7 tonnes/TeV).
- An absence of large cold-to-warm magnetic forces due to the symmetry of the "Double-C" design.
- An Invar cryogenic pipe for the center conductor which eliminates bellows for thermal shrinkage.
- An inexpensive warm-bore vacuum system [4,5] using extruded aluminum and NEG pumping.
- Low Magnetic Stored Energy (60MJ/TeV). This translates into small power supplies for ramping and a simple quench protection system [6].

2 PROTOTYPE SYSTEM

In the last year a proof-of-principle 50kA Transmission Line Magnet system was constructed. To avoid the cost and complexities of high current leads, a current transformer approach with a floating superconducting secondary loop was used. The "Double-C" iron structure was mounted on the 5m long secondary loop which served as both the experimental transmission line and the curent return.

2.1 Current Transformer

The current transformer yoke was the iron structure from an accelerator magnet. The primary windings were the 24 turn x 2.5kA water-cooled copper windings of that magnet. The copper windings were driven by a 15V 2.5kA conventional SCR power supply.

Under ideal conditions a single turn shorted secondary should develop 24 x 2.5kA = 60 kA according to the turns ratio of the current transformer. Nearly ideal coupling can be expected as long as the iron yoke of the transformer does not saturate. The current at which the yoke saturates depends on the inductance of the load plus the stray inductance of the secondary loop. Calculations of the expected electrical and magnetic behavior of the prototype are detailed in [7].

2.2 *Superconducting Secondary*

The superconducting secondary consisted of 7 turns of surplus SSC dipole inner coil cable, and was located in a loop cryostat 5m long which serves as the prototype transmission line. The SSC Cable was looped through the cryostat 7 times and then spliced to itself by soldering over a length of ~40cm. This approach reduced the effective resistance of the joint by a factor of seven, since the current only passes through the splice every 7th time around the loop. An L/R decay time of order 10 hours is expected for the current in the superconducting secondary.

The superconductor was supported inside the 2.5cm diameter helium cryopipe at ~10cm intervals by UHMW form-fitting spacers which were clamshelled around the conductor and tied in place by twisted steel wire. Less than 10% of the cross sectional area was available for helium flow.

The superconducting line is supported in symmetric positions and accurately centered in both the transmission line magnet and drive transformer to avoid large magnetic forces. The drive transformer has a pair of copper primary coils which are placed on either side of the superconducting secondary to maintain the symmetry. In the "Double-C" magnet the conductor experiences nominally zero force but a decentering "negative spring constant" of approximately 100 kgf per mm of displacement per meter of transmission line. In the drive transformer the decentering force is about half of this.

2.3 *Cryogenic System*

The system consisted of a loop cryostat cooled by a convective "bubble pump" from a 30" high x 12" diam. LHe filled Dewar at one end. Liquid Helium enters the loop from the lower end of the Dewar, is heated (and perhaps vaporized) by the heat leak along the length of the transmission line loop. Bubbles travel upward in the U-turn region at the far end of the loop, and 2-phase flow is forced back out the top (return) half of the loop and back into the Dewar. The flow is convective and needs no special pumps, etc. for a system of this size.

The loop cryostat consists of a 2.5cm diameter Helium-filled stainless cryopipe with a 180-degree bend at the far end (5m from the Dewar). The 180-degree bend used a rigid U-tube 60cm in diameter. The cryopipe was enclosed in a vacuum jacket consisting of 2.5" stainless pipe and a 4" diameter flexible stainless bellows hose in the region of the U-turn. The cryopipe was superinsulated and supported from the vacuum jacket by G-10 "spiders". The spacing of the supports was ~30cm along the length of the cryopipe and ~15cm in the region underneath the test magnet where conductor forces are greatest.

Helum was provided to the system from a 500L Dewar. Liquid level in the experimental Dewar was monitored by a superconducting liquid level probe which was also used to control the automatic transfer system.

2.4 *Instrumentation*

Temperature measurements were made 3 places along the loop cryostat and two places inside the Dewar using. Pressure in the Dewar was logged and there were 4 voltage taps on the 7-turn winding for quench detection and studies.

Current in the secondary was monitored with a Hall probe fixtured ~10cm away from a clear section of the drive conductor. A secondary Hall probe was used to monitor the field in the gap of the test magnet as well as various stray fields which were monitored for safety reasons.

Rapidly changing data (currents, voltages, pressures) were logged with a Sony DAT data logger. Slowly changing data (temperatures and fill levels, etc.) were logged using a computerized slow-scan system from Fermilab's Magnet Test Facility.

3 PRELIMINARY TEST RESULTS

The initial running of the prototype took place a few days prior to this conference (PAC97).

3.1 *Cool Down of Loop Cryostat*

Cooldown began by initiating a transfer of liquid helium into the dewar at room temperature. A liquid level was quickly established and regulated ~60cm above the bottom line of the loop cryostat (i.e. near the level of the return line of the loop). Cooldown of the loop was initially very slow. After 3½ hours the far end of the loop cyostat was still at room temperature as the "cold wave" propagated slowly down the lower half of the loop. Shortly after this the cold wave reached the far end of the loop, travelling at ~2m/hr. as it passed the temperature transducers at the turnaround. The cooldown of the top (return) half of the cryoloop was much faster, taking only ~1/2 hour for the entire 5m return leg to reach 4.3K.

The system operated very stably after initial cooldown had been achieved. Recovery following quenches was also rapid (<2 mins), indicating that the convective flow, once established, has significant excess capacity to keep the system cool.

3.2 *Electrical and Magnetic Measurements*

The magnet was cooled down with the power supply off, so that nominally zero flux was trapped in the superconducting loop. The primary was then energized to various DC current levels and the currents and magnetic fields were observed. At low excitation (10kA of secondary current) the expected 24:1 current transformer ratio was observed. The transfer function between transmission line curent and B-field in the gap of the Transmission Line Magnet structure was measured to be 25kA/Tesla and agreed with calculations. Stray fields

were recorded for ES&H reasons and agreed with estimates based on 2-d calculations.

In the initial running of the prototype the iron size of the coupling transformer yoke limited the circulating current in the secondary to 25kA. This behavior was calculated in advance, and served the useful side purpose of limiting the maximum energy which could be transferred to the cryogenic system until preliminary tests were completed. A larger transformer yoke is under construction which should allow us to reach the full 50kA/2T design goal in the next run.

3.3 Quench Behavior

At full current in the prototype, the SSC Cable used for the conductor is being run at a small fraction (~20%) of the nominal short-sample current carrying limit at 4.3K and 1 Tesla. However, there were (and are) concerns due to the fact that the conductor is very loosely clamped in the transmission line cryopipe, which could make the device prone to quenches induced by mechanical motion of the drive conductor. Thus the quench behavior is interesting even at the half-current tests run to date.

A conservative calculation [8] indicated a final conductor temperature following a quench of less than 300K, and hence no protection was necessary. Nonetheless quench detection and protection circuitry was included in the prototype to permit quench studies and protect against unforseen circumstances.

Two 60cm long stainless heater strips were embedded between cables of the superconducting loop and connected to Tevatron Quench Heater Firing Units to allow manual initiation of quenches. The heater units had 2/3 of the capacitance removed to limit the energy delivered to the heater tapes. In practice it was not possible to induce a quench by firing the heater tapes with the secondary current at 10kA or below. At ½ current (25kA) firing the heater tapes induced a quench which blew off only ~ 3 liters of LHe. No spontaneous quenches have been observed.

4 SUMMARY AND FUTURE PLANS

The first goal of the next run is operation of the system at the full 50kA design current. This requires a larger transformer yoke which is currently under fabrication. If still higher current is to be achieved, a polarity reversing switch on the copper primary would allow a 4 Tesla swing of the iron in the transformer yoke and a doubling of the load inductance which can be driven. The ultimate current limit of the existing setup is ~60kA given by the ideal turns ratio of the coils.

The full-current quench behavior and decay time will be studied, as well as any effects from decentering conductor forces in the Double-C magnet iron.

The present Double-C magnet iron test structure does not have contoured pole tips and hence no precision magnetic field quality measurements are planned. An interesting measurement which can be made is the ramp rate dependence of the sextupole arising from eddy currents in the solid-iron Double-C magnet yoke. This measurement is important since we anticipate substantial cost savings from using solid extruded/cold drawn steel yokes instead of laminations for the full scale machine.

A potential follow-on use of the test setup will be to evaluate persistent-current switches to extend the range of the transformer coupling technique to longer (higher inductance) prototypes. If feasible, this technique could allow dewar-based operation of prototype magnets with lengths up to ~100m.

5 ACKNOWLEDGEMENTS

The authors thank the Fermilab Technical Divison (especially B. Bianchi, J. Garvey, J. Sim, D. Sorensen, and D. Validis) and the staff of the Magnet Test Facility for their support during this project. Thanks also to M. May, D. Snee, and J. Volk of the FNAL Beams Division for fabrication Double-C magnet structure and the coupling transformer. Alvin Tollestrup is thanked for useful discussions in the initial stages of this project.

REFERENCES

[1] 'The Pipetron, a Low-Field Approach to a Very Large Hadron Collider', selected reports submitted to the Proceedings of the DPF/DPB Summer Study on New Directions in High-Energy Physics (Snowmass '96), compiled by Ernie Malamud (malamud@fnal.gov) Jan 1997. Current project information can be found at http:://www-AP.fnal.gov/PIPE and ../VLHC

[2] G.W.Foster, 'Magnetic Calculations for the Pipetron Transmission Line Magnet', in Ref. 1. The crenelation technique was described by R.R. Wilson in Snowmass 1982 and evaluated numerically by S. Snowdon in a 1983 Fermilab TM.

[3] M. McAshan, P.O.Mazur, "Cryogenic Systems for the Low Field RLHC Study Cases", in Ref. 1.

[4] H. Ishimaru, "Conceptual Design for a Very Low Cost Aluminum Alloy Vacuum Chamber in a High Energy Low-Field Collider", in Ref. 1.

[5] William C. Turner, "Beam Tube Vacuum in Low Field and High Field Very Large Hadron Colliders", in Ref. 1, also LBNL-39482, UC-414.

[6] K. Koepke, A Zlobin, G.W. Foster, "Power Circuit and Quench Protection for the Pipetron Transmission Line Magnet", in Ref. 1.

[7] G.W. Foster "Magnetic Calculations for the Transmission Line Magnet and Current Transformer Test Setup", FNAL Tech. Div. Note #TD-97-014

[8] A. Zlobin, contribution to FNAL Tech. Div. Electrical Safety Review documentation for transmission line magnet protoype system.

Cryogenic Systems for the 3 TeV Injector Study

M. McAshan
Fermi National Accelerator Laboratory, Batavia, IL 60510
December 18, 1997

I. CHOICE OF CONDUCTOR OPERATING TEMPERATURE

At the 1996 Snowmass workshop [10] several alternative cryogenic system arrangements were identified for different versions of the transmission-line magnet. For a NbTi conductor a system providing a conductor temperature between 4.5 and 5 K was suggested, and for NbSn the temperature range was 4.5 - 6.5 K. The first of these is of the SSC type with a transmission line flow of subcooled helium in series passing through recooler heat exchangers where heat is exchanged with boiling saturated helium at 4.5 K. In the second of these systems the transmission line is cooled by supercritical helium streams which are connected in parallel. There is no boiling helium in this second system. Instead heat is transported by the sensible heat of the supercritical stream, but operating just outside the critical region and expanding the stream as it passes through the transmission line produces a large effective heat capacity. Thus the temperature of the stream rises only 1.5 K while taking up heat of 28 J/g. The heat capacity of boiling helium in the saturated system is infinite and the temperature rise zero, but the latent heat is only 18 J/g.

The supercritical system requires lower flow rates for a given heat removal and tolerates larger pressure drops than the saturated system. In addition it is simpler, requiring no recoolers. The price that is paid for these advantages is a higher conductor operating temperature. Thus the trade-off is between current density in the superconductor and cost of cryogenics. In a high field magnet of small cross-section, high current density is an extremely important cost driver because the number of ampere-turns needed for a given central field increases as the current density decreases, and because the size of the coil drives the size of the whole magnet. In general, this trade-off in systems such as the Tevatron, SSC and LHC favors lower temperature and higher current density. In the Low-field transmission line magnet, however, all of the current density in magnet is equally effective in driving the magnet gaps, and the conductor current density does not drive the size of the magnet. The size of the conductor is instead dominated by the amount of copper needed to give adequate quench protection and the space needed for helium flow. The trade-off in this case, therefore, is strictly between the cost of the cryogenics and the cost of the additional NbTi in the conductor. This is a very different cost equation and it gives a different answer.

To make this concrete it is useful to use recent cost information from IGC. For 80,000 A at 4.2 K, this vendor suggests 23 strands each 1.30 mm in diameter with CuSc ratio 1.35:1. For this strand they quote $0.5844 per foot. It is not clear how much margin is included in this recommendation. Ignoring any included margin and assuming that we would like a critical current at 100,000 A, and taking a linear relationship of critical current with temperature, $I_c = I_o(1 - T/8.8)$, costs for conductor at various temperatures can be determined and are shown in Table I.

Table I
Magnet Transmission Line SC Cost and Quench Characteristics

For 100,000 A conductor, I_c = 6654 A for strand

Temp.	# strands	Cost per m	T for quench at 70,000 A
4.2 K	29	$63.95	5.60 K
5.0 K	35	$77.18	6.15 K
6.0 K	47	$103.64	6.83 K

A factor of 1.15 has been applied to these costs to provide for cable lay.

This suggests that the SC cost difference between a transmission line designed for 6 K and one for 5K is less that $30 per meter or $9000 for a 300 m unit. With the line sizing given in Table I, 40 g/s of flow can be used for heat transfer in the transmission line. With a temperature rise of 4.5-5 K, the sensible heat is about 2 J/g, making the recooler capacity 80 W. With the heat load budget shown in Table IV, 0.26 W/m, one recooler would be required for every 300 m transmission line unit. The cost of this recooler with its J-T valve, level regulation, and instrumentation is surely greater than $9000. The costs developed for these objects for the SSC was considerably greater than this. Of course the heat load budgeted may be greater than that eventually achieved, and the operating tempera-

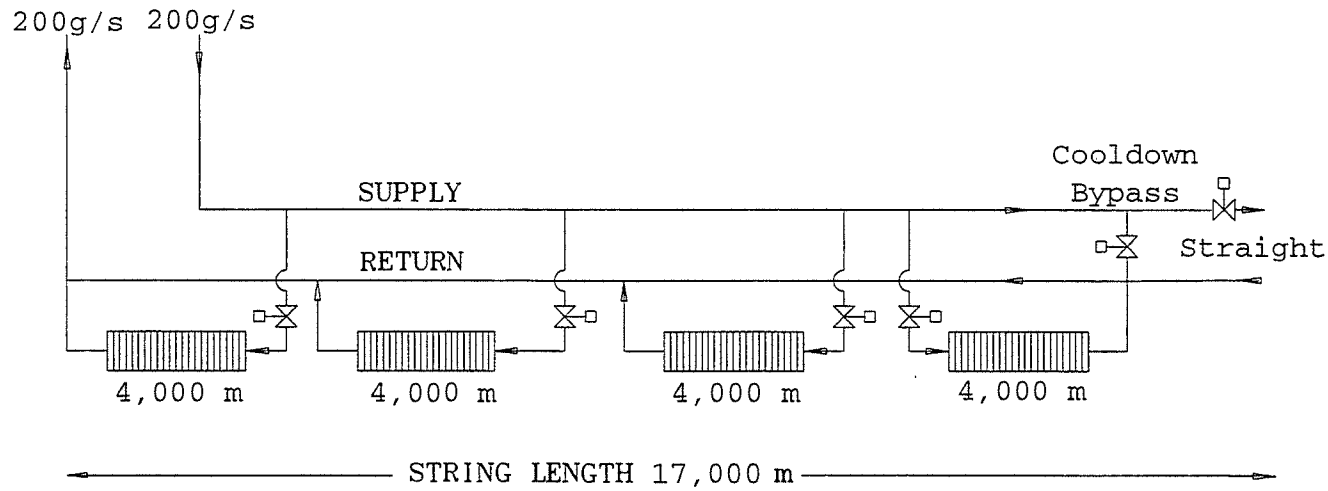

Figure I Layout of a String

ture range could be increased, but whether or not it can be argued that the cost for this major simplification of the cryogenic system is actually negative, it is certainly modest and definitely worth it.

This argument only extends the discussion at Snowmass. It is clear that the low-field magnet option to be viable must have a low cost per meter. At the same time, the accelerator will be large. This puts a major pressure on for simplification of all of the accelerator systems. This argues for increased pressures and increased temperatures of operation allowing increased temperature and pressure gradients, increased unit sizes, decreased line sizes and reduced instrumentation requirements.. The supercritical system will be cheaper to construct and more robust in its operation than the saturated system, and although attention will be paid in the course of system design studies to the issues raised by the increased operating temperature, the choice now is to adopt the supercritical system as first choice for the 3 TeV Injector. This system will be described in the following sections.

II CRYOGENIC SYSTEM LAYOUT AND OPERATION

For the 3 TeV Injector which is proposed with the modest circumference, at least on an RLHC scale, of 34,000 m, the minimum number of 1 refrigeration station is required. The choice of the number of stations is the balance between the cost of the stations, which have many economies of scale, and the costs of dealing with longer strings. These include the costs of larger piping, cost of underground real estate and installation, the logistics of underground work, the larger heat load and cryogen inventory associated with a unit length of the larger piping, and string voltage and quench protection issues. This is not just an economic calculation, because the costs of surface stations are likely to be political as well as economic. The work at Snowmass showed that piping and electrical string length do not begin to present problems at 20,000 m. In addition, the total refrigeration plant capacity required for the 3 TeV machine is within the current experience. In this case, therefore, the choice is a simple one, and the system can be laid out in two strings connected to a single service station containing both refrigeration plant, power supply, and dump. Table II presents some of parameters of the system.

Table II
System Parameters

Circumference	m	34,000	Number of Sections/String		4
Number of Refrigeration Stations		1	Straight Length	m	1,000
Number of Strings		2	Section Length	m	4,000
Number of Straights		2	Cell length	m	300

The layout of each string is likewise simple. The string consists of a cryogenic pipeline containing supply and return headers. In the current picture of the 3 TeV system, the vacuum jacket of this

pipeline doubles as a support member for the magnet. The magnet transmission line is connected in four parallel passes between the supply and the return, and the flow of supercritical helium through each pass is controlled by a valve and flowmeter. The general arrangement is illustrated in Figure I.

Also shown connected in parallel with the four sections of the magnet transmission line is a fifth circuit for one of the two long straights that are part of the layout. This can, of course, go anywhere along the string. Further, it is assumed that the cryogenic pipeline carries across the straight, so that the arrangement can be adapted to suit the final arrangement of all of the components.

Table III
String Heat Load

Load by Type	Number/String	Supply Line W/unit	Supply Line W	Magnet Line W/unit	Magnet Line W	Return Line W/unit	Return Line W
MLI	17,000 m			0.08	1,360	0.32	5,440
Gas Cond.	17,000 m	.002	34	Inc in MLI		Inc in MLI	
Support	17,000 m	.002	34	0.18	3,060	0.10	1,700
Connections	60	1.2	72	5	300	22	1,320
Vac Barrier		2x0.1		2x1		2x6	
Splice		1		1		0	
Connection				2		10	
Control Devices	10			8	80		
Refr. Connection Piping			100		0		400
Total Load per String W			240		4,800		8,860
Total Load for Two Strings W			480		9,600		17,720

A heat load breakdown for one of these strings is given in Table III. This is intended to represent a heat load that can be achieved with straightforward design at low risk. This is thus a high point with which to begin optimization. It is desirable to have a cryogenic system that will operate feasibly at this load so that costs and benefits associated with optimization can be assigned values. The basis on which this load was developed will be discussed below. For the moment consider the total refrigeration requirement in each category and compare it to the process that is outlined in Table IV.

Table IV
Refrigeration and Ideal Power: 400 g/s Total Flow

Point or Load	P bar	T K	h J/g	exergy J/g	Load W	Eff. W/W	Ideal Powr MW	%
Refr. Supply State	4.5	4.548	12.47	1045				
Delivery & Cont. ΔP	3.25	4.633	12.47	1107			.0248	1.85
Supply Line Load					812	61	.0496	3.70
Mag. Line inlet	3.25	5.000	14.5	1231				
Magnet Line					9,600	61	.5816	43.4
Mag. Line Outlet	1.90	5.891	38.5	2685				
Return Line Load								
Refr. Return State	1.3	13.60	84.5	4393	18,400	37	.6832	51.0
Total					28,812		1.339	100

The supply stream from the refrigeration plant is 400 g/s at 4.5 bar and 4.55 K. This is divided between the two strings, flowing in the supply line. At 4000 m intervals along this line flows of 45 g/s are drawn off through flow control valves and pass into the magnet transmission line. This is illustrated in Figure I. An initial estimate of the line ΔP is 0.4 bar, half of which appears in the first 4000 m, but this calculation is complicated by the bus carried in this line. Table IV shows that a pressure drop of 1.25 bar has been budgeted for the flow in the supply line plus the drop in the control valve. This is adequate to cover the requirements plus a contingency, and as is indicated in the last column of the Table, the ideal power associated with this pressure drop is less than 2% of the total.

About an average of 2 J/g (800 W) is budgeted for the heat load of the supply line system and again there is a contingency. This goes into the fluid unevenly, the maximum rise being 3 J/g at the end of the string. Few-percent flow adjustments in the magnet transmission line compensates for this.

In the magnet transmission line, pressure drop is made a virtue since expansion keeps the temperature down. The flow enters at a nominal 3.25 bar and 5 K and exits at 1.9 bar and 5.9 K. The enthalpy increases by 24 J/g, and the density of falls by a factor of 6 along the stream. Computer calculations of the pressure and temperature along the transmission line show that the flow state remains single-phase and keeps well away from the critical everywhere. Calculations also show that the heat transfer coefficients [8] between the conductor and the helium are large enough everywhere that the temperature differences within the transmission line are negligible compared with the end-to-end temperature rise.

This scheme works well over a fairly large range of flow rates. For turn-down of a factor of two, if this is required, a back-pressure valve about 2/5 of the way along the line will have to be added. Calculations so far show that the largest dynamic load in this system is the loss due to conductor splices, and this does not present a significant control problem.

At the exit of the magnet transmission line sections, the flow is collected in the return line. The arrangement shown in Figure I gives a minimum of 65 g/s and a maximum of 155 g/s. This minimizes pressure drop while providing enough flow everywhere to pick up the heat load. The pressure drop has been estimated to be 0.45 bar and 0.6 bar has been budgeted in Table IV. The heat load of this line and shield raises the enthalpy of the flow by an average of 46 J/g. The flow returns to the refrigeration plant at 1.3 bar and 13.6 K.

In addition to the steady operating mode just described, the cryogenic system must be capable of transient modes of operation to accomplish system cool-down, warm-up, and quench recovery. String cool-down in this system is straightforward: After readiness testing, the cooldown process is established by passing helium at 5 bar down the supply line and back through the return line to the refrigeration plant at 1.3 bar. This is a pressure-controlled process, and about 25 g/s will flow when the system is warm All of the section control valves and the bypass valve at the end of the string are open, so there is flow established in all of the circuits. The system has a volume of about 200 cu-m and holds 200 kg of helium. The circulation replaces this inventory every 2-1/2 hours, and purification will be complete in less than a day. After cleanup, the flow from the refrigeration plant is cooled to about 20 K, and cooldown begins. As the cooling wave reaches the outlet of each section of the transmission line, the control valve for that section is closed to keep the cooling wave moving . As the system cools down, the flow rate will increase. The cold mass of the whole system is about 170,000 kg with a heat content of 24 GJ. the first wave cooldown will be complete after 16,500 kg of helium has circulated. This is estimated to take about 4 days. In the third day, therefore, the inlet temperature to the string will be slowly lowered to the operating temperature and the refrigeration process will be supplemented with helium from storage. An important point is reached when the return temperature to the refrigeration plant approaches the 13.6 K operating point. When the flow rate into the string reaches 200 g/s, the pressure will be reduced to the 4.5 bar nominal operating pressure. The operating inventory of the string is about 18,500 kg, and at 200 g/s unbalanced flow, filling will take about 1 day. We can estimate, therefore that something like 2-1/2 days will be required to complete the second wave of cooldown. Adding a day to condition the string to the right temperature profiles, the cooldown will require 7-8 days. This is about the same time that is required by the Tevatron system.

Warming up is the reverse process to cool-down. The first step in warm-up is storage of the inventory. This is done by adjusting the refrigeration plant to supply to the string a flow of 25 g/s at 4.5 bar and 13.6 K, and at the same time expanding the 200 g/s at 4.5 K into the storage tank. This is the same volume flow as the 200 g/s at 4.5 K, and so the inventory comes out of the string at the 200 g/s rate and is re-liquefied by the refrigerator into storage. After the inventory is recovered, the string is warmed up by circulation of gas. Because of the variation of heat capacity of solids with temperature, warm-up waves spread out in a system, and the warm-up process is not as efficient as the cooldown. It is reasonable to assume that a warm-up will take something like two weeks.

The last transient process to be considered here is quench recovery. Quench in the transmission-line magnet is a non-event from the cryogenic point of view because almost all of the magnet stored energy is dumped in the dump resistors. The quench propagation velocity in the conductor is adjusted to be just large enough to provide resistance growth for quench detection. Thus all there is to quench recovery is getting some warm helium out of the transmission line section. The rate at which this can be done is determined by the transit time of the helium through the 4000 m path. This is about

two hours. The warm gas in the return line goes directly to the refrigeration plant without disturbing neighboring sections and the refrigeration process has no difficulty in dealing with the small amount of heat involved.

III MAGNET TRANSMISSION LINE DESIGN ISSUES

From a cryogenic point of view, the most important system component is the magnet transmission line. In the system that proposed here the transmission line heat load determines the helium flow required and thus sets the sizes of all of the piping in the system. It has been mentioned above that the heat loads for the cryogenic lines in Table III are suggested as starting points for development. We will here present arguments for these numbers.

The space provided in the magnet iron for the transmission line cryostat is 3 inches diameter, and the superconducting bus has a cross-sectional area of about 3.5 sq-cm. This insulated bus is enclosed in a cryogen-carrying pipe 1.5 inches outside with a wall 0.049 inches, and the inside clear diameter for helium flow is 1.125 inches diameter

The conductor inside the magnet is at a point of unstable equilibrium in the vertical direction, and feels a force gradient of about C = 2 MN/sq-m or 290 lb. per inch of conductor per inch of displacement from the center of the magnet iron. If the cold pipe is supported at intervals by spiders, the field gradient gives rise to an instability in which the current-carrying pipe bends into a sinuous curve with a period twice the support distance. Surprisingly, this problem is one that can be solved exactly. The elastic curve of the pipe is actually a sinusoid, and the unstable support interval, L_o, is given by the root of the first equation when the frequency of the transverse sinusoidal motion of the pipe is zero:

$$-\varepsilon \cdot \omega^2 = C - T \cdot \left(\frac{\pi}{L}\right)^2 - E \cdot J \cdot \left(\frac{\pi}{L}\right)^4 = 0$$

$$L_0 \cong \pi \cdot \left(\frac{EJ}{C}\right)^{1/4} \left(1 + \frac{T}{2\sqrt{CEJ}} + \frac{1}{2}\left(\frac{T}{2\sqrt{CEJ}}\right)^2\right)^{1/2} \quad for \frac{T}{2\sqrt{CEJ}} << 1$$

An approximate solution is given in the second equation. Here T is the tension, E is the modulus of elasticity and J is the moment of area of the section of the pipe.

Some of the mechanical parameters of the conductor and pipe are given in Table V. Here the spring constant of the support spiders has been chosen to be a factor of 4 greater than the value at which the pipe is unstable at the support point. This is C·L = 1MN/m. The conductor will not be exactly on the magnetic center of the iron, so there will be an off-center force. This misalignment has been chosen to be at a maximum 0.5 mm, and the force is given in the table. The maximum force that will be felt at the supports is the sum of the off-center force and force due to the weight of the pipe and conductor. This total is about 700 N.

Note that the frequency of the support loaded by the pipe mass is lower than the pipe frequency. Thus the compliance of the support is mass-like rather than stiffness-like at this frequency, and it is certainly necessary to carefully review what is meant by a stiff support. The simple model presented here will have to have some correction terms.

Table V
Magnet Transmission Line Mechanical Parameters

Vacuum Jacket	SS 3 inch od x 0.083 wall	Magnetic Spring Constant, C	$2 MN/m^2$
Inner line	Invar, 1.5 inch od x 0.049 wall	Support stiffness, SC = n·C·L	4 MN/m
Support Interval, L	0.50 m	Max. center misalignment, d	0.5 mm
Max Support Interval, L_o	0.67 m	Max.Off-center force, n·C·L·d/(n-1)	667 N
Conductor area	3.5 sq-cm	Mass of pipe + conductor, ε	4 kg/m
Weight of conductor	2.84 kg/m	Lowest pipe freq., ω/2π	318 Hz
Support stiffness factor, n	4	Vert. support freq., $((n-1)\cdot C/\varepsilon)^{1/2}/2\pi$	195 Hz

To get a feeling for the scope of the support problem, neglect bending and elastic failure, and consider the limiting case of pure tension or compression. The heat flow, Q, can be is related to the stress, σ, and l, the length of the thermal and mechanical path in the simple way shown below.

$$Q = \lambda \cdot \frac{F}{\sigma \cdot l} \quad and \quad SC = \frac{F \cdot E}{\sigma \cdot l} \quad \Rightarrow \quad Q = \lambda \cdot \frac{SC}{E}$$

In these equations λ is the thermal conductivity integral of the support material at 300 K. Clearly, the spring constant varies inversely with the allowed stress and the length, and there are two possible limits to the Q that can be achieved. One is represented in the last equation with the required spring constant, and the second in the first equation with the limiting stress. Thus there is a heat vs allowed stress trade-off for heat loads above the minimum set by what is required to achieve the needed spring constant.

At this point it is useful to look at some properties of real materials, and a likely candidates are fiber reinforced composites. There is a great deal of experience with these materials in the support of cryogenic tankage, in spacecraft, and other similar applications. There is a good understanding of how to design and manufacture these materials and what their fatigue properties are [3,4]. In the application under discussion here fatigue is important , since the 3 TeV injector will cycle on the order of 10^7 times in a 20-year lifetime. Table VI shows some properties of two of these materials [3] and the heat loads that are predicted from them. For both materials the properties are those of uniaxial straps in tension. Small diameter glass-epoxy tubular struts in compression have a somewhat higher cyclic compressive stress limit and carbon somewhat lower.

Table VI
Support Materials

	S-Glass Epoxy	Low-Modulus (LM) Carbon Epoxy
Young's Modulus, E	60 GPa	140 GPa
Thermal Conductivity Integral, λ	150 W/m	550 W/m
Limiting Stress for 10^7 Cycles, σ	0.2 GPa	1 GPa
$Q = \lambda \cdot SC(required)/E$	20 mW/m	31 mW/m
$Q = \lambda \cdot F/\sigma \cdot l$ ($l = 0.025$ m)	21 mW/m	31 mW/m

It is remarkable that both the stress limited and the stiffness limited heat leaks of both of these materials coincide at the scale of .025 m support length.

A design program for this support must deal with many requirements besides the few fundamental ones considered above. Care must be taken with the way that the loads are transmitted through the support: the way that the magnetic load on the conductor is transmitted to the pipe; from the pipe to the support; from the support to the vacuum jacket; and from the vacuum jacket to the magnet iron. All of these things are important in achieving the needed stiffness. In addition to the magnetic forces the support system must resist assembly and transportation forces and forces due to thermal contraction of the inner pipe during cooldown and warmup, and it must be manufacturable and reasonably cheap (there are 70,000 in the system). The heat leak that is budgeted in Table III, 180 mW/m, is a reasonable place to begin this design process. This provides adequate room for optimization in the heat leak-stress-stiffness space with a good prospect of getting a fully satisfactory result.

Although the support heat load is the most critical in the magnet transmission line, the thermal radiation heat load must also be controlled by the use of multi-layer insulation (MLI). There is little to add on this topic to the discussion at Snowmass. A dimpled mylar MLI system has been used in a number of large systems and is commercially available [1]. It is reported as performing at the level of 0.3 W/sq-m for 40 layers in a 1 cm thickness. This would produce a radiation heat load of 0.06 W/m in the transmission line. In addition, a variable-density MLI system with fiberglass paper spacers has demonstrated an average heat flux of 0.21 W/sq-m in testing on a hydrogen calorimeter with a 310 K warm boundary [2]. There are about 54 layers in this package which is 57 mm thick. The behavior of both of these package is almost that of ideal floating shields. This demonstrates that a reasonably sim-

ple understanding of the functioning of these MLI packages is adequate to predict their performance. The radial space available in the transmission line is 17 mm, so the limit as to what can be achieved in the line is something like 0.2 W/sq-m; but the insulation package is interrupted by the supports, providing paths for radiation leakage. Because of this 0.08 W/m has been budgeted for radiation heat load. It is likely that in order to achieve this the supports will have to be integrated with the MIL package at a few levels by means of aluminized mylar cuffs. Again in this case cost optimization will determine the final form that the insulation package will take.

In the discussion so far it has been ignored that it is only in one plane that the conductor feels the decentering gradient. The gradient in the other plane produces centering forces, and the support system can be designed to take advantage of this. However, if this is done means will have to be found to orient the support inside the vacuum jacket and the vacuum jacket within the iron. This is not impossible, clearly. There can be ears or pins in the wall of the outer pipe that engage both the support spiders and the iron. But this has implications for manufacturability, assembly and maintenance as well as performance and cost of the system, and consideration of the cost-benefit optimization of a non-round transmission line system must come after the issues of the round design are more fully understood.

To finish up the discussion of the magnet transmission line, some ideas concerning construction should be mentioned. In the current picture, the accelerator is constructed in 300 m lengths, transported into the tunnel and installed. The 300 m sections of the cryogenic lines are terminated with vacuum barriers and permanently evacuated. This vacuum is maintained during operation by adsorbent and getter packages distributed in the vacuum space. Assembly in the tunnel involves what is termed in the cryogenics business a field joint. The conductor is spliced by soft soldering on a copper mandrel. This also serves to anchor the conductor longitudinally, and longitudinal forces on the inner line are transmitted through the vacuum barrier to the outer jacket. The inner line is connected by welding in place a sliding sleeve. MLI is then installed and a second sleeve is welded to make up the vacuum insulation. This leaves a small volume of vacuum insulation to be roughed out and checked and pumped by sorption material in a frangible capsule. The vacuum barrier in this picture is a piece of stainless steel pipe about 2 inches in diameter with 0.035 inch wall 16 inches long. This has a heat leak of 1 watt that appears in the budget of Table III.

Table VII
Line Sizing and Inventory

Length	OD	Wall	Inlet State			Outlet State			Flow	Wght	Invntory
			T	P	Flow	T	P	Flow	Area		LHe
m	in	in	K	bar	g/s	K	bar	g/s	sq-cm	kg/m	cu-m
Magnet transmission line: In 4 parallel 4,000 m flow paths plus straight per string. 34,000 m total length											
4,000	1.5	0.049	5.000	3.25	45.0	5.891	1.90	45.0	6.41	3.99	21.8
Supply line: In 2 strings. Line is 2-1/2 Sch 5 SS pipe carrying conductor. 34,000 m total length											
17,000	2.875	0.083	4.548	4.5	200.0	5.000	4.00	**	33.6	6.13	114.2
Return line: In 2 strings. Line is 3-1/2 Sch 5 SS pipe. 34,000 m total length											
17,000	4.000	0.083	5.891	1.90	**	13.6	1.30	155.0	74.5	4.61	16.9
Total Inventory											152.9
Times 1.2											183.4
											About 50,000 gal.

IV CRYOGENIC SUPPLY AND RETURN PIPING

Here there are two thermally isolated pipelines in a single vacuum jacket. The supply line contains the transmission line return bus and carries the supply flow of cryogen from the refrigeration station. The return line carries the return flow of cryogen back to the refrigeration station. In contact with this pipe is a thermal shield surrounding the supply line. Thus almost all of the heat leak into the pair of lines is taken as sensible heat in the flow of the return line.

These lines will fit into a 12 inch vacuum jacket, so the circumference of the cold boundary is somewhat less than 1 meter. If the same dimpled insulation system is used here, one could expect a radiative heat load of about 0.32 W/m. There is more room for the supports in this cryostat than in the magnet transmission line, and although the weight to be supported is greater, the magnetic forces are smaller. The support problem is therefore much less complicated. The load estimate in Table III is based on having S-glass epoxy support posts for the return line, 7/16 inch in diameter and 4 inches long, a pair every three meters. This provides more than adequate support and scope for optimization. The supply line is supported from the return line by stainless steel straps, 0.02 inches thick, 0.5 inches wide and 3 inches long, a pair every two meters. These straps are pictured as being hinged at top and bottom with pins so that some longitudinal motion is allowed. This is necessary to provide for thermal motions of the lines during cooldown or warmup of the system. Table VII gives the sizes and weights of the cryogenic lines and the helium inventory of the system.

V. REFRIGERATION PLANT

The refrigeration requirements for the 3 TeV machine are given in Table IV. The system operates with a flow of 400 g/s of helium supplied at 4.5 bar and 4.55 K and returning at 1.3 bar and 13.6 K. The total refrigeration load is 28.812 kW and the refrigeration ideal power is 1.339 MW. This ideal power is equivalent to 20.4 kW at 4.5 K, and so the overall capacity is close to the plants that were planned for the SSC and close also the plants to be used for the LHC [5]. There is a further similarity to the LHC in that part of the load is absorbed by sensible heat. In LHC the cold compressor load and part of the load in the beam screen circuit are taken at temperatures above the saturated level. Such a "cold compressor cycle" operates at Thomas Jefferson Laboratory and there has been considerable recent study of this kind of process in the context of TESLA [6] and APT. Thus the refrigeration plant required here lies along the main path of development of large-scale helium refrigeration today, and the both process design and plant engineering issues will be widely familiar ones as a plant for the 3 TeV machine is planned and procured.

To get an idea of what a plant suitable for FNAL might look like, the process for a satellite refrigerator for the 3 TeV application has been investigated [7]. This is a large version of the satellite refrigerator familiar Fermilab with two engines rather than one at the low temperature end to cover the refrigeration required up to the 13.6 K temperature. In order to supply 400 g/ s of flow under the conditions mentioned above, this process requires 103 g/s of liquefier flow at 3 bar and an enthalpy of 14 J/g. This is typical of the Fermilab CHL which will produce approximately 200 g/s of flow with these conditions from the upgraded cold box. The satellite heat exchanger requires 1.03 kg/s of flow at 19 bar and returns the 1.13 kg/s at 1 bar. The engines have inlet temperatures of 15.03 K and 9.82 K and produce work of 11.8 and 4.9 kW respectively at an efficiency of 0.7. Taking a compressor efficiency of 0.5 for the satellite flow, and proportioning the compressor and nitrogen plant power requirement of the CHL, the total power requirement of the process is 6.7 MW for an overall efficiency of 20% of Carnot.

This exercise is not to be taken seriously as a design, but it does provide a set of parameters for a plant that although not optimized, is entirely realizable and provides for all of the operating modes required for the 3 TeV machine. The goal in continuing this work is the development of concepts and simple cost models for a stand-alone and for a satellite plant. These concepts need to include such site-specific requirements as tunnel depth and location relative to the currently installed Fermilab cryogenic plant and utilities.

VI. CONCLUSION

The cryogenic system outlined here is meant to be both an investigation of feasibility and a starting point from which to develop an optimized conceptual design. Of course, optimization proceeds throughout the design of any of the systems of the 3 TeV machine. However, we are not yet to square one in this process. The basic ideas of the Pipetron need enough development to form a beginning that is complete and self-consistent at the most basic technical level. To move in this direction three undertakings present themselves. These are briefly described below:

1) There is a complete enough set of requirements to begin a preliminary design of the magnet transmission line. The goal here is to produce a first-order consistent design together with a complete mechanical analysis and a thermal model. Follow-on to this work is development of a cost model for the transmission line and the design of some appropriate verification and demonstration testing.

2) The supply and return pipeline is simpler in its mechanical requirements that the transmission line. In this case MLI performance is very important, and it is very desirable to develop an appropriate system. The most promising candidate is the dimpled mylar system that has been previously investigated here at FNAL. We should procure supplies and undertake calorimeter testing to confirm previous results and develop competence to handle the system. Then it would be reasonable to build a return pipeline prototype for a demonstration heat leak test. This MLI would also be used in the transmission line.

3) As mentioned above, steady-state calculations of the thermodynamic state of the helium coolant in the transmission line have been carried out. This work should be extended to a dynamic simulation of the thermo-hydraulics of the line. This is needed for two reasons: the first is to support the design of a control system for the helium flow. It is important to confirm that a temperature measurement every 1000 m, which is the system currently contemplated, is sufficient to permit efficient control of the cryogenics under conditions of ramping and other transient operations. The second need is for the further understanding of the stability margin of the conductor and the development of a quench. The Pipetron conductor is to operate in a regime of cooling that is different from that investigated before [9] and unfamiliar in accelerator magnets. This is not discussed above, and it is worth mentioning the issues here.

The Pipetron concept employs a conductor cooled by an internal flow, but one that is to be protected by active detection of a quench and switched ramp-down of the magnet system. This certainly seems to be the most appropriate and economical system that can be employed. The conductor has been designed estimating quench velocity and resistance growth in the adiabatic limit [11], but there is a large amount of helium heat capacity per unit length. The magnetic stored energy is 66 J/g in the helium, and if this is absorbed at constant volume, the final state is at about 28 K (and 9 MPa). The steady state heat transfer in the conductor produces only a small reduction in the adiabatic quench velocity [12], but the heat transfer is large enough so that the flow of the helium accelerates very rapidly after a quench. The heat transfer increases on time scales smaller than that required to produce a detectable quench voltage, and will certainly affect the resistance growth time. This is the same situation that produces stability in cable-in-conduit conductors with static or slowly-flowing helium, but the heat transfer coefficients are clearly larger in that case.

Thus further work is needed to get the design basis of the Pipetron conductor into satisfactory shape. Some quantitative understanding of the minimum quench energy and margin, minimum propagating zone sizes, quench growth resistance, and so on is absolutely needed in order to support a conductor testing program; and if history is a guide, complete control of these issues will be needed to get to a fully finished design.

VII. REFERENCES

[1] T. Ohmori, et. al., "Multilayer Insulation with Aluminized Dimpled Polyester Film", *Proceedings of the Eleventh International Cryogenic Engineering Conference*, Berlin, April 1986, editor Prof. G.Klipping and Dr. I. Klipping, pages 567-571. Butterworth and Co., Guildford, Surrey GU2 5BH, UK.

[2] R. J. Stochl, et. al., "Variable Density MLI Test Results", *Advances in Cryogneic Engineering*, **Vol. 41a**, Plenum Press, Inc. New York (1996) pages 101-107

[3] R. P. Reed and M. Golda "Cryogenic Composite Supports: A Review of Strap and Strut Properties", Cryogenics, **Vol. 37** (1997) pp 233-250

[4] V. L. Morris, "Engineered Composite Structures for Cryogenic Systems", *Advances in Cryogneic Engineering*, **Vol. 39b**, Plenum Press, Inc. New York (1994) pages 2021-2030

[5] B. Chromec et. al., "A Highly Efficient Helium Refrigerator for the LEP 200 Project at CERN", in *Supercollider 5*, Plenum Press, New York (1994)

[6] M. Kauschke, C. Haberstroh, and H. Quack, "Safe and Efficient Operation of Mulitstage Cold Compressor Systems", *Advances in Cryogneic Engineering*, **Vol. 41a**, Plenum Press, Inc. New York (1996) pages 921 - 926

[7] M. McAshan, Technical Note (unnumbered) 7/97

[8] P. Giarratano, V. Arp, and R. Smith, "Forced Convection Heat Transfer to Supercritical Helium", *Cryogenics*, **October, 1971**, pages 385 - 393

[9] L. Dresner, "Stability of Internally Cooled Superconductors: A Review", *Cryogenics*, **October, 1980**, pages 558 - 563

[10] M. McAshan and P. O. Mazur, "Cryogenic Systems for the Low-Field RLHC Study Cases" in *Proceedings of the DPF/DPB Summer Study on New Directions for High Energy Physics (Snowmass '96)*

[11] K. Koepke, A. Zlobin, and W. Foster, "Power Circuit and Quench Protection for the Pipetron Magnet Transmission Line" in *Proceedings of the DPF/DPB Summer Study on New Directions for High Energy Physics (Snowmass '96)*

[12] M. Wilson, *Superconducting Magnets*, Oxford University Press, New York, 1983

EXAMINATION OF THE PROPOSED VLHC VACUUM SYSTEM

Terry Anderson
BD/MS

During the Summer Studies period the "current thinking" for the Very Large Hadron Collider's (VLHC) vacuum system was reviewed. The basis for the "current thinking" was the papers by H. Ishimaru and W.C. Turner submitted to the Proceedings of the DPF/DPB Summer Study on New Directions for High-Energy Physics, Snowmass '96 and information obtained directly from Bill Foster, Mike May, and H. Ishimaru. The goal of this investigation was to identify areas where an R&D effort should be initiated, identify problems in the "current thinking", and comment on the validity of the current cost estimate. The following is a list of my questions, concerns, and recommendations.

1) How much will the channel between the elliptical chamber and the side pump channel collapse? Using the current chamber design section this can easily be determined using finite element analysis or by direct measurement.

2) If there are no bellows:
   a) What affect will thermal expansion and no bellows have on alignment?
      1) Beam pipe movement could cause alignment issues with the magnets.
      2) The lack of bellows will make it necessary to have very small incremental movement between magnets during alignment.
   b) Thermal expansion due to NEG conditioning could be significant.
   c) Full penetration welds will be needed to ensure structural integrity.

3) The use of dichloro-propane:
   a) Potential for chlorine to attack stainless steel components.
   b) Pump down will need to be discharged to outside or containment.

4) If internal pumping mechanism (NEG Strips) needs repair how do we do this?

5) Roughing the system down.

Vacuum System parameters:

Gas is Air at 20 C
Camber Surface Area / meter = 3040 cm^2/m
Chamber Volume / m = 3002 cm^3/m = 3 l/m
Outgassing rate prior to degass = $6.3(10)^{-9}$ Torr-l/cm^2-s
Conductance / cm^{-1} = $1.8(10)^3$ l-cm/s
Pump Speed = 100 l/s

For pump spacing of 150 m and $q_D = 6.3(10)^{-9}$ Torr-l/cm^2-s:

Mid-point pressure = $3(10)^{-3}$ Torr
Delta P = $3(10)^{-3}$ Torr
Pressure at port = $3(10)^{-5}$ Torr

For pump spacing of 150 m and $q_D = 6.3(10)^{-13}$ Torr-l/cm^2-s:

Mid-point pressure = $3(10)^{-7}$ Torr
Delta P = $3(10)^{-7}$ Torr
Pressure at port = $1(10)^{-9}$ Torr

As can be seen by the above calculations if we want to have a pump spacing on the order of 150 m it is critical that we make the effort to degass the chamber prior to the conditioning of the NEG material. Whether this is done by bake-out, gas flow, or pumping over a long period of time has yet to be determined.

6) Recommendations for R&D efforts.

a) Engineering analysis of thermal effects on the vacuum chamber and magnet assembly. An analysis should be done on what affect a 500 C bake out would have on the chamber and magnet assembly. If it is possible to bring the system to this temperature for a long enough period of time to condition the NEG material it should be possible to eliminate the problems and cost of ceramic feed-throughs, stand-offs, processed NEG strips with conductors, and any repair problems associated with the NEG strips.

b) Whether the NEG material is heated from the outside or the inside, installation of the material in tubes of the length we are talking about will require considerable development work. It would be very useful to understand this up front so that the impact on cost and installation is understood.

c) It would be useful to have a working vacuum system mock-up. This would allow us to measure system parameters such as outgassing rates, pump spacing requirements, and system response times.

d) There will be numerous difficulties in working with tubes of extreme length. Examples would include initial cleaning and handling, machining at port locations and mating ends, straightening process, and transportation. Some R&D work up front here would go a long way towards eliminating bottlenecks and problems down the road.

As an R&D effort, a test set up of approximately 150 m should be initiated. This would allow us to investigate all of the above issues. The cost for equipment would be minimal due to the availability of existing Lab equipment. The main material costs would be the aluminum extrusions and the NEG material.

Instrumentation
Beam Intensity and Longitudinal Measurements

A. Hahn

The instrumentation to measure the Beam Intensity and bunch lengths is straight-forward extensions of the technology used in the Tevatron.

Fast Toroids are used to measure the injected beam intensity. They are located in injection lines and near the point of injection into the ring. They are typically used in measuring the transfer efficiency of beam lines since they share a common calibration.
Cost : $4k per installation (includes support electronics of a sample and hold).

DCCT (Direct Current Current Transformer) measures the dc component of beam current with absolute accuracy <1-2%. One is needed per beam pipe. They provide a reliable and redundant intensity measurement .
Cost: Commercially available along with front end electronics for $25k/ installation.

SBD (Sampled Bunch Display) and **FBI** (Fast Bunch Integrator) both use a high bandwidth (3 kHz -6 GHz) Resistive Wall Detector (RWD) to measure individual bunch intensities. The SBD uses a fast scope to capture the waveform, while the FBI simply integrates over the rf bucket. The absolute accuracy of the SBD is <2%, while the FBI is typically 5%. The update rate on the SBD is 2 Hz (with today's technology), while the FBI can work at turn by turn speeds. The SBD also measures the bunch length, but in order to measure the bunch length, it is important to preserve the bandwidth of the signal to the scope/digitizer. This could involve locating the scope near the detector, or converting the electrical signal into an optical one for transmission on a fiber).
Cost: One RWD ($10k including helix cable, perhaps $20k if fiber is used) installation per beam pipe, but only one SBD and FBI support system per Machine. Cost is $40k (primarily the commercial scope/digitizer) for SBD, $15k for the FBI.

Transverse Measurements
Currently the Tevatron uses 2 systems to measure the transverse size of the beam, a Flying Wire System and a Synchrotron Light Monitor. Both are described below. As the beam energy is increased, the transverse size of the beam decreases inversely proportional to the square root of energy (relativistic damping). This will make the measurement of transverse beam size more difficult than it is in the Tevatron. Larger lattice beta's will offset this effect somewhat, but not eliminate it entirely. Development effort will be needed for the current systems as well as new devices such as the Electron Beam Monitor.

Flying Wires (FW) fly a 30 micron diameter carbon filament wire through the beam. The interaction of the beam on the wire produces a shower (primarily pions) which are detected in downstream scintillators. This system should still work fine for 3 TeV machine, and at

injection for the 50 GeV machine. It isn't clear how high in energy (before the beam gets too small) one can go with this technology. A measurement at the B0 IR with small beam sizes (start of Run 2) should provide insight into this question. In any case the FW should be installed at a high beta region to maximize the beam size and increase the precision of the measurement. One installation is comprised of three FW's- two horizontal and one vertical in reasonable proximity to each other so they can share electronics and controls. In the case of a very large machine, it may be advantageous to install 2 sets of 3 wires at opposite sides of the ring in order to look for lattice inconsistencies.
Cost: It may be possible to locate the wire can so that it could fly through both beams pipes. Cost per installation $100k.

Sync Lite uses synchrotron radiation from the edge of a dipole magnet to make a 2D (transverse), and 3D (transverse and longitudinal) measurement of beam size. A pickup mirror, internal to the beam pipe reflects the synchrotron light beam through a transparent window into a telescope where an image of the beam is formed. A system similar to the Tevatron one could easily be imagined for the 3 TeV machine, as long as a provision is made to collect the synchrotron light beam before it hits the wall of the beam pipe). A least 2 telescopes are needed (one for each beam pipe--for pp operation). A system for the 50 TeV machine will need **development** work to extend the telescope into the hard uv-xray (short wavelength λ) region in order contend with diffraction effects (scaling as $\lambda\gamma$) and with smaller beam sizes, (naively scaling as $\sqrt{\gamma^{-1}}$).
Cost: For a 2D system, $75k for one installation, plus 2 man years (a physicist and an engineer spread over a 2 year period) of development of the new telescope. A 3 D system would add another $250k, primarily for a streak camera. Most software would have already been done for the Tevatron version.

Electron Beam Monitor scans a 10 keV electron beam across the proton beam. By measuring the deflection one can infer the transverse charge distribution.(SSC was working on a device like this for the 20 TeV machine).
Cost: Estimate $100k/installation, with 2 man-years of **development**. This work could be started in the Tevatron.

Multi-electrode pickup measures the rms of the beam (transverse and longitudinal using time slicing) . A Multi-electrode detector is sensitive to the beam multipoles. It is in principle possible to extract the moments of the charge distribution. The small beam pipe should be a plus here, although it would need to be round in shape. Although the SSC rejected this option as lacking the needed sensitivity, it should be reevaluated as a fast (and dirty) transverse beam size monitor.
Cost: $20k for a detector (either a stripline or a resistive wall detector), and a man year of **development** (spread over a couple of years).

Position Monitors for 3 TeV High Energy Booster

James Crisp

Propose 1 bpm per half cell, 350 bpm's and 350 blm's for each beam. Provides about 350/(2*33) = 5.3 bpm's per betatron wavelength. Main Injector has 3.8, Main Ring and TeV have 6.4 bpm's per betatron period. MI note 75 indicates for Main Injector, measuring both planes would improve the rms closed orbit distortion correction by only 10%. The ratio of beta max to beta min makes it less important to measure the orthogonal plane.

With 132 nsec between bunches it's tempting to measure each bunch using a log amp processor. Both logA/B and logAB would be digitized to determine position and intensity.

The main ring AM to PM rf module cost about $5k to reproduce, however, a log amp module costs $1k per channel. The 4 plate detector cost $1000 but the split tube detector is about $500. In comparison, Main Injector tunnel cost about $2400 per foot.

Linearity is much better for split tube detectors as can be seen in the following figures.

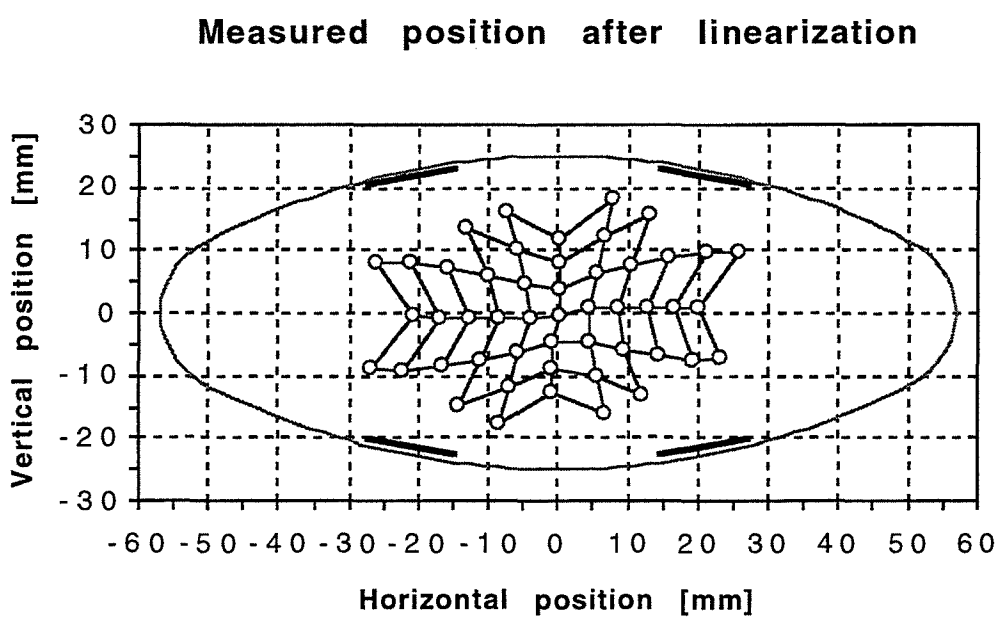

Figure 1. Main Injector 4 plate detector.

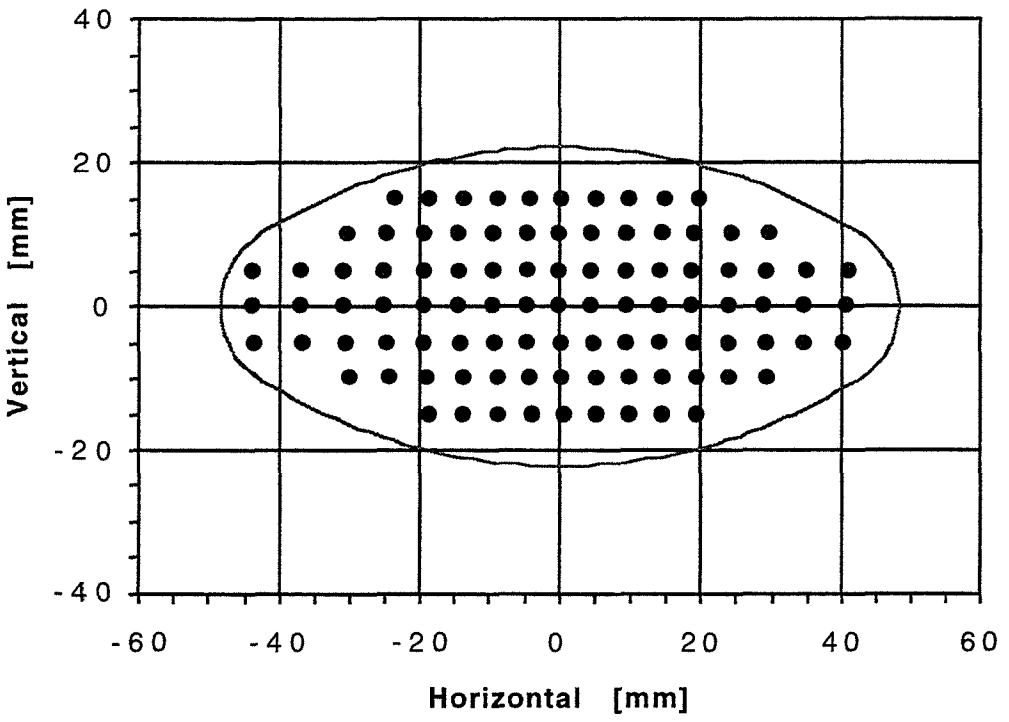

Figure 2. Recycler ring horizontal split tube detector.

The detector plate acts like a differentiator as beam current is induced onto the plate and then removed. The signal induced on a 10 cm detector is estimated below.

$$I = \frac{Ne}{\sigma_t \sqrt{2\pi}} \exp^{-\frac{1}{2}\left(\frac{t}{\sigma_t}\right)^2}$$

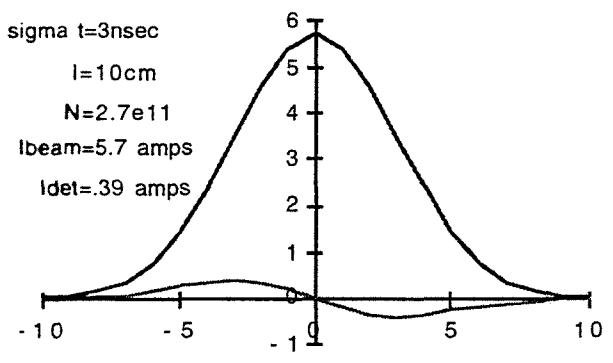

Measured beam position is proportional to the log of the ratio of the two bpm signals.

$$pos = \frac{mm}{db} 20 \log_{10} \frac{A}{B}$$

The effects of thermal noise limit how small the electrodes can be. The equivalent position noise is estimated below.

$$\frac{A}{B} = \frac{V_{out} + V_{noise}}{V_{out} - V_{noise}} = \frac{1 + V_{out}/V_{noise}}{1 - V_{out}/V_{noise}}$$

$$\ln\frac{1+x}{1-x} = 2x + \frac{2}{3}x^2 + \frac{2}{5}x^3 + \cdots \quad \approx 2x$$

(use $\sqrt{2}x$ since x represents uncorrelated noise)

$$\log_{10}\frac{A}{B} = \log_{10} e \quad \ln\frac{A}{B}$$

$$pos\ \ noise = \frac{mm}{db} 20\log_{10} e \ \sqrt{2}\frac{V_{noise}}{V_{out}}$$

$$V_{out} = Z_{plate} I_{\det} \quad \text{and} \quad V_{noise} = \sqrt{4kTBZ} \quad \text{(thermal kTB noise)}$$

$$\boxed{pos\ \ noise = \frac{mm}{db} 20\log_{10} e \ \sqrt{2}\frac{\sqrt{4kTB}}{I_{\det}\sqrt{Z_{plate}}}}$$

10cm split tube detector
I det = .2 amps, 2.7E11/bunch
sigma t = 3 nsec
4 MHz bandwidth
50 ohm impedance, (higher requires cables < 2ft)
1 db/mm, (scaled from RR 5x12cm pipe)

Thermal noise 2.4 um RMS

In order not to waste signal, plate capacitance should provide an impedance greater than the amplifier at frequencies less than 50 MHz. To satisfy this, the detector housing should be at least 20% larger than plates. This may require the bpm not be placed within the magnet. If the cables between the bpm and the log amplifiers is longer than two feet the amplifier input impedance should match the characteristic impedance of the cable. Split tube detector with log amp $1500/BPM

Loss Monitors

Ion chambers with 116 cc of Argon at 725 mm of Hg is currently used in the TeV, MR, and MI. At 1 or 2 KV, they provide about 1 uamp for 14.3 Rads/second. The amplifier response is shown in the figure below. They cost about $200 for the detector and $300 for the supporting electronics.

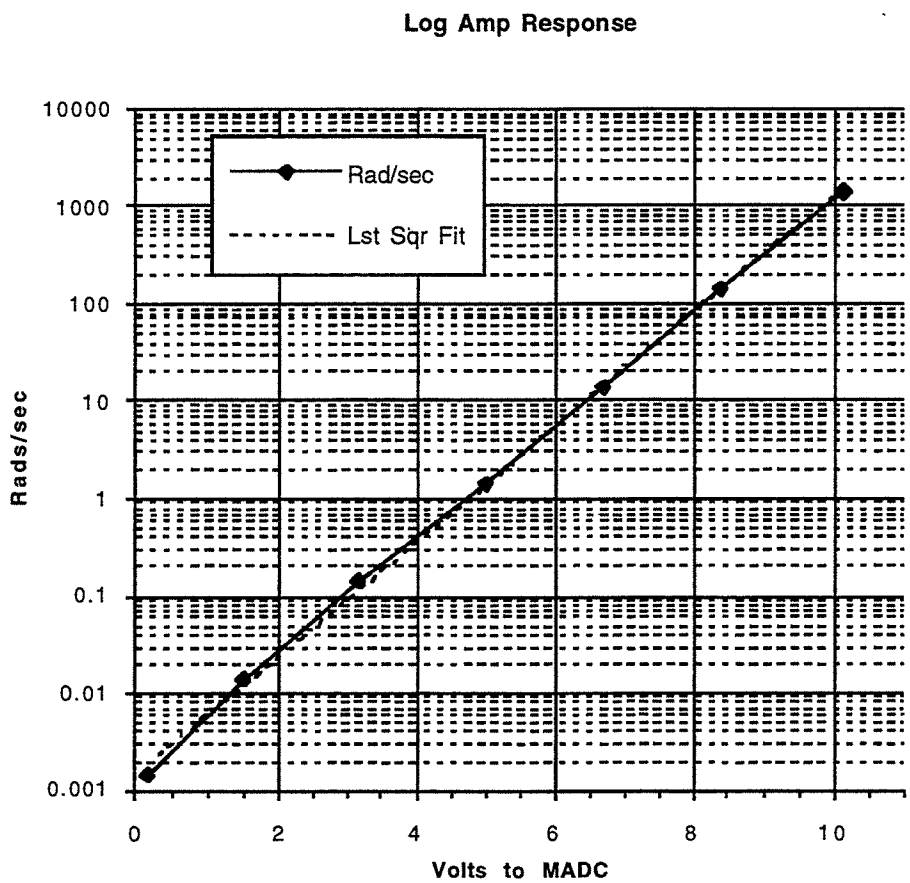

Figure 3. BLM amplifier response.

The Ion chamber could be made from air dielectric coaxial cable which runs the length of each half cell. If more position resolution is desired, each half cell could be subdivided with loss monitor cables which run up and downstream of the controls node.

1/4" Andrew coaxial air dielectric cable
- $5.91/m
- 1.6 KV
- 26 cc/m

Since the half cell is about 100m, the cost of 1/4" cable is comparable to the present ion chamber. It would contain about 22 times the volume of gas, however, the type of gas, pressure, and voltage could be selected to provide the desired sensitivity.

Air dielectric CATV cable may provide a less expensive alternative, however, the types I could find would not work. One used plastic disks to support the center conductor but each disk is water tight making it impossible to flow gas through the cable. The other used splines to support the center conductor but the center conductor was completely surrounded by dielectric making it impossible to collect ions.

Commercial diode loss monitors cost about $500 in small quantities. They have a hundred nsec time constant and large dynamic range but very small volume sensitive to radiation. They are interesting for specific applications but may not be desirable everywhere.

High Field Magnet R&D for VLHC

H. Glass, P. Limon, J. Tompkins, A. Zlobin

Overview

Two approaches for a VLHC machine involve the use of low-field magnets (i.e., Pipetron) and high field magnets (HFM). In a machine with the nominal Snowmass-96 parameters, 50 TeV on 50 Tev, the HFM option has the advantages of utilizing synchrotron radiation damping to improve beam stability, and also to minimize tunnel circumference [1]. The required fields have yet to be determined, although an operational field between 9 – 13 T is probably what is needed. A 9 T dipole may be sufficient to provide radiation damping in a 50 TeV machine; damping would be improved at higher fields, and the Snowmass group chose 12.5 T as a nominal field.

The choice of magnet technology and the required level of R&D will significantly depend on the field one chooses. Magnets with 9 T fields will be achievable through continued improvements in NbTi. The technology for producing cos-theta magnets in the 10-12 T range using Nb_3Sn is a reasonable goal in the next few years, while a magnet with fields > 12 T will require new magnet designs and significant improvements in the utilization of superconducting materials with higher H_c and J_c than what is attainable with NbTi; these include the A15 materials (e.g., Nb_3Sn) and the less well known high temperature superconductors (HTS).

LHC HGQ program

A natural bridge to a VLHC magnet is the High Gradient Quadrupole (HGQ) program now getting underway in the Technical Division. This project will result in the construction of a number of quads with gradients in the range 210-250 T/m and a bore of 70 mm. These magnets will be used in the low beta interaction regions of the LHC. Arc quadrupoles in a VLHC will undoubtedly have gradients at least as large, most likely in the 250-300 T/m range, but with smaller magnet bore.

Fermilab will construct low-beta triplets for the LHC. Each triplet will consist of 4 cold masses each of length ~6 m. A major milestone in this project will be the construction of a full-scale prototype in FY2000. Prior to this, we will need to have completed short model R&D. Production will result in about 20 magnets to be completed by FY2004. These magnets will use NbTi conductor made from SSC strands cooled with superfluid He at 1.9 K.

The high-field in the LHC quads will be about 9.5 T. Hence, the HGQ program naturally leads to development of dipoles in the 9 T to 10 T range.

Dipole options

Lessons learned from the HGQ program can be applied to a 9 T or perhaps 10 T dipole made with NbTi. Two key issues in the structural design of a high field dipole are: 1) Sufficient control of global winding deflections to preserve field quality, and 2) Sufficient control of local conductor motions to avoid premature quenches. Both issues become more difficult as the magnetic field increases [2].

NbTi:

The advantage of building magnets with NbTi is obviously that we know this material so well, and we have a lengthy experience with this magnet technology. Hundreds of short (~1 m long) and full-scale (6-15 m long) SC NbTi magnets have been fabricated and tested in large accelerator/collider projects as Tevatron, UNK, HERA, SSC, RHIC, LHC. The key points can be summarized as follow:

- NbTi magnets allow one to achieve 7.5-8 T maximum field (6-7 T operating field) at 4.4 K and 10 T at 1.8 K in the magnet bore of 50 mm. The required field quality in the magnet bore of 50 mm, reproducible from magnet to magnet, has been obtained. All sources of the field errors are well understood.
- Magnets show reliable behavior in thermal and current cycles over long times in hard radiation environments.
- Coil cooling can be provided by liquid helium at 4.2-4.8 K or superfluid helium at 1.9 K. Liquid helium cryogenic systems can provide the magnet thermal stabilization at levels of localized heat deposition up to ~10 W/m.
- Magnet quench protection is provided by internal quench heaters.
- The technology of NbTi magnets has been demonstrated in mass production in industry (HERA, RHIC) at acceptable costs.

Nb_3Sn:

Significant progress in attaining higher magnetic fields has been achieved using Nb_3Sn in the past 3-5 years. The High Field Magnet group at LBNL has had some success at building R&D magnets using a hybrid scheme [3] using an inner coil of Nb_3Sn and an outer coil of NbTi. This magnet reached a quench plateau of 7.56 T at 4.3 K, and is expected to reach nearly 10 T at 1.9 K. More recently, the LBNL group had a significant success with an all Nb_3Sn dipole (D20) which reached fields above 13T at 1.8K [4]. The magnet group at Twente University (Netherlands) had achieved 11 T with a Nb_3Sn model magnet[5].

The main problem is that unlike NbTi, Nb_3Sn is brittle. Even worse, Jc degrades when it is subjected to strain. An alternative which may have lower strain sensitivity is Nb3Al. To minimize the strain problem, one usually winds the Nb_3Sn into a coil shape prior to preparing the material in its final state. In this wind-and-react method, the coil must be reacted at high temperatures (~650 C) for many days. Coil insulations which can withstand this temperature include fiberglas and ceramics.

Some useful results obtained with Nb_3Sn short dipole models are:

- A magnetic field of 13 T has been achieved in the magnet bore of 50 mm at 4.3 K with a Nb_3Sn shell type dipole magnet. The magnet critical current degradation of 5-10% was observed in the magnets for both wind+react and react+wind winding technologies.
- Coil cooling by pressurized liquid helium at ~4.4 K provides the magnet thermal stabilization at high heat depositions. These magnets have a bigger temperature margin and therefore they are good for fast cycle or high heat load operation.
- Well understood quench protection systems based on internal quench heaters can provide reliable magnet protection.

- Field quality and its reproducibility from magnet to magnet as well as long term magnet behavior are not well known because of the small number of models built.

Magnets employing coil designs other than the proven cosine theta design are being investigated at various facilities. For example, A block-coil design using Nb_3Sn is being developed [6] with the goal of achieving 16 T. These designs are driven by the need to provide better mechanical support for the conducter, which is subject to very high forces at high fields. Unfortunately, such designs are not efficient in their use of conductor, typically requiring twice the conductor of cosine-theta geometries.

High Temperature Superconductors (HTS):

The most promising of the new materials include $Bi_2Sr_2CaCu_2O_x$ (BSCCO-2212), with $T_c \sim$ 85K, and $Bi_2Sr_2Ca_2Cu_3O_x$ (BSCCO-2223), having $T_c \sim$110K. Kilometer-length quantities of these materials have been made in the form of multifilamentary tapes (typically 10:1 aspect ratio), suitable for a magnet using the parallel wall design [2].

Another material, YBCO, shows even more promise of being useful at high fields. Very high critical current densities have been achieved at high fields in short samples. Commercial production of this material lags well behind BSCCO. A good review of the new HTS materials is given in [7].

The first direction to be taken at Fermilab in the immediate future will be investigating the use of HTS materials in superconducting leads with the possibility of replacing the existing 5kA leads in the Tevatron to reduce the overall thermal load on the 4K system. An additional R&D step to be taken soon will be the installation of an HTS short sample test facility.

Other issues which have not been addressed here, but will clearly need attention in a HFM program, include quench protection, cryogenics, and structural issues. All of these areas should be addressed concurrently with the conductor R&D outlined above. A comprehensive program is needed to develop the magnet technology for a future collider, but we believe this program has a high probability of success given appropriate R&D support from DOE.

References:

[1] Holmes, Really large hadron collider summary report, in Proceedings of Snowmass96 workshop.

[2] Scanlan et al., Superconducting Magnet technology for future hadron colliders, in Frontiers of Accelerator Technology, World Scientific, 1996, pp. 359-378.

[3] Caspi et al., Design & construction of a hybrid – Nb_3Sn, NbTi dipole magnet, in IEEE Transactions on Applied Superconductivity, June 1997, p. 547

[4] McInturff et al., Test results for a high field (13 T) Nb_3Sn dipole, Particle Accelerator Conference (PAC97), Vancouver, Canada, 1997.

[5] den Ouden & ten Kate, Application of Nb_3Sn superconductors in high-field accelerator magnets, in IEEE Transactions on Applied Superconductivity, June 1997, p. 733.

[6] Elliott et al., 16 Tesla Nb_3Sn dipole development at Texas A&M University, in IEEE Transactions on Applied Superconductivity, June 1997, p. 555.
[7] Larbalestier, The road to conductors of high temperature superocnductors, IEEE Transactions on Applied Superconductivity, June 1997, p. 90.

Thoughts on Controls/Instrumentation for 3 TeV booster/VLHC

Working Team: Bob Goodwin, Peter Lucas, Elliott McCrory and Mike Shea.
Thursday, July 31, 1997

Introduction & Outline

Ideas and (mostly) questions about the character of the controls and instrumentation for a low-field 3 TeV injector/collider are presented. First the required **Diagnostics** are outlined, followed by some of the anticipated **Instrumentation** needs. Finally, a series of **Questions** are presented about these aspects. The questions are broken down into three categories:

1. What is in the "diagnostic lumps"?
2. How do we communicate with these lumps?
3. What are some of the global issues here?

Given the size of the 3 TeV low-field machine (and, thus the size of the VLHC), the most important considerations are (a) to keep is simple and (b) to keep it cheap. One would also presume that we could make it good (violating the commonly held principle that you get to choose two out of those three qualities!).

This document can be found on the web as:

`http://www-linac.fnal.gov/~mccrory/papers/VLHC_Controls`

Diagnostics

Most diagnostics are contained in diagnostics "lumps" placed at each half period (according to GWF). Some lumps may be denser than others may, but it seems like all of the lumps around the ring will be basically the same.

Here is a list of probable diagnostics *(stolen from Mike Marten's list of Tevatron diagnostics)*. First, the diagnostics which will appear in a diagnostic lump:

Item	Number	Data Rate	Questions/Comments
BPM	4/period	4 MHz	One per beam * two beams per diagnostics lump
Loss Monitor	4/period	1 kHz	One per beam * two per period. Maybe continuous.

Next, the diagnostics which come in small quantities:

Tune Measurement	a few/ring	10 Hz	One per lump using local computer for FFT??
Sampled Bunch Display	1/ring	1 Hz	
Fast Bunch Integrator	1/ring	1 Hz	
Synchrotron Light Monitor	0/ring	1 Hz	
Ion Profile Monitor	1/ring?	.1 Hz	
Flying Wires	1/ring		

For the costs here, as pointed out by A. Hahn, much of this can be taken from a decommissioned Tevatron.

Other Controls/Instrumentation needs

Item	**Rate**	**Description/Comments**
Controls Local Computer	2/period	Like an IRM in controls functionality; like a PC/Mac in OS functionality.
Digitizers	2/period	4 chans @ 4 MHz, 2 chans @ 1 kHz, "many" chans @ 1 Hz.
Correction Power supply	2/period	At each lump
Magnet pushers	2/magnet? Robot?	*GWF...?*
Vacuum control/readback	@ 150 m	Can arrange for vacuum readbacks to be at a lump
Cryo instrumentation	?	Similarly, arrange to have these readbacks near a lump
Gate valves	@ 750 m	Can EM-controlled valves be used?
Ion pumps	@ 150 m	
RF System Controls		To be determined elsewhere
Electron Cooling?		
Stochastic Cooling?		
Dampers?		

Questions

Having outlined the diagnostics and other instrumentation needed, what questions need to be answered? There are three basic categories for questions, and many sub-questions under each.

I. What is in the Lumps?

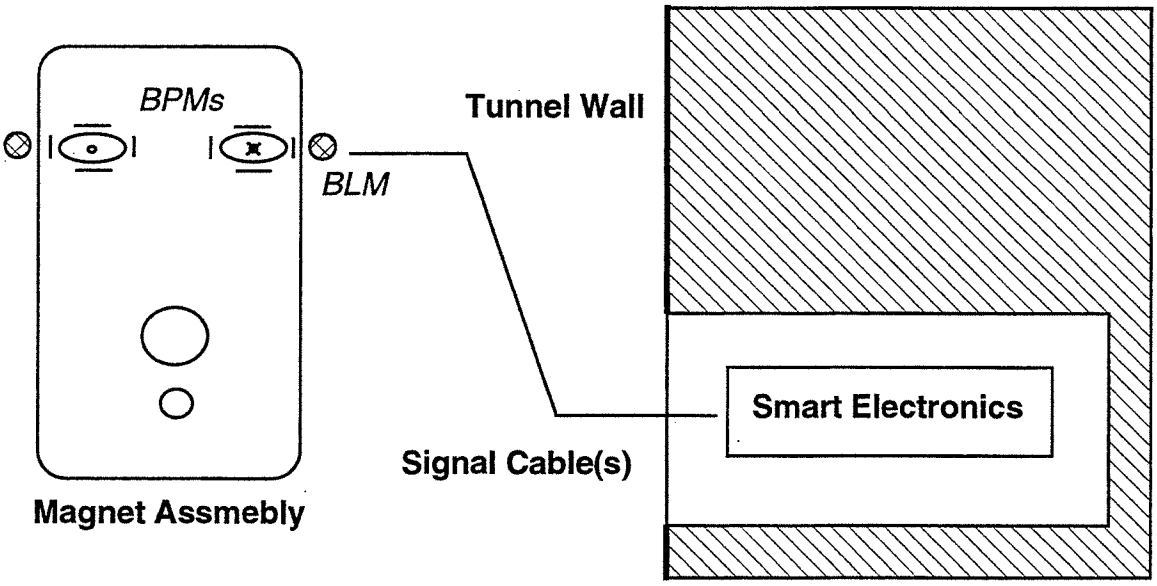

What is in a lump?

A split ring BPM and a loss monitor for each ring. A continuous loss monitor has better coverage of this enormous accelerator that the Main Ring style we commonly use today. Log amplifiers for the BPM signals are cheaper and almost as good as expensive AM/PM circuitry. These signals could be interpreted by the local "smart electronics" as either position or intensity.

Technical and cost analysis of both the BPM and the BLM systems are required.

Digitizers would be attached to the internal bus of the local computer. Would need four channels of fast for the BPMs; two moderately fast digitizers for the loss monitors and a few (~10) plain (multiplexed) digitizers for miscellaneous signals, like vacuum gauges. Depending on the nature of the correctors, may also need ~kHz digitizer(s) for that.

Dampers may also be distributed around the ring, and this would need consideration.

The "smart electronics" would be a highly configurable, Internet computer system, much like today's Pentium Pro PC or PowerPC Macintosh. The signal cables from the pickups would be directed to the digitizers located on the internal bus of the PC. The local computer will do the digital signal processing to produce the desired position and intensity information. It will probably be necessary to shield these electronics in a nearby alcove, drilled into the wall of the tunnel. Automated maintenance needs to be designed in to these components (i.e., by robot hands).

Note that this local "smart electronics" box looks a lot like today's Internet Rack Monitor (IRM). Note also that the topology of the control system here is geographic, not functional.

What are the anticipated functions of the local computer?

Here is today's list:

1. Direct the digitization of 10-20 local signals at both a leisurely rate and fast rates. For beam spacing of 250 nsec, the BPMs would require 4 MHz digitizers, probably similar to today's "quick Digitizers", but not within a VME context (too expensive). If the beam spacing goes beyond 100 nsec (10 MHz), digitizing individual bunches may be impractical. Would use the local PC bus for this new piece of electronics.
2. Provide Flash, First-turn, Turn-by-turn and/or scalar information from BPMs, using local memory as required; ~400 bunches per beam in the ring implies 2 kB per turn; 1000 turns would require 2 MB—no big deal!
3. Most, if not all, of the digital signal processing will be done directly on the local computer. The speed of new PC's these days, like the 250 MHz Pentium Pro and the 350 MHz PowerPC, is so high that some electronics houses are turning to programming these PC's instead of programming DSPs. We see if this trend continues.
4. Respond to requests for data from the network,
5. Allow remote access to the internal workings of the computer (the OS) for configuration,
6. Connect with "central database"
7. Report bad conditions to the network (alarms)
8. Allow users/operators to add software functionality, including the possibility of local software feedback mechanisms.
9. Provide general access to the local works, like an HTTP server (web access)
10. ...

How much redundancy is necessary (a) in the instrumentation lumps? (b) in the smart electronics? (c) in the cabling?

What are the control requirements of the corrector system?

Can you get valves that do not require compressed air?

Probably.

What is the overall power budget? How much power is needed at each lump and how much heat is dissipated?

Here is a preliminary table.

Item	Power	#/Lump	Comments
Local Computer & digitizers	50 W	1	Today's fully configured IRM takes less than 60 W, and this device has more hardware connectivity than we need.
BPM signal processing	20+ W	1	Log amps use a lot of power.
BLM HV	1 W	1	1 mA at 1 KV
Vacuum Valve	5 W?	0.2	A guess at the power requirements for an EM-controlled vacuum valve
Corrector Power Supply	200W?	1	Another guess
Totals	***280 W***		*Depends mostly on corrector power.*

II. How do we communicate with the lumps?

What will the network be?

This local computer would be on a ring-wide computer network. Today's technology offers high-speed Ethernet switches, which are being installed in our offices now. There are at least two possible topologies for this network: a ring or a star. The favored topology would be based on performance and cost consideration nearer the time of construction.

First topology; "Ring":

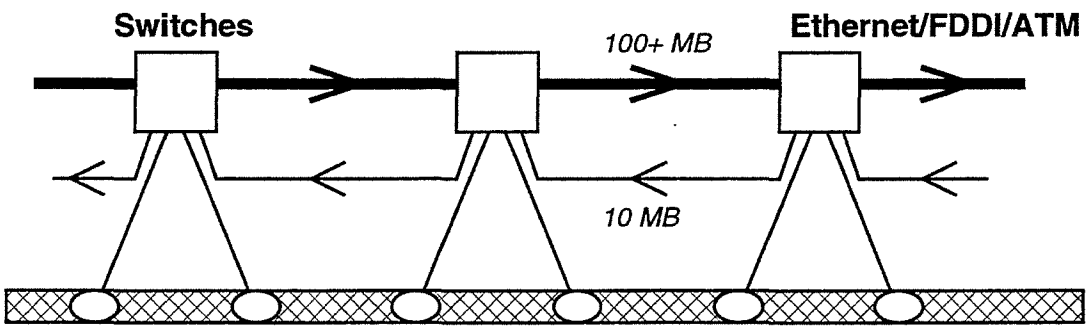

Lumps, within Magnet String

A global, high-speed computer network goes around the ring, inside the tunnel. A number of fast switches, one for a few lumps (two shown in figure) controls the message traffic for its lump. Since these switches work on a "store-and-forward" mechanism, collisions on the network are not seen. The ring would be fiber; the branches to a lump could be fiber or copper.

The other possible topology is a "Star" topology. The figure is attached.

A router is stationed at the top of each of the four vertical access shafts. Six fibers are dropped down the shaft for further distribution. At the end of each fiber in the tunnel is another network branch, this one is to another six-port switch, which then connects to a four-way fiber-to-copper "CAT 5" distribution. The three ports here attach to the three nearby lumps. This is very close to the topology in most large office buildings.

This topology presumes that the costs of fiber and the reach of a single router are reasonable. Using today's standards, this seems like a good alternative. Single-mode fiber can easily go over 5 km; routers now can handle 100+ nodes. A big benefit of this topology is that single-point failures of the entire network can only occur on the ground, not in the tunnel. At the top of the access points is a natural place for message "consolidation,' so that if you, in a central control room, ask for all the BPM data, you are not flooded with little messages.

Approximate costs for this last system are presented separately.

It is important to note that anything we decide on today is unlikely to be the best choice in 5 years. The best choice today is 5 times cheaper than what was available 5 years ago, and probably 5 times better. We will need to be flexible until then.

How many/few cables do we need?

MI experience shows that the cost of one installed fiber is approximately equal to that of 36 installed fibers. If fiber is inappropriate for the tunnel, then the question remains unanswered. Probable uses for individual fibers (each one with a backup):

1. Computer network connection
2. Beam-sync clock
3. Event clock

We need a list of how fibers are being used in the Main Injector.

The notion that a lot of fiber runs costs a lot is wrong. The phone company is leading the way in bringing down the cost of fiber communications.

How much communications between *lumps is necessary?*

None/very little. Communications between lumps would be easy, but experience with large circular machines seems to indicate that this functionality is not really necessary.

What cable-hanging scenario do we use?

- Under the floor: requires a floor
- On the magnet: requires rad-hard cables
- in cable trays: neat and tidy, but requires rad-hard cables
- strung on hooks along the walls: low-cost, messy, but requires rad-hard cables

Is it necessary to shield the electronics and cabling? Can naked fiber optics cables (i.e., fiber that is not shielded by concrete) be used in the tunnel?

That is, how much radiation will the tunnel have, and how hardened will the electronics need to be. We think that maybe the RHIC people may have something to say about that. The SSC people apparently didn't get that far. LHC experience?

This is a critical issue. If we cannot use fiber in this tunnel, then it is going to be hard to take advantage of the cheap communication mechanisms being devised today.

What is the nature of the beam sync clock and the event clock system(s)?

The event clock will probably be needed everywhere, but the beam sync clock may be needed only in the RF region (we can put the one-of-a-kind beam diagnostics there, too). It would be nice to use the (highly-underutilized) computer network for the event clock too, but this technology does not currently exist.

Beam-sync clock issues for a ring as big as the 3 TeV low-field injector are difficult ("synchronicity" is tough to define, for example; note that $v \approx 0.6\ c$ in a light fiber). We are told that putting repeaters in a beam sync line destroys the time stability of the signals, so it would be necessary to have direct connections to everywhere that requires beam sync. If there was no beam sync at the lumps, one would require that the local computers, which all have BPM information available, use these signals as their beam sync, and count from the abort gaps to determine which bunch is present.

This obviously needs further development.

III. What are some of the Global Issues?

What is the nature of the beam abort system and how will this interact with the control system?

Will there be a central database? What will it do?

What about exiting controls frameworks like EPICS and ACNET?

Do the benefits of using these old systems (familiarity, established user interface mechanisms, central services like datalogging) outweigh the benefits of using a modern, open, commercial OS? If we were not to use these systems, it would take significant effort to rebuild their controls functionality into a generic PC.

Section 4: CONVENTIONAL CONSTRUCTION AND SITE CONSIDERATIONS

J.Lach et al, "Geology and Tunneling"

S.Krstulovich et al, "Dehumidification Options"

J.A.Satti, "3 TeV RF Cooling System Design Proposal and Cost Estimate"

Geology and Tunneling

Joseph Lach, Ernest Malamud, Michael P. May

September 5, 1997

Geology

The geology and hydrology of the Fermilab region are ideally suited for a new large collider project. Site conditions at Fermilab are well understood. The Illinois State Geological Survey (ISGS) has extensive data on the regions under consideration from drill holes, and additional data compiled when there was active consideration given to siting the SSC in Illinois. [1]

There are predictable rock and tunneling conditions and relatively homogenous rock mass. There are no settlement problems at the depths being considered. The region is seismically stable. There is a relatively vibration free environment, important to minimize emittance growth problems. A systematic vibration measurement program is now underway.

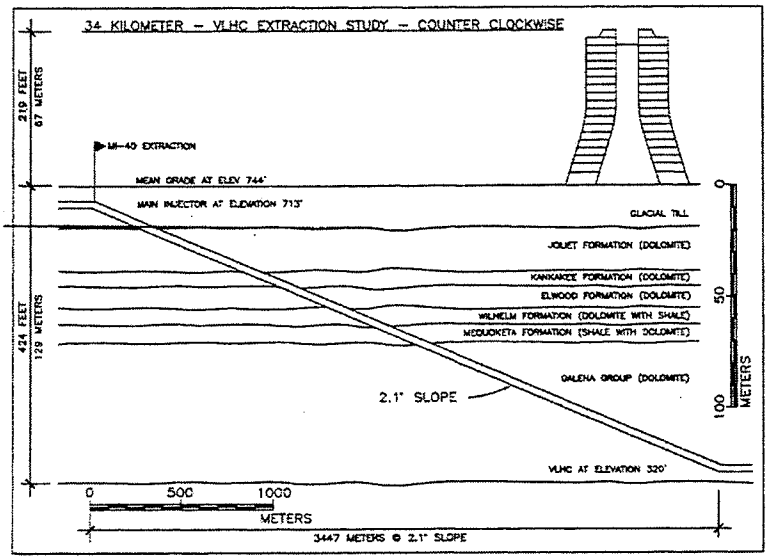

The dolomite layers under Chicago and under Fermilab are quite uniform. The large regional extent of dolomite can serve as an excellent host for a tunnel in the Fermilab region. A tentative decision by the VLHC Study Group to site both the 3 TeV and 50 TeV rings at an elevation of 320 feet above sea level (msl) has been made. This places both machines in the Galena-Platteville dolomite layer. This layer has sufficient thickness so even with variations in depth the 3 TeV ring can most likely lie in a plane and be parallel to the surface. The depth below the surface is about 400 feet. At the North Aurora quarry that a group of us visited on September 3, we learned that the Galena-Platteville layer is 297 feet thick and does not vary much going to the east.

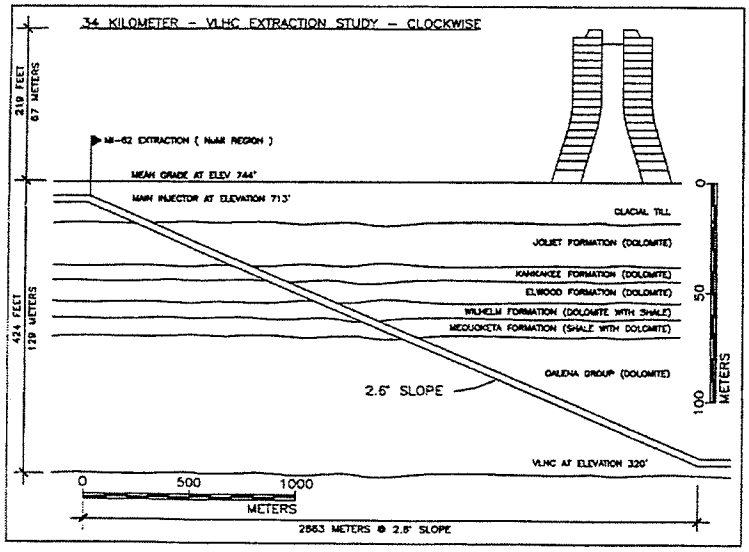

Since it is easier to transfer 150 GeV beams than 3 TeV beams, it is felt advantageous to have the 3 TeV injector at the same depth as the final 50 TeV ring. Shown are injection lines from the Main Injector to the 3 TeV ring using MI-62 (NuMI stub) and MI-40 (abort) as the extraction points from the Main Injector.

Hydrology

As one goes down through the various layers shown in the figures, the water seepage varies by 3 orders of magnitude. The Galena-Platteville layer is an aquatard and water seepage is very small, confirmed on our recent field trip.

Trenchless Technology

Trenchless Technology is a generic term for tunnel or pipe construction without surface disturbance. Trenchless Technology is growing in importance as a practical solution to expansion and repair of underground utilities. Trenchless construction is helping solve huge, complex underground infrastructure problems economically, safely, and with minimum of inconvenience to the public and damage to the environment. This is an area where the VLHC will benefit from the expanding technologies but may also be a catalyst to this environmentally crucial industry by pushing the envelope on advance rate over very large distances.

Two of the techniques used in trenchless technology are microtunneling and "standard" Tunnel Boring Machines (TBM). Microtunneling can be as large as 6 ft in diameter but refers to construction methods without human access. TBM's bore tunnels over a large size range. In this technique humans are in the tunnel during construction.

Fermilab is a member of the North American Society for Trenchless Technology as well as the American Underground Construction Association. Through these connections we are keeping up with this rapidly evolving field. We have learned that for smaller diameter tunnels in the range 6 - 14 ft, there is a merger of technologies in the direction of more automated tunneling with less need for human access. These advances are gradually improving the utilization rate and thus the linear advance rate which, in turn, is lowering the cost. R&D in the trenchless technology industry is aimed at several advances that will aid us in the construction of the VLHC tunnel:

- increasing distances between shafts
- utilization of remote liner installation methods
- development of long-distance muck removal strategies
- development of guidance for tunneling in a gentle curve and following the best terrain to stay in the optimal geology
- system monitoring to improve utilization percentage

Tunnel Costs and local experience

Preliminary estimates for tunnels in hard rock in the 10 - 14 ft diameter range vary from $300/foot to $1500/foot. In order to sharpen up these numbers Fermilab has issued purchase orders for two independent consultants to develop a cost model for the 3 TeV, 34 km tunnel used as a model for us to study siting and the effect of varying parameters such as depth, number of accesses, diameter on the cost and construction time.

Besides having excellent geology for the VLHC enclosure, we are benefiting greatly from local expertise in hard rock tunneling. In the TARP (Tunnel and Reservoir Plan) under Chicago in the similar rock as we are proposing for the VLHC 93.4 miles of tunnel in the diameter range 8 to 33 ft has been completed out of a total planned length of 109 miles.

Choosing the tunnel size

There are three considerations in choosing the tunnel size:

- lowest cost
- room for other machines (Fermilab & CERN strategy)
- although we will strive to automate the installation, alignment, and repair as much as possible one must retain the ability to deal with unknown problems using human access

As a starting point we consider a 10 foot diameter tunnel. The invert and its infrastructure is an item which will need a lot of attention. There are many different design scenarios which will work and each one has different advantages and disadvantages. The design which is depicted in the cross sections below can save money in the fact that it only needs to be installed once, and is used for both the tunnel contractors needs, and later for the technical components. During construction (by a TBM with conveyor belt muck removal) the contractor will install a rail system for bringing people and equipment to the tunnel face. We are investigating whether or not the rail system installed by the contractor could be retained and used by us for the magnet installation vehicles. The risk that is taken is that the inverts are installed behind the TBM after the tunnel walls have been sealed for moisture, and as a result, the TBM cannot be removed from the tunnel for major repair by pulling it backward.

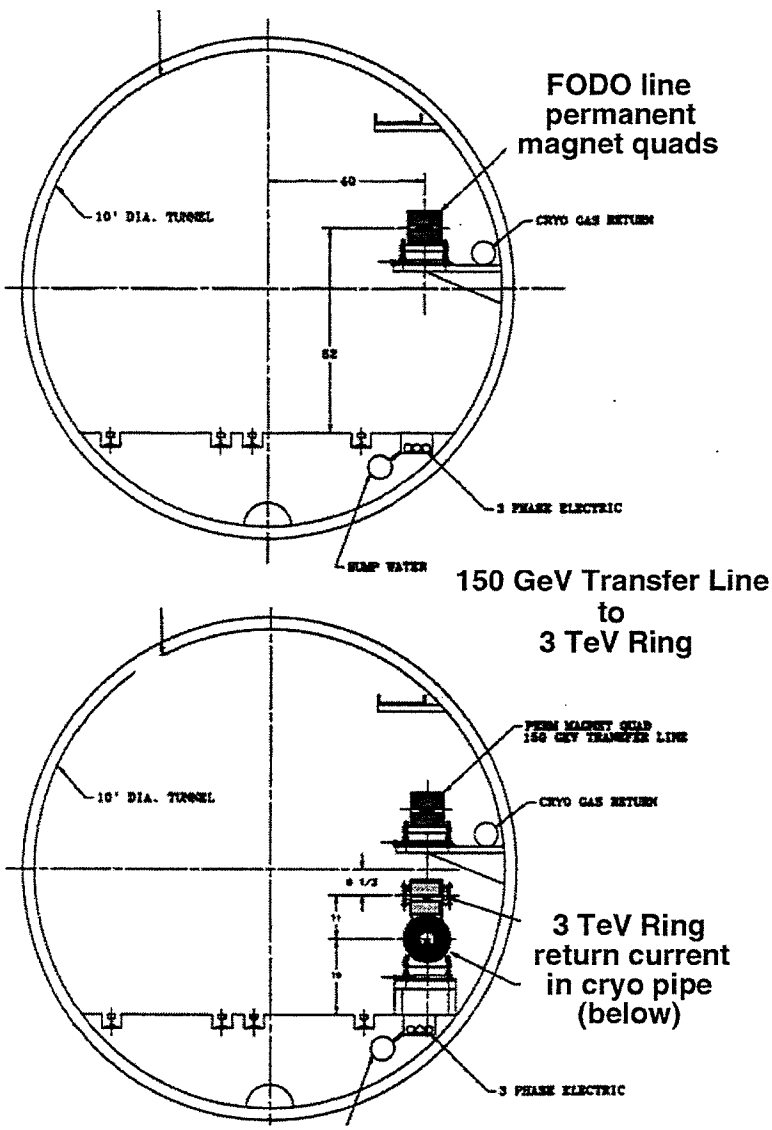

The usual way that tunnels are bored, is to have the contractor bore a tunnel to a given size. The construction infrastructure is removed, and the tunnel is turned over to another contractor to install the infrastructure that is needed for its final use. Power, air and transportation are common needs of the contractor and of Fermilab. If there is a way of installing these functions once, money can be saved.

Shown are two cross sections, one of the injection tunnel where the 150 GeV beam is transported in a simple FODO line made out of permanent magnet quadrupoles, and the second cross section showing the main tunnel at the point where the transport line is approaching the injection point.

Sharing the tunnel with other machines

The small magnet aperture and the large number of bunches makes it unattractive to attempt to have counter rotating beams of protons and antiprotons in the same vacuum tube. A better solution for a 6 TeV cm antiproton-proton collider is to put in a second set of VLHC magnets and only use one magnet gap of each. The return current then can power the other string. Furthermore at a later stage, when the 50 TeV/beam machine is built, it may be possible to recycle the second 3 TeV ring and use it for a portion of the 50 TeV ring (or for the 3 TeV transfer lines).

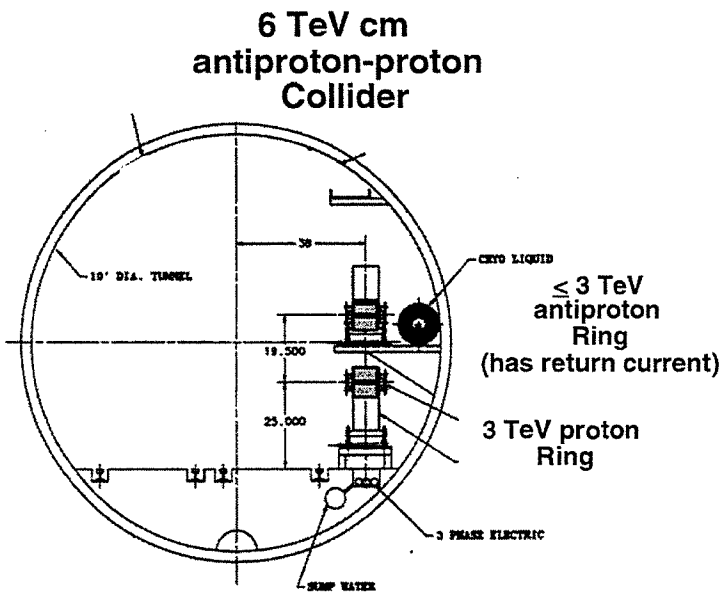

Another idea is to put an electron ring in the 3 TeV tunnel and do ep physics during the several year period that the "ultimate" VLHC is under construction. Heat removal and operating costs are an important issues for the electron ring. If the RF power is limited to 50 MW, then the electron energy would be 81 GeV.

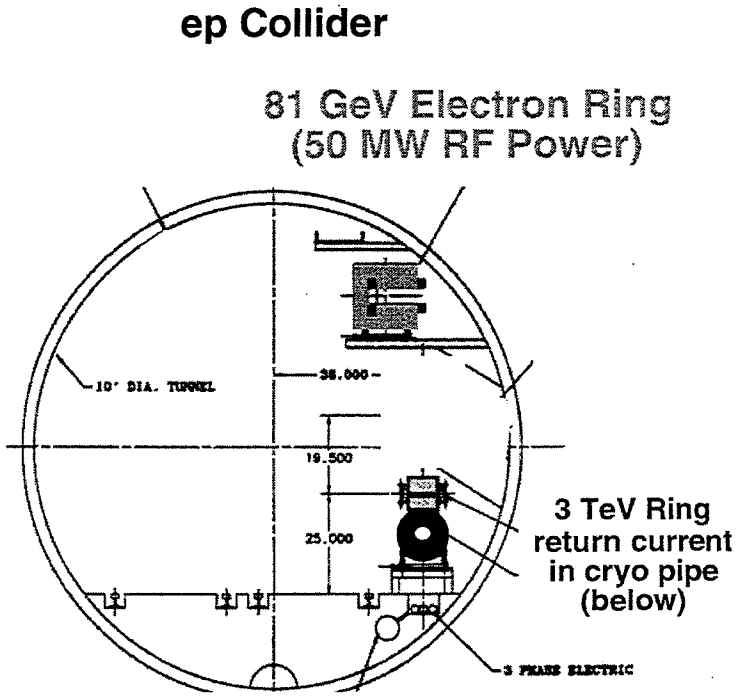

Reference:[1] R. A. Bauer & D. L. Gross, "Geology of the Greater Fermilab Region," Snowmass '96.

Dehumidification Options

Steve Krstulovich, Mike May, Ray Stefanski

Tunnel Moisture Load:

The cost of dehumidification is directly related to the moisture the tunnel air will pick up from water sources in the tunnel. To keep the air dry at low cost, it will be essential that water sources are eliminated or kept to a minimum. Areas where tunnel walls show excessive infiltration should be sealed if possible. Water should not be allowed to pool or run through open trenches - drainage should be provided in a closed piping system.

The 35km tunnel is approx. 6 times the size of the current Main Ring tunnel. A recent study of dehumidification issues in the Main Ring showed that humidity comes from 3 principle sources besides the ventilation air intake. These are:

1. Transmission through concrete = 5 lb/hr
2. Trench and sump evaporation = 170 lb/hr
3. Allowance for water spray from leaks = 70 lb/hr

which gives a figure for moisture build-up in the Main Ring of 245 lb/hr. If we multiply this by the factor of 6 increase in tunnel length for the 3 TeV machine we would have over 1000 lb/hr in moisture released to the tunnel air.

This straight forward scaling does not directly apply, because water spray from leaks should not be an issue as only cryogens are anticipated in the tunnel. However, trench and sump evaporation, if multiplied by a factor of 6, would result in 1000 lbs/hr release to the air. Because the dolomite is not a good water conductor at a depth of 400 feet, we can be optimistic about controlling water penetration through the tunnel rock, especially if care is taken to seal the bad spots. Trench and sump evaporation can be improved by use of enclosed drain lines and sealed sumps.

With these considerations in mind, we would design a basic dehumidification system to handle 200 lbs/hr, with provision for expansion if conditions prove more extreme in reality.

Ventilation System Capacity:

The ventilation system shown in figure 1 allows for the minimum breathing requirements for tunnel personnel. Air is introduced into the tunnel at one of the two access shafts, and released at the other, the two halves of the ring being fed in parallel. The system shown has a capacity of about 15,000cfm which results in a 100fpm wind (1mph) through the tunnel and a 1"wc differential pressure end to end. This minimal ventilation reduces moisture load from outside air intake to a minimum, however, it also results in a 10 hour air purge time for the tunnel. The cost for this scale of system (not including tunnel ducting) would be about $700K[1]. It would have

---

1

150 ton air cooled chiller (1 ea)	$100K
15,000 cfm air handler with run around coils (1 ea)	$30K
15,000 cfm exhaust fan (1 ea)	$5K
250 gpm glycol pumps - chiller & run around (4 ea)	$20K
DDC controls and interlocks allowance	$50K
Piping and accessories allowance	$60K
Electrical allowance	$30K
Ductwork to and from shafts allowance	$40K
Equipment pads and supports allowance	$5K
TOTAL CONSTRUCTION COST W/ OH&P	$390K (w/o tunnel ductwork)
EDIA allowance (15%)	$60K

the ability to remove 200 lb/hr of tunnel moisture (in addition to outside air moisture) to keep the tunnel moisture below the dew point at 55F. The ventilation unit will have to be fitted with heating capacity for winter operation.

The ventilation system could be increased to allow for additional capacity. For every 1 lb/hr of tunnel moisture, 75cfm of additional air flow would be needed, at a unit cost of about $3.5K (not including tunnel ductwork). At a size of 150,000cfm (allowing the tunnel to be purged in 1 hour) the ventilation system would be able to remove 1800 lb/hr of moisture and with economies of scale would cost about $5M (not including tunnel ductwork). Air velocities in the tunnel would be about 1000fpm (10 mph) and require a differential pressure of 8"wc across the tunnel, which would require special design considerations.

Auxiliary Dehumidifiers:

Auxiliary tunnel dehumidification units could be placed down the tunnel length. At a half mile spacing between units, 44 units would be required. To preclude dead spots in the tunnel air movement, due to these units simply recirculating on themselves, it would probably be necessary to run the ventilation system concurrently. These units normally range from 10 lb/hr (size 300 unit) to 32 lb/hr (size 1200 unit) moisture removal capacity each. This would total 440 to 1408 lb/hr capacity for 44 units. The unit cost of this type of equipment runs about $2.5K per lb/hr capacity (not including electrical installation and assuming that no ducting is necessary). An example of a ventilation unit mounted in a 10 foot tunnel is shown in figure 2.

Other Considerations

The 3 TeV accelerator adds about 3 watts per meter in heating to the tunnel. This represents about a 100 kwatt heating load. This would increase the tunnel air temperature by about 20 degrees F at the exhaust point. This actually serves to help the dehumidification system in the following sense: In the Winter, the chiller system is turned off and the outside air is heated before injection into the tunnel. The extra heating from the accelerator components helps this process.

An Electron Ring

An electron ring will loose energy in the tunnel due to synchrotron radiation at a rate that may be as high as 50 Mwatts. Such a high heating load could not be air cooled, and would have to revert to another cooling medium - presumably water. The addition of a large water cooling capability into the tunnel could complicate the dehumidification problem, because of the potential for leaks. Recall that the Main Ring must allow for as much as a 70 lb/hr load that could come from leaky water systems.

Conclusions

A ventilation system for a 3 TeV ring need not be an excessive cost to the project. A great deal depends on the care taken to seal potential water sources in the tunnel. Based on the experience gained at the Main Ring tunnel, a system that can handle a 200 lb/hr load could very well be sufficient.

However, the 200 lb/hr system should be treated somewhat optimistically as a target. As more data become available, and plans for the electron machine firm up, the dehumidification requirements can be predicted with greater certainty.

Management Reserve allowance (25%)	$115K
G&A allowance (23%)	$130K
TOTAL PROJECT COST (w/o escalation)	$695K (say $0.7M)

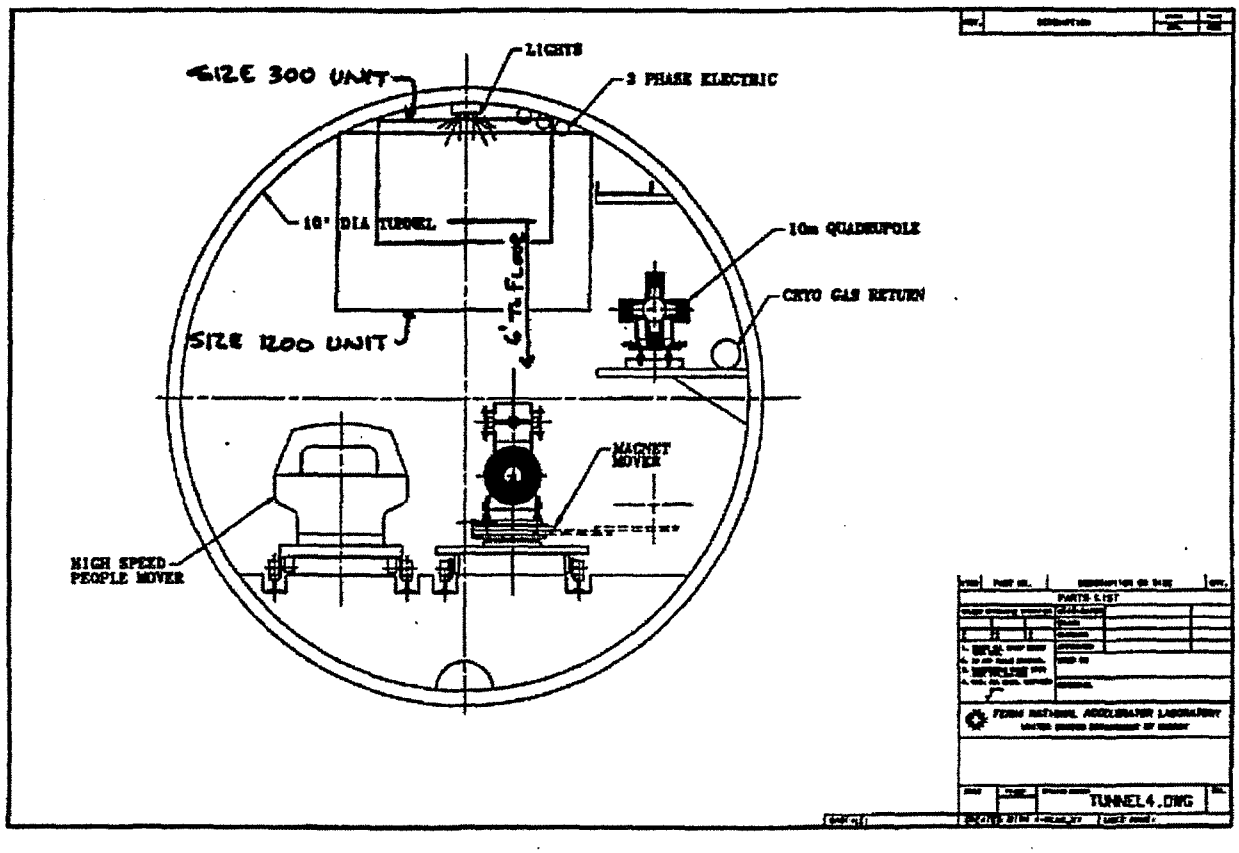
SIZE 300 UNIT
LIGHTS
3 PHASE ELECTRIC
10' DIA TUNNEL
10m QUADRUPOLE
CRYO GAS RETURN
SIZE 1200 UNIT
6' TO FLOOR
MAGNET MOVER
HIGH SPEED PEOPLE MOVER
PARTS LIST
FERMI NATIONAL ACCELERATOR LABORATORY
TUNNEL4.DWG

FERMILAB
ENGINEERING NOTE

SECTION | PROJECT | SERIAL-CATEGORY | PAGE

SUBJECT: 35 KM RING VENTILATION SYSTEM

NAME | DATE | REVISION DATE

VENTILATION AIR REQ = 25 CFM/PERSON x 600 PEOPLE (27 PEOPLE/MILE)
= 15,000 CFM NOMINAL

TUNNEL PURGE TIME = 10 HOURS

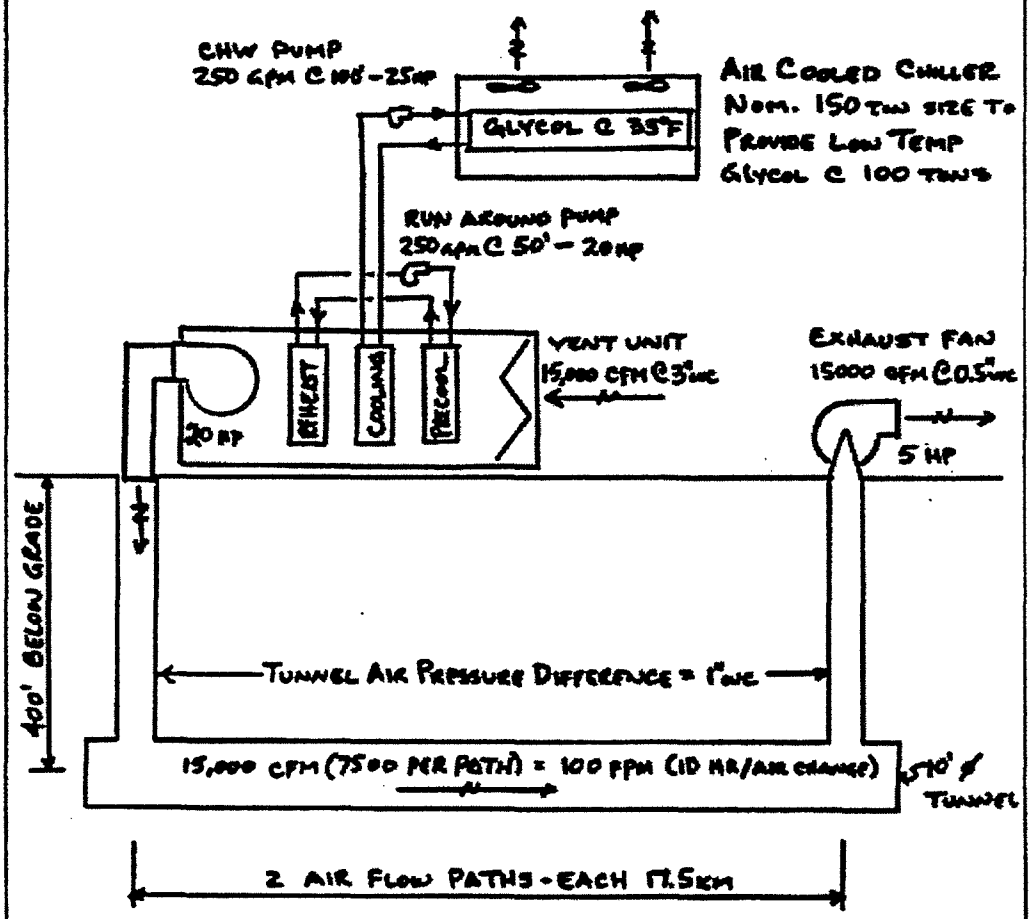

3 TEV RF COOLING SYSTEM
DESIGN PROPOSAL AND COST ESTIMATE

John A. Satti
July 1997

The proposed system for connecting the water to the 3 TeV rf accelerating system is similar to the existing Tevatron rf installation at F0. Air cooled chillers will be used since existing cooling ponds are too far from the 3 TeV location (~ 1.3 km) and chilled water is still required for tuning the cavities. For redundancy, a stand-by chiller will be installed per system. As shown on Figures 1 and 2, the power modules and the temperature control skids will be installed in a room near the accelerator enclosure. The average cooling load for the power supplies is 1600 kW and for the cavities tuning system 400 kW. The existing LCW temperature control skids for the eight cavities will be moved and retrofitted for the new location.

<u>3 Tev RF Power Amplifier-Driver Cooling System (Fig. 1)</u>

3/270 ton (948 kW ea.) reciprocating packaged chillers with air cooled condensers.	$177K x 3 =	$ 531K
Pump, tank, heat exchanger, piping, electric & controls for chillers.		$ 300K
95°F LCW System (700 GPM) for eight power stations		$ 510K

<u>3 TeV Cavities Temperature Control System (Fig.2)</u>

3/80 ton (280 kW ea.) air cooled chillers	$58K x 3 =	$ 174K
Pump, tank, heat exchanger, piping, electric and controls for chillers.		$ 250K
45°F Chilled Water System (350 GPM) for eight temperature control skids		$ 410K
Eight skids moved, retrofit work, and connection to cavities.		$ 180K

<u>Total Estimate Including EDI&A ('97 $) $ 2,355K</u>

The above costs are based using Means estimate and experience from the MI Utilities project.

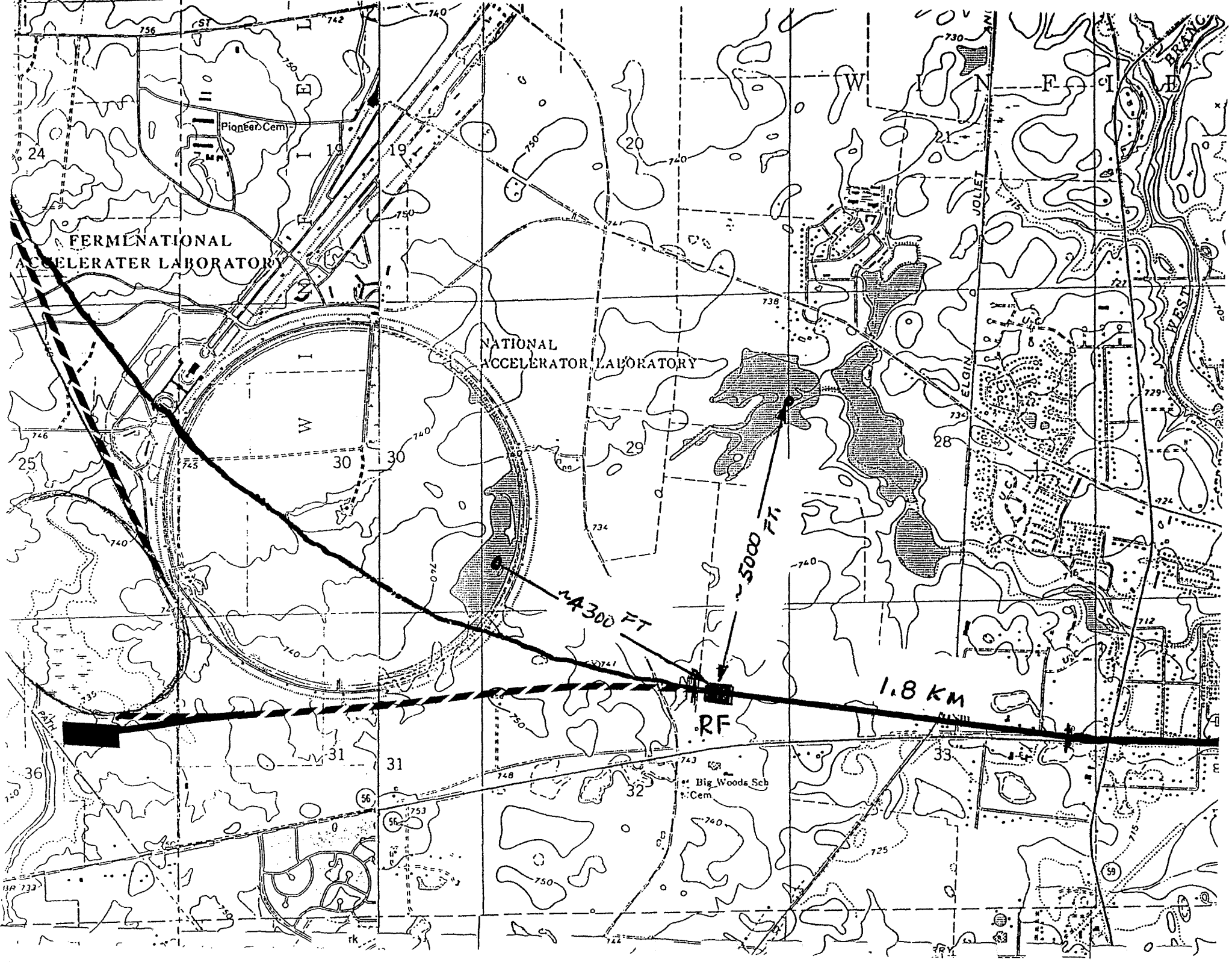
FERMI NATIONAL
ACCELERATER LABORATORY
NATIONAL
ACCELERATOR LABORATORY
Pioneer Cem
Big Woods Sch
Cem
~4300 FT
~5000 FT
1.8 KM
RF
JOLIET
ELGIN
WEST
BRANCH

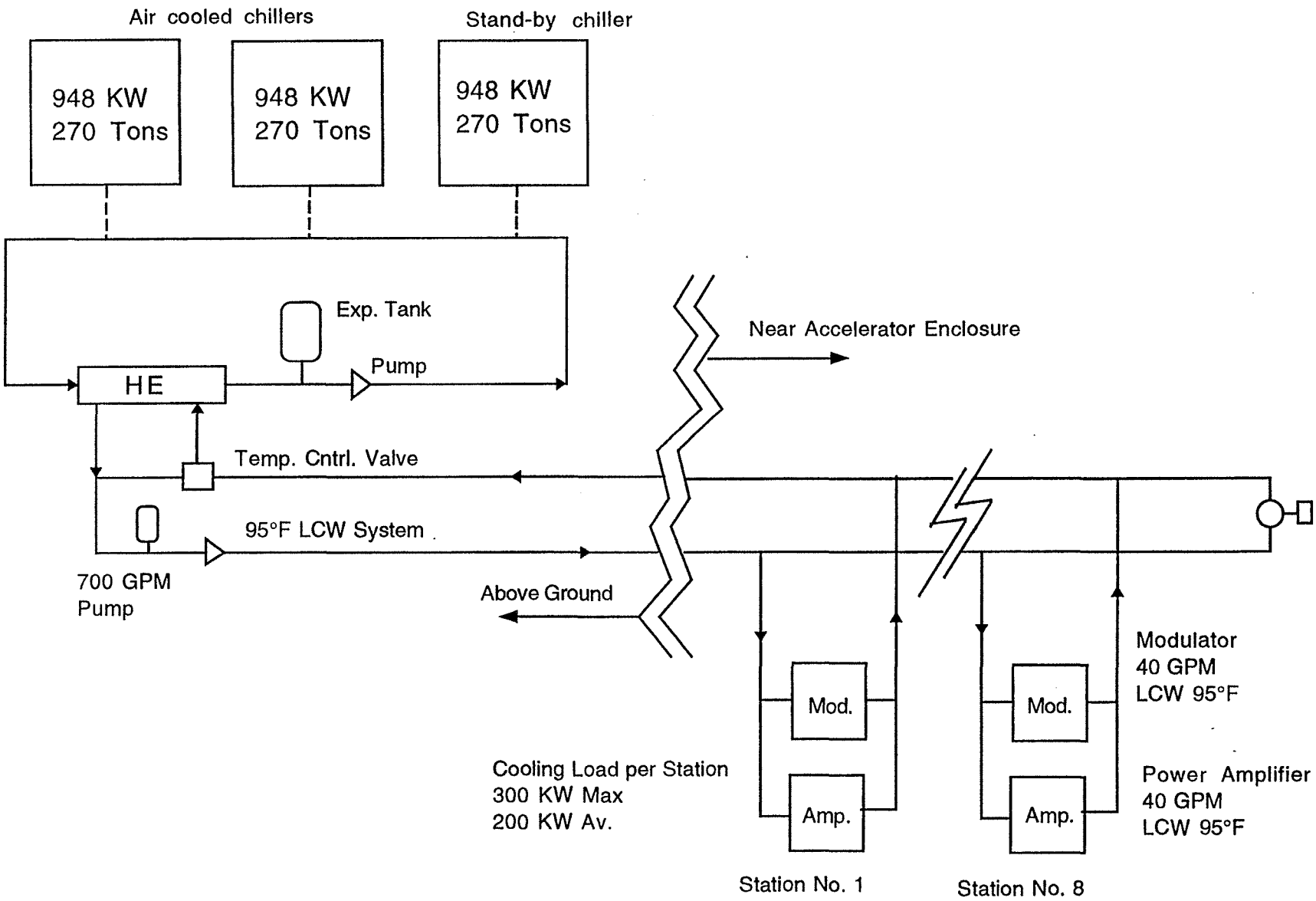

3 TeV RF Power Amplifier-Driver Cooling System

Simplified Schematic

Fig. 1

John Satti, July 1997

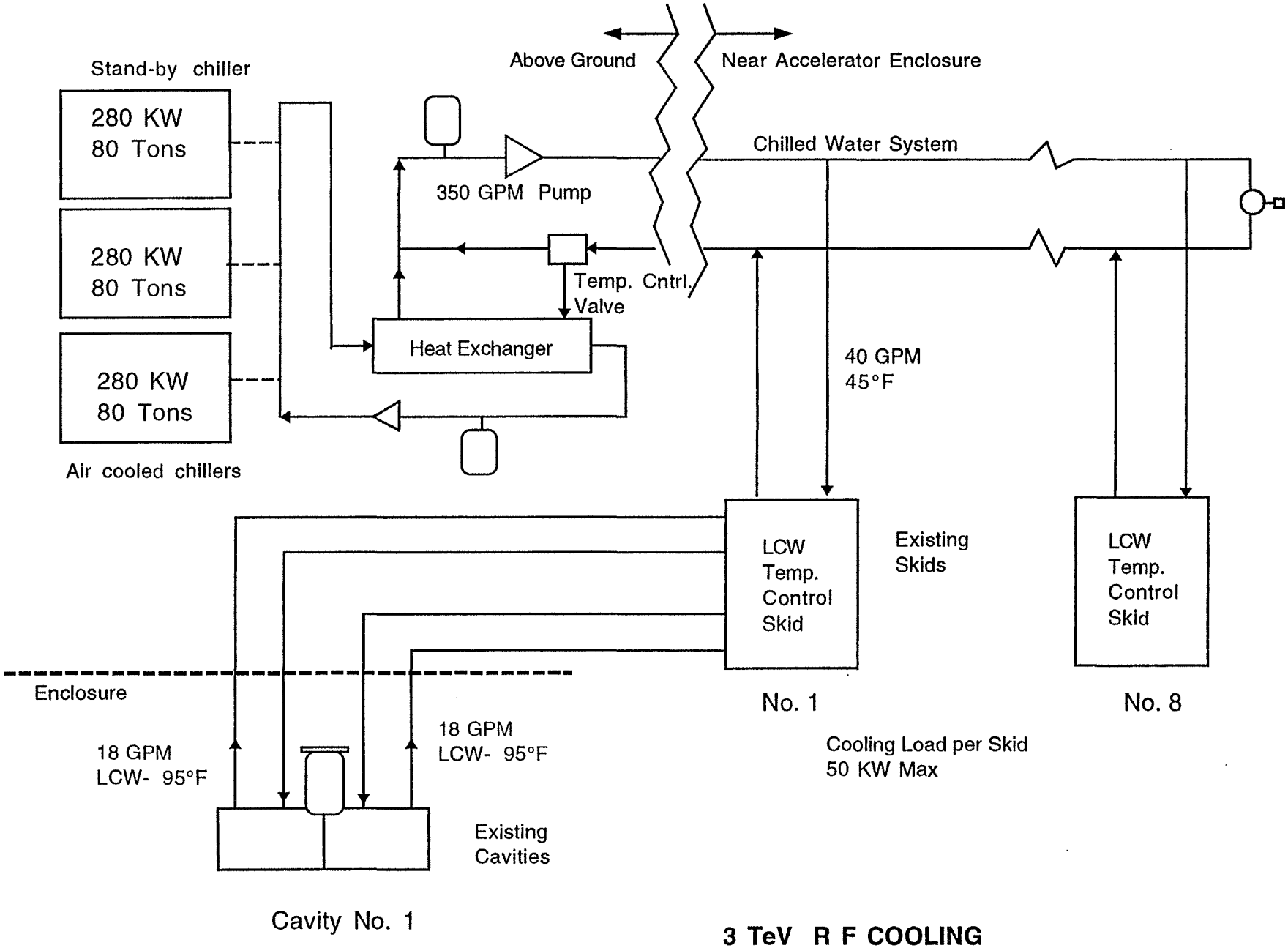

3 TeV R F COOLING
TYPICAL CAVITY TEMPERATURE CONTROL SYSTEM
Simplified Schematic

Fig. 2

John Satti, July 1997

Section 5: Five Year Plan for R & D

Proposed Research and Development Plan

Ernest Malamud

September 1, 1997

The overall R&D goal of the VLHC Study Group over the next 1-2 years is to evaluate feasibility and cost. Cost goals not only include lowering the capital cost for the collider, but also lowering the operating cost by efficient cryogenics, strong emphasis on reliability, and the use of automated installation, alignment, and repair methods wherever possible.

More specifically:

- The VLHC Study Group will produce a detailed design with cost estimates for 3 TeV (low-field) and 3 TeV (medium field) injectors so a choice can be made. This includes carrying out prototype work on all components of the low-field design.

- A Design Study for a 100 TeV cm pp collider built in the Fermilab region using either low or high field magnets will also be done on a somewhat longer time scale. An outline for this Design Study exists, responsibility for chapters and sub-chapters is being assigned and work is getting done.

- Prototype work will lead in a few years to a technical design.

- The High Field approach has a longer time scale. The key is the magnet. A goal is to have an accelerator usable magnet in 5 years

The proposed R&D plan is divided into 7 areas, each with a set of goals. For each a rough estimate of the necessary personnel, materials and supplies can be made. In the tables that follow the personnel costs are based on the following SWF multipliers:

physicist	$72,800
engineer	$79,900
designer/drafter	$60,450
technician	$46,100
administrative	$33,500

To the SWF totals 10% is added for support: computers, office supplies, travel etc. Escalation is not included.

5-year totals by system			
	M&S	personnel	total
Physics/Detector	$220	$1,725	$1,945
Accelerator Physics	$400	$3,462	$3,862
Magnet	$5,800	$3,967	$9,767
Cryogenics	$825	$1,713	$2,538
Vacuum	$350	$735	$1,085
Instrumentation & Controls	$525	$1,686	$2,211
Construction & Installation	$690	$2,700	$3,390
Total	**$8,810**	**$15,988**	**$24,798**

This 5-year effort totals approximately $25M of which 2/3 are personnel costs.

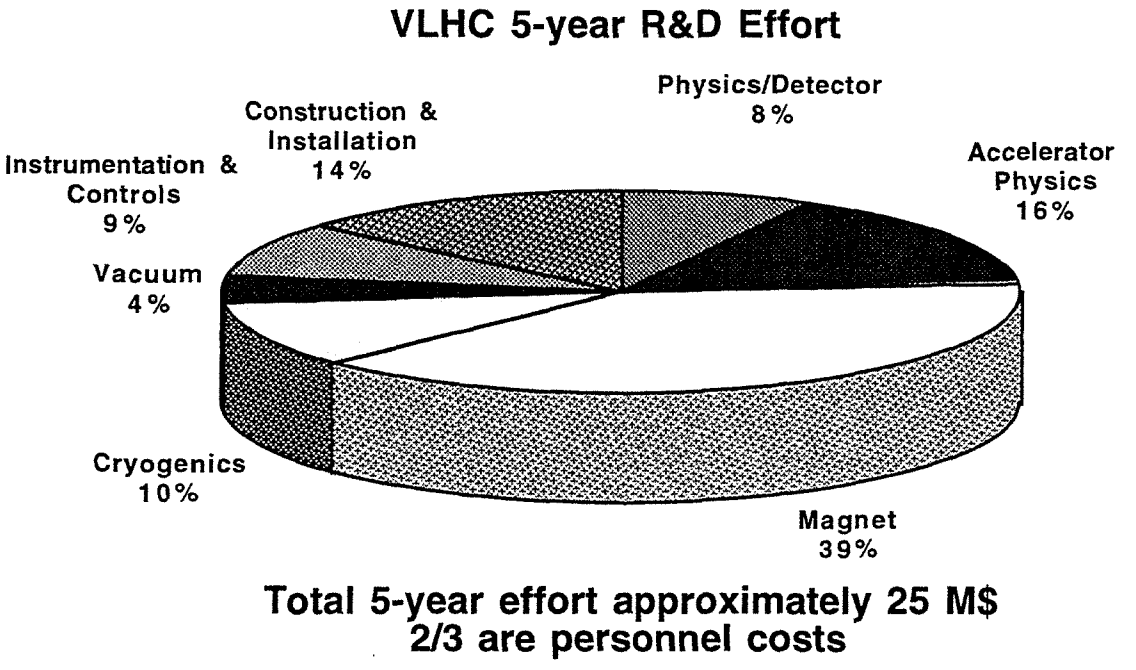

This vigorous R&D program will develop the physics case for the VLHC including preliminary detector parameters, work on accelerator dynamics and find limits imposed by and solutions to instabilities, produce preliminary parameters, conduct R&D on magnets including possible the use of the new emerging high-temperature superconductors. Furthermore we will work with industry on tunneling and robotics. Partnerships with the private sector will be one of the components of our plans to build public support for the VLHC.

Physics and Detector Team

- Hold an annual Spring VLHC Physics/Detector Workshop
- beginning in FY 98 a part-time physicist will work on the detector/machine interface
- FY 00 - 01 begin detector R&D

		FY 98	FY 99	FY 00	FY 01	FY 02	5 yr tot
People required (FTE)							
	physicist	0.5	0.5	1	4	8	
	engineer		0.5	0.5	1	2	
	designer/drafter			0.5	0.5	0.5	
	technician			1	1	1	
	adminstrative						
TOTAL		**0.5**	**1**	**3**	**6.5**	**11.5**	
K$:							
TOTAL M&S		$10	$10	$20	$60	$120	$220
TOTAL SWF		$36	$76	$189	$447	$819	$1,568
add 10 % to SWF		$4	$8	$19	$45	$82	$157
TOTAL		$50	$94	$228	$552	$1,020	$1,945

Accelerator Physics Team

- Has primary responsibility for the Design Study -- goal is distribution by Dec. 1998
- In Spring 1998 hold a workshop on VLHC Accelerator Physics
- During FY 98-99 mostly computational work
- $\geq$ FY 00 Accelerator experiments can begin
- Development of lattice parameters for all machines
    - Low-field 3 TeV
    - Medium (high) field 3 TeV
    - Low-field 50 TeV
    - High field 50 TeV
- Theoretical and experimental investigation of the Resistive Wall Instability
- investigate feasibility of optical stochastic cooling

		FY 98	FY 99	FY 00	FY 01	FY 02	5 yr tot
People required (FTE)							
	physicist	3	4	4	6	8	
	engineer			3	4	4	
	designer/c	0.5	0.5	0.5	0.5	0.5	
	technician			1	2	2	
	adminstrative				1	1	
TOTAL		**3.5**	**4.5**	**8.5**	**13.5**	**15.5**	
K$:							
TOTAL M&S		$50	$50	$75	$100	$125	$400
TOTAL SWF		$249	$321	$607	$912	$1,058	$3,148
add 10 % to SWF		$25	$32	$61	$91	$106	$315
TOTAL		$323	$404	$743	$1,104	$1,289	$3,862

Low-field Magnet Team

- Iron design including crenelations
- Transmission line conductor R&D
- Advanced iron fabrication techniques
- Power Supply, Quench protection, and conductor design

- FY 98 - 99 materials research (with industry); joints
- FY 00 100 meter prototype
- FY 00 100 kA power supply and current leads
- FY 02 low-field VLHC systems test
- prototypes for beam lines (continue perm magnet program)
- correction magnet prototypes
- Alternate low-field magnet, E-magnet

High-field Magnet Team
- FY 98 materials investigations
- FY 99 physics and engineering calculations
- FY 00 initial prototype effort begins
- FY 02 first high field magnet

		FY 98	FY 99	FY 00	FY 01	FY 02	5 yr tot
People required (FTE)							
	physicist	1.5	3	3	3	5	
	engineer	0.5	1.5	2.5	4	5	
	designer/c	0.25	2	3	4	4	
	technician	0.25	1	2	3	4	
	adminstra	0.25	0.5	1	1	1	
TOTAL		**2.75**	**8**	**11.5**	**15**	**19**	
K$:							
TOTAL M&S		$300	$500	$1,000	$1,500	$2,500	$5,800
TOTAL SWF		$184	$522	$725	$952	$1,223	$3,606
add 10 % to SWF		$18	$52	$73	$95	$122	$361
TOTAL		$503	$1,074	$1,798	$2,547	$3,846	$9,767

Cryogenics Team:
- heat Leak measurements
- evaluation of new-technology superinsulation
- low heat leak spider development,
- cold-pipe material evaluation and prototype
- cryogen distribution line design
- conceptual design and cost optimization of cryo system
- this team will also be concerned with powering the magnets and quench protection

		FY 98	FY 99	FY 00	FY 01	FY 02	5 yr tot
People required (FTE)							
	physicist	0.25	0.5	1	1	1	
	engineer	0.25	0.5	1	2	3	
	designer/drafter		1	1	1	1	
	technician	1	1	2	2	2	
	adminstrative		1	1	1	1	
TOTAL		**1.5**	**4**	**6**	**7**	**8**	
K$:							
TOTAL M&S		$50	$100	$200	$200	$275	$825
TOTAL SWF		$84	$216	$339	$419	$499	$1,557
add 10 % to SWF		$8	$22	$34	$42	$50	$156
TOTAL		$143	$338	$573	$661	$824	$2,538

Vacuum Team

- It is expected that some of this work will be carried out KEK under the Japan-US collaboration
- Engineering analysis of thermal effects
- Determine if NEG material heated from inside or outside
- build vacuum system to measure system parameters
- determine pump spacing and system response times
- learn how to handle long length objects
- build 150 m test setup (most equipment available)
- perform roughing calculations and tests
- purchase/evaluate aluminum, non-air operated gate valves
- welding machines to join ends

		FY 98	FY 99	FY 00	FY 01	FY 02	5 yr tot
People required (FTE)							
	physicist	0.25	0.5	0.5	1	1	
	engineer	0.25	0.25	0.25	0.5	1	
	designer/drafter		0.25	0.25	0.5	0.5	
	technician	0	0.5	1	1	1	
	adminstrative						
TOTAL		**0.5**	**1.5**	**2**	**3**	**3.5**	
K$:							
TOTAL M&S		$40	$60	$75	$75	$100	$350
TOTAL SWF		$38	$95	$118	$189	$229	$668
add 10 % to SWF		$4	$9	$12	$19	$23	$67
TOTAL		$82	$164	$204	$283	$352	$1,085

Instrumentation and Controls Team

- "Standard" devices: BLM's, BPM's
- Special devices: construct one/year -- test on Tevatron
    - electron beam transverse emittance measurement
    - synchrotron light device
    - multiple electrode pickup

- controls: prototype a "LUMP"; this includes:
    - two split-ring BPM's with log amps, sample & hold
    - extruded-aluminum or heliax loss monitors, with power
    - 10 MHz digitizers for BPM signals
    - local controls computer
    - network connection
    - correction element power supplies
    - vacuum controls and readback
    - clock system-- event clock and beam sync clock
- packaging, heat loads, demonstrate connectivity
- research on radiation hardness of single-mode fibers

		FY 98	FY 99	FY 00	FY 01	FY 02	5 yr tot
People required (FTE)							
	physicist	0.5	1	3	3	4	
	engineer	0.25	0.25	1	1	2	
	designer/drafter		0.25	0.5	0.5	0.5	
	technician			1	2	2	
	adminstrative						
TOTAL		**0.75**	**1.5**	**5.5**	**6.5**	**8.5**	
K$:							
TOTAL M&S		$50	$50	$100	$150	$175	$525
TOTAL SWF		$56	$108	$375	$421	$573	$1,533
add 10 % to SWF		$6	$11	$37	$42	$57	$153
TOTAL		$112	$169	$512	$613	$806	$2,211

Construction and Installation Team

- Develop cost models to understand effect of varying parameters -- this work has already begun with two independent efforts; results will be available before the end of CY 97.
- carry out (or observe) Tunnel Lining experiments
- Utilities: tunnel environment, beam loss and radiation issues
- power distribution to "lumps"
- work on installation issues: layout (more than one machine), invert (tunnel floor), stands
- build full-scale tunnel mockups
- conduct vibrations studies and investigate other causes of emittance growth; this work has already begun -- some of it will be carried out in TARP tunnels to understand the change of the noise spectrum with depth
- begin cutter optimization in FY 00 (subcontract to the Colorado School of Mines)
- FY 00 design of installation vehicles, alignment robot followed by prototype work

		FY 98	FY 99	FY 00	FY 01	FY 02	5 yr tot
People required (FTE)							
	physicist	0.25	0.25	2	4	5	
	engineer	0.25	0.5	3	4	6	
	designer/drafter		0.25	1	1	1	
	technician		1	2	2	2	
	adminstrative						
TOTAL		**0.5**	**2**	**8**	**11**	**14**	
K$:							
TOTAL M&S		$75	$90	$150	$175	$200	$690
TOTAL SWF		$38	$119	$538	$763	$996	$2,455
add 10 % to SWF		$4	$12	$54	$76	$100	$245
TOTAL		$117	$221	$742	$1,015	$1,296	$3,390

Ramp up of the effort

An organization now exists that is focusing and coordinating the efforts. Our R&D goals are aggressive and depend on sufficient resources becoming available. Clearly, Fermilab's rich future physics program must take priority, but gradually resources will become available. e.g. upon completion of accelerator physics calculations for the Main Injector/Recycler -- accelerator physicists will be freed up to work on VLHC. Completion of magnet building (retrofitting main ring parts) for the Main Injector may free up a few magnet designers and specialists. Some of these people are already working part-time on the VLHC magnets. With completion of the 1997-1998 long shutdown some mechanical and electrical engineers will be available.

		FY 98	FY 99	FY 00	FY 01	FY 02	5 yr tot
People required (FTE)							
physicists		6.25	9.75	14.5	22	32	84.5
engineers		1.5	3.5	11.25	16.5	23	55.75
designers/drafters		0.75	4.25	6.75	8	8	27.75
technicians		1.25	3.5	10	13	14	41.75
adminstrative		0.25	1.5	2	3	3	9.75
TOTAL		**10**	**22.5**	**44.5**	**62.5**	**80**	**219.5**
K$:							
TOTAL M&S		$575	$860	$1,620	$2,260	$3,495	$8,810
TOTAL SWF		$686	$1,458	$2,891	$4,103	$5,397	$14,535
add 10 % to SWF		$69	$146	$289	$410	$540	$1,453
TOTAL		$1,330	$2,464	$4,800	$6,774	$9,431	$24,798

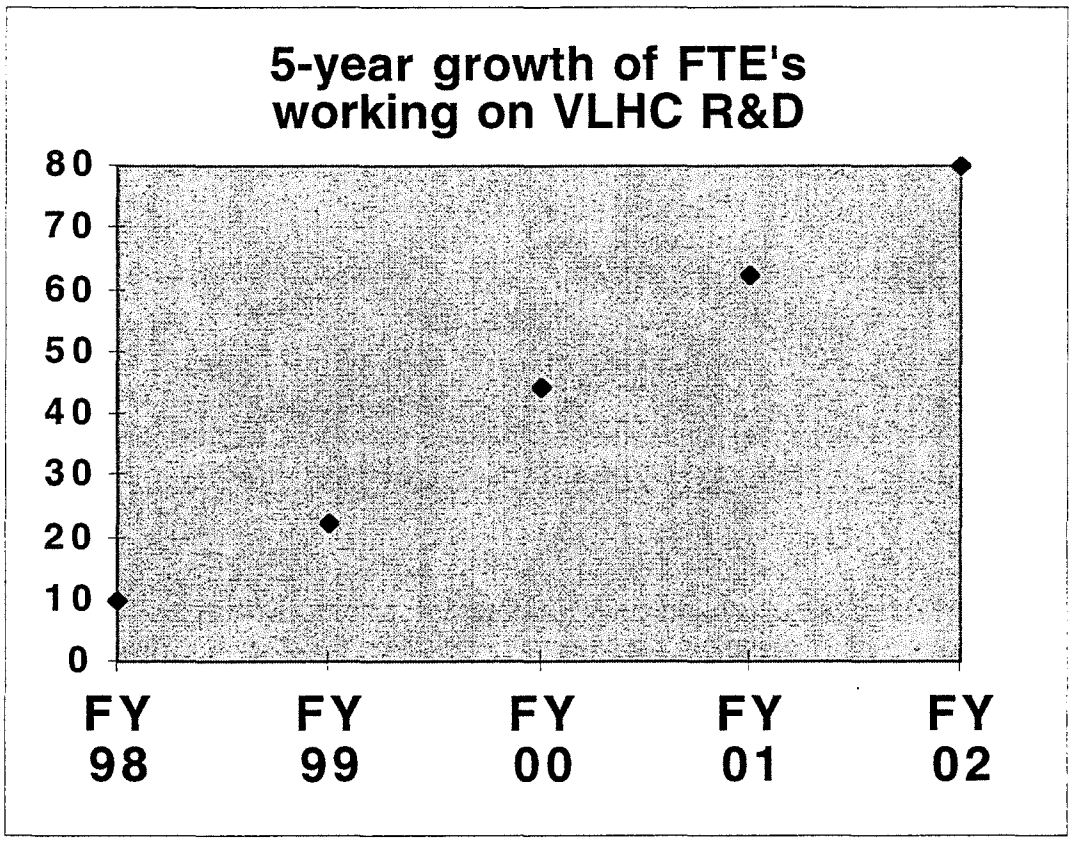
5-year growth of FTE's working on VLHC R&D
80
70
60
50
40
30
20
10
0
FY 98
FY 99
FY 00
FY 01
FY 02

APPENDIX

J. Norem et al, "An e^+e^- Top Factory in a 50 + 50 TeV Hadron Collider Tunnel''

J. Norem, "Electron/Proton and Electron/Positron Collider Options''

D. Krakauer and J. Norem "The e/p Option in the 3 TeV Booster"

AN e^+e^- TOP FACTORY IN A 50 + 50 TeV HADRON COLLIDER TUNNEL

J. Norem, J. Jagger, S. Sharma, Argonne National Laboratory, Argonne IL 60439 USA
E. Keil, CERN, CH-1211 Geneva 23 Switzerland
G. W. Foster, E. Malamud, Fermilab, Batavia IL 60510 USA
E. Chojnacki, Cornell University, Ithaca NY 14853
D. Winn, Fairfield University, Fairfield CT 06430 USA

Abstract

We present the parameters of an e^+e^- collider sized for the tunnel of a 50 + 50 TeV superferric hadron collider[1]. Assuming a diameter of 170 km and a maximum radiated power of 100 MW, this collider should have a maximum energy of 500 - 600 GeV (c.m.) and should be able to produce a luminosity $L = 0.9 \cdot 10^{33}$ $cm^{-2}sec^{-1}$ at a center of mass energy of 360 GeV, (somewhat less at higher or lower energies) which would make it useful for producing top quarks or light Higgs bosons. Design problems include the very low field magnets, synchrotron radiation power, beam stability, and heat removal systems. Preliminary magnet, vacuum chamber and cooling designs are presented along with possible construction techniques, and some costing algorithms. We also consider an ep collider with 70 GeV electrons and 5 TeV protons as an injector.

1 PARAMETERS

We have considered an e^+e^- collider[2] located in the tunnel of a 50 + 50 TeV hadron collider, which could operate at energies sufficient to study $e^+e^- \rightarrow t\bar{t}$ and light Higgs production[3]. If this facility was operated as an ep collider, a c.m. energy of $\sqrt{s} = 7$ TeV could be reached.

The most important parameters of a $t\bar{t}$ factory operating at a beam energy of 180 GeV are shown in Table I. A complete parameter set is on the WWW[4]. We assume a total RF generator power available at the cavity windows of 100 MW, and a superconducting RF system similar to that of LEP operated at a gradient of 5 MV/m. We assume that the collider consists either of a single ring, operated with pretzels and parasitic beam-beam collisions every quarter betatron wavelength, and have adapted phase advance, arc tune Q and number of bunches k accordingly, or of two rings. Wiggler magnets are used to make the horizontal emittance a factor of 10 higher than its equilibrium value without wigglers. The advantage is a smaller value of the synchrotron tune, the disadvantages are a smaller dispersion in the arcs, a possibly smaller dynamic aperture and a larger momentum spread in the beam. We have not checked that the dynamic aperture is large enough.

We assume that the aperture is filled and that the beam power limit is reached at a beam energy of 180 GeV. If we control the beam size such as to remain at the beam-beam limit over a range of energies, the luminosity is proportional to E^2 for $E \leq 180$ GeV, and proportional to E^{-3} for $E \geq 180$ GeV. We increase the phase advance of the arc cells in steps from $\pi/8$ at 100 GeV to $\pi/2$ at 250 GeV. In order to satisfy the pretzel condition, all phase advances are integral fractions of $\pi/2$. We assume that wiggler magnets, installed in wiggler insertions where H has four times the arc value, are used to make the horizontal emittance a factor of ten larger than its equilibrium value without wigglers. Table II shows the proposed variation of phase advances and wiggler excitation. At energies below 250 GeV, the desired beam size can often be reached by more than one combination of phase advance $\mu/2\pi$ and emittance increase F_ε. In Table II, we favor higher values of $\mu/2\pi$ and F_ε in order to restrict the variation of the synchrotron tune Q_s with the energy E. It is indeed possible to achieve the strong variation of the beam radii with E by adjusting the phase advance in steps and using emittance wigglers.

Table I: The Parameters of a Very Large Lepton Collider

Beam energy E /GeV	180
Circumference C /m	531000
Luminosity L /$cm^{-2}s^{-1}$	9.15E+32
Beam-beam tune shift $\xi_x = \xi_y$	0.03
Beta functions at IP $\beta_x^* : \beta_y^*$ /m	1.0 : 0.05
Beam emittances $\varepsilon_x : \varepsilon_y$ /nm	32.5 : 1.7
Beam radii at IP $\sigma_x^* : \sigma_y^*$ /μm	180 : 9.01
Bunch population N	8.04E+11
Total current / beam I_b /mA	37.2
Number of bunches /beam k	512
Bending radius ρ /m	72628
Injection Energy E_{inj} / GeV	50
Dipole fields $B_{max} : B_{inj}$ /mT	8.3 : 2.3
Phase advance / cell $\mu/2\pi$	0.125
Arc tune Q	258
Cell Length L_p /m	249
Beta functions in arcs $\beta_{max} : \beta_{min}$ /m	488 : 218
Beam radii $\sigma_x : \sigma_y$ /mm	4.3 : 2.8
Synchrotron radiation loss U_s /MeV	1376
Aperture radii $A_x : A_y$ /mm for 10σ	53 : 38
Center of mass energy spread σ_E /GeV	0.26
RF voltage V_{RF} /MV	1616
Total generator power P_g /MW	102

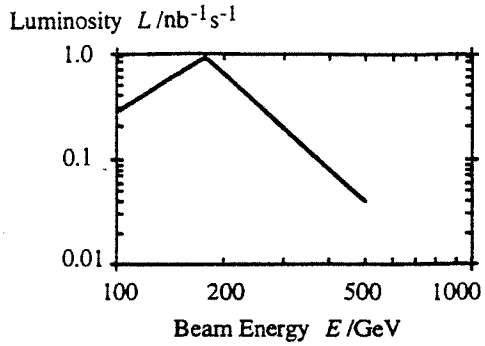

Figure 1, The energy dependence of the luminosity

The aperture limited luminosity is given by the expression $L_a = \pi f k \xi \sigma_x^* \sigma_y^* \gamma^2 / r_e^2 \beta_y^*$, where the revolution frequency $f \propto 1/\rho$, and the number of bunches $k \propto \rho$ if the bunch spacing is fixed by the hardware required to separate the beams, thus L_a is independent of ρ. If power limited, $L_P = (3/16\pi)\xi\rho P / r_e^2 E_e \beta_y^* \gamma^3$, where E_e is the rest mass of the electron and r_e its radius[2]. The maximum luminosity occurs when $L_a = L_P$, and this energy, E_{max}, is proportional to $\rho^{1/5}$. Thus the specific dimensions of the tunnel only weakly affect the operating parameters.

The energy resolution of the collider, σ_E ~0.26 GeV, in the center of mass at the $t\bar{t}$, would be useful for high resolution studies of threshold behavior and may be better than other collider options.

The polarization time is about 19 hours at 180 GeV, and comparable to the typical duration of a physics fill. The tolerance on the closed orbit harmonic at the spin tune is very tight, even with Siberian snakes. Therefore, no useful degree of polarization is expected.

The requirements that all three degrees of freedom are damped by synchrotron radiation imposes constraints on the length of all quadrupoles, as does nonlinear radiation damping [3].

Table II. Luminosity L, proposed phase advances $\mu/2\pi$ in the arc cells, emittance increase factors F_ε with wiggler magnets and circumferential RF voltage V as functions of the beam energy E, (L, I and V are evaluated at the lower end of the energy range).

E /GeV	L /nb^{-1}s^{-1}	$\mu/2\pi$	I /mA	F_ε	V /GV
100→136	0.28	0.0625	21	4→2.2	0.2
136→180	0.52	0.0833	29	5.2→3	0.7
180→250	0.92	0.125	39	10→1	1.8
250→335	0.34	0.25	10	8→1	5.3

2. RF SYSTEM

Table II also shows the total current in one beam I, the luminosity L, and the total circumferential RF voltage V as a function of energy. The total RF generator power at the cavity windows increases proportional to E^5 up to 180 GeV. There it reaches 100 MW, and remains at that value for higher energies by design, although the required voltage continues to rise as E^4. Above 250 GeV, the RF voltage and the length of the RF system, assuming ~6 MV/m, become absurd.

Current technology limits input power to superconducting cavities to about 500 kW. Using a very reasonable gradient of 6 MV/m in a superconducting cell with 0.425 m active length, operating at a synchronous angle of 31.6° and matched at 160 mA beam loading gives 3 cells per cavity for 588 kW input power. Klystrons providing 1.7 MW at 350 MHz determine 3 cavities per klystron and 70 klystrons for 1.4 GV synchrotron loss. This system should benefit from expected improvements in RF coupler and window technology, superconducting gradients and klystron power.

Instabilities related to higher order monopole and multipole modes can be managed by aggressive higher order mode damping techniques, which are available. Coupled bunch longitudinal instabilities, exacerbated by cavity detuning being comparable to the revolution frequency are a concern.

3 MAGNET ISSUES

Since the maximum dipole field required is only 23 mT even for 500 GeV, one could use thin steel laminations separated by large nonmagnetic spacers, as in LEP, and stabilized against thermal expansion with materials like invar. Error fields should be on the order of 4 x 10^{-4} of the dipole fields, and the earth's field is on the order of 0.05 mT, thus it will be necessary to carefully shield this field from the beam, particularly at injection when the dipole field is ~2.3 mT, (assuming E_{inj} = 50 GeV). If the electron ring was used in combination with the hadron ring for e/p collisions, even larger fields from the superferric magnet and return current must be shielded.

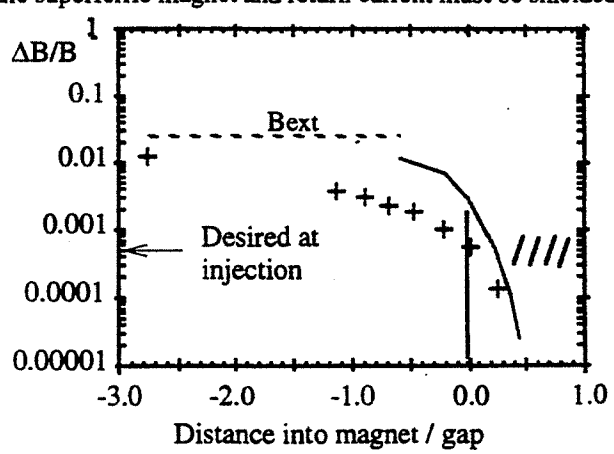

Figure 2, Measured error fields after degaussing, with parametrizations of Brown and Spencer. ΔB/B = (measured field) / (field at injection), which is equivalent to the measured field in mT. The hatched line shows level of residual fields.

In order to evaluate experimentally the degree of shielding one would expect from the normal magnet yoke itself we constructed a prototype of a C magnet from 0.025" laminations spaced by 0.25". This prototype is 0.2 m long and made from magnet laminations cut and glued to make a C magnet with a gap height of 3.81 cm. Measurements were made with a Bartington MAG-01 single axis fluxgate magnetometer. The magnet was degaussed by exciting it at 60 Hz, with slowly decreasing amplitude from 700 A-turns to zero. The results are shown in Figure 2, above, compared with Brown and Spencer[5].

Since the total mass of iron required is ~ 20 kg/m the magnet will rely on an external support structure against mechanical motion and thermal expansion. Possible component dimensions are shown in Figure 3.

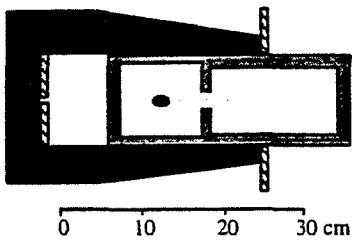

Fig 3. Dipole yoke, 4 conductors and vacuum chamber

4 VACUUM ISSUES

The vacuum system is defined by the comparatively small amount of photoproduced gas per unit length, and the large radius of the ring, which makes the vacuum chamber effectively straight between discrete absorbers. The average photodesorption of gas per meter by synchrotron light is given by $Q_{gas}/m = 24.2EI\eta/2\pi R$ [6], where Q_{gas} is the gas load in Torr-L/s, and η is the photodesorption coefficient, roughly 10^{-5}- 10^{-6}. At 180 GeV a pressure of 10^{-9} Torr could be reached with an average pumping speed of ~ 2 $Ls^{-1}m^{-1}$.

We consider a vacuum chamber with a beam channel and a antechannel containing NEG strips, discrete absorbers and ion pumps. The slot impedance is a concern for beam stability. OFHC copper absorbers 0.6m long protruding into the antechannel would protect the vacuum chamber from synchrotron radiation. With discrete absorbers the gas load and ionizing radiation would be localized and handled more efficiently. Each absorber would intercept 19 kW of power with a surface temperature rise of 150 °C. Bulk water temperature rise in the absorber with 4 gpm of water flow would be 18 °C.

Since the machine would be far underground and distances would be large, we have considered sinking the 200 W/m of synchrotron power directly into the rock by taking the cooling water from the synchrotron absorbers through an array of pipes extending from the tunnel. Since the conductivity of rock is low but the specific heat is high, heat tends to be absorbed rather than conducted away. The required power can be absorbed by an array of pipes extending on the order of 3 m in one direction from the tunnel, water in the rock would help heat conduction.

We anticipate sharing a ~3 m diameter tunnel with the hadron collider magnets and a two way railroad, with access points to the surface located far apart.

5 COST MINIMIZATION

The cost of the facility is expected to be dominated by the cost of the tunnel, magnet/vacuum systems and RF. Tunnel costs have been estimated at 1000 $/m from a number of sources[1]. Bending magnet costs for a system of length l should roughly scale like $Bl \propto B\rho \propto E$ for a given magnet cross section, however the very low dipole field permits the use of more compact coil structures which should permit a considerably smaller and lighter stamping than that used in LEP. The RF cost has been roughly estimated at <0.25 $/V, although R&D directed at producing higher gradients could perhaps reduce this.

6 THE INJECTOR: AN ep COLLIDER

The injector for the hadron and e^+e^- colliders would be a proton ring of 3-5 TeV and an electron ring, both with a circumference of 15 - 30 km. If the >1.8 GV, 100 MW rf system for the e^+e^- collider were installed in the injector ring, an energy E_e ~ 80-100 GeV might be obtained. Use of these rings as an ep collider would thus be possible up to $\sqrt{s}$ ~1000 - 1350 GeV. The power to the vacuum chamber, P_{av} ~8 W/mm, can be cooled with simple water channels on the outside circumference.

7 CONCLUSIONS

An e^+e^- collider could be added to a 50+50 TeV low field hadron facility permitting high energy lepton physics as well as ep physics in an integrated facility.

8 REFERENCES

[1] G. W. Foster and E. Malamud *Low-cost Hadron Colliders at Fermilab - A Discussion Paper,* Fermilab TM-1976 June 1996. Updated parameters and references are located at http://www.ap.fnal.gov/PIPE/.

[2] E. Keil, *Storage Ring Design,* Physics of High Energy Accelerators, Fermilab '81, AIP Conference Proc.#87 (1982), 824.

[3] J. Norem and E. Keil, *1996 Snowmass Workshop Proceedings.*

[4] http://wwwslap.cern.ch/keil/Design/vllc100-500.lis

[5] K. Brown and J. E. Spencer, 1981 Part. Accel. Conf. Washington, D. C. (1981) p2568

[6] *PEP-II, An Asymmetric B Factory,* SLAC-PUB - 418, (1993).

Electron Options at Fermilab

	Site Buster injector	HERA	LHC w LEP	VLHC
coll. options	ep	ep	e^+e^-/ep	e^+e^-/ep
C, km	34000	6336	26660	550000
Proton Ring				
E_{Max}, GeV	3000	820	7000	50000
B(dipole), T	2.1	4.6	8.46	2.1
Electron Ring				
E_{Max}, GeV	81	28	100	250
B(dipole), T	0.068	0.355	0.135	0.008
P, MW	50	6.1	100	100
Pwr Den, kW/m	2	1.2	4	0.2
V(rf), MV	1000	122	3000	3000
I, A	0.05	0.06	0.050	0.050
ep Collider				
$\sqrt{s}$, GeV	988	*300*	1673	7071
L, 10^{30} $cm^{-2}s^{-2}$	47	16	57	142
$cost_{e\ ring}$, * HERA	2.9	1	4	4
$cost_{rf}$, M$	250	30	750	750
const. start	2007	*1984*	2015	2015

7/30

Electron/Proton and Electron/Positron Collider Options

James Norem
Argonne National Laboratory

We are considering both ep and e^+e^- colliders which would operate in the tunnels of the VLHC proton collider system. The large 500 - 1000 km circumference tunnel could be used for an e^+e^- collider which would reach a center of mass energy of 500 - 600 GeV and a ep collider collider operating at $\sqrt{s} \sim 7$ TeV, and the 34 km circumference injector tunnel could accommodate an ep collider which would reach $\sqrt{s} \sim 1$ TeV. These machines would have a physics reach far beyond what is available today.

The proposed facility could be built in stages, with the electron ring in the 34 km injector built first and used for e/p collisions. Since the same rf system would be required for maximum performance of the two machines, it seems logical to assume that the rf could be used first in the injector to produce 80 GeV electrons. The majority of the rf could then be moved to the larger ring to produce high energy ep and e^+e^- collisions when that ring became available, leaving the injection energy at about 50 GeV.

e/p Colliders

Although a design has not been done, we assume the parameters of the interaction points and arcs can be made similar to those at the DESY HERA collider[1] and parameters would scale according to simple scaling laws. The proposed e/p collider parameters are given in Table I.

Table 1, Preliminary e/p Collider Parameters

	Injector	VLHC
Circumference, km	34	500
Proton Ring		
E_{Max}, TeV	3	50
B(dipole), T	2.1	2.1
Electron Ring		
E_{Max}, GeV	81	250
B(dipole), T	0.068	0.008
P, MW	50	100
Pwr Den, kW/m	2	0.2
V(rf), MV	1000	3000
I, A	0.05	0.05
ep Collider		
$\sqrt{s}$, GeV	988	7071

The 34 km electron ring would use comparatively standard, but low field, magnets, however the rf system and synchrotron radiation power produced by the beam would be significant concern, both due to vacuum and thermal problems.

The design luminosity of both machines must be maximized order to match the large increase in accessible kinematics. The luminosity limits of HERA are determined by the interaction point parameters, (quadrupole gradients, spacings etc.) and the maximum charge/bunch that can stably circulate. The single bunch current limit in HERA is determined by multibunch instabilities which are driven by parasitic modes in the accelerating cavities. The instabilites are cured by broadband feedback systems.

The e^+e^- Collider

The and e^+e^- collider located in the tunnel of the 50 + 50 TeV hadron collider has been described elsewhere [2,3]. This facility has a maximum luminosity of $9 \cdot 10^{32}$ $cm^{-2}s^{-1}$ at a center of mass energy of about 360 GeV, and lower luminosities above or below this energy. Table II gives the parameters of this facility.

Table II, The and e^+e^- Collider in the VLHC Tunnel

Beam energy E /GeV	180
Circumference C /m	531000
Luminosity L /$cm^{-2}s^{-1}$	9.15E+32
Beam-beam tune shift $\xi_x = \xi_y$	0.03
Beta functions at IP $\beta_x^* : \beta_y^*$ /m	1.0 : 0.05
Beam emittances $\varepsilon_x : \varepsilon_y$ /nm	32.5 : 1.7
Beam radii at IP $\sigma_x^* : \sigma_y^*$ /μm	180 : 9.01
Bunch population N	8.04E+11
Total current / beam I_b /mA	37.2
Number of bunches /beam k	512
Bending radius ρ /m	72628
Injection Energy E_{inj} / GeV	50
Dipole fields $B_{max} : B_{inj}$ /mT	8.3 : 2.3
Phase advance / cell $\mu / 2\pi$	0.125
Arc tune Q	258
Cell Length L_p /m	249
Beta functions in arcs $\beta_{max} : \beta_{min}$ /m	488 : 218
Beam radii $\sigma_x : \sigma_y$ /mm	4.3 : 2.8
Synchrotron radiation loss U_s /MeV	1376
Aperture radii $A_x : A_y$ /mm for 10σ	53 : 38
Center of mass energy spread σ_E /GeV	0.26
RF voltage V_{RF} /MV	1616
Total generator power P_g /MW	102

A number of features of this machine are noteworthy including the good luminosity and the small center of mass energy spread.

The basic design of the large collider would somewhat follow that of LEP, however the scalings effect various components in different ways. The energy at which the maximum luminosity occurs is proportional to $\rho^{1/5}$, thus the specific dimensions of the tunnel only weakly affect the operating parameters of the machine. It is anticipated that the low fields and power loadings will permit cost savings in the design of both accelerator components and support systems.

Although the arcs of this machine would be very long, the very low dipole field and low excitation current required to produce this field seem to imply that the magnet system would be very light and simple. The machine would use pretzel orbits produced by electrostatic deflectors at the ends of the straight sections. RF, controls and interaction regions would be very similar to existing machines. Air cooled aluminum conductors are a possibility, for example. Likewise, the pumping requirements for photo produced gas per unit length would be minimal, ~2 $Ls^{-1}m^{-1}$. We have assumed that vacuum pumping would be done by 500 L/s TM pumps at discrete synchrotron absorbers spaced about 100 m apart. The synchrotron power would then be transmitted by water coolant to coils in the tunnel walls. The rf system required by both machines would provide 1 - 3 GV, which would be most efficiently produced by superconducting rf cavities operating at a frequency of 350 - 500 MHz.

Design Issues for Electron Options

A number of specific concerns require attention. Efficient use of the large kinematic range accessible to the ep colliders would require high luminosity interaction regions and large beam currents operating with significant rf voltages /turn. In the large ring, the effects of synchro-betatron coupling on the dynamic aperture must be understood.

An electron ring in the VLHC injector tunnel would use magnets and vacuum components similar to those used in large storage rings and colliders. The electron ring in the large tunnel would look quite different from existing machines and would have to solve problems associated with low fields and efficient heat removal at low power densities. The design of a vacuum chamber with lumped absorbers and an acceptable wall impedance is also an issue.

An efficient injector system is also required for both machines.

References

[1] R. Brinkmann, Proceedings of the 1995 Particle Accelerator Conference, Dallas, (1995), 410
[2] J. Norem, E, Keil, Proceedings of the 1996 Snowmass Workshop, (1997)
[3] J. Norem, J. Jagger, S. Sharma, E, Keil, G. W. Foster, E. Malamud, E. Chojnacki, D. Winn, Proceedings of the 1997 Particle Accelerator Conference, Vancouver CA, (1997)

The e/p Option in the 3 TeV Booster

D. Krakauer, Argonne
J. Norem, Fermilab/Argonne
12 / 5 / 97

I. Introduction

While the eventual aim of the VLHC experimental program is the construction of a large circular hadron collider, this machine would require an injector, and a significant experimental program could take place in the tunnel of the 3 TeV injector. This note considers the costs and benefits of colliding leptons on hadrons.

II. Physics goals at the ep collider

Lepton-hadron deep inelastic scattering (DIS) experiments have played important roles in development of the Standard Model. The discovery of partons inside the nucleon and weak neutral currents occurred in (nowadays) low-energy DIS, and more recently low-energy DIS in fixed target experiments have been used for increasingly precise measurements of the strong coupling constant , α_S, and the electroweak mixing angle, $\sin^2\theta_W$. When the HERA collider, operating at $\sqrt{s}$ ~ 300 GeV, extended precise measurements of the proton's internal structure up two orders of magnitude in momentum-transfer (Q^2), or equivalently down two orders in parton-momentum-fraction x, theoretical interest was sparked many areas of Quantum Chromodynamic (QCD). These include investigations of perturbative QCD in exclusive and inclusive processes, at the interface of pertubative and nonperturbative interactions, in diffractive and non-diffractive scattering, into regions where there are two-or-more hard-scales, and so on. The relatively high center-of-mass also allowed tests for new phenomena beyond the Standard Model, that were competitive or complementary to searches performed at e^+e^- and $p\bar{p}$ colliders.

A new *ep* collider with $\sqrt{s}$ ~ 1 TeV would provide a unique method to continue and enhance this rich program. A partial list and short description of a fraction of the physics that could be done at this new facility is contained in the next three subsections. Before describing the physics, it should be noted that the experiments/detectors at this collider do not require any great technological improvements compared to present detectors at HERA. Furthermore, lessons learned at the present experiments could be used to optimize the design of the new detectors taking full advantage of technological advances that have occurred in the recent past since HERA was commissioned.

IIa. QCD and the Structure of the Proton

The *ep* collider is first and foremost a QCD-factory - designed to provide a multitude of interesting inclusive and exclusive measurements relevant to the test and improvements of our theory of hadron interactions. Compared to HERA, the new collider will extend measurements of the proton structure functions up by a factor of ten in both Q^2 and/or $1/x$. The covered kinematic reach also nicely overlaps with some of the (x, Q^2) region at HERA providing immediate and necessary cross checks of absolute cross sections and structure functions measured. The extension into higher Q^2 will allow more precise measurements of α_S by reducing sensitivity to systematic uncertainties that are predominant at low-Q^2.

In the early days of the new collider, the experiments can concentrate on exploring the interface of perturbative-to-nonperturbative physics at very small-x. The wide-band-beam of real and virtual photons colliding with the proton will allow extension of inclusive measurements of total, diffractive and inelastic cross-sections to three-times higher center-of-mass than now possible. New measurements of the photon structure function to lower-x than possible at any other collider.

Proton structure functions will be measured over the extended kinematic range. There may be a chance to reach a low-enough x at large-enough Q^2 that the parton densities will become saturated, and the first effects of non-linear dynamics in gluon interactions can be explored quantitatively. The ability of QCD to properly describe the parton density distributions in the new kinematic region will be severely tested, and may lead to insights on the proper evaluation of QCD evolution -- so called "BKFL vs DGLAP" dynamics.

The event rate at $Q^2 > 1000$ GeV^2 will be roughly a thousand times that at HERA, and so it should be possible (using combinations of electron and positron beams) to measure both F_2 and xF_3 cross sections with vastly improved precision. This enables one to determine the parton distributions separately for each flavor of quark and anti-quark. It is likely that such precise data will be needed by the groups operating at LHC and its successors in order to evaluate their QCD background and physics rates.

IIb. Electroweak physics

Unlike at HERA, where the cross-sections and event rates for Charged Current reaction (W-exchange) are minuscule compared to Neutral Current (Z and virtual photon exchange) - at this new facility event rates of > 100,000 NC and CC per year for $Q^2 > 10000$ GeV^2 are expected. In addition to the precise measurements of F_2, xF_3 mentioned above, this non-trivial event rate for electroweak scattering opens up the possibility for Electroweak measurements in both DIS and in direct production of the weak-vector bosons. For instance, details here (must confirm sensitivity).

Secondly, it is likely that by the time this collider is operational, the limited factor in sensitivity to fundamental parameters (weak-couplings, weak-mixing angles) in certain direct measurements at hadron colliders, will be due to uncertainty in the (anti)proton's parton structure. Improvements by large factors compared to present data are inevitable if the data from this collider are available to constrain the quark/anti-quark/gluon densities of the proton.

IIc. Searches for new physics

It is generally true that the sensitivity to directly produce new particles is greatest in colliders achieving the highest center-of-mass per collision. Therefore, a $\sqrt{s} = 1$ TeV ep machine is at some disadvantage to the LHC in absolute "mass reach" for new particles. Nevertheless, for some selected channels, particularly those with leptons in the final state, or with lepton-flavor violation in the production mode, the mass reach is comparable for the proposed machine and for LHC. More crucially, should a new particle, such as a LeptoQuark, with mass less than ~600 GeV be discovered at LHC or during the Tevatron Run II, then the proposed machine will be an ideal "factory" for producing and understanding the particle's interactions. For instance, combining data from electron and positron scattering, especially if polarized interactions are possible, would allow one to disentangle the spin-isospin-flavor quantum numbers of a singly produced leptoquark or squark.

The proposed machine does have some advantage for discovering 'new interactions' that do not result in mass-resonances, but instead lead to changes in the observed distributions of high-mass final states {Such as "contact interactions" or quark/lepton-compositeness}. Firstly, discovery limits for such interactions depend crucially on accurate and precise predictions for the standard model "background" cross-sections. These background distributions typically rely on estimates of 'parton distributions' in kinematic regions where such have not been directly measured and where some (in particular gluon-density distributions) are not precisely constrained. Because on parton in the *ep* collision is the 'structureless' lepton, sensitivity to parton distributions is smaller than at *pp* colliders and background predictions usually better constrained by previous measurements. In fact, measurements of structure functions here may even reduce the uncertainties at hadron colliders and thereby eliminate a fundamental limitation of their sensitivity to some forms of new physics and interactions.

III. A Large e^+e^- Circular Top Factory

In addition to the ep options, an electron/positron injector chain would permit the eventual construction of a large circular e^+e^- collider in the VLHC tunnel, which could be used to produce large numbers of $t\bar{t}$ pairs or light Higgs. A preliminary design of this option has been produced and published in the Proceedings of the Snowmass workshop and the 1997 Particle Accelerator Conference.

IV. Collider Requirements

The ep collider would would face many of the problems of HERA, although at beam energies three times higher. A total power consumption limit of 50 MW would correspond to an electron beam of about 80 GeV, giving $\sqrt{S} \sim 1$ TeV. The dimensions of the 34 km tunnel for the 3 TeV collider are roughly comparable to the 27 km LEP tunnel, so magnets and rf could be scaled from this machine.

The performance of the collider must be sufficient to produce a physics program complementary to the LHC and other machines which will be operating in 20 years. This facility should have high luminosity and the flexibility to be study the complete range of available physics. This effectively means that the luminosity of the collider will have to permit counting rates on the order of one fb^{-1} per year. In addition it will be necessary to be able to look at both e^+/p and e^-/p collisions. This will require an injector chain that can produce both polarities, requiring either that ring magnets are reversed or injection and extraction systems for both polarities are provided. A further requirement of the ep program would be that the operation of the machine would be compatible with lepton polarization. Since the Sololov-Ternov times, $\tau_p^{-1} = 5\sqrt{3}\, \gamma^5 \hbar e^2 / \; 8\, \rho^3 m^2 c^2$, are on the order of 30 minutes for beams of 80 GeV, operation with polarization seems possible. The design of the lattice must also be compatible, however, with spin rotators incorporated into the design from the beginning.

Experimental access to the beam must also be provided for small angle (low Q^2) events. These counters would be located in both the proton and lepton lines and, at HERA are inserted almost into the halo of the beam. Since the events have a large cross section and counting rates, these measurements can be carried out in the early stages of the experimental program before the machine reaches full luminosity and special tunes can be used, for example to move the interaction point up

or downstream where detection would be easier.

V. Injector Chain

It will be necessary to adapt the Fermilab injector to provide high energy leptons. This could be done as shown in Fig 1. The system consists of: 1) a new e+e- linac system. 2) an accumulator ring for positrons, 3) A lattice correction package, together with a new injector and extraction system for the Booster, 4) and beamlines to carry the beams to and from the Main Injector.

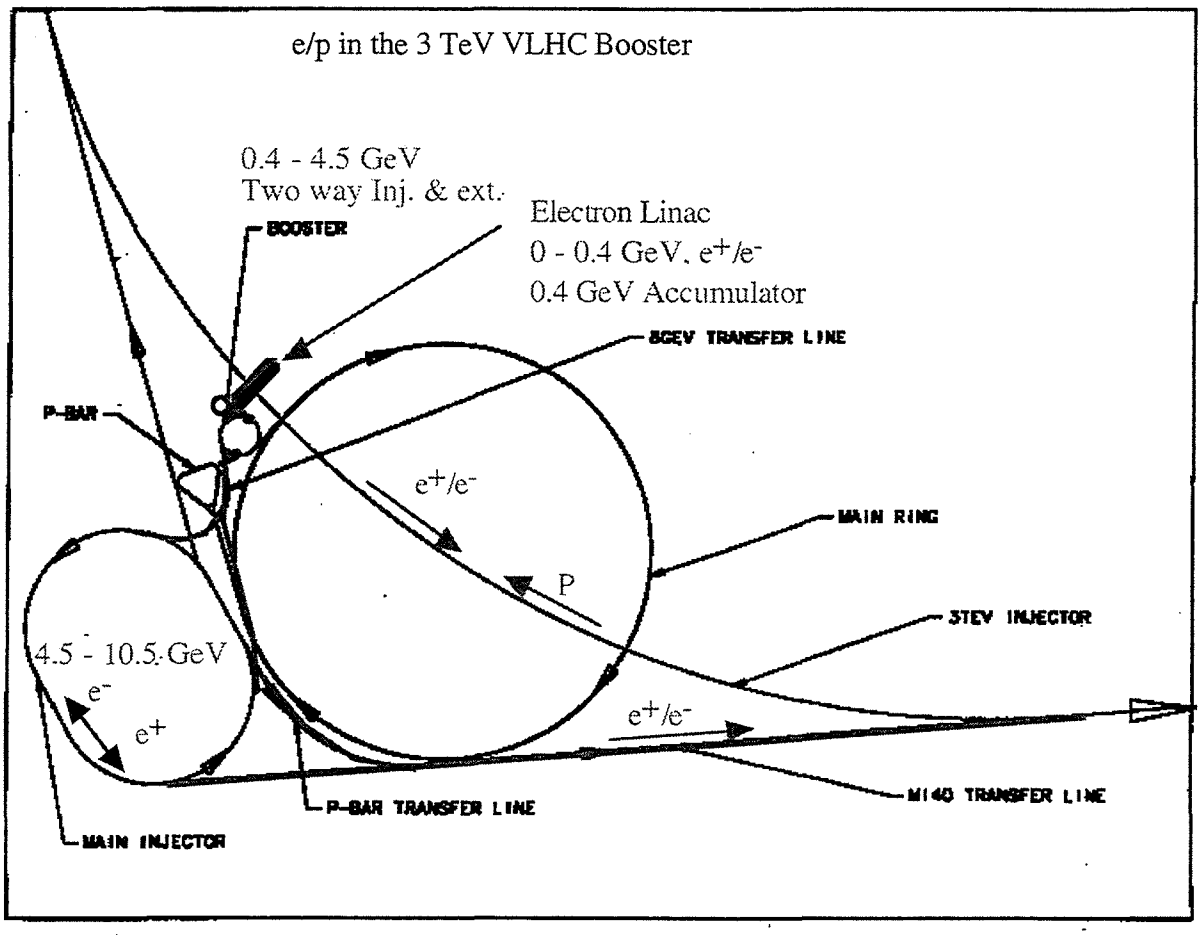

Figure 1. The injector chain for an e/p collider.

The electron linac would be based on those at DESY, CERN and the Argonne APS. There seems to be sufficient space in the present proton linac vault to construct an electron linac and the klystron gallery also has sufficient space for the electron linac power supplies, however the positron accumulator would require a new shielded room.

It is assumed that the Booster would operate from 0.4 to ~ 4 GeV, and the Main Injector would accelerate leptons from ~4 to ~10 GeV, the energies being determined by the requirements that the existing rf system provide the power required to replace synchrotron loss. More rf could be provided at a cost of ~0.7 $/V if needed, however it is not clear that the low injector energies

introduce problems. The injection fields for both the Booster and Main Injector would be about half of the design fields for these machines. The magnets of the Main Injector have been measured and should be adequate at these field levels, and it is assumed that the Booster would also be able to operate in this mode, since the required aperture at low energies should be small. Synchrotron radiation problems such as heat removal and radiation doses have not yet been considered.

It will be necessary to provide correction packages to control the damping partition numbers in the Booster. These packages would consist of gradient magnets, dipole magnets and quadrupoles which would compensate for the effects of the alternating gradient lattice. These packages should be on the order of 5 - 8 m long and could be distributed among the five empty long straight sections.

The costs of modifications to the injector chain seem to be primarily in the new linac and accumulator ring, and in the new injection and extraction systems for the booster. It is unclear what modifications required for synchrotron radiation in the Booster and Main Injector would cost.

VI. Services

Additional services must be provided to the 34 km circumference injector due to magnet cooling and the removal of synchrotron radiation power. Ultimately the most of the 50 MW of power produced by the rf system appears as heat at the outside edge of the vacuum chamber. The usual solution to heat removal would be to provide cooling towers at intervals around the ring, however the superconducting magnets require no comparable services. Synchrotron radiation would also produce radiation doses of 10^6 - 10^8 rads/yr (depending on location) due to the high energy part of the synchrotron photon spectrum. This dose could damage insulators and cause a variety of problems. The radiation dose can be absorbed by local lead shielding.